SOA FORMATION: CHAMBER STUDY AND MODEL DEVELOPMENT

Final Report to the

California Air Resources Board
Contract No. 08-326

By

William P. L. Carter, Gookyoung Heo, David R. Cocker III, and Shunsuke Nakao

May 21, 2012

Center for Environmental Research and Technology
College of Engineering
University of California
Riverside, California 92521

ABSTRACT

An experimental and mechanism development study was carried out to enhance the recently developed SAPRC-11 gas phase aromatic mechanism so it can predict secondary organic aerosol (SOA) formation from the atmospheric reactions of aromatics. This phase of the project covered dry conditions and 300K. A total of 158 dual reactor chamber experiments were carried out using the UCR-EPA environmental chamber, and their results were combined with previous data from this chamber to provide a database of 315 separate reactor irradiations for mechanism evaluation. A total of 14 representative aromatic hydrocarbons and 7 representative phenolic compounds were studied with varying reactant and NO_x levels and in some cases with different light sources and other added reactants. Methods were developed and evaluated to represent gas-particle partitioning, nucleation, and chamber effects when modeling the experiments. Alternative mechanisms were examined and SOA yield and gas-particle partitioning parameters were optimized to simulate the available chamber data. The model simulated most of the data without large biases but with larger run-to-run variability in model performance than observed in ozone mechanism evaluations, and potential evaluation problems were observed for some compounds. It is concluded that this new mechanism reflects the current state of the science. Recommendations are given for the next phase of SOA mechanism development and other needed research.

ACKNOWLEDGEMENTS AND DISCLAIMERS

This work was funded by the California Air Resources Board (CARB) through contract number 08-326. with additional support for the experiments provided by National Science Foundation contracts ATM-0449778 and ATM-0901282. An instrumentation grant from the W. M. Keck Foundation provided instrumentation that was used in experiments for this project.

The environmental chamber experiments were carried out at the College of Engineering Center for Environmental Research and Technology (CE-CERT) by Wendy Goliff, Dylan Switzer, Christopher Clark, Xiaochen Tang and Ping Tang, with assistance from Kurt Bumiller and Charles Bufalino. Mr. Dennis Fitz provided assistance in administration of this project, and Robert Griffin provided input and useful comments on this report. We also wish to acknowledge the contributions of Bethany Warren, who helped initiate the concept for this project and worked on the initial mechanism development work.

TABLE OF CONTENTS

TABLE OF CONTENTS (continued)

LIST OF TABLES

LIST OF FIGURES

LIST OF FIGURES (continued)

LIST OF FIGURES (continued)

LIST OF FIGURES (continued)

EXECUTIVE SUMMARY

Background

Secondary organic aerosol (SOA) formed from atmospheric reactions of volatile organic compounds (VOCs) constitutes an important component of atmospheric particulate matter (PM) that impacts visibility, climate, and health. Development of reliable and effective SOA control strategies depends on models that can reliably simulate its formation based on an adequate understanding of SOA formation processes. Previous work has resulted in various parameterized methods for modeling SOA in airshed models that have known limitations and whose validity in atmospheric simulations is doubtful. Ultimately, we need detailed mechanisms that can predict SOA based on our understanding of actual chemical reactions and species involved, but developing such mechanisms is many years away.

Adapting existing gas-phase mechanisms to SOA modeling is what is needed at the current phase of SOA mechanism development. It should start with developing SOA mechanisms for well-defined chemical systems reacting under well-controlled and well-characterized conditions, and then continue with enhancing them to cover additional types of chemical compounds and the other atmospheric conditions that need to be represented. This project represents the first phase of this plan, covering aromatics reacting under dry conditions at ~300K without added seed aerosol.

Objectives and Methods

The objectives of this project were to carry out the experimental and mechanism development work to enhance existing gas-phase mechanisms so they can predictively model SOA formation from the reactions of aromatics under well-defined conditions. Environmental chamber experiments were carried out to measure PM formation in both the presence and absence of NO_x in the UCR-EPA chamber, which has been used extensively for gas-phase mechanism evaluation studies at atmospherically relevant reactant levels and is well characterized for this purpose. The results were used to develop and evaluate enhanced versions of the current SAPRC aromatics mechanism that can predict the SOA formation observed in the experiments. The compounds studied represented the major types of aromatics, including 14 different representative aromatic hydrocarbons and 7 different representative phenolic compounds, and the experiments had varying reactant levels and in some cases differing light sources and addition of other reactants. The experiments in this phase of the project were restricted to dry conditions and 300K, to allow for differences among compounds and reactant levels to be comprehensively evaluated. Models and methods were developed and evaluated to represent gas-particle partitioning, nucleation and chamber effects when modeling our experiments. The results were used to derive mechanisms and parameters to predict SOA formation from the 14 aromatic hydrocarbons and 3 representative phenolic products, and also to develop mechanisms for lumped aromatic model species for airshed models.

Results and Discussion

A total of 158 dual reactor environmental chamber experiments were carried out for this project to provide data needed for aromatic SOA mechanism development. Of these 316 separate reactor irradiations, 40 (13%) were analyzed or modeled for chamber characterization purposes, and 217 (69%) were judged to be useful for SOA mechanism evaluation. These were combined with relevant

experiments carried out previously in our chamber, to yield a combined dataset of inputs and results for 334 well-characterized and quality-assured reactor irradiations useful for SOA mechanism evaluation.

The recently developed SAPRC-11 gas-phase aromatics mechanism was used as the starting point to develop a mechanism for predicting aromatic SOA. The SOA model used a level of detail similar to that used for the gas-phase mechanism, and represented five different SOA formation processes using 11 new model species, for which yields and partitioning parameters had to be estimated or derived based on simulations of the chamber data. Various alternative mechanism formulations and alternative partitioning parameter values were examined in test calculations, with the results being used to select a baseline mechanism that seemed to be chemically reasonable, and to fit the available data with the least bias, once the various adjustable yield parameters (two for each aromatic hydrocarbon, and six in total for the four phenolic model species) were optimized. The mechanism predicted that approximately ~5-60% of the SOA formed from aromatic hydrocarbons come from the reactions of phenolic products, with the remaining coming from primary hydroperoxide formation and from secondary reactions of non-phenolic aromatic oxidation products. The relative importance of these processes varied with reaction conditions.

The mechanism was evaluated by conducting model simulations of the 315 SOA mechanism evaluation experiments. The model simulated most of the data without large overall biases because parameters in the mechanism were adjusted to minimize biases, and in most cases no clear dependence of model performance on experimental conditions could be found, which tends to support the model formulation used. More run-to-run variability in model performance was observed in the evaluation results than is the case in ozone mechanism evaluations, and some potentially significant biases and evaluation problems were seen for some compounds. However, other than the variability and some inconsistencies in the data for toluene, the problems did not appear to be significant for most of the compounds, particularly for m-xylene, the compound that was the most extensively studied.

Conclusions and Recommendations

We believe this work represents significant progress and what is necessary at this stage in the process of adapting gas-phase mechanisms to predicting SOA formation in the atmosphere. There were mechanism evaluation issues such as greater scatter in the fits to the data than observed when evaluating gas-phase mechanisms, and clearly many uncertainties exist in the mechanism as well as the modeling methods and chamber effects model, but this reflects the current state of the science.

The major recommendations coming from this project are that additional phases of the work needed to provide improved models for SOA formation in the atmosphere should be carried out, and that longer-term research is also needed. The next phase should be to enhance the mechanism developed for this work so that it can cover compounds other than aromatics and conditions of varying humidity, temperature, and other types of PM present. Studies of the level of detail appropriate for representing SOA formation in airshed models are needed to guide future SOA mechanism development and implementation. Additional work is needed to evaluate and improve our ability to model the transformation of gas-phase species to particles (and back), both in the context of atmospheric models and when developing mechanisms using chamber data. Uncertainties in SOA-related chamber effects need to be reduced, and inter-laboratory comparison studies of chamber experiments for SOA mechanism evaluation need to be carried out. The appropriateness of the absorptive partitioning assumptions needs to be evaluated and better methods for measuring or estimating partitioning coefficients are needed. Finally, work needs to continue to characterize the compounds present in SOA and exactly how they are formed so that ultimately the models can be based on fundamental scientific understanding rather than adjustments to fit chamber data.

INTRODUCTION

Secondary organic aerosol (SOA) formed from atmospheric reactions of volatile organic compounds (VOCs) in the presence of NOx constitutes an important component of atmospheric particulate matter (PM) that impacts visibility, climate, and health. Development of reliable and effective SOA control strategies depends on models that can reliably simulate SOA formation, which in turn requires an adequate understanding of SOA formation processes. Due to limited knowledge of chemical and physical processes involved in SOA formation, SOA modeling is afflicted by large uncertainties (Volkamer et al, 2006; Zhang et al, 2007).

Data on SOA formation in well-characterized environmental chamber experiments representing a range of atmospheric conditions are essential to test and improve our theories and models for predicting SOA in the atmosphere. Emerging evidence obtained from such experiments demonstrates that NO_x levels during atmospheric simulations impact the extent of gas-to-particle conversion measured for atmospherically relevant hydrocarbons (Chen et al, 2005; Hurley et al, 2001). Previous findings widely cited and used in atmospheric airshed models are derived from atmospheric chamber simulations at elevated NO_x concentrations far exceeding those typically encountered in urban airsheds (e.g., Odum et al, 1996, 1997; Griffin et al, 1999; Cocker et al, 2001; Izumi and Fukuyama, 1990; Jang and Kamens, 2001). Previous data from our group (Song et al, 2005) and at EUPHORE (Johnson et al, 2005) indicate that current environmental chamber data obtained under elevated NO_x conditions may significantly underestimate SOA formation. For aromatic systems, Song et al (2005, 2007) performed a series of experiments demonstrating that aerosol production is elevated at low NO_x concentrations and that this cannot simply be predicted by ozone, hydroxyl, and nitrate concentrations present in the chamber. A significant portion of the underprediction in aerosol formation may be resulting from improperly evaluating aerosol formation at atmospherically relevant VOC to NO_x ratios.

Previously, our group developed a preliminary model that tracks the gas phase precursors and applies a semi-empirically determined gas-to-particle partitioning coefficient to single precursors (Warren et al, 2007, 2008a). This model involved adding representations of SOA formation processes to the SAPRC-07 mechanism previously developed by Carter (2010a). Although SAPRC-07 was developed primarily to represent gas-phase processes and calculate ozone reactivity scales, it is well suited for adaptation to models for SOA prediction because of its ability to represent mechanism differences of individual VOCs, and because of its significantly improved capabilities of predicting hydroperoxide formation, which we believe are important PM precursors (Carter, 2010a). Although this model showed promise for tracking the influence of NO_x on SOA formation, it did not correctly simulate all of the available data, and it incorporates assumptions that need to be experimentally tested. In addition, because of limited available data, its scope was limited to SOA predictions from m-xylene. Although this represented a useful starting point, it needed significant development and experimental evaluation before it could be adapted for regulatory modeling.

This project was carried out to address the need to develop and evaluate improved models for predictions of SOA formation from aromatic compounds. The approach used and the results obtained are documented in this report. Briefly, the approach consisted of carrying out well-characterized environmental chamber experiments to measure PM formation from the irradiations in both the presence and absence of NO_x, and using the results to develop and evaluate mechanisms to predict SOA formation from the compounds that were studied. The aromatic - NO_x irradiations were carried out at various aromatic, NO_x, and aromatic / NO_x levels, and the experiments without NO_x consisted of aromatic - H_2O_2

irradiations with varying initial aromatic and H_2O_2 levels. Experiments with m-xylene were carried out with varying light intensities and different light sources, though most experiments were carried out using blacklight irradiation. Mechanism evaluation experiments were conducted with a total of 14 different non-phenolic aromatic hydrocarbons, consisting of benzene and all the possible C_7-C_9 alkylbenzene isomers, and also with a number of representative phenolic products.

The chemical mechanism used as the starting point in this work was the SAPRC-11 gas-phase aromatics mechanism, which is an updated version of SAPRC-07 that was also developed for this project and is documented in a separate report (Carter and Heo, 2012). Model species and reactions were added to this mechanism to represent SOA formation from various processes, and yield and other parameters representing these processes were adjusted based on the model simulations of the experiments carried out for this project.

Because of limited time and resources the experiments were restricted to dry conditions and a single temperature (~300K) with no added seed aerosol, so the mechanism developed for this work is limited to this set of conditions. Although a wider variety of conditions need to be represented in air quality modeling under ambient conditions, this is a necessary first step in the process of developing improved models for predicting SOA in regulatory models. Recommendations for additional work that is needed to continue making necessary progress towards this goal are discussed in this report.

EXPERIMENTAL METHODS

Chamber Description

All of the environmental chamber experiments for this project were carried out using the UCR EPA environmental chamber. This chamber was constructed under EPA funding to address the needs for an improved environmental chamber database for mechanism evaluation (Carter et al, 1999, Carter, 2002). The objectives, design, construction, and results of the initial evaluation of this chamber facility are described in more detail elsewhere (Carter et al, 1999; Carter, 2002, 2004; Carter et al, 2005a,b). A brief description of the chamber is given below.

The UCR EPA chamber consists of two ~85,000-liter fluorinated ethylene propylene (FEP) Teflon® reactors located inside a 16,000 cubic ft temperature-controlled "clean room" that is continuously flushed with purified air. The clean room design is employed in order to minimize infiltration of background contaminants into the reactor due to permeation or leaks. Two alternative light sources can be used. The first consists of a 200 KW argon arc lamp with specially designed UV filters that give a UV and visible spectrum similar to sunlight. This light source could not be used for this project because it was not operational during this period. Banks of blacklights are also present to serve as a backup light source for experiments where blacklight irradiation is sufficient, and this was used for the experiments for this project because of availability and because use of blacklights was judged to be sufficient to satisfy the project objectives. These blacklights were upgraded to yield a higher light intensity as part of a previous project funded by the California Air Resources Board (CARB) (Carter, 2011). The interior of the enclosure is covered with reflective aluminum panels in order to maximize the available light intensity and to attain sufficient light uniformity, which is estimated to be ±10% or better in the portion of the enclosure where the reactors are located (Carter, 2002). A diagram of the enclosure and reactors is shown in Figure 1. The spectrum of the blacklight light source is given by Carter et al (1995).

The dual reactors are constructed of flexible 2 mil (0.05 mm) Teflon® film, which is the same material used in the other UCR Teflon chambers used for mechanism evaluation (e.g., Carter, 2000a, 2010a, and references therein). A semi-flexible framework design was developed to minimize leakage and simplify the management of large volume reactors. The Teflon film is heat-sealed into separate sheets for the top, bottom, and sides (the latter sealed into a cylindrical shape) that are held together and in place using bottom frames attached to the floor and moveable top frames. The moveable top frame is held to the ceiling by cables that are controlled by motors that raise the top to allow the reactors to expand when filled or lower the top to allow the volume to contract when the reactors are being emptied or flushed. These motors in turn are controlled by pressure sensors that raise or lower the reactors as needed to maintain slight positive pressure which contributes to preventing background contaminants from infiltrating into the chamber reactors. During experiments the top frames are slowly lowered to maintain a constant positive pressure of approximately 0.03 inches of water (7.5 Pa) as the reactor volumes decrease due to sampling or leaks. The experiment is terminated if the volume of one of the reactor reaches about 1/5 the maximum value, where the time this took varied depending on the amount of leaks in the reactor, but was greater than the duration of most of the experiments discussed in this report. Since at least some leaks are unavoidable in any large Teflon film reactor, the constant positive pressure is important to minimize the introduction of enclosure air into the reactor that may otherwise result.

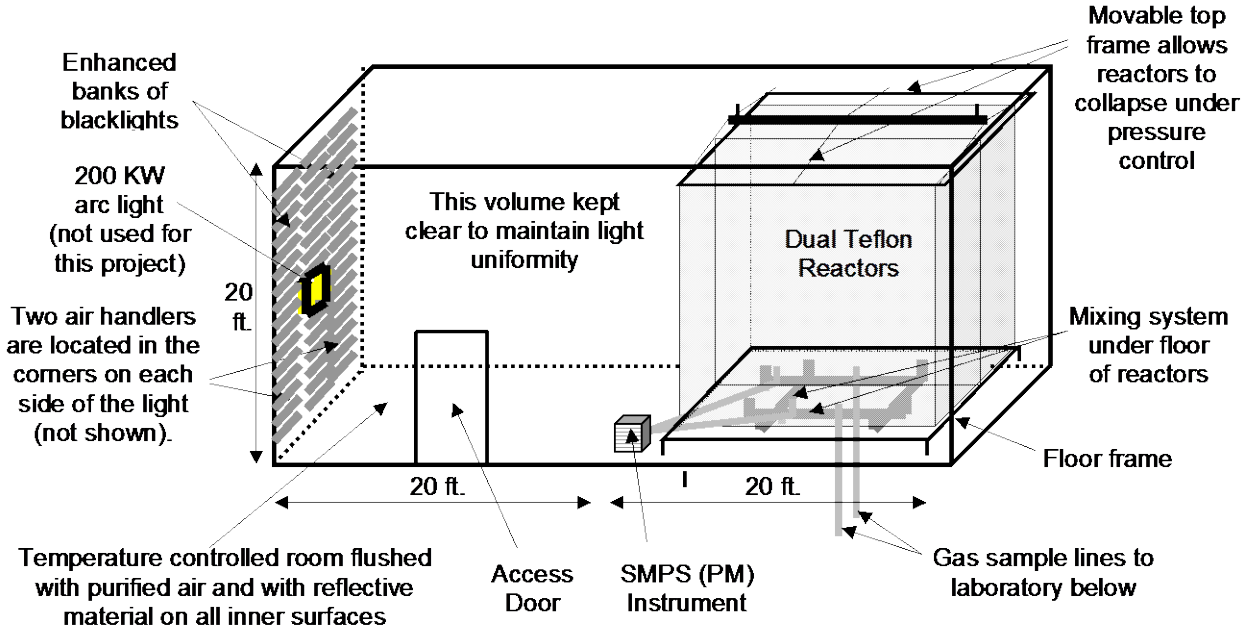

Figure 1. Schematic of the UCR EPA environmental chamber reactors and enclosure.

As indicated in Figure 1, the floor of the reactors has openings for a high volume mixing system for mixing reactants within a reactor and also for exchanging reactants between the two reactors to achieve equal concentrations in each reactor. This utilizes four 10" Teflon pipes with Teflon-coated blowers and flanges to either blow air from one side of a reactor to the other, or to move air between each of the two reactors. Teflon-coated air-driven metal valves are used to close off the openings to the mixing system when not in use, and during the irradiation experiments.

An air purification system (AADCO, Cleves, OH) that provides dry purified air at flow rates up to 1500 liters min^{-1} is used to supply the air to flush the enclosure and to flush and fill the reactors between experiments. The air is further purified by passing it through cartridges filled with Purafil® and heated Carulite 300® which is a Hopcalite® type catalyst, and also through a filter to remove particulate matter. The measured NO_x, CO, and non-methane organic concentrations in the purified air were found to be less than the detection limits of the instrumentation employed (see Analytical Instrumentation, below).

The chamber enclosure is located on the second floor of a two-floor laboratory building that was designed and constructed specifically to house this facility (Carter, 2002). Most of the analytical instrumentation is located on the ground floor beneath the chamber, with sampling lines leading down as shown in Figure 1.

Analytical Instrumentation

Table 1 gives a listing of the analytical and characterization instrumentation whose data were utilized for this project. Other instrumentation was available and used for some of these experiments, as

Table 1. List of analytical and characterization instrumentation for the UCR EPA chamber whose data were used for mechanism evaluation.

Type	Model or Description	Species	Sensitivity	Comments
Ozone Analyzer	Dasibi Model 1003-AH. UV absorption analysis.	O_3	2 ppb	Standard monitoring instrument.
NO - NO_y Analyzer	TECO Model 42 C with chemiluminescent analysis for NO, NO_y is converted to NO by catalytic conversion.	NO NO_y	1 ppb 1 ppb	Useful for NO and initial NO_2 monitoring. Note that converter used for NO_2 analysis also converts peroxy acyl nitrates (PANs) and organic nitrates, so these are also detected as NO_2. Quartz fiber filters soaked in a 9% solution of NaCl and dried were used to remove HNO_3 prior to entering the converter, to avoid a non-quantitative interference by HNO_3.
CO Analyzer	Thermo Environmental Instruments Inc. Model 48 C	CO	50 ppb	Standard monitoring instrument
GC-FID Instruments	HP 6890 Series II GCs with dual columns, loop injectors and FID detectors. Controlled by computer interfaced to network.	VOCs	~10 ppbC	30 m x 0.53 mm GS-Alumina column used for the analysis of light hydrocarbons such as ethene, propene, *n*-butane, trans-2-butene and perfluorohexane and 30 m x 0.53 mm DB-5 column used for the analysis of C_{5+} alkanes and aromatics, such as toluene and *m*-xylene. Loop injection is suitable for low to medium volatility VOCs that are not too "sticky" to pass through valves.
GC-FID Instruments with cartridge sampling	Agilent 6890 GC with FID detection interfaced to a ThermoDesorption System (CDS analytical, ACEM9305, Sorbent Tube MX062171) with Tenax-TA/Carbopack/ Carbosieve S111.	Lower Volatil-ity VOCs	~1 ppbC	Sample collection tubes were packed with Tenax-TA/Carbopack/Carbosieve S111. The tubes were thermally desorbed at 290°C. The column used was a 30 m Restek® Rtx-35 Amine (0.53 mm ID, 1.00 micron). This system was used for the analysis of low-volatility compounds such as phenolic compounds.
Gas Calibrator	Model 146C Thermo Environmental Dynamic Gas Calibrator	N/A	N/A	Used for calibration of NO_x and other analyzers. Instrument under continuous use.
Data Acquisition System	Windows PC with custom LabView software, 16 analog input, 40 I/O, 16 thermo-couple, and 8 RS-232 channels.	N/A	s, temperatu re	Used to collect data from most monitoring instruments and control sampling solenoids. In-house LabView software was developed using software developed by Sonoma Technology for ARB for the Central California Air Quality Study as the starting point.

Table 1 (continued)

Type	Model or Description	Species	Sensitivity	Comments
Temperature sensors	Various thermocouples, radiation shielded thermocouple housing	Tempera -ture	~0.1^{o}C	Primary measurement is thermocouples inside reactor. However, comparison with temperature measurements in the sample line suggests that irradiative heating may bias these data high by ~2.5^{o}C. See text.
Scanning Mobility Particle Spectrometer (SMPS)	TSI 3080L column, TSI 3077 ^{85}Kr neutralizer, and TSI 3760A CPC. Instrument design, control, and operation Similar to that described in Cocker et al (2001)	Aerosol number and size distribut-ions	Adequate	Provides information on size distribution of aerosols in the 28-730 nm size range, which accounts for most of the aerosol mass formed in our experiments. Data can be used to assess effects of VOCs on secondary PM formation.

discussed by Carter (2002), Carter et al (2005a), Qi et al (2010a, 2010b), and Nakao et al (2011a), but the data obtained were either not characterized for modeling or required additional analysis that was beyond the scope of this project, and were not used in the mechanism evaluations for this project. Table 1 includes a brief description of the equipment, species monitored, and their approximate sensitivities, where applicable. These are discussed further in the following sections.

Ozone, CO, NO, and NO_y (i.e., NO, NO_2 and other nitrogen-containing species that are converted to NO using a heated catalytic converter) were monitored using commercially available instruments as indicated in Table 1. The instruments were spanned for NO, NO_2, and CO and zeroed prior to most experiments using the gas calibration system indicated in Table 1, and a prepared calibration gas cylinder with known amounts of NO and CO. O_3 and NO_2 spans were conducted by gas phase titration (GPT) using the calibrator during this period. NO_2 concentrations established during sampling from the zero air (purified air) and during GPT using reaction between NO and O_3 to generate a specified concentration of NO_2 were used as reference NO_2 concentrations (for GPT, refer to Singh et al (1968), Fried and Hodgeson (1982), Bertram et al (2005) or Hargrove and Zhang (2008)). Span and zero corrections were made to the NO, NO_2, and CO data as appropriate based on the results of these span measurements, and the O_3 spans indicated that the UV absorption instrument was performing within its specifications.

Organic reactants were analyzed by gas chromatography (GC) with flame ionization detector (FID) as described elsewhere (Carter et al, 1995; see also Table 1). Propylene and perfluorohexane (n-C_6F_{14}; used as a dilution tracer) were monitored by using 30 m megabore GS-Alumina column and the loop sampling system. The second signal of the same GC outfitted with FID, loop sampling system and 30 m megabore DB-5 column was used to analyze liquid-state compounds: benzene, toluene, ethylbenzene, and the propylbenzene, xylene, ethyl toluene, and trimethylbenzene isomers. A GC-FID interfaced to a thermal desorption system with a 30 m Rtx-35 Amine column (RESTEK, Cat No. 11355) was used to analyze less volatile compounds such as phenol, cresol, dimethylphenol, and catechol isomers. The sampling methods employed for injecting the sample with the test compounds on the GC column depended on the volatility or "stickiness" of the compounds.

Both the GC instruments were controlled and their data were analyzed using HPChem software installed on a dedicated PC. The GC's were spanned using the prepared calibration cylinder with known amounts of ethylene, propane, propylene, *n*-butane, *n*-hexane, toluene, *n*-octane and *m*-xylene in ultrapure nitrogen. Analyses of the span mixture were conducted approximately every day an experiment was run, and the results were tracked for consistency.

GC response factors that are required for quantitative detection were obtained as follows: GC response factors for propene, toluene and m-xylene were determined using the calibration cylinder and GC span analyses, and verified by injecting and sampling known amounts of the compound in a calibration chamber of known volume. GC response factors for the other aromatic hydrocarbon isomers and perfluorohexane were determined based on the injected amounts and GC areas obtained during representative runs. For the phenolic compounds and catechols, liquid calibration was used to obtain their GC response factors.

The amounts of gaseous compounds injected, such as NO, NO_2, and propene, were determined by using a custom-built vacuum rack, an MKS Baratron® precision pressure gauge, and bulbs of known volume, determined by weighing when filled with water. The amounts of liquid compounds injected, such as most organic reactants, were determined by measuring amounts injected using microliter syringes. The volumes of the calibration chambers were determined by injecting and analyzing compounds whose analyses have been calibrated previously. For solid-state compounds, such as phenol, catechol, p-cresol, 2,6- and 3,5-dimethylphenol, a small cut of the solid-state material was weighed using a balance, melted using an oven integrated with the injection system and injected into the reactors by using heated N_2 gas. The injection oven was also used for o-/m-cresol and 2,4-dimethylphenol. CO and H_2O_2 were also used for this project. CO was directly injected from the cylinder of CO using a flow controller, and liquid H_2O_2 (50 wt% in water) was injected using the injection oven as well as microliter syringes to minimize the time needed to inject H_2O_2, a sticky compound.

The amount of H_2O_2 injected into the gas phase was not monitored, but had to be calculated from the volume and concentration of the liquid H_2O_2/water solution injected and the volume of the chamber. The concentration of H_2O_2 in the solution (50wt%, Sigma-Aldrich) was confirmed by weighing a known volume of the solution (accurate within 5%). The experimental hydrocarbon decay rates agreed reasonably with the predicted decay rates based on the amount of H_2O_2 injected into the reactors.

Particle size distribution between 27 and 685 nm was monitored by a scanning mobility particle sizer (SMPS) similar to that described in Cocker et al (2001). Particle sizing was periodically verified by aerosolized polystyrene latex (PSL) particles (90, 220, and 350 nm) (3000 series Nanosphere Size Standards, Thermo Scientific). (See also Table 1). Information from this SMPS was used to obtain particle numbers and particle volumes for this study. Size-resolved particle numbers were converted into particle volumes by assuming that the particles formed were ideally spherical in shape (in other words, particle volume = $(\pi/6)\cdot D^3$ where D is the particle diameter) and had a uniform density of 1.4 gm/cm^3 based on previous studies at this chamber facility (Malloy et al. 2009; Nakao et al, 2011a). Particle volatility was monitored with a Volatility Tandem Differential Mobility Analyzer (VTDMA), in which mono-disperse particles of mobility diameter Dmi are selected by the first DMA followed by transport through a Dekati thermodenuder (TD; residence time: ~17 s, temperature: 100^{o}C). The particle size after the TD (Dmf) is then measured by fitting a log-normal size distribution curve from the second SMPS. Volume fraction remaining (VFR) is then calculated as the before and after the TD volume ratio, i.e., $VFR = (Dmf/Dmi)^3$. The VTDMA was calibrated for each diameter setting using VFR of non-volatile seed particles (e.g., dry $(NH_4)_2SO_4$ seed aerosol) (Qi et al. 2010b; Nakao et al. 2011a).

Most of the instruments, other than the GCs and aerosol instrument, were interfaced to a PC-based computer data acquisition system under the control of a LabView program written for this purpose. These data, and the GC data from the HP ChemStation computer, were collected over the CE-CERT computer network and merged into Excel files that were used for applying span, zero, and other corrections, and preparation of the data for modeling.

Sampling Methods

Samples for analysis by the continuous monitoring instrument were withdrawn alternately from the two reactors and zero air, under the control of solenoid valves that were in turn controlled by the data acquisition system discussed above. For most experiments the sampling cycle was 5 minutes for each reactor, the zero air, or (for control purpose) the chamber enclosure. The program controlling the sampling sent data to the data acquisition program to indicate which of the two reactors was being sampled, so the data could be appropriately apportioned when being processed. Data taken less than 3-4 minutes after the sample switched were not used for subsequent data processing. The sampling system employed is described in more detail by Carter (2002).

Samples for GC analysis of surrogate compounds were taken at approximately every 20-minute directly from each of the reactors through the separate sample lines attached to the bottom of the reactors, as shown in Figure 1. The GC sample loops were flushed for a desired time with the air from reactors using a pump. Samples for analysis of the phenolic compounds were taken by using Tenax-TA/Carbopack/Carbosieve S111 cartridges that were then thermally desorbed onto the GC for analysis.

Characterization Methods

Use of chamber data for mechanism evaluation requires that the conditions of the experiments be adequately characterized. This includes measurements of temperature, humidity, and light intensity and spectral distribution, and wall effects characterization. Wall effects characterization for gas-phase mechanism evaluation is discussed in detail by Carter (2004) and updated by Carter and Malkina (2005) and Carter (2010a), and most of that discussion is applicable to the experiments for this project. Additional characterization is required for SOA mechanism evaluation as discussed below in the Characterization Results section, below. The instrumentation used for the other characterization measurements is briefly summarized in Table 1, and these measurements are discussed further below.

Temperature. Air temperature was monitored during chamber experiments using calibrated thermocouples attached to thermocouple boards on our computer data acquisition system. The temperature in each of the reactors was continuously measured using relatively fine gauge thermocouples that were located a few inches above the floor of the reactors. These thermocouples were not shielded from the light, though it was expected that irradiative heating would be minimized because of their small size. Experiments where the thermocouple for one of the reactors was relocated to inside the sample line indicated that radiative heating is probably non-negligible, and that a correction needs to be made for this by subtracting ~2.5^{o}C from the readings of the thermocouples in the reactors. This is discussed by Carter (2004).

The temperature was not varied for the experiments carried out for this project. The average temperature for the UCR-EPA chamber experiments used for mechanism evaluation was in the range of 296-307^{o}K, with the average being 299±2^{o}K.

Light Spectrum and Intensity. The spectrum of the light source in the 300-850 nm region has been measured using a LiCor LI-1800 spectroradiometer, which is periodically calibrated at the factory (e.g., see Carter et al, 1995). Based on previous extensive measurements the spectrum of the blacklight light was assumed to be constant, and was not measured during the time period of this project. The method used to derive the light intensity using the blacklight light source was based on that discussed by Carter et al (1995), updated as described by Carter and Malkina (2007). Briefly, the absolute light intensity is measured by carrying out NO_2 actinometry experiments periodically using the quartz tube method of Zafonte et al (1977) modified as discussed by Carter et al (1995). In most cases the quartz tube was located in front of the reactors. Since this location is closer to the light than the centers of the

reactors, the measurement at this location is expected to be biased high, so the primary utility of these data are to assess potential variation of intensity over time. However, several special actinometry experiments were previously conducted where the quartz tube was located inside the reactors, to provide a direct measurement of the NO_2 photolysis rates inside the reactors.

Additional blacklights were added to the chamber in the year 2010 as part of a previous CARB-funded project (Carter, 2011). The light intensity was measured once the construction of the new lights were completed using the quartz tube method discussed above, both inside and outside the reactors. These measurements are discussed by Carter (2011), and are summarized, along with results of more recent measurements made during the later period of this project, are discussed in the "Experimental Results" section, below. Since the same type of blacklight bulbs (115W Osram Sylvania 350 BL; part no. 25251) was used with the new lights as those already in the chamber, we assume that the spectral distribution of the light source did not change.

Experimental Procedures

The reaction bags were collapsed to the minimum volume by lowering the top frames, and then emptied and refilled at least six times with the lights being turned off after each experiment, and then were filled with dry purified air on the night before each experiment. Span measurements were generally made on the continuously measuring instruments prior to injecting the reactants for the experiments. The reactants were then injected through Teflon injection lines (that are separate from the sampling lines) leading from the laboratory on the first floor to the reactors on the second floor. The common reactants were injected in both reactors simultaneously, and were mixed by using the reactor-to-reactor exchange blowers and pipes for 10 minutes. The valves to the exchange system were then closed and the other reactants were injected to their respective sides and mixed using the in-reactor mixing blowers and pipes for 1 minute. The contents of the chamber were then monitored for at least 30 minutes prior to irradiation, and samples were taken from each reactor for GC analysis to get stabilized initial concentrations and air temperatures inside the reactors.

Once the initial reactants are injected, stabilized, and sampled, the blacklights were turned on to begin the irradiation. During the irradiation the contents of the reactors were kept at a constant positive pressure by lowering the top frames as needed, under positive pressure control, to minimize infiltration of background contaminants into the reactors. The reactor volumes therefore decreased during the course of the experiments, in part due to sample withdrawal and in part due to small leaks in the reactors. A typical irradiation experiment ended after about 6 hours, by which time the reactors are typically down to about half their fully filled volume. Larger leaks are manifested by more rapid decline of reactor volumes, and the run is aborted early if the volume declines to about 1/5 the maximum. This was not the case for most of the experiments discussed in this report. After the irradiation the reactors were emptied and filled six times as indicated above.

The procedures for injecting the various types of reactants were as follows. NO, NO_2, and propene were prepared for injection using a vacuum rack. For example, known pressures of NO, measured with MKS Baratron capacitance manometers, were expanded into Pyrex bulbs with known volumes, which were then filled with nitrogen (for NO) or purified air (for NO_2). The contents of the bulbs were then flushed into the reactor(s) with nitrogen. For experiments with added CO, CO was purified by passing it through an in-line activated charcoal trap and flushing it into the reactor at a known rate for the amount of time required to obtain the desired concentration. Measured volumes of volatile liquid reactants were injected, using a micro syringe, into a 2 ft long Pyrex injection tube surrounded with heat tape and equipped with one port for the injection of the liquid and other ports to attach bulbs with gas reactants. H_2O_2 was also injected using a microliter syringe and an oven used for injecting low-volatility compounds and sticky compounds such as phenols and cresols. For injections into both reactors, one end

of the injection tube was attached to the "T"-shape glass tube (equipped with stopcocks) that was connected to reactors and the other end of injection tube was connected to a nitrogen source. The injections procedures into a single reactor were similar except the "T" tube was not used.

Injection of low-volatility compounds such as phenol, o-cresol and catechol into the chambers was carefully performed using a heated oven through heated transfer line maintained at a temperature higher than oven for 30 minutes. The oven temperature can be adjusted, and a temperature of 60°C was used for this project. The glass manifold inside the oven was packed with glass wool to increase the mass transfer surface area. Nitrogen (N_2) was used as the carrier gas. All the gas and liquid reactants intended to be the same in both reactors were injected at the same time. The injection consisted of opening the stopcocks and flushing the contents of the bulbs and the liquid reactants with nitrogen, with the liquid reactants being heated slightly using heat tape that surrounded the injection tube. The flushing continued for approximately 10 minutes.

Materials

The NO, CO, H_2O_2 and the other reagents used in this project came from various commercial vendors as employed in previous projects at our laboratory. CO (Praxair, CP grade) was scrubbed with carbon charcoals before injection into the reactors to remove carbonyl-containing compounds produced by reaction of CO and the cylinder surface. NO_2 was generated in-situ by chemical conversion of NO (Matheson, UHP grade) using reaction of NO with O_2 (i.e., $NO + NO + O_2 = 2\ NO_2$) inside small Pyrex bulbs with known volumes. H_2O_2 was purchased from Sigma-Aldrich as H_2O_2 solution in water (Sigma-Aldrich, 50 wt. % in H_2O, stabilized, 516813) to use as a radical source. The concentration of H_2O_2 in the solution was measured so that the amounts of H_2O_2 injected into the chamber could be determined from the volume of solution used. Propene and ethene were purchased from Matheson, and the other organic reagents used in this study were purchased from Sigma-Aldrich.

MODELING METHODS

Simulation Inputs and Procedures

Simulations of Chamber Experiments

The procedures used in the model simulations of the environmental chamber experiments for this project were based on those discussed in detail by Carter (2004) and were employed in more recent studies (Carter and Malkina, 2005, 2007; Carter, 2008 and references therein), except as indicated below and in the "Characterization Results" section later in this report. Carter (2004) should be consulted for details of the characterization model and chamber effects parameters employed. The temperatures used when modeling were the averages of the temperatures measured in the reactors, corrected as discussed by Carter (2004). The temperature was not varied and averaged 299±2^{o}K for the experiments for this project. The photolysis rates were derived from the NO_2 photolysis rate measurements and the spectral distribution for the light sources employed was derived as discussed in the "Characterization Results" section. The chamber effects model and parameters used when modeling the experiments in this chamber were the same as those given by Carter (2004) except for the HONO off-gasing parameters, which were derived based on results of characterization runs carried out in conjunction with these experiments, and those related to PM formation, which were developed for this project. The chamber effects model and the derivation of its associated parameters are discussed in more detail in the "Characterization Results" section later in this report.

The initial reactant concentrations used in the model simulations were based on the measured values except for experiments where the added reactant could not be accurately measured using the available methods. This included H_2O_2 in those experiments where H_2O_2 was added and the few experiments where catechol was added. In those cases, the amounts of the compounds injected into the reactors, and the volumes of the reactors were used to calculate the initial concentrations used for modeling. Although the reactors are flexible, their initial volumes were very consistent from run to run because of the use of the pressure control system when filling the reactor to its maximum volume prior to the reactant injections (see Chamber Description section, above, and Carter, 2004).

Adjustment of OH Radical Levels

As indicted in the Introduction, a major objective of this project is to develop and evaluate mechanisms for prediction of SOA formation from the reactions of aromatic hydrocarbons. Predictions of the amounts of SOA formed when modeling a mechanism evaluation experiment depends not only on the ability to predict how much SOA is formed when the aromatic compound reacts (i.e., the SOA yield), but also on the ability to predict *how much* of the aromatic compound reacts during the experiment. The latter is determined primarily by the ability of the mechanism to predict OH radical levels in the experiment, which is the main species with which most of the aromatic compounds react. Prediction of radical levels is a part of the gas-phase chemical mechanism, whose development and evaluation is not strictly speaking within the scope of this report. However, if the model does not predict OH radical levels correctly it will not correctly predict the amounts of aromatics that react in the mechanism evaluation experiments, which means that it will not correctly predict SOA levels measured in the experiments unless there are compensating errors in the portions of the model used to predict SOA yields.

As discussed in the Chemical Mechanism section of this report the gas-phase chemical mechanism used to represent the gas-phase aromatics reactions in this work is the SAPRC-11 aromatics mechanism that is documented by Carter and Heo (2012). The mechanism is enhanced to predict

formation of condensable species for the purpose of SOA predictions, but the portions involved in the predictions of purely gas-phase species such as OH radical levels have not been modified during this enhancement for SOA prediction, because that would require re-adjusting and re-evaluating the gas-phase mechanism for ozone formation. Unfortunately, as discussed by Carter and Heo (2012), and also observed for previous versions of the SAPRC aromatics mechanisms (Carter, 2000a,b, 2010a) and other aromatics mechanisms (e.g., see Bloss et al, 2005), the mechanism systematically underpredicts OH levels and amounts of aromatic hydrocarbon reacted in model simulations of most aromatic - NO_x mechanism evaluation experiments. This will introduce a bias in the evaluation of SOA mechanisms, since an underprediction of radical levels would mean that a correct SOA mechanism should underpredict amounts of SOA formed from the aromatics.

The approach used to address this problem is to adjust the OH radical levels when modeling the SOA mechanism evaluation experiments to force the model to predict the correct amounts of aromatic VOC reacted in the simulation of the experiment. This is done by implementing versions of the mechanism where the OH levels are specified as a function of time in the input file used for the simulation of the chamber experiment, rather than being simulated by the model using the mechanism. These are referred to as the "adjusted OH" versions of the mechanism in the discussion in this report, to distinguish them from standard or "unadjusted" versions where the OH levels are simulated using the mechanism.

The method used to derive the OH levels for input into the adjusted OH mechanisms is as follows. Each experiment is divided into a minimum of 2, and more typically 3, time segments where plots of $R^{expt} = \ln(C_0/C_t)$ vs. time can be fit by various line segments, where C_0 and C_t are the measured concentration of the aromatic VOC at time t=0 and time t= t, respectively. The default is to use 3 segments, the first being 0 to 60 minutes after the run starts, the second being between 60 minutes and halfway to the end of the experiment, and the last being from then to the end of the experiment. These can be adjusted manually if judged to be necessary to fit the data with line segments. The value of C_0 is the initial concentration assigned for modeling. For the end of each of the n segments, values of R^{fit} are derived such that the sum of squares differences between the R^{expt} and the R^{fit} values interpolated for the time of each R^{expt} are minimized. The Excel solver function is used to derive these R^{fit} values. The [OH] level for each segment is then derived from

$$kOH \cdot [OH]_n + dil = (R^{fit}_n - R^{fit}_{n-1}) / (t_n - t_{n-1})$$
$$[OH]_n = (1 / kOH) \cdot \{(R^{fit}_n - R^{fit}_{n-1}) / (t_n - t_{n-1})\} - (dil / kOH)$$

where kOH is the OH rate constant for the added aromatic, $[OH]_n$ in the average OH radical concentration derived for segment n, dil is the dilution rate assigned for the experiment (usually zero), R^{fit}_n is the R^{fit} value for the end of the segment, and R^{fit}_0 is set at 0, This follows from integrating the kinetic equation

$$C_t = C_0 \, e^{-t(kOH \cdot [OH] + dil)}.$$

Concentration-time plots of R^{expt} and R^{fit} values derived for a representative experiment, the adjusted OH levels derived from the R^{fit} values, and the "experimental" and "adjusted OH" model calculated concentrations for toluene are shown on Figure 2.

Results of unadjusted model calculations for OH and toluene are also shown on Figure 2, where the extent of underprediction of the unadjusted model is noticeable. This is typical of aromatic - NO_x experiments used for mechanism evaluation (Carter and Heo, 2012). However, the unadjusted model generally performed better in simulating the aromatic consumption rates in the aromatic - H_2O_2 experiments, because the calculated OH levels for these experiments with H_2O_2 added are determined primarily by the injected H_2O_2 and aromatic levels and are not as influenced by uncertainties in the gas-phase aromatic mechanisms as for aromatic – NOx experiments. Nevertheless, for consistency, adjusted

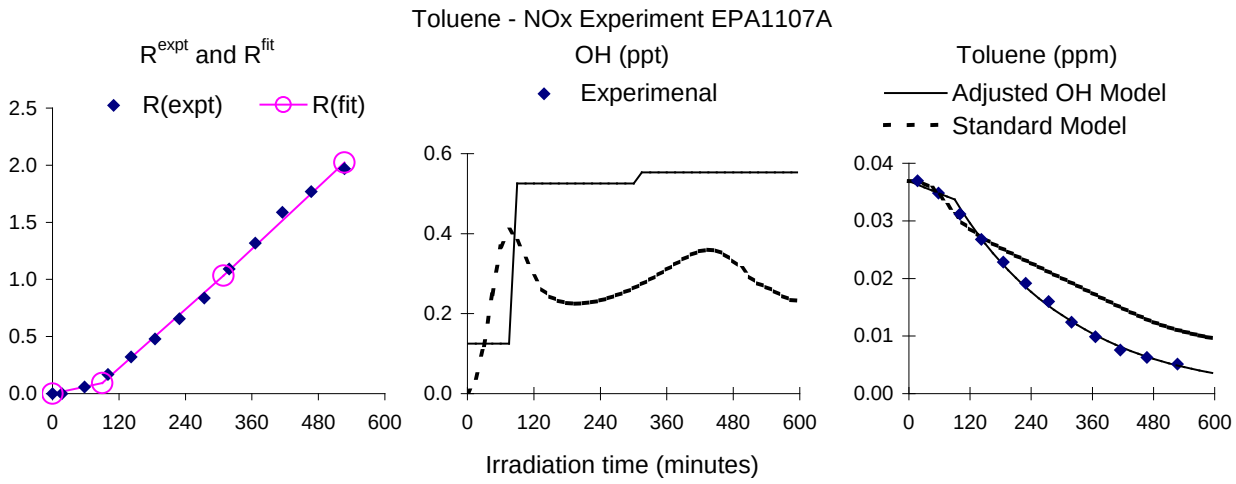

Figure 2. Concentration-time plots of R^{expt} and R^{fit} values derived for a representative toluene - NO_x experiment, and the experimental and calculated toluene and calculated OH levels for that experiment.

model calculations were used for all the aromatic SOA mechanism evaluation experiments where this is appropriate. Such experiments with no reliable aromatic reactant data to derive adjusted OH levels were not used for SOA mechanism evaluation.

Although use of an adjusted OH mechanism is obviously not an appropriate approach for gas-phase mechanism evaluation, it provides a means to test the model's capability to simulate SOA formation from aromatics with the correct amounts of the aromatic hydrocarbon consumed by reaction with OH, and also with better approximations of the amounts of secondary reactions of product species that react with OH radicals and form SOA. Therefore, except for some sensitivity calculations where the effect of not using the adjusted OH is examined, this approach was used when modeling experiments for compounds where use of this approach is appropriate. This is considered appropriate for all aromatic hydrocarbons except for benzene, but not for phenolic products such as cresols or xylenols when they react in the presence of NO_x. This approach could not be used for benzene because it reacts with OH too slowly for OH radical levels to be reliably derived from its rate of consumption, and is not used for phenolic products because they react to a significant extent with NO_3 radicals as well as with OH radicals in the presence of NO_x. Although in principle this adjustment can be used in the phenolic - H_2O_2 experiments, it was found not to be necessary for the cresols and the xylenols because the unadjusted model fit the consumption rate for the phenolic compound reasonably well. However, it was used for the phenol - H_2O_2 experiments because the unadjusted model tended to overpredict the phenol consumption rate in these experiments.

Note that the tendency for the aromatics mechanisms to underpredict OH radical levels does not necessarily mean they will underpredict OH in ambient simulations to a comparable extent. However, further discussion of this problem, which is applicable to all current aromatics mechanisms, is beyond the scope of this report.

Modeling PM formation

The model simulations in this work use a kinetic and equilibrium approach to simulate PM formation. The rates of sorption of condensable species onto existing PM, which is assumed to be

dominated by absorption (Pankow, 1994a, 1994b), are calculated using a gas-kinetic and diffusion approach as discussed by Stroud et al (2004). The rates of evaporation or desorption of the condensed species back to the gas-phase are calculated from the condensation rate and the equilibrium partitioning coefficient for the condensable species as discussed below. Because our experiments do not have initial seed aerosol available for sorption, it is also necessary to use a simple model to approximately simulate new particle formation, as also discussed below.

The species and parameters used in our model for calculating PM formation from a condensable gas-phase species are listed and described in Table 2. The table and discussion below give the parameters and species for an example condensable species called "CND1" in this discussion, but the same is applicable for all the condensable species in the model. The condensation and evaporation of CND1 on and off particles are represented by the following reactions that are added to the model.

$$\text{CND1} + \text{PMmass} \rightarrow \text{pmCND1} + (1+\text{fCND1})\ \text{PMmass} \qquad k = \text{kOnCND1} \quad (1)$$

$$\text{pmCND1} \rightarrow \text{CND1} - (\text{fCND1})\ \text{PMmass} \qquad k = \text{kOnCND1} / \text{KpCND1} \quad (2)$$

As indicated on Table 2, pmCND1 is the condensed form of CND1, PMmass is the total PM mass, fCND1 is a conversion factor relating the amount of pmCND1 formed or lost to the change in PMmass, kOnCND1 is the condensation rate constant calculated as discussed below, and KpCND1 is the gas-particle equilibrium partitioning coefficient specified in the SOA mechanism for CND1, defined as [pmCND1]/([PMmass][CND1]) under equilibrium conditions. In addition, the following reactions are included in order to represent loss of particles or condensable material to the walls:

$$\text{PMmass} \rightarrow (\text{loss of PM to walls}) \qquad k = \text{PMwall} \quad (3)$$

$$\text{pmCND1} \rightarrow (\text{CND1 on walls}) \qquad k = \text{PMwall} \quad (4)$$

$$\text{CND1} \rightarrow (\text{CND1 on walls}) \qquad k = \text{WallCond} \quad (5)$$

$$(\text{CND1 on walls}) \rightarrow \text{CND1} \qquad \text{Assumed negligible} \quad (6)$$

where PMwall is the particle wall loss rate that is specified for the experiment being modeled, and WallCond is the rate of condensation of gas-phase condensable species onto the walls. Reactions (3) and (4) are part of our chamber wall model that was developed based on characterization data as discussed in the Characterization Results section of this report. Reactions (5) and (6) are discussed further below in the subsection below on absorption and desorption of organics from the walls. They are both assumed to be negligible in this work except for sensitivity calculations where the effects of varying WallCond in Reaction (5) are examined.

Finally, since the above reactions will not simulate the formation of PM in the absence of initial PM, nonzero PMmass is required for the rate of Reaction (1) to be nonzero. Therefore, it is necessary to have some process to represent new particle formation. This is not straightforward to model exactly, and care must be taken to avoid situations where predicted nucleation rates are so slow that predictions of SOA yields are highly sensitive to highly uncertain and arbitrary nucleation parameters, or are so fast that they affect the gas-particle partitioning at high PM levels. In this work we represent nucleation as a bimolecular reaction between condensable species,

$$\text{CND1} + \text{CND1} \rightarrow 2\ \text{pmCND1} + (2 \times \text{fCND1})\ \text{PMmass} \qquad k=\text{NC\_CND11} \quad (7)$$

$$\text{CND1} + \text{CND2} \rightarrow \text{pmCND1} + \text{pmCND2} + (\text{fCND1}+\text{fCND2})\ \text{PMmass} \qquad k=\text{NC\_CND12} \quad (8)$$

Such "nucleation" reactions are given for each or each pair of condensable species in the model, with the rate constant depending on the equilibrium partitioning coefficients as discussed below. The mechanism developed in this work (discussed later in this report) has only four condensable model species, so all of the possible cross reactions (8) are represented in our model. Because this is a relatively minor process throughout most of the simulations, a different approach, such as that used for peroxy + peroxy reactions

Table 2. Description of species and parameters used to model PM formation from calculated concentrations of condensed species in the model simulations of the chamber experiments.

Name [a]	Description
	Active Species (concentrations calculated in simulations from rates of reaction)
CND1	Gas-phase form of the condensable species "CND1". Formed in the gas-phase reactions in the mechanism and also from evaporation from the condensed phase as shown below. The current mechanism has several such condensable species. Units of ppm are used in the model simulation software.
pmCND1	Condensed form of the condensable species CND1. Units of ppm are used in the model simulations.
PMmass	Total mass of species in the condensed phase. Calculated in units of $\mu g/m^3$
PMmassCorr	Mass of species in the condensed phase, corrected for wall loss as discussed in the "Particle wall loss characterization" subsection of the "Characterization results" section below. Calculated from calculated PMmass + amount of PMmass calculated to undergo wall loss.
	Dummy Species (time-varying concentrations calculated from active species)
PMVOL	Total volume of species in the condensed phase, in units of $\mu m^3/cm^3$, for comparison with experimental PM volume measurements. Calculated from PMmass / PMden, where PMden is the average density of all PM species. Note that if PMden=1 gm/cm^3 (i.e., the density of water), then a PM volume of 1 $\mu m^3/cm^3$ has a PM mass of 1 $\mu g/m^3$. However, the actual density used in this work is 1.4 gm/cm^3 (see below).
PMVolCorr	Volume of species in the condensed phase (PMVOL), corrected for wall loss as discussed above for PMmassCorr. Units are $\mu m^3/cm^3$. Calculated from PMmassCorr / PMden. The calculated PMVOLcorr values are compared with the experimental values that are calculated by Equation (VII) in the "Particle wall loss characterization" subsection, below.
	Constant Parameters (values specified as inputs for the simulations)
T	Temperature in degree K. Can vary with time, depending on the experiment inputs.
KpCND1	Partitioning coefficient used in the model for CND1 in units of $\mu g^{-1}m^3$. This is specified for each condensable model species as part of the SOA mechanism and is used to calculate the rate of evaporation of the particles from the condensed phase given the calculated rate of absorption onto particles. These are highly uncertain and the values used are somewhat arbitrary, but with approximate magnitudes are derived based on model simulations of the chamber experiments as discussed later in this report. Although these are expected to be temperature dependent, the temperature dependence is not represented in the current model because temperature was not varied in the SOA evaluation experiments. Note that some compounds are represented as being non-volatile, which is approximated by $Kp=\infty$ (i.e., $1/Kp \approx 0$).
MwCND1	Molecular weight of CND1 in units of gm/mole. This is used to calculate changes in PMmass from changes in pmCND1.

Table 2 (continued)

Name [a]	Description
PMden	PM density in gm/cm^3. Used for calculating PMVOL from PMmass. The default value of 1.4 gm/cm3 is used based on SOA densities reported previously from our laboratory (Malloy et al. 2009; Nakao et al, 2011a).
PMwall	PM wall loss rate, in units of min^{-1}. Derived from experimental data to fit measured rates of decrease of PM number once new particle formation ends as discussed in "Characterization Results" section of the report. Generally specified for each experiment where sufficient PM is formed for this to be derived. Default value is 4.2 x 10^{-3} min^{-1} (~25%/hour), the average for experiments with PM wall loss rates in the normal range.
WallCond	Rate of condensation of gas-phase species onto the walls. This is a highly uncertain parameter that may affect the modeling results, but is assumed to be negligible in most of the model calculations except for sensitivity calculations where the effect of varying this parameter is assessed. It is expected to vary from compound to compound but is assumed to be the same for all condensable species for the purpose of the sensitivity calculations.
PMradius	Particle radius in nm, which is used to calculate rate of condensation of condensable species. This is estimated by an empirical relationship between the particle radius and volume measurements, corrected for wall losses, derived from the SMPS data as discussed in the text.
DiffParm	A parameter used to estimate the gas-phase diffusion coefficient given the molecular weight of the model species, where the diffusion coefficient is one of the inputs used to calculate the rate of absorption of condensable species on the wall. The diffusion coefficients tabulated for various condensable aromatic oxidation product model species by Stroud et al (2004) are reasonably well approximated by Diffusion Coefficient = DiffParm / sqrt(molecular weight) with DiffParm = 0.9 when diffusion coefficients are in units of cm^2/sec and molecular weights are in units of grams/mole. This default value of 0.9 was used for all model calculations in this work.
ACCOM	Accommodation coefficient used to calculate rate of absorption of condensable species on particles or the walls. Default value of 0.2 used for all calculations, based on the discussion by Stroud et al (2004). Unitless.
NCrateI	The value of the nucleation rate constants (e.g., NC_CND1) for non-volatile species, i.e., with species where Kp=∞. The default value is 10^3 ppm^{-1} min^{-1}, which is about 1% of the gas-kinetic limit of around 10^5 ppm^{-1} min^{-1}. This value gives the best simulations of the background PM formation in the pure air runs, assuming that the SOP precursors formed from reactions of contaminants off the wall are non-volatile.
MaxNucM	A parameter used to determine nucleation rate constants for semi-volatile species, given their equilibrium partitioning coefficient (e.g., KpCND1) and the NCrateI parameter. The method used to calculate nucleation rate constants is discussed below in this table. For species with low or moderate Kp values, the nucleation rate constant is approximately proportional to Kp/MaxNucM, so a higher MaxNucM value means lower nucleation rate constants for semi-volatile compounds. The appropriate value for this parameter is uncertain, but a default of 10 μg/m^3 is assigned because it gave acceptable results of test calculations discussed in the subsection on nucleation.

Table 2 (continued)

Name [a]	Description
	Calculated Parameters (calculated from other parameter values) (One set for each condensable species)
fCND1	Conversion factor used to convert CND1 concentrations in ppm units to PMmass units in $\mu g/m^3$. Used to calculate change in PMmass resulting from absorption or evaporation of CND1. Calculated from $fCND1 = 1.2186 \times 10^4 \times MwCND1 / T$ where 1.2186×10^4 is a conversion factor for the units used, MwCND1 is the molecular weight of CND1 in units of gm/mole, and T is the temperature in units of degree K.
kOnCND1	Rate constant for the conversion of gas-phase CND1 to PM-phase pmCND1, which is represented as a reaction between CND1 and PMmass. Calculated from $kOnCND1 = (k[dif] \times k[kin]) / (k[dif] + k[kin])$ where k[kin] is the free molecular kinetic limit and k[dif] is the continuum diffusion limit. As discussed by Stroud et al (2004), $k[kin]=3\alpha_i c_i/(4\rho r)$ and $k[dif]=3D/(\rho r^2)$, where α_i is the accommodation coefficient for species i, (given by the parameter ACCOM in this case), c_i is the mean gas-phase molecular speed of species i (given by sqrt{8RT/πM}, where R is the gas constant, T is the temperature and M is the molecular weight, or MwCND1 in this case), ρ is the density (PMden), r is the particle radius (PMradius), and D is the diffusion coefficient (given by DiffParm / sqrt{MwCND1} in this case). In terms of the parameter names given above, these are calculated from $k[kin] = 7.18 \times 10^{-4} \times ACCOM \times sqrt(T) / \{PMden \times PMradius \times sqrt(mwCND1)\}$ $k[dif] = 1.8 \times 10^4 \times DiffParm / (PMden \times PMradius \times PMradius \times sqrt(mwCND1)\}$ where 7.18×10^{-4} and 1.8×10^4 are conversion factors incorporating the gas constant R and units of ppm for CND1 and $\mu g/m^3$ for PMmass.
NC_CND11 NC_CND12	Rate constant used to approximate the nucleation rate for the bimolecular reaction of the condensable species CND1 with itself (NC_CND11) or with another condensable species, CND2 (NC_CND12). Given as a bimolecular rate constant (units of ppm^{-1} min^{-1}). Depends on the parameters NCrateI and the equilibrium partitioning coefficients, KpCND1 and (for NC_CND12) KpCND2. Calculated from $NC\_CND11 = NCrateI \cdot NF\_CND1^2$ $NC\_CND12 = NCrateI \cdot NF\_CND1 \cdot NF\_CND2$ where $NF\_CND1 = 1 / (1 + [MaxNucM / KpCND1])$ $NF\_CND2 = 1 / (1 + [MaxNucM / KpCND2])$ Note that these are zero and NCrateI at the limits of low and high Kp values, respectively.

[a] The names "CND1" and "CND2" are used to designate the condensable species, of which there are several in the model. There is such a set of parameters or species for each condensable species or each pair of species (in the case of NC_CND12).

in the base mechanism (e.g., Carter, 2000a, 2010a) would be needed for mechanisms with large numbers of condensable model species.

Using constant values of the bimolecular nucleation rate constant for all nucleation reactions does not give satisfactory results in our model simulations, and it is not reasonable to assume it is independent of volatility. Using a value that is too low results in the model significantly underpredicting the onset time for particle formation in background characterization and other low PM experiments, and using a value that is high enough to eliminate this problem results in these bimolecular nucleation reactions being fast enough to perturb the gas-particle equilibrium even at high PM levels. To address this, we assume that the bimolecular nucleation rate constant is approximately proportional to the equilibrium partitioning coefficients, Kp, for low Kp values, and approaches a constant maximum value for non-volatile compounds. This is reasonable since highly volatile compounds, i.e., compounds with Kp near zero, should not nucleate, while completely non-volatile compounds ($Kp \rightarrow \infty$) should nucleate the fastest, though not at an infinite rate. We also assume that the nucleation rate depends on the volatility of both reactants in the bimolecular nucleation process.

Based on these considerations, the rate constants for the bimolecular nucleation reactions involving condensable species CND1 and CND2 (e.g., Reactions 7 and 8, above) are calculated using

$$NCrate = NCrateI / (1 + [MaxNucM / KpCND1])^2 \qquad (I)$$

for nucleation involving the same species (Reaction 7) and

$$NCrate = NCrateI / (1 + [MaxNucM / KpCND1]) \cdot (1 + [MaxNucM / KpCND2]) \qquad (II)$$

for nucleation involving different species (Reaction 8). Note that

$$NCrate = 0 \qquad \text{if one of the Kp's} = 0$$
$$NCrate \rightarrow NCrateI \qquad \text{if both of the Kp's} \rightarrow \infty \text{ (non-volatile).}$$

Here, NCrateI is the nucleation rate assumed for non-volatiles and MaxNucM is the Kp where NCrate is half that of non-volatiles (with higher values resulting in lower nucleation rates for semi-volatile compounds). This representation is arbitrary, but at least it has appropriate limiting behavior for low and high Kp values. The choices used for NCrateI and MaxNucM are given in Table 2, and are discussed below in the subsection on nucleation.

A series of test calculations with a simplified aerosol model was carried out in order to assess model sensitivity to the uncertain input parameters and to determine reasonable default values to use for this work. The model consisted of only the reactions given above for CND1, pmCND1, and PMmass, plus a reaction providing input for CND1 at a constant rate. Some of the calculations also had formation of a non-volatile condensable species at variable rates. PM formation from non-volatile species are represented in the same way as discussed above for semi-volatile model species, except that the rate constant for evaporation (Reaction 2) is set at zero, and the nucleation rate constants have the maximum values[1]. The input rate for CND1 was varied to yield specified maximum PM levels that would occur at the end of the 6-hour simulated experiment if all the CND1 were converted to PM (i.e., pmCND1 and PMmass). The levels used in these calculations corresponded to either ~2.3 μg/m3 to represent mechanism evaluation experiments with relatively low PM levels, or to ~23 μg/m3 to represent experiments with average PM levels used in this mechanism evaluation study. Model simulations of

[1] Note that formation of a non-volatile model species does not mean instantaneous formation of PM, since condensation (Reaction 1) is not instantaneous and its rate is assumed not to depend on the volatility. Under conditions of very low PM formation the calculation may give a significant ratio of non-volatiles in the gas relative to the PM phase.

experiments with higher PM levels tended to be less sensitive to these input parameters and are not shown. For simplicity the wall loss rate (PMwall) was set to zero. The molecular weight for CND1 was set at 157.2, which is the value used for CNDp2p (the condensable species formed from the reactions of the lumped catechol model species) in our aromatics SOA model. The input values of KpCND1 (called Kp in the discussion below), PMradius, and NCrate were also varied in the calculations. These values were held constant in the calculations. The results of these calculations are discussed in the following subsections.

Calculation of Rates of Condensation on Particles

The method used to calculate the condensation rates, (e.g., kOnCND1) shown on Table 2 is based on the kinetic modeling approach developed by Kamens et al (1999) as discussed by Stroud et al (2004). The condensation rates depend on the size of the PM particles, being approximately proportional to the reciprocal of the particle diameter for particles less than about 100 nm. Unfortunately, we do not have a means to calculate the evolution of the particle size with the model used in this work, so the particle diameter has to be specified. Stroud et al (2004) used the particle sizes measured during the course of the irradiations as inputs to the calculations for this purpose, but this is not practical given the large number of experiments modeled in this study. It is also inappropriate to use measured particle data as input when evaluating mechanisms for particle formation. Therefore, we had to use a more approximate approach of specifying a default PM radius when simulating the experiments.

Figure 3 shows plots of the fractions of condensable material in the particle phase as a function of PM radius values calculated for Kp values and two maximum PM levels. (In the context of this section, "maximum PM" means the PM levels that would occur at the end of the experiment if all the condensable material appeared in the particle phase, and "fraction in the PM phase" means the ratio of the calculated PM to this maximum PM".) The left plot shows the final fraction as a function of PM radius, and the right plot shows the fractions as a function of time for a radius of 50 nm. For very small particles the condensation rate is sufficiently fast that it does not affect the amount of PM formation, and the fraction in the particle phase is determined by the equilibrium, i.e., Kp x Max PM. However, when the particle radii are greater than about 10 nm, the condensation rate becomes sufficiently low that the amounts of condensable material in the particle phase are affected by the condensation rate and therefore the PM radius, and are less than the equilibrium values. As discussed below (see Figure 4, below) a radius range of 15-20 nm is representative of the initial stages of the experiments, so the results could be affected by the condensation rates at least to some extent. This will result in an uncertainty in the model calculations, though this is less important for experiments with higher PM levels and for models where most of the condensable material has higher partitioning coefficients. Note that for particles having their radius of > 20 nm, the Kelvin effect should be negligible (Bowman et al, 1997) and was not considered in this work.

The average particle radius at a given time in a given experiment can be calculated from 3 x the ratio of the calculated PM volume to the calculated PM area for each time of the experiment, using the measured particle size distribution data. The factor of 3 comes from the relationships between radius and volume and surface areas, assuming the particle is a sphere. Using the surface area and volume to derive the average radius is appropriate since it is the surface area that is the most important factor determining the rate of condensation on the particles for the size range in these experiments, but the rate of condensation (Reaction 1, above) is calculated using the PM mass (related to the volume) times a rate constant that is approximately inversely proportional to the radius.

It is reasonable to expect that the radius of the particles would increase as more PM is formed and that it might be correlated with the PM volume corrected for wall losses. However, the radius will also increase with the irradiation times, since existing particles tend to grow with time. Guidance on which

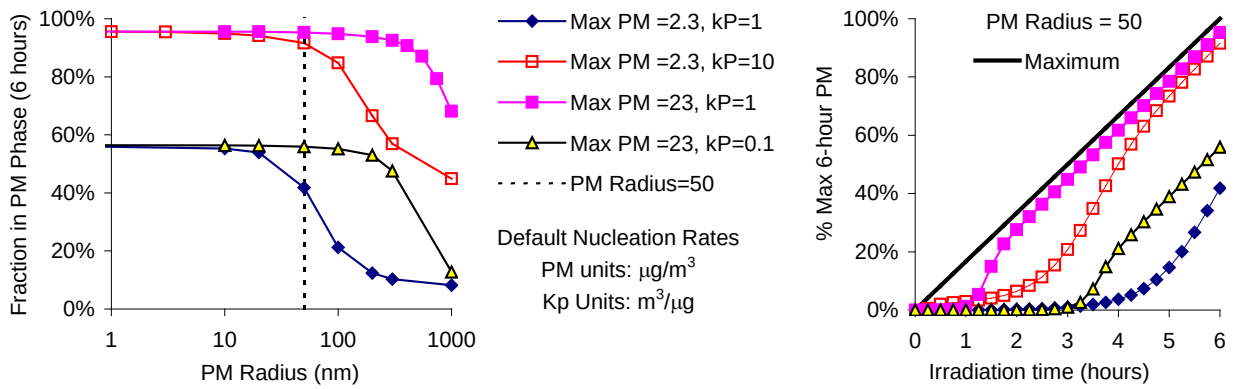

Figure 3. Plots of fraction of condensable material in the PM phase as for various levels of maximum possible PM formation (max PM), partitioning coefficients (Kp) and PM radius values.

factors might be most useful to derive estimates of particle radius values was obtained by examining correlations between hourly particle radius values for the SOA mechanism evaluation experiments with quantities that can be calculated in the model simulations. The best correlation coefficients found for the hourly radius values were as follows

vs. hour of irradiation:	51%
vs. PM volume uncorrected for wall loss:	54%;
vs. PM volume corrected for wall loss:	61%
vs. (PM volume corrected for wall loss)$^{1/3}$:	79%

Based on this, the cube root of the volume corrected for wall loss appears to be the most useful method to estimate PM radius values for the purposes of the model simulations of the chamber experiments

Figure 4 shows plots of hourly particle radius values against the cube root of the PM volume corrected for wall loss for all the SOA mechanism evaluation experiments. The plots show data for all the experiments and various types of experiments as indicated. The lines show fits to all the data, with the same lines being given on each of the plots. The data are fit by the empirical relationship

$$\text{PM radius (nm)} = 13.81 + [20.51 \cdot (\text{PMVolCorr in } \mu m^3/cm^3)^{1/3}] \qquad \text{(III)}$$

where PMVolCorr is the PM volume corrected for wall loss as discussed in Table 2. This is obtained by minimizing the sum of (measured hourly radius - radius derived from volume data) / average (measured radius, radius derived from volume data) for all the hourly data for all the mechanism evaluation experiments where the PM number exceeds 1000 and where wall loss corrections could be derived. The figure also shows subjectively drawn "low limit" and "high limit" curves that are used for predicting lower and upper limit particle radius values for sensitivity calculations discussed later in this report.

Note that the approach we use for estimating PM radius values assumes a minimum particle radius of ~14 nm. Strictly speaking the minimum particle radius should be on the order of the size of a few molecules, each of which are expected to be on the order of 1-2 nm for aromatic oxidation products (Finlayson-Pitts and Pitts, 1999). However, for such small clusters the assumptions used in the condensation approach employed are not applicable, and in any case the methods used to treat nucleation, discussed below, are much more important in affecting predictions of PM growth at such an early stage in

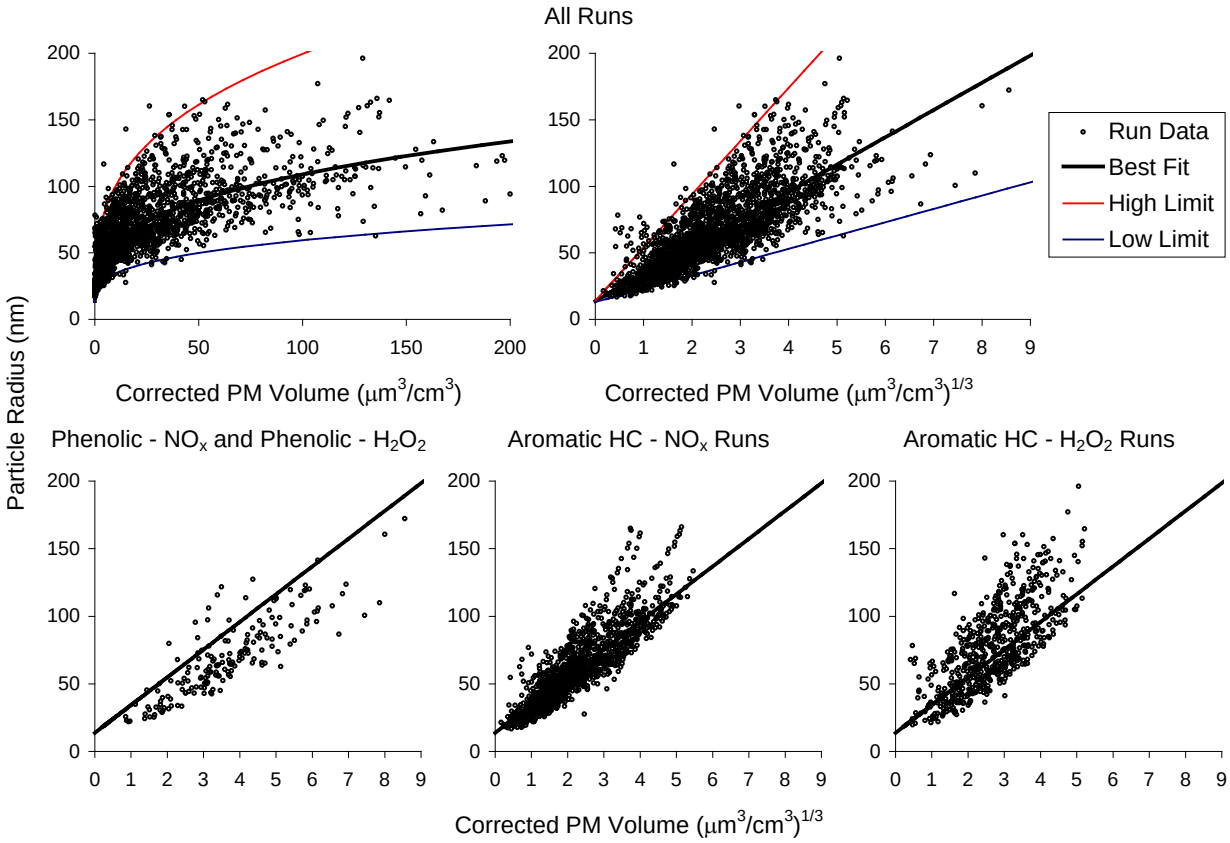

Figure 4. Plots of hourly PM radius values calculated from total PM number and volume data against the PM volume corrected for wall loss for all the experiments used for SOA mechanism evaluation..

the process. Therefore, the use of ~14 nm as the minimum particle radius is considered to be reasonable for predictions of absorption onto existing particles.

Figure 4 shows that the corrected PM volume is not a perfect predictor of particle radius, and that the method derived by fits to all the data may overpredict the radius values for the runs with the phenolic compounds. On the other hand, there does not seem to be a significant difference between the dependence of the radius values on corrected volume for the aromatic - NO_x and aromatic - H_2O_2 experiments. Although using different parameters to estimate the radius values for the experiments with phenolic compounds may be appropriate, for this work the radius assignments given by Equation (III) were used when modeling all the experiments. The test calculations indicate that the PM radius is primarily important in model simulations of low PM experiments, and almost all of the experiments with phenolic reactants had high measured and modeled PM levels.

Nucleation

Another uncertain aspect of the model and the model input is the treatment of nucleation. It is necessary to have some process to form PM when none is initially present because the major PM formation process is assumed to be condensation on existing aerosol (e.g., Reaction 1, above), and all the experiments used in this work for mechanism evaluation had no aerosol initially present. It is reasonable to assume that nucleation starts when condensable gas-phase species react with each other, so the

bimolecular reaction used in our model (e.g., Reactions 7 and 8 above) is not inappropriate. It is also reasonable to assume that the nucleation rate depends on the volatility of the material, and since the nucleation is assumed to be a bimolecular reaction we assume it is inversely related to volatility of both species, as shown in Equations (I and II). These equations have two parameters that need to be specified in addition to the equilibrium partitioning coefficients, the maximum nucleation rate for non-volatile materials (NCrateI), and the MaxNucM parameter that determines nucleation rates for semi-volatiles. The most appropriate parameters to use for these parameters are highly uncertain, and the defaults chosen for modeling are somewhat arbitrary. We assume that the nucleation rate for completely non-volatile materials is 1 x 10^3 ppm^{-1} min^{-1} (6.8 x 10^{-13} cm^3 $molec^{-1}$ s^{-1}), based on the somewhat arbitrary but not unreasonable assumption that it is approximately 1% of the gas collision rate. This value also gives the best simulations of PM formation in the pure air experiments under the assumptions that the background SOA precursor is non-volatile (see the "Characterization Results" section, below). The value of the MaxNucM parameter is chosen so that nucleation rates are sufficiently high that the calculated PM levels for most experiments are not highly sensitive to this parameter, but not so high that the rate of nucleation is high enough to significantly perturb the equilibrium ratio of condensable materials in the gas and particle phase under the conditions of the experiments used for mechanism evaluation. This was assessed in various test calculations that are discussed below.

Figure 5 and Figure 6 show plots of calculated fractions of condensable materials in the particle phase (left side), and of ratios of these fractions to the equilibrium fractions (right side), against the equilibrium partitioning coefficients (Kp) for various nucleation rates or methods for calculating the nucleation rates from the Kp values. Figure 5 shows plots for various nucleation rates independent of the Kp values, and Figure 6 shows plots where the nucleation rates were calculated using Equation (I) with various values of the MaxNucM parameter. Note that the nucleation rates are the same for the curves on the two plots with the same color and symbol when Kp = 1 $m^3/\mu g$, i.e. MaxNucM = 3, 10, 32, and 100 $\mu g/m^3$ give NCrate = 100, 10, 10, and 0.1 ppm^{-1} min^{-1} when Kp=1 $m^3/\mu g$. The two plots look similar when Kp > 1 $m^3/\mu g$, but Equation (I) gives smaller fractions in the particle phase when Kp < 1 $m^3/\mu g$. In both cases higher particle fractions than equilibrium are calculated when Kp < 1 $m^3/\mu g$. Figure 6 shows that using MaxNucM of 10 $\mu g/m^3$ gives the highest nucleation rates that do not calculate PM levels exceeding equilibrium if Kp is above ~0.5 $m^3/\mu g$ for the conditions of this simulation.

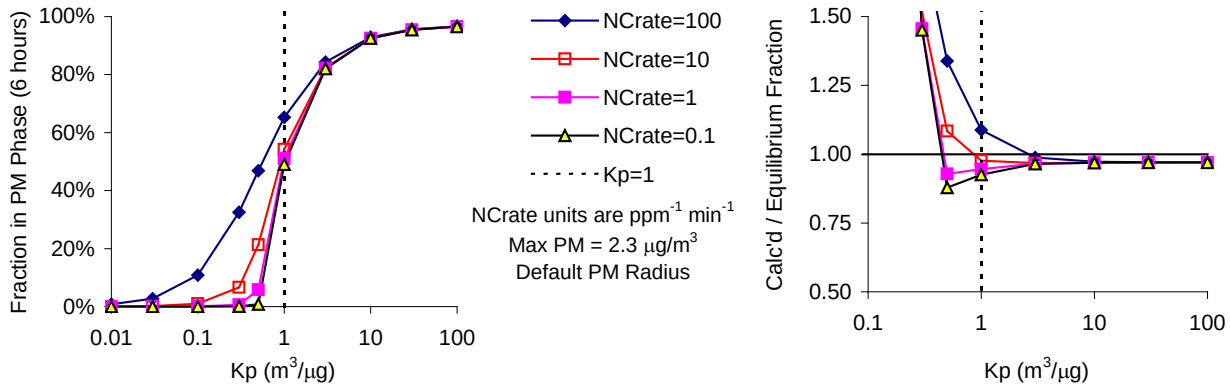

Figure 5. Plots of fractions of condensable material in the PM phase and ratios of calculated to equilibrium fractions of condensable materials in the PM phase against the equilibrium partitioning coefficient (Kp) for various nucleation rates.

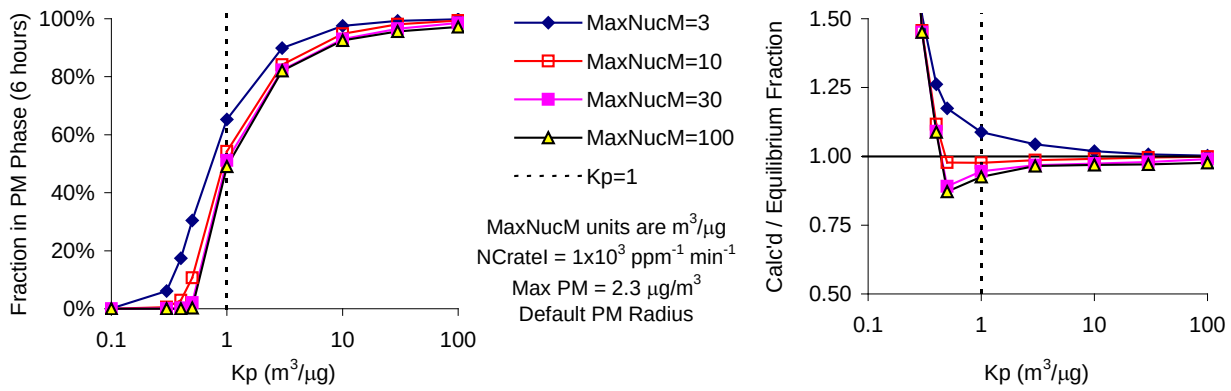

Figure 6. Plots of fractions of condensable material in the PM phase and ratios of calculated to equilibrium fractions of condensable materials in the PM phase against the equilibrium partitioning coefficient (Kp) calculated using Equation (I) for various values of the MaxNucM parameter.

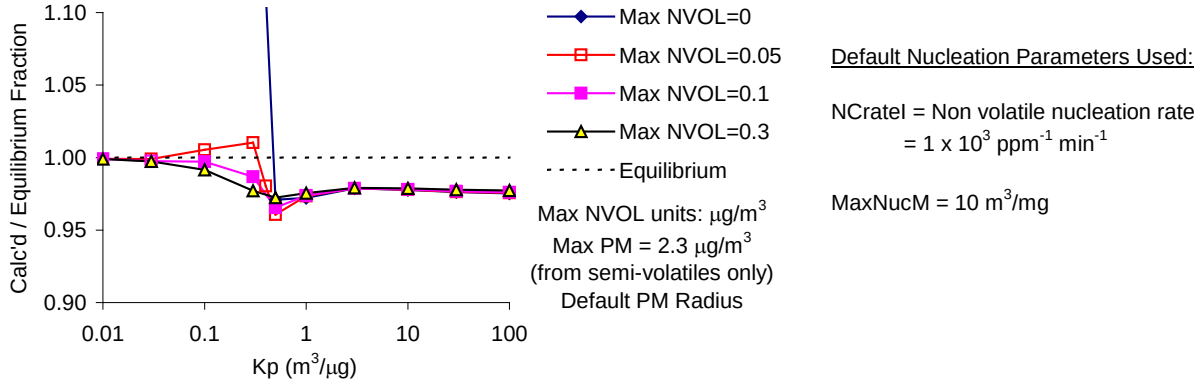

Figure 7. Plots of ratios of calculated to equilibrium fractions of condensable materials in the PM phase as a function of equilibrium partitioning coefficients (Kp) for various levels of non-volatile materials also formed in the simulations, using the default parameters for calculation of nucleation rates.

However, the simulations on Figure 5 and Figure 6 with Kp ≤ 0.5 $m^3/\mu g$ represent conditions where the only condensable materials formed have low Kp values, and these simulations give maximum particle levels no greater than ~0.3 $\mu g/m^3$ when MaxNucM = 10. Most runs used for aromatic SOA mechanism evaluation have much higher PM levels than this. Perhaps a more representative situation would be test calculations where some formation of lower volatility species also occurred. Figure 7 shows plots of ratios of fractions of semi-volatile materials in the PM phase relative to equilibrium fractions against Kp for various levels of added non-volatile materials also being formed. The nucleation rates were calculated using Equation (I) with MaxNucM = 10 $\mu g/m^3$. These results show that when these parameters are used the fractions of semi-volatiles in the PM phase will not be calculated to be significantly above the equilibrium if at least 0.05 $\mu g/m^3$ of non-volatiles are also formed in the simulation. Based on these

considerations, these are the parameters used to calculate the nucleation rates in our simulations, except for sensitivity calculations where the effects of varying these parameters are examined.

Absorption and Desorption of Organics from the Walls

The presence of the chamber walls could affect the amount of PM formed in the experiments if any of the condensable material formed in the reactions of the VOCs being studied are absorbed onto the walls rather than onto the particles that are dispersed within the chamber. As discussed by Matsunaga and Ziemann (2010), this might result in lower SOA yields than might occur under similar circumstances in the atmosphere, especially in experiments with low PM levels and with relatively high volatility products. Based on data they obtained in smaller Teflon® film chambers (5.9 m^3 and 1.7 m^3) made of the same material as used in our chamber, they estimated that the "sorption properties of the chamber walls were equivalent to organic aerosol mass concentrations of .. up to ~4 orders of magnitude larger than concentrations used in most laboratory studies of SOA". This includes the conditions of the experiments used in our study. This means that given a sufficient time to attain full equilibrium, all the condensable material would be on the wall even if there were no particle wall loss. On the other hand, the rate of condensation on the particles is expected to be faster than condensation on the walls (Bowman et al, 1997), so on short time scales condensation to the particles dominates, and the material will stay on the particles if the volatility is sufficiently low. However, in the 2-6 m^3 chamber they employed the estimated time scale for absorption on the walls was on the order of 10-60 minutes (Matsunaga and Ziemann, 2010), so wall absorption may not be slow enough that it can be neglected in our experiments, which typically last on the order of 4-12 hours.

Figure 8 shows a portion of a figure in the paper of Matsunaga and Ziemann (2010) on results of their model calculations on how PM from SOA in the chamber ($[OC]_p$) would be affected after 100 minutes of irradiation, for various PM levels in the chamber (C_p) and gas-particle partitioning coefficients (K_p). This is calculated using a model they developed based on measurements they made in their chamber (1.7 m^3), which is smaller than ours, of absorption data for C_{11}-C_{13} 2-ketones, which are probably more volatile than most of the SOA formed from aromatics. This model predicts that the presence of the walls will significantly affect PM in the chamber if the PM is less than about 30 $\mu g/m^3$, or if K_p is less than about 1 $m^3/\mu g$. Note that the maximum PM levels in the mechanism evaluation experiments in this work ranged from ~1-100 $\mu g/m^3$, and most of the condensable model species in the mechanism developed in this work (see below) are assigned K_p levels below 1 $m^3/\mu g$.

The applicability of these estimates to experiments measuring SOA formation from aromatics in our chamber is uncertain, and needs to be experimentally investigated. First, whether semi-volatile compounds formed from oxidation of aromatics used in this study indeed partition into the Teflon FEP walls in a large amount is not clear. Based on Kamens et al (1995) and Matsunaga and Ziemann (2010), relatively non-polar semi-volatile compounds (e.g., pyrene, fluoranthene; C_{16} 1-alkene, C_{13} 2-alcohol, C_{13} 2-ketone) can partition to Teflon FEP walls in large amounts. To our best knowledge, there is no strong direct evidence of significant wall partitioning of polar semi-volatile compounds similar to expected oxidation products from aromatics under dry conditions, though Loza et al. (2010) observed wall-loss of polar compounds such as glyoxal under humid conditions. Second, Kamens et al (1995) and Matsunaga and Ziemann (2010) provide some experimental evidence showing the impact of the chamber surface-to-volume (S/V) on wall partitioning. The impact of wall partitioning is expected to be smaller in the UCR EPA chamber because its surface/volume ratio is smaller at least by a factor of 2 than that of the 1.7 m^3 chamber used by Matsunaga and Ziemann (2010). Third, the estimated time constants for gas-wall partitioning were calculated by using an effective organic mass concentration of the walls for the 1.7 m^3 chamber and a particle radius of 100 nm. Therefore, time constants for gas-wall partitioning of semi-volatiles in the EPA chamber are expected to be longer than those estimated by Matsunaga and Ziemann (2010).

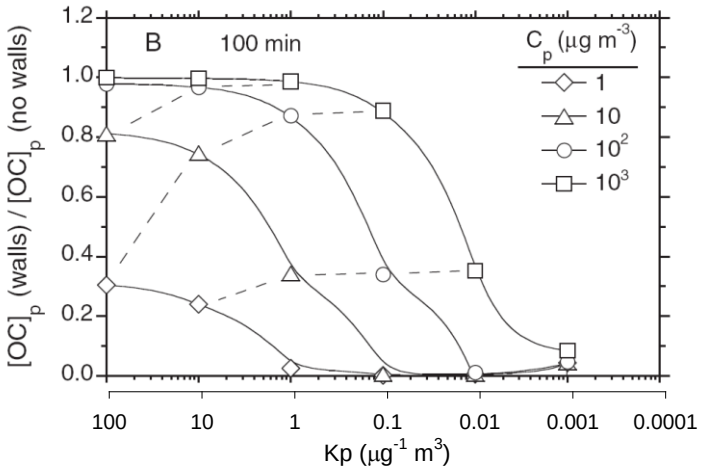

Figure 8. Plots of fractions of ratios of condensed organic materials in the particle phase in the presence of walls, relative to the absence of walls after 100 minutes of irradiation for various PM levels (C_p) and partitioning coefficients, calculated by Matsunaga and Ziemann (2010) for the conditions of their Teflon® chamber and the observed partitioning behavior for high molecular weight 2-ketones. Taken from Figure 8 of Matsunaga and Ziemann (2010).

Kroll et al (2007) proposed that chamber experiments carried out without seed particles systematically underpredicted SOA yields of aromatic hydrocarbons due to loss of semi-volatile products onto chamber walls during an "induction period", a period of time during which the parent hydrocarbon reacts away but no aerosol is formed. However, in our previous study, Warren et al. (2008b), there was no significant difference between SOA formation from m-xylene with and without seed particles, which could be due to smaller surface/volume ratio of UCR EPA chamber than that of the Caltech chamber (28 m^3) used by Kroll et al (2007). Although the absence of apparent seed effect suggests that semi-volatile loss is minor in our experimental conditions, this deserves further investigation.

For the time being, because of the significant uncertainties and lack of available data, we assume that this is not significant for the conditions of our experiments and do not include this in our chamber wall model. However, the modeling results discussed below includes results of sensitivity calculations showing the wall absorption rates (values of the WallCond parameter in Reaction (5), above) necessary for this to affect the data, and how the modeling of the chamber data are affected. As discussed later in this report, assuming wall absorption occurs at 25% per hour, the average rate of particle wall loss in our chambers, has a significant effect on the mechanism evaluation results, and calculations with this assumption tend to predict that PM volume is lost to the wall faster than PM number, which is not consistent with the experimental results. However, the wall absorption rates may be less than this and still affect the results of the experiments. This represents an uncertainty in this work and represents an area where additional chamber effects characterization work is needed.

A related issue is desorption of organics from chamber walls, i.e., the rate of Reaction (6), above. The issues of desorption of background or contaminant organics are discussed in the Characterization Results section below, but briefly the characterization data indicate that desorbing of condensable contaminants is not an issue, though desorbing of contaminants that react with OH radicals to form condensables is an issue. Semi-volatile organics formed in the experiments could also be absorbed in the walls and subsequently desorb and condense in the particle phase. We assume that this is not likely to be

an important factor when modeling our data based on the estimate of Matsunaga and Ziemann (2010) that the equivalent organic mass levels on the walls are orders of magnitude higher than that in the particle phase. If this is the case, then any particles with sufficiently low volatility to condense in the particle phase would have a much greater affinity for the walls than the particle phase, and once on the walls would likely remain there for the time scale of our experiments. Therefore, the rate of Reaction (6) above is assumed to be negligible for all model species in the mechanism representing condensable gas-phase compounds.

EXPERIMENTAL AND CHARACTERIZATION RESULTS

Summary of Experiments

Experiments Carried Out for this Project

A total of 158 dual reactor environmental chamber irradiations were carried out for this project, resulting in a total of 316 separate reactor irradiations that could potentially be used for mechanism evaluation. These are listed on Table A-1 in Appendix A, along with a brief indication of the type of mixture irradiated and a code indicating how it was used if used for modeling, or why it was not used if not. Each of these separate reactor irradiations, referred to as "runs" in the remainder of this report are designated as "EPAnnnnA" or EPAnnnnB", where "nnnn" is the run number and "A" or "B" indicates the reactor used, where "A" is always used for the west reactor and "B" is used for the east reactor. Of these 316 irradiations or runs, 40 (13%) were analyzed or modeled for chamber characterization purposes, 217 (69%) were judged to be useful for SOA mechanism evaluation, and 59 (23%) were judged not to be useful because of experimental or data problems, lack of relevance or out of the scope of this project, calculated high sensitivity to chamber background effects, or questionable modeling results based on apparent inconsistencies with results of modeling similar experiments. (The latter two categories consisted of respectively 8 and 7 experiments, or 5% of the total.) The codes in Table A-1 indicate why these runs were not used for modeling.

The data from these 40 characterization and 217 SOA mechanism evaluation experiments were added to the dataset of previous EPA chamber experiments whose results are judged to be useful for chamber characterization and mechanism evaluation for this project. These consist of 20% of the total number of characterization experiments used to derive the chamber model for this report and 67% of the mechanism evaluation experiments. The smaller fraction of characterization experiments reflects the fact that the characterization data reflect much of the time when the UCR EPA chamber was used, which was for many projects and purposes over the years. The larger fraction of mechanism evaluation experiments reflects the fact that this project focused on obtaining data useful for the purpose of this report, and while there were 98 previous experiments that were judged to be useful, they reflected only 1/3 of the total.

The results of all the characterization experiments are discussed together in the following section, followed by a section summarizing the results of all the mechanism evaluation experiments. The results of the model simulations of the mechanism evaluation experiments are discussed later in this report after the mechanism that was evaluated is described.

Characterization Methods and Results

The characterization results discussed in this section will include not only those applicable to the mechanism evaluation experiments carried out for this project, but also to the previous UCR-EPA chamber experiments whose data were used for mechanism evaluation in this report. Additional details concerning the previous characterization experiments are available in previous reports from this laboratory (e.g., Carter, 2004, 2008, 2010a, 2011; Carter et al, 2005a,c and references therein), and much of this detail is applicable to the newer experiments whose results are discussed below. The use of these results to assign characterization inputs for modeling is also discussed, with additional information given in the "Modeling Methods" section below.

The individual characterization experiments whose data are discussed in the sections below are listed in Table A-2 in Appendix A. These include experiments used to derive chamber background effects related to the chamber radical source, NO_x offgasing, and background PM formation, as discussed below. They do not include NO_2 actinometry experiments whose results are discussed in the following section. These data are available upon request.

Blacklight Characterization

All of the experiments carried out for this project used the blacklight light source, and although most were carried out using the upgraded light source with additional blacklights as described by Carter (2011), some were carried out with the original blacklights with lower light intensity, as were most of the previous UCR EPA chamber experiments used in this evaluation.

Methods for characterizing the intensity of the original blacklight light source were discussed by Carter et al (2005b), though some revisions were made as a result of subsequent measurements. As discussed by Carter et al (2005c), for the original blacklights the results of these and other measures of light intensity indicated a steady decline in light intensity with time, with the results being best correlated with the "blacklight run count", which is the number of experiments carried out in the chamber using the blacklights, and is thus an indicator of the ageing of the lights due to use. However, after around early 2006, or around the time of run EPA500 or a blacklight run count of around 200, the light intensity appeared to level off at a NO_2 photolysis rate of around 0.13 min^{-1}. This is shown on Figure 9a, which gives plots of NO_2 photolysis rates measured or estimated for the reactors against the blacklight run count. The "reactor" values give the results of the in-reactor actinometry measurements, and the "enclosure (adjusted)" values show the results of the measurements made in front of the reactor, adjusted by a factor of 0.698, which is the ratio of reactor to enclosure actinometry measurements made previously (Carter et al, 2005c).

The results of the NO_2 actinometry measurements made after the blacklights were upgraded for this project are shown on Figure 9b. The "enclosure (adjusted)" points shown on Figure 9b are results of

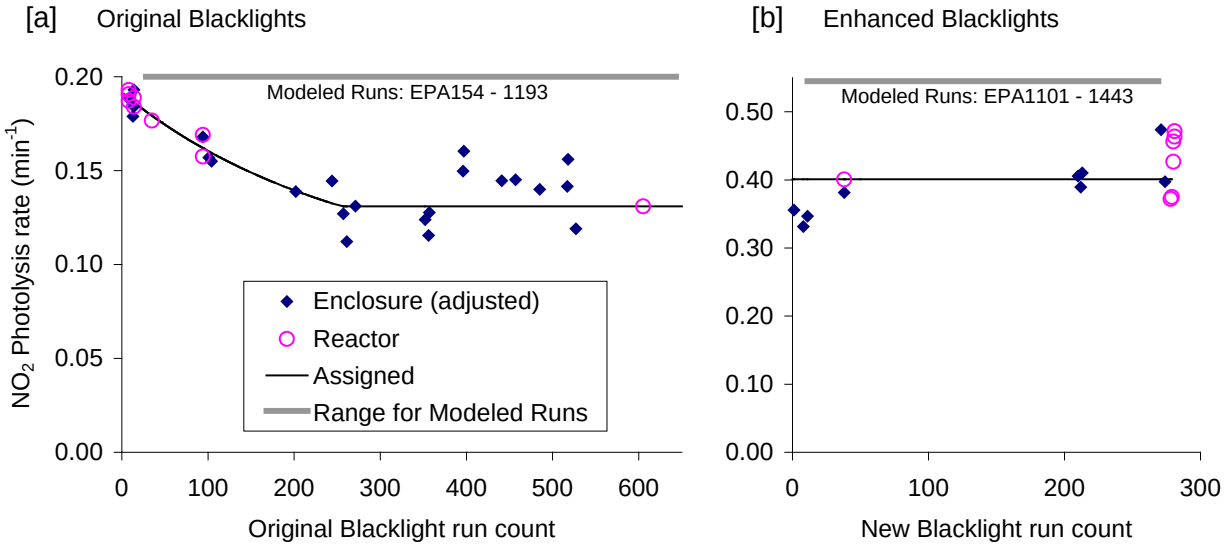

Figure 9. Plots of light intensity data used to assign NO_2 photolysis rates for the blacklight light source.

measurements made in front of the reactors, multiplied by the correction factor 0.698, derived from the data for the original blacklights discussed above. The enclosure actinometry results indicate no significant change of light intensity with time when the upgraded lights were employed, in contrast with the results with the original lights when they were new.

The lines on Figure 9 show the NO_2 photolysis rates that were assigned to the runs for modeling purposes. For the enhanced blacklights, a constant NO_2 photolysis rate of 0.401 min^{-1} is used, based on the initial in-chamber actinometry measurements. As discussed by Carter (2011), for the old lights up to blacklight run count of around 400, the results are reasonably well fit by the empirical expression k_1 (min^{-1}) = max {0.131, 0.0958 x [1 + exp(-Blacklight Run Count x 0.003914)]}.

The spectrum of the blacklights in this chamber has been measured periodically and is assumed to continue to be the same as the spectrum recommended by Carter et al (1995) for modeling blacklight chamber runs. There is no reason to expect the spectrum to change with the light upgrade made during this project, since the same type of lights is employed as the original lights.

Arc Light Characterization

No arc light experiments were carried out for this project because the arc light system is no longer functioning and requires major repairs, but a number of arc light experiments that were carried out previously were used for the mechanism evaluation in this work. As discussed by Carter (2004) and updated by Carter and Malkina (2007), the results of the actinometry experiments with this light source indicate that an NO_2 photolysis rate of 0.260 min^{-1} is appropriate for modeling all arc light experiments using the normal power setting, as is the case for all arc light runs modeled for this project. The spectrum of the light source was measured periodically using our LI-1800 spectroradiometer, and the results indicated that the spectrum did not change significantly with time. Therefore, the spectrum given by Carter (2004) is also assumed to be applicable for all arc light experiments modeled for this project (see also Carter and Malkina, 2007).

Chamber Effects Characterization for Gas Phase Mechanism Evaluation

Except as discussed below, the characterization results relevant to gas-phase mechanism evaluation for the more recent experiments for this project are consistent with those discussed by Carter et al (2005c) and Carter and Malkina (2005, 2007), and the same characterization parameters were used for modeling. The most important chamber effect, and the only chamber effect parameter that appears to vary with time, concerns the apparent HONO offgasing, which is believed to be responsible for both the chamber radical source and NO_x offgasing effects (Carter, 2004, Carter et al. 2005c). This is represented in the chamber effects model by the parameter RN-I, which is the HONO offgasing rate used in the simulations divided by the light intensity as measured by the NO_2 photolysis rate. Figure 10 shows the HONO offgasing parameters that best fit the radical or NO_x - sensitive characterization experiments during the period relevant to the experiments modeled for this project, which covers most of the period when the UCR EPA chamber was operational. The run numbers for the experiments used for mechanism evaluation in this report, and the range of run numbers for the experiments carried out for this project, are also indicated on the figure.

Figure 10 shows that the HONO offgasing parameter tends to vary significantly from run to run, and also varies with the reactor employed. Occasionally the data suggested different HONO offgasing rates in the "A" and "B" reactors, and this was the case during the first sets of reactors employed for the experiments carried out for this project. However, the parameter values derived from radical-sensitive experiments such as CO - NO_x irradiations tend to be in the same range of those derived from NO_x-

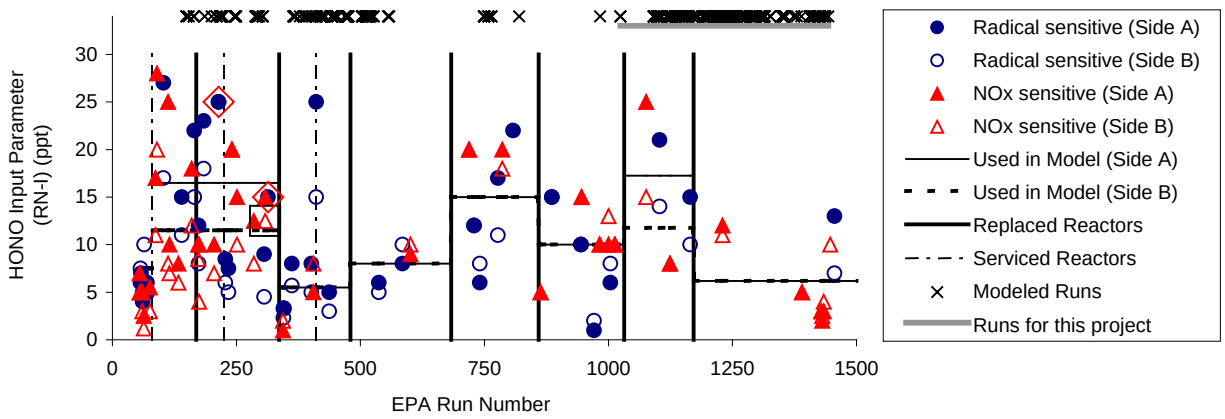

Figure 10. Plots of best fit HONO offgasing parameters against UCR EPA run number.

sensitive experiments such as CO - air or H_2O_2 - air irradiations, supporting our assumption that both radical and NO_x input comes from the same process, namely the photolysis of HONO. The results obtained during the period of this project are consistent with those derived previously (e.g., Carter, 2004; Carter et al, 2005c; Carter and Malkina, 2005, 2007) and need not be discussed further here.

The lines on Figure 10 show the HONO input rates that were incorporated in the wall model when modeling the experiments for this project. These were derived by averaging the parameters derived from the experiments in the various reactors. The variability of the results indicate the uncertainty of the RN-I parameter when modeling the runs, which is generally about a factor of two. However, sensitivity calculations do not indicate that the variability or uncertainty in this parameter is a significant factor affecting the results of modeling SOA in these experiments. This is discussed further below in the "Modeling Methods" section.

Particle Wall Loss Characterization and Corrections

Additional characterization information is needed when modeling particle formation in environmental chamber experiments, and this is discussed in this and the following subsections. Probably the most important chamber effect regarding particle formation in chamber experiments is loss of particles to the chamber walls. Evidence that this is occurring at non-negligible rates comes from the particle number data obtained from the SMPS measurements, which indicates that the particle numbers peak prior to the time of maximum particle volume (i.e., mass) formation, and then decline at approximately first-order decay rates. This is observed in essentially all chamber studies where PM formation is measured (McMurry and Grosjean, 1985; Pierce et al, 2008), and is observed in our chamber as well (Carter et al, 2005c).

Examples of particle data from the SMPS for four representative experiments carried out for this project are shown on Figure 11. The top two plots are representative of the majority of the experiments where the wall loss characterization and correction approach, discussed below, fit the data reasonably well, with the left hand plot being an experiment with very low SOA formation and the other being an experiment with very large amounts of PM volume formed. The bottom two plots are examples of runs with phenolic compounds where the correction approach did not fit the data quite as well, but use of the approach is still considered to be sufficient for the purpose of this project.

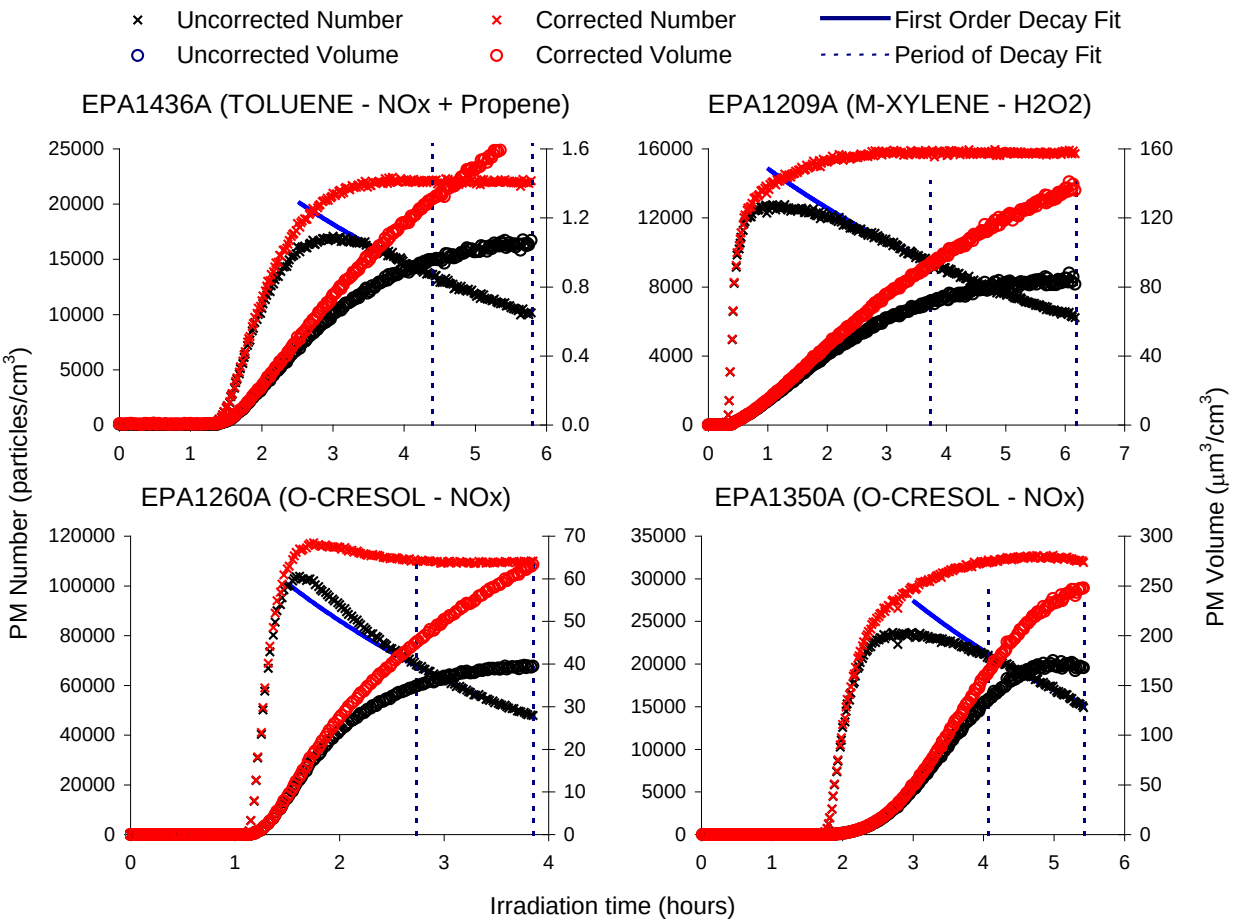

Figure 11. Examples of particle wall loss rate calculation and correction for four representative chamber experiments.

The wall loss rate is calculated by fitting the particle number data for the period of the experiment following the maximum particle number to a first order decay curve. The fit curves and the time periods for the fits to the data are shown for the representative experiments on Figure 11. The time period for the fits was set at halfway between the time of the maximum particle number and the time of the end of the experiment, and went through to the end of the experiment. For most experiments the particle numbers during this period fit a first order decay curve reasonably well, though in a few cases the time period was adjusted by manually inputting the start time to assure that the appropriate period was used. If this time period was less than 30 minutes, if the particle number was still increasing when the experiment was terminated, or if the number of particles formed in the experiment was too low for quantitative analysis (a lower threshold of 1000 particles/cm^3 was used in our analysis), then the wall loss rate could not be calculated and in most cases the particle data were not used for model evaluation except for background PM characterization runs, where a default wall loss rate was used.

Figure 12 shows the wall loss rates plotted against run number and Figure 13 shows these plotted against the amounts of PM formed in the experiments. Figure 12 indicates which of the dual reactors (Side A or B) was used and Figure 13 indicates the general type of experiment. The results indicate that the PM wall loss rates are highly variable from experiment to experiment, ranging from as low as ~10%/hour to as high as ~50%/hour, with no significant dependence on reactor, when the run was

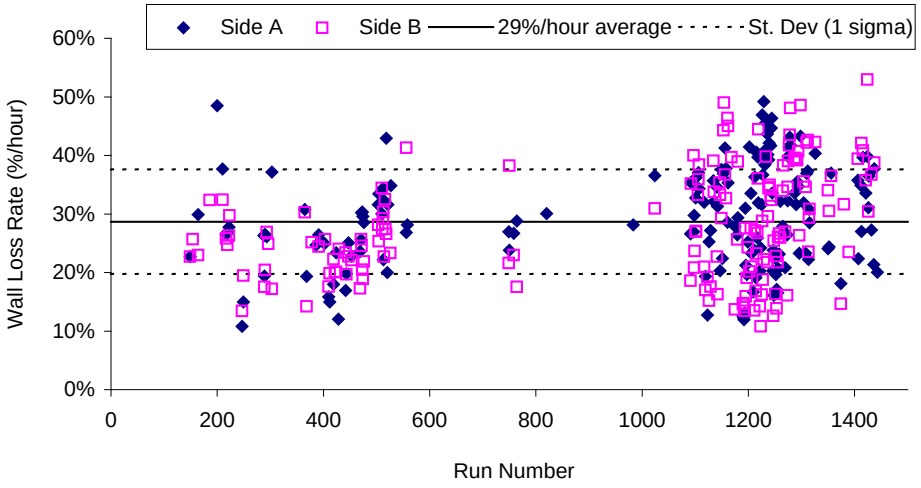

Figure 12. Plots of PM wall loss rates against UCR EPA chamber run number for all experiments used for mechanism evaluation.

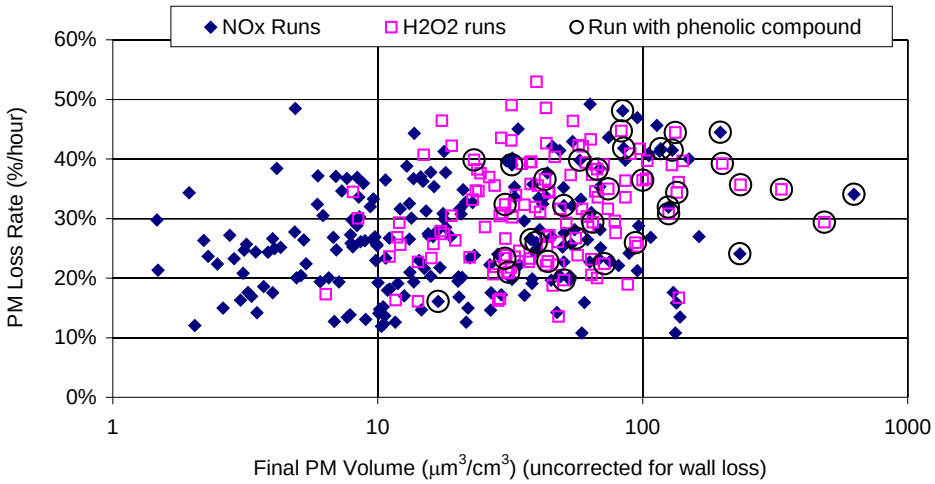

Figure 13. Plots of PM wall loss rates against amount of PM formation for all experiments used for mechanism evaluation.

conducted and type of experiment. There may be a very small dependence on the amount of PM formed, but it is much less than the run to run variability. The average wall loss rate was 29±9%/hour, which is close to 8 x 10^{-4} s^{-1} (29%/hour), the overall wall loss rate for benzoic acid aerosol reported by McMurry and Grosjean (1985) but is lower than 2.0 x 10^{-5} s^{-1} (7%/hour), the wall loss rate used by Stroud et al (2004). This average wall loss rate (29%/hour) was used when modeling those few experiments (mainly background characterization runs) that were modeled despite the lack of useable wall loss data.

The wall loss rates for the individual experiments were used to correct the PM number and volume data for wall loss, to obtain estimates of what they would be if particle wall loss were not occurring. The procedure used was the same for particle volume as for particle number, and was as follows:

$$PMcorr(t0) = PM(t0)$$
$$PMcorr(t2) = PM(t2) + Average(PM(t2),PM(t1)) \cdot \{1-exp(-Wloss \cdot [t2-t1])\} \quad \text{(VII)}$$

where PM(t) is the PM number or volume measurement at time t, t0 is the first time in the experiment, t1 and t2 are two consecutive time with PM data, PMcorr(t) is the PM number or volume measurement corrected for wall loss, and Wloss is the wall loss rate derived from the PM number data in the experiment as discussed above. Note that PMcorr can be either corrected PMmass or PMVOL (PMmassCorr or PMVolCorr on Table 2).

Note that this approach assumes that the wall loss rate is not dependent on the particle sizes, which generally increase throughout the experiments. This is an approximation, because in theory wall loss rates should depend on particle size (McMurry and Grosjean, 1985; Pierce et al, 2008). However, the apparent lack of significant dependence of the wall loss rates on the total volume of particles formed, which in general should affect particle sizes, suggests that this is probably not a large factor compared to the large run-to-run variability. Measured and simulated results of McMurry and Grosjean (1985) and simulated results of Pierce (2008; specifically, results shown for "HYBRID" in Fig.5 of Pierce (2008)) indicate that particle wall loss rates in Teflon chambers with volume larger than 10 m^3 and a reasonable surface to volume ratio for particles of ~50 nm to ~500 nm are not dramatically different but approximately within a factor of two around the wall loss rate for particles of ~ 100 nm. Most particles were in a range narrower than this range of 50 nm to 500 nm for most experiments for this project except during the early stages of the experiments when small-diameter particles dominated. Therefore, size-dependent particle wall loss rates were not used, and a constant particle wall loss rate was used after being estimated as illustrated in Figure 11

The corrected PM number data provides a test of the appropriateness of this approach and the Wloss value derived, since if they are appropriate then the corrected PM number should level off at a constant value during the last stages of the experiment. This was the case for most of the experiments, with the top two plots on Figure 11 being representative. As indicated on the bottom two plots on Figure 11, the particle number data for some of the experiments with the phenolic compounds were not as well fit by this approach, and the wall losses may be occurring at a non-exponential rate or the wall loss rates may be affected by changes in the particle sizes. However, the errors introduced by using this method are probably not large compared to run-to-run variability or other uncertainties.

Background Particle Formation

Another potential chamber effect that must be considered when modeling PM formation in chamber experiments is the possibility of background particle formation. This could come from physical release of particles from the walls, emissions of low volatility compounds from the walls that subsequently form particles, and emissions of volatile compounds from the walls that react in the gas phase to form low volatility products that then condense to form particles. This can be assessed by conducting various types of characterization experiments as discussed below.

Results of characterization experiments concerning background particle formation in the UCR EPA chamber have been discussed previously (Carter et al, 2005a-c), and characterization experiments carried out during the course of this project generally yielded comparable results. Results of relevant characterization experiments are briefly summarized below. Briefly, no measurable particle formation is observed when dry pure air is injected into the reactors and allowed to sit for extended periods of time in the dark. Furthermore, no measurable particle formation is observed in the many CO - air or CO - NO_x irradiation experiments carried out for radical source or NO_x offgasing characterization. However, particle formation is observed in dry pure air irradiations, with the amount of particle formation varying from experiment to experiment. The amounts of particles formed were relatively small, generally less than 1 $\mu g/m^3$, but well within the detection limits of our SMPS.

The observation that no significant particle formation is observed in the dark or in CO - NO_x or CO - air irradiation experiments indicates that particles are not introduced from the pure air system and that emissions of particles or condensable compounds from the walls is probably not significant. The fact that measurable levels of particles are formed in pure air irradiations but not CO - air experiments means that the presence of CO inhibits background particle formation. The presence of CO enhanced O_3 formation, but O_3 is also formed in most pure air runs, so the differences in O_3 levels are probably not the relevant factor causing the differences in particle levels. The more likely factor is the fact that the addition of CO significantly suppresses OH radical levels, as predicted by model calculations and expected by its known rate of reaction with CO. This suggests that the background particle formation in the pure air experiments is due to offgasing of some volatile compound that reacts with OH radicals to form low volatility products that subsequently condense to form the PM observed in the pure air experiments. This is suppressed when CO or other reactants are present to suppress the OH radical levels.

The identities of the PM precursor compounds or their condensable oxidation products leading to background PM formation are unknown. The levels of PM formed in the pure air experiments are generally too low for collection and chemical analysis using the methods currently available in our laboratory, so no information about this is currently available. For lack of more detailed information, the background PM formation in our chamber experiments is modeled as follows:

Walls + hν → PM-Precursor	Rate = WallPMparm · $k^{phot}(NO_2+h\nu)$
PM-Precursor + OH → CNDwall	kOH = 1 x 10^{-11} cm^3 $molec^{-1}$ s^{-1}
CNDwall → → PMwall	(condensation and nucleation)
Kp(CNDwall) = ∞	

Here, "WallPMparm" is the wall offgasing parameter that is adjusted to fit the amounts of PM formed in pure air and other appropriate background PM characterization experiments, "PM-Precursor" is the emitted gas phase compound(s) that react with OH radicals to form condensable products, kOH is the rate constant for this reaction, "CNDwall" is the unknown condensable compounds(s) that are formed in the gas phase in this reaction, "PMwall" represents the compounds when they are in the particle phase and contribute to the total PM mass or volume, and kP(CNDwall) is the partitioning coefficient between the gas-phase (CNDwall) and particle phase (PMwall) form of the condensable material. The method used to represent condensation and nucleation of the background PM materials is the same as used for modeling PM formation from other condensable compounds in the mechanism, as discussed above in the "Modeling PM Formation" section of this report.

Because of the variability of the apparent background PM formation and lack of information needed to derive a multi-parameter model for background PM formation, it is not practical to model this process with more than one adjustable parameter. This means that the rate constant for the reaction of the PM precursor with OH radicals and the partitioning coefficient for condensable material have to be estimated. We assume a moderately high rate constant of 1 x 10^{-11} cm^3 $molec^{-1}$ s^{-1} that is reasonably representative of many higher molecular weight VOCs, and expect that using a different rate constant would affect primarily the WallPMparm values that fit the data, rather the results of the model simulations with the best fit parameters. We also assume that the condensable material is non-volatile, i.e., Kp(CNDwall) is infinite, since there are no data available to derive a partitioning coefficient for this process, and better model simulations of the data are obtained if relatively high nucleation rates are assumed, as discussed below. It is reasonable to expect that the condensable materials are not very volatile because otherwise relatively large amounts of CNDwall would have to build up in the gas phase before significant condensation would occur on the ≤ 1 $\mu g/m^3$ PM levels found in most of the pure air experiments. The molecular weight used for PMwall also affects the results, and we arbitrarily use a molecular weight of 200 g/mole for this model. Using different values would affect the absolute values of the WallPMparm value that fit the data, but not the results when the WallPMparm value is adjusted to fit the data.

It should also be noted that because of the relatively low PM levels formed in most of the pure air experiments, the WallPMparm values that fit the data are also sensitive to the method used to represent nucleation in the experiments. If nucleation is not assumed to be sufficiently rapid in the experiments, the model predicts that most of the CNDwall remains in the gas phase and the rate of nucleation is the rate determining step for PM formation. As discussed above in the "Modeling PM Formation" section, the nucleation rate constant used for non-volatile species such as CNDwall is determined by the NCrateI parameter. The effects of varying this parameter on model simulations of the pure air experiments, with the WallPMparm value adjusted so the model simulates the maximum PM levels, are shown on Figure 14. The left plot shows the model error as a function of irradiation time for the model simulations adjusted to fit the maximum PM levels and the right plots show the fraction of PM that is formed from nucleation as opposed to condensation.

It can be seen from the right plot on Figure 14 that most of the PM formed in experiments with less than about 1 $\mu g/m^3$ comes from nucleation rather than condensation, so the nucleation rate is important in affecting the modeling of these background PM runs. It can be seen from the left plot that using a nucleation rate of 100 ppm^{-1} min^{-1} significantly underpredicts the amount of PM formed in the earlier stages of the experiment, while using a nucleation rate of 1 x 10^4 ppm^{-1} min^{-1} tends to overpredict PM in the first hours of the experiment. Using a nucleation rate of around 1000 ppm^{-1} min^{-1} seems to give reasonable fits to the data, which is one reason that 1000 ppm^{-1} min^{-1} was chosen for the default value of NCrateI.

Results of our analysis of the pure air and H_2O_2 - air experiments carried out in our chamber whose data were judged to be useful for background PM characterization are shown on Figure 15. Figure 15a shows the maximum PM volume levels in these experiments in up to 6 hours of irradiation, which ranged from near or below the detection limit of our SMPS to ~2 $\mu g/m^3$. The uncorrected PM volume data are shown because it was not possible to obtain a wall loss correction for the experiments with low PM levels. Results of H_2O_2 - air experiments are also shown because background PM formation is also observed in these experiments, and as with pure air runs the only significant source of PM should be wall

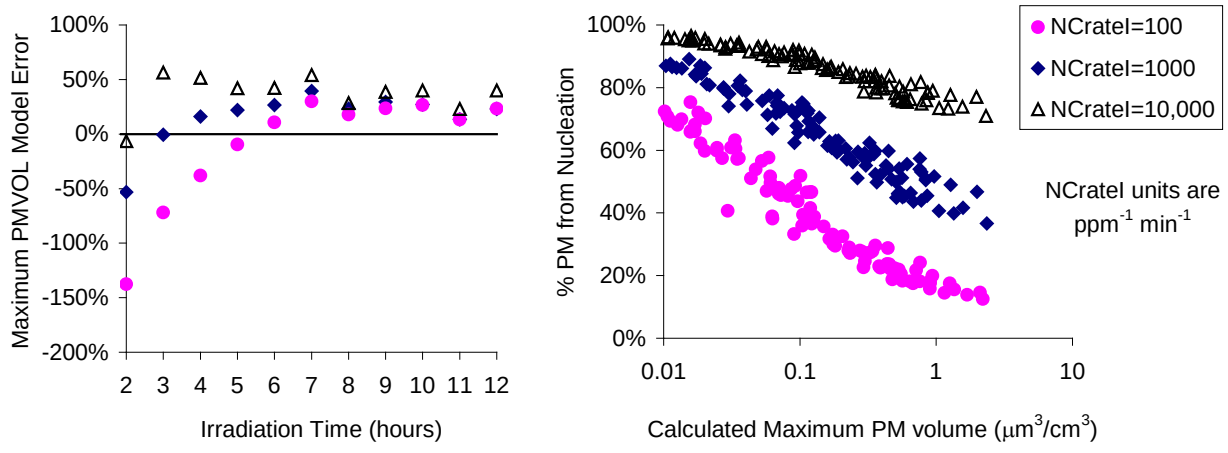

Figure 14. Effects of varying the nucleation rate on model simulations of PM formation in the model simulations of the pure air experiments, using WallPMparm values adjusted so the model fit the maximum PM levels in each run. (a) Plot of average maximum PM volume model errors against irradiation time. (b) Plot of fractions of final particle mass formed from nucleation as opposed to condensation.

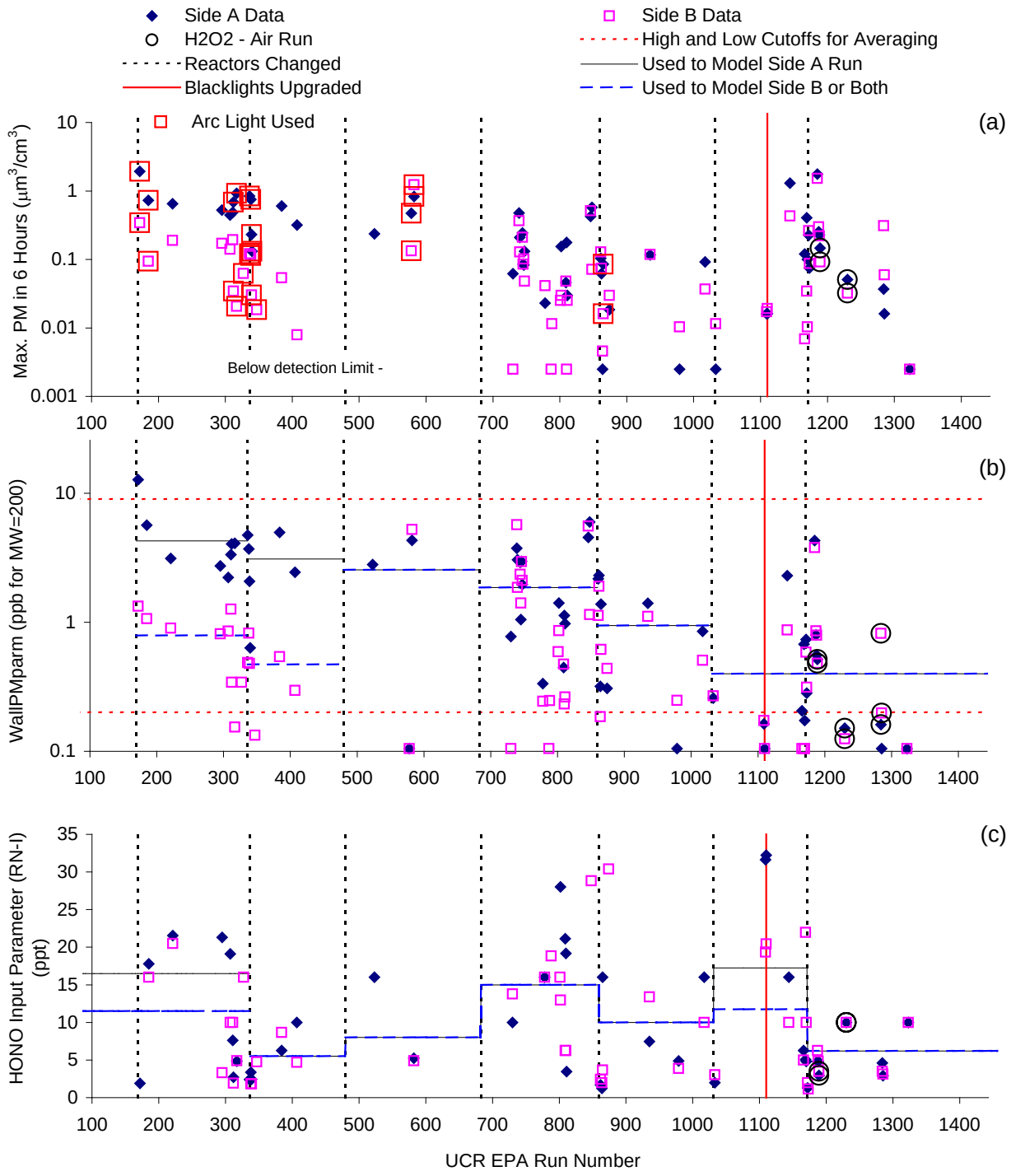

Figure 15. Plots of selected results of background PM characterization experiments against EPA chamber run number. (a) Maximum PM volume level in 6 hours; (b) Values of WallPMparm parameters that fit PM formation; and (c) HONO input parameters that fit ozone formation. Times when reactors were changed and parameter values assigned for modeling are also shown

effects. Figure 15a also shows that the PM levels in those experiments were in the same range as those for pure air experiments carried out around the same time. Note that the apparent background PM in Side A was higher than that in Side B for the first two set of reactors employed, but the differences between the two sides were insignificant for subsequent sets of reactors. The reason for this higher apparent contamination of Side A for the first two reactors is unknown.

Note that the initial pure air experiments employed only the arc light system while the experiments between runs 221 and 582 include runs with either the arc light or blacklights. The light intensity of the arc light experiments corresponded to an NO_2 photolysis rate (k_1) of 0.26 min^{-1}, while the k_1 for those with the blacklights prior to the blacklight upgrade decreased from 0.18 to 0.13 min^{-1}. There was no apparent effect of light source on the amounts of PM formed in the pure air experiments during this period, despite the fact that one might expect higher background PM from the arc light runs because the higher IR levels might cause more radiative heating on the walls. However, around the time of run 1100 the blacklights were upgraded, resulting in an increase in k_1 from 0.13 to 0.40 min^{-1}. This caused an increase in the background PM from the relatively low levels observed in the previous reactors to higher levels more comparable to those observed in the first two set of reactors with PM data.

Figure 15b shows the WallPMparm values that fit the maximum PM data for these background PM characterization experiments. These were calculated using the default nucleation rate parameter for non-volatiles (NCrateI) of 1000 ppm^{-1} min^{-1}. We found that the WallPMparm values that fit the data were affected by NO_x offgasing and radical source rates used in the chamber wall model, so we adjusted the HONO and NO_x offgasing parameter, RN-I, so that the model predictions fit the amounts of O_3 formed in these experiments, before determining the WallPMparm value that fit the PM data. (The adjustment was done in this order because the WallPMparm value did not affect predictions of O_3 or any other gas-phase species.) The RN-I parameters that fit the data for these pure air runs are shown on Figure 15c, where they can be seen to be in reasonably good agreement with the magnitudes of the RN-I values assigned for modeling based on results of the radical source or NO_x offgasing characterization experiments discussed previously. Note that these pure air experiments were not used to derive the RN-I parameters because background VOC levels could affect the result, though the fact that the results appear to be consistent suggest that background VOC levels in this chamber were not large enough to affect ozone formation, even though they apparently affect PM formation.

Figure 15b shows that the WallPMparm values that fit the results of these characterization experiments was highly variable from run to run, but tended to be higher in Side A than Side B for the first two reactors, then about the same in each side for the subsequent sets of reactors, where the WallPMparm values tended to decrease with time. There is no apparent effect of light source or light intensity in the WallPMparm values that fit the PM data in these experiments, with the results for the arc light runs being not significantly different than those for the blacklight experiments, and the blacklight upgrade also not significantly affecting the results. This tends to support our assumption that the input rate for the PM precursor is approximately proportional to the light intensity.

Figure 15b also shows the values of the WallPMparm values that were assigned for modeling the mechanism evaluation experiments. These were derived by averaging the WallPMparm parameters that fit the individual experiments, as follows. If the experiment had a WallPMparm value higher than the high cutoff limit of 9 ppt, then the high cutoff limit of 9 ppt was used instead of the value for the run. Likewise, if the WallPMparm parameter for the run was less than the low cutoff limit of 0.2 ppt, or if no measurable PM formation was observed in the experiment, then the low cutoff limit of 0.2 ppt was used. This approach was used to reduce the effects of extreme points and to utilize data from runs where the PM or WallPMparm was too low to measure. The high and low cutoff limits used are shown on Figure 15b, and are based on a subjective examination of the data. For the purpose of assigning the WallPMparm values for modeling and averaging the data, the experiments are grouped as follows: The first two

reactors with PM data are treated separately and Side A and Side B are also treated separately. The two sides do not appear to be significantly different for the subsequent reactors and so the Side A and B data are grouped together for averaging and assigning the parameter for modeling. Each set of reactors is treated separately for the purpose of averaging and assigning the parameters, except for the last two sets of reactors, which do not appear to be significantly different and are grouped together.

The WallPMparm values shown on Figure 15b were used when modeling all runs for mechanism evaluation based on the set of reactors and (for the first two sets) the reactor side except for sensitivity calculation purposes as discussed below. For the purpose of assessing sensitivity of modeling results to this uncertain and variable parameter, we used lower limit WallPMparm values of zero and upper limit values of 9 ppt, the latter being the high cutoff limit shown on Figure 15b.

Reproducibility of PM Formation

Characterization of the level of reproducibility of the data is obviously important when using data to evaluate models. For our dual chamber experiments, reproducibility can be assessed by conducting "side equivalency" tests where the same mixture is irradiated simultaneously in the two reactors, as well as by comparing results of duplicate or near-duplicate experiments carried out on different days. Generally good side equivalency in formation of O_3 and measurements of other gas-phase species is observed in our chamber (see reports at Carter, 2012, website), but this may not necessarily imply good reproducibility of particle results. For this reason, a number of side equivalency experiments where the same SOA-forming mixture was simultaneously irradiated in both reactors, and the mechanism evaluation dataset includes a number of replicate or near-replicate experiments carried out on different days, including some in different reactors.

Table 3 lists the pairs of side equivalency tests or near-replicate experiments in our SOA mechanism evaluation dataset that are judged to be useful for assessing reproducibility of our SOA data, Figure 16 plots relative differences in PM volume formation against EPA chamber run number for the earlier experiment of the pairs, and Figure A-1 and Figure A-2 in the Supplementary Materials show plots of PM volume and number data, both uncorrected and corrected for particle wall loss as discussed above, in the order they are listed on Table 3. Experiments carried out on different days are included in the list if the initial concentrations of the compounds were all within 5%, the experiments had the same light source and light intensity, and there are no reasons to suspect that any of the results or conditions were unusual or questionable. Note that for the purpose of the Table 3 and Figure 16, the relative difference is defined as the difference in PM formation between the two experiments (Side B - Side A for side equivalency tests or later - earlier for different runs), divided by the average of the PM in the experiments. The maximum PM level within the time period of the shorter duration experiment is used for uncorrected PM volume, and the PM level at the time of the end of the shorter duration experiment is used for PM volume corrected for particle wall loss.

These data show that the reproducibility of the corrected and uncorrected PM volume data is on the order of ±30%, with the average differences in the corrected final PM volume being 18±13% for all pairs, 12±11% for side equivalency tests, and 29±15% for runs on different days. The differences for the uncorrected maximum PM volume levels are essentially the same, being respectively 18±13%, 14±7%, and 26±16%, respectively. The correlation coefficients for the differences are shown on Table 4. The fact that the corrected and uncorrected data have about the same reproducibility and the low correlations between the differences in PM volume and differences in wall loss rates indicate that the differences cannot be necessarily attributed to run-to-run differences in particle wall loss rates. Figure A-1 and Figure A-2 shows that there are some experiments with better reproducibility in the corrected data and some with better in the uncorrected data, as well as some where neither are well reproduced. The negative correlation between the PM volume differences and the amount of PM formed would be expected since

Table 3. Comparison of PM formation in irradiations of the same reaction mixtures with the same light intensities.

Run ID		Compound Added		NO_x	H_2O_2	Hour	Wall Loss (/hr)		Corr. PM ($\mu m^3/cm^3$)			Uncorr.
Run 1	Run 2	Compound	(ppm)	(ppb)	(ppm)		Run 1	Run 2	Run 1	Run 2	Diff	diff
					Side Equivalency Tests							
EPA217A	Side B	m-Xylene	0.04	10		10	27%	26%	10	8	-19%	-12%
EPA247A	Side B	m-Xylene	0.40	477		10	11%	13%	133	136	2%	-8%
EPA249A	Side B	m-Xylene	0.16	247		11	15%	19%	21	20	-5%	-22%
EPA410A	Side B	m-Xylene	0.52	137		6	16%	18%	134	131	-3%	-8%
EPA474A	Side B	m-Xylene	0.11		4.0	9	30%	19%	79	75	-5%	21%
EPA476A	Side B	m-Xylene	0.05		1.0	11	29%	22%	25	26	1%	12%
EPA556A	Side B	m-Xylene	0.16	79		11	27%	41%	107	116	8%	-8%
EPA750A	Side B	m-Xylene	0.07		1.2	10	24%	38%	24	24	-1%	-29%
EPA1097A	Side B	m-Xylene	0.58	196		6	27%	40%	129	150	15%	-8%
EPA1175A	Side B	m-Xylene	0.08	51		8	28%	14%	17	11	-44%	-22%
EPA1193A	Side B	m-Xylene	0.07	45		7	13%	13%	9	8	-16%	-18%
EPA1205A	Side B	m-Et. toluene	0.10		1.0	6	34%	28%	86	79	-8%	4%
EPA1179A	Side B	o-Et. toluene	0.09	53		9	26%	26%	62	54	-14%	-7%
EPA1406A	Side B	o-Et. toluene	0.10		1.0	4	36%	39%	30	38	24%	18%
EPA1194A	Side B	p-Et. toluene	0.20	90		7	31%	28%	60	50	-17%	-13%
EPA1206A	Side B	Phenol	0.05		1.0	5	23%	21%	30	31	3%	7%
					Runs on different days							
EPA293A	396A	m-Xylene	0.05	22		6	26%	25%	8	10	20%	27%
EPA472B	514B	m-Xylene	0.11		1.0	9	25%	23%	28	37	29%	33%
EPA1256A	1426B	n-Prop. benz.	0.10		1.0	5	21%	30%	27	19	-36%	-55%
EPA1205A	1211A	m-Et. toluene	0.10		1.0	4	34%	24%	63	57	-11%	0%
EPA1211B	1218B	m-Et. toluene	0.20		1.0	3	14%	36%	48	77	45%	22%
EPA1218B	1416A	m-Et. toluene	0.20		1.0	6	36%	40%	137	114	-18%	-22%
EPA1242B	1326A	o-Et. toluene	0.10		1.0	5	33%	40%	23	42	59%	45%
EPA1227A	1239B	p-Et. toluene	0.20		1.0	5	37%	35%	83	66	-22%	-18%
EPA1266B	1427A	o-Cresol	0.10		1.0	3	38%	36%	67	54	-21%	-14%

Notes: "Corr PM" is PM volume corrected for wall loss; "Diff" is [(run 2) - (run 1)] / Average [(run 1), (run 2)]; "Uncorr diff" is difference for maximum uncorrected PM values.

chamber effects might have relatively greater influence on experiments with lower PM levels, but the correlation is not very large. There are more cases of poor reproducibility (i.e., differences greater than 50%) for the more recent experiments that were carried out for this project than for those that were carried out previously. The reason for this is not known.

This ~30% run-to-run reproducibility is most likely due to irreproducible chamber effects since there is no obvious correlation with any measurement data or differences in known run conditions. This needs to be taken into account when assessing what is an acceptable fit of the model simulations to the PM data when evaluating the performance of the mechanism in simulating the chamber data.

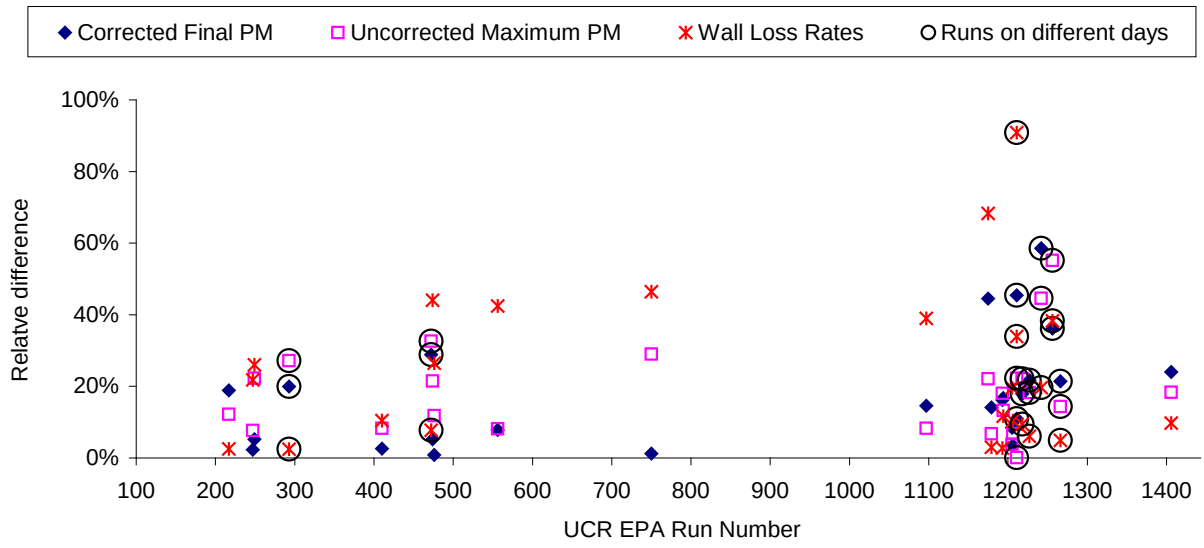

Figure 16. Plots of relative differences in PM formation in replicate experiments against UCR EPA chamber run number.

Table 4. Correlation coefficients for differences between PM volume formation in the various pairs of side equivalency or replicate experiments

Correlation Coefficients with:	Difference in Corrected Final PM Volume	Difference in Uncorrected Maximum PM Volume
Difference in PM Wall Loss Rate	28%	15%
Difference in Uncorrected maximum PM Volume	63%	
UCR EPA chamber run number		
Runs on different days	-9%	20%
Side Equivalency Tests	-7%	49%
Difference in average temperature	6%	-5%
Duration of shortest experiment	-11%	-49%
Maximum Uncorrected PM Volume	-44%	-26%

Mechanism Evaluation Experiments

List of Experiments

Data from a total of 315 separate aromatic - NO_x or aromatic - H_2O_2 experiments were used for SOA mechanism evaluation for this project, including 98 such experiments carried out previously as well as the 217 carried out for this project. These experiments are listed on Table A-3 in the Supplementary Materials. Note that by "experiment" in this context we mean irradiation of a separate mixture in a single reactor (Side A or B) in our dual reactor chamber, which is designed such that two experiments are typically carried out at the same time. Although dual reactors were designed in part for conducting incremental reactivity experiments where the effect of adding a test compound to a standard base case

mixture is examined, in this project the experiments in the different reactors are considered independently. Although some of these experiments consisted of simultaneous irradiations of the same mixture and can be used as side equivalency tests as discussed in the "Reproducibility" subsection of the "Characterization Results" section above, most had different mixtures in the different reactors. For experimental purposes usually the two reactors had the same reactants, but the concentration levels were different for at least one reactant. There is no evidence for interaction of contents of different reactors, so for the purpose of this project they are treated as independent in the mechanism evaluation.

The types and numbers of experiments modeled for this project are summarized on Table 5. These consisted of aromatic - NO_x irradiations with various aromatic and NO_x levels to evaluate the mechanisms for SOA formation in the presence of NO_x, aromatic - H_2O_2 irradiations to evaluate mechanisms for SOA formation in the absence of NO_x, and a few experiments, primarily with m-xylene or toluene, where the effects of adding CO or another reactive organic compound was added. Most of these were aromatic - NO_x - added VOC experiments but a few were aromatic - H_2O_2 - CO experiments. As indicated on Table 5, about 2/3 of these experiments were carried out for this project, and almost 3/4 of the VOCs listed on Table 5 were not studied previously. Most of the previous experiments were with m-xylene, though a few other compounds were studied as well.

Not all aromatic experiments carried out for this project or aromatic experiments with PM data carried out in our chamber previously were used for mechanism evaluation. Experiments where data judged to be critical for modeling were missing or suspect and experiments with characterization or procedure problems that may affect the validity of the results were rejected for use in mechanism evaluation. Modeling was sometimes used as part of this screening process. However, judgments to reject a given experiment were not based on how well the model could simulate ozone or SOA formation, but only on whether the modeling results indicate that the experiment was improperly characterized or the results are clearly anomalous. Many of the earlier m-xylene experiments did not have satisfactory quality assurance procedures and because of the large number of available experiments with this compound we were somewhat more selective when selecting runs for modeling. Experiments where results of model simulations of either gas-phase results or PM formation appeared to be highly atypical compared to modeling of similar experiments, were considered to have questionable data quality or characterization and were not used for modeling, but only if there was a sufficient number of other experiments to support a judgment that these data are atypical and suspect. Note that a similar procedure was used when judging whether an experiment is suitable for gas-phase aromatic mechanism evaluation (Carter and Heo, 2012), though some runs that were used for evaluating the gas-phase mechanism used for that work were not used in this study because of missing or suspect PM data.

Additional criteria were used to reject otherwise suitable experiments for mechanism evaluation in order to conduct the evaluation on a consistent basis for all compounds and experiments. As discussed in the "Modeling Methods" section above for most compounds, we evaluated mechanisms for SOA formation based on model simulations of SOA yields with OH radicals levels adjusted so the model will correctly predict the amount of the aromatic compound that reacts. This is because the gas-phase mechanism tends to underpredict radical levels in aromatic - NO_x experiments (Carter and Heo, 2012), and not making this adjustment would introduce biases and potential compensating errors in the SOA mechanism evaluation. This could not be used for benzene because it reacts too slowly to reliably derive OH levels and could not be used for phenolic compounds in the presence of NO_x because they can react with NO_3 radicals as well as with OH radicals, but was used for all other aromatics. It was also used for the phenol H_2O_2 experiments because the model tended to overpredict amounts of phenol consumed in those experiments, but was not necessary for the H_2O_2 experiments with the other phenolic compounds. For this reason, experiments for such compounds that lacked reliable measurements of consumption of the starting aromatic hydrocarbon had to be excluded from the SOA mechanism evaluation dataset. These excluded experiments included some experiments that could be used for gas-phase mechanism evaluation

Table 5. Summary of types of SOA mechanism experiments that were modeled for this project. All experiments were carried out in one of the reactors of the UCR EPA chamber.

Aromatic Compound	Total Experiments [a]			Aromatic-NO_x	Aromatic - H_2O_2	2nd Cmpd Added
	All	New	Old			
Benzene	17	15	2	10	6	1
Toluene	20	11	9	11	5	4
Ethyl Benzene	8	8	-	4	4	-
o-Xylene	15	9	6	9	6	-
m-Xylene	103	27	76	50	33	20
p-Xylene	11	6	5	6	5	-
n-Propyl Benzene	8	8	-	2	6	-
Isopropyl Benzene	8	8	-	4	4	-
o-Ethyl Toluene	17	17	-	11	6	-
m-Ethyl Toluene	18	18	-	10	8	-
p-Ethyl Toluene	12	12	-	8	4	-
1,2,3-Trimethyl Benzene	6	6	-	4	2	-
1,2,4-Trimethyl Benzene	21	21	-	17	4	-
1,3,5-Trimethyl Benzene	8	8	-	4	4	-
Phenol	9	9	-	4	5	-
o-Cresol	11	11	-	6	5	-
m-Cresol	2	2	-	-	2	-
p-Cresol	5	5	-	-	5	-
2,4-Dimethyl Phenol	9	9	-	4	5	-
2,6-Dimethyl Phenol	3	3	-	-	3	-
3,5-Dimethyl Phenol	2	2	-	-	2	-
Catechol	2	2	-	-	2	-
All Compounds	315	217	98	164	126	25

[a] "New" refers to experiments carried out for this project and "Old" refers to experiments carried out previously.

(Carter and Heo, 2012) because at least the initial concentration of the aromatic hydrocarbon was reasonably well characterized. Fortunately, there were not many such experiments, so this requirement was not a significant problem.

A potentially more substantive problem is that we also did not model experiments where the levels of PM formed were so low that we could not use the experimental data to reliably derive a particle wall loss rate. The particle wall loss rate is a significant input to the modeling that varies significantly from experiment to experiment (see discussion of PM characterization results, above), and if it is unknown or has to be estimated without reliable data, the SOA mechanism evaluation is uncertain, regardless of whether the evaluation uses PM data corrected or uncorrected for wall loss. If the evaluation is done using PM data corrected for wall loss, as is the case for most of this study except for evaluation of PM characterization runs, the wall loss rate does not affect the model simulation of the corrected PM yields but it affects the correction used to derive the corrected PM data from PM measurements. If the evaluation is done using uncorrected PM data, the model simulation of the PM data will be affected by the wall loss parameter used in the model input. This means that very low PM runs had to be excluded from the evaluation. This presents a potential source of bias in the mechanism evaluation, as there may be

cases where the model may predict high PM levels with the data showing that this is may not be case being excluded. However, most of the mechanism evaluation experiments had sufficient PM levels to derive wall loss corrections, and even PM levels as low as ~1 $\mu g/m^3$ are sufficient to derive wall loss rates.

We also did not use experiments for mechanism evaluation where the final PM levels calculated in the model simulations were found to be unduly influenced by the chamber background PM formation, as discussed in the "Background Particle Formation" section of the characterization results, above. This was evaluated by conducting model simulations of the experiments by setting chamber background particle formation to zero (i.e., setting the WallPMparm value to 0), and comparing the results of model simulations using the baseline mechanism with parameters adjusted to fit the chamber data. If eliminating the chamber background caused the calculated final PM to drop by more than 40%, the run was rejected from the evaluation dataset. This resulted in a total of 18 runs being removed from the evaluation set, 9 with m-xylene, 4 with toluene, 2 each with 1,2,4- and 1,3,5-trimethylbenzene, and 1 with ethylbenzene. Because of the variability of the background PM formation, runs with this level of sensitivity to this background were not considered to be sufficiently well characterized for use for mechanism evaluation. Removing there runs did not affect SOA yield parameters derived for m-xylene and 1,2,4-trimethylbenzene, but did affect those derived for toluene, ethylbenzene, and 1,3,5-trimethylbenzene.

PM Formation in the Mechanism Evaluation Experiments

Table 5 shows that there were a number of experiments judged to be suitable for evaluating SOA formation mechanisms for a variety of aromatic hydrocarbons and representative phenolic products. Table 6 lists the range of PM volume levels (corrected for wall loss as discussed above) and the highest SOA yields observed for all the experiments for each compound, and Figure 17 and Figure 18 show plots of these yields against the final PM volume in the experiments for each of the compounds. Different symbols are used on Figure 17 and Figure 18 for aromatic - NO_x and aromatic - H_2O_2 experiments because lower yields were generally observed in experiments where NO_x was present. Results of one-product Odum (Odum et al, 1996) model fits, discussed below, are also shown on the table and plots. Although there are a sufficient number of data points for some compounds, such as m-xylene, to fit the data with a two product model, the fits are not significantly better than those with the one-product model, so using the larger number of parameters for the two product model is not considered to be meaningful.

For the purpose of Table 6 and the discussion in this section, the SOA yield, Y, refers to the final mass-based yield in the experiment, and is defined as follows:

$$Y = PMmassCorr / \Delta VOCmass \qquad (IV)$$

where

$$PMmassCorr = PMVolCorr \cdot PMden,$$

$$\Delta VOCmass = (VOCmass_0 - VOCmass_{final}) \cdot e^{-Dil \cdot t},$$

Y is the SOA yield at the end of the experiment, PMden is the density assumed for the PM (see Table 2), PMmassCorr and PMvolCorr are the measured final PM mass and volume corrected for wall loss as described above, ΔVOCmass, $VOCmass_0$, and $VOCmass_{final}$ are the mass of VOC reacted in the experiment and the initial and final VOC mass in $\mu g/m^3$, respectively, Dil is the dilution rate assigned for the experiment (usually zero), and t is the duration of the experiment. The duration is defined as the last hour of the irradiation where there are valid PM and VOC data, and the $VOCmass_{final}$ value is derived by interpolation if the last measurement is not exactly at the last hour. Note that measured SOAyields are uncertain for benzene because of the relatively small fraction that reacts (i.e., uncertain ΔVOCmass), and yield data are not available for all experiments because of lack of final VOC data. However, sufficient

Table 6. Summary of PM volume and yields formed in the aromatic SOA mechanism evaluation experiments and fits to the 1-product model for the aromatic - H_2O_2 runs.

Compound	PM Volume ($\mu m^3/cm^3$) [a] (Wall Loss Corrected)			1-Product Model Fits to H_2O_2 Experiments [b]				
				Kp Adjusted			Kp = 0.02 $m^3/\mu g$	
	Min	Max	Y(max)	Y∞	Kp(Fit)	Y(50)	Y∞	Y(50)
Benzene	2.6	95	30%	41%	0.028	24%	47%	24%
Toluene	1.5	61	23%	24%	0.232	22%	51%	25%
Ethyl Benzene	3.0	58	32%	35%	0.082	28%	66%	33%
m-Xylene	1.5	163	40%	45%	0.021	23%	46%	23%
o-Xylene	12.9	54	31%	47%	0.022	25%	50%	25%
p-Xylene	2.9	96	28%	26%	0.064	20%	37%	19%
n-Propyl Benzene	8.5	48	30%	29%	0.074	23%	48%	24%
Isopropyl Benzene	7.9	44	25%	28%	0.117	24%	54%	27%
m-Ethyl Toluene	5.4	142	46%	50%	0.022	26%	52%	26%
o-Ethyl Toluene	20.2	113	26%	33%	0.031	20%	39%	20%
p-Ethyl Toluene	11.9	103	30%	32%	0.093	26%	48%	24%
1,2,3-Trimethyl Benzene	15.8	68	32%	30%	[c]	30%	51%	25%
1,2,4-Trimethyl Benzene	2.8	54	28%	21%	[c]	21%	45%	23%
1,3,5-Trimethyl Benzene	3.2	64	32%	27%	[c]	27%	48%	24%
Phenol	16.9	196	56%	44%	0.074	34%	68%	34%
o-Cresol	39.6	627	69%	56%	0.033	35%	65%	33%
m-Cresol	29.0	32	28%	100%	0.008	28%	55%	27%
p-Cresol	30.3	74	73%	63%	0.107	53%	93%	47%
2,4-Dimethyl Phenol	32.1	485	107%	100%	0.013	40%	95%	48%
2,6-Dimethyl Phenol	42.8	133	44%	43%	[c]	43%	63%	32%
3,5-Dimethyl Phenol	30.3	83	26%	39%	0.018	18%	37%	19%

[a] Minimum and maximum PM volume and maximum PM yields [Y(max)] in all the experiments with the compound. Yields are given on a mass basis and are calculated based on an assumed PM density of 1.4.

[b] Fits to the yields observed in the aromatic H_2O_2 experiments using the 1-product model as described in the text. Y∞ is the limiting high PM SOA yield, Kp(fit) is the best fit partitioning coefficient in $m^3/\mu g$, and Y(50) are the yields calculated for PM levels of 50 $\mu g/m^3$ using the best fit parameters.

[c] The data are best fit assuming the SOA is non-volatile.

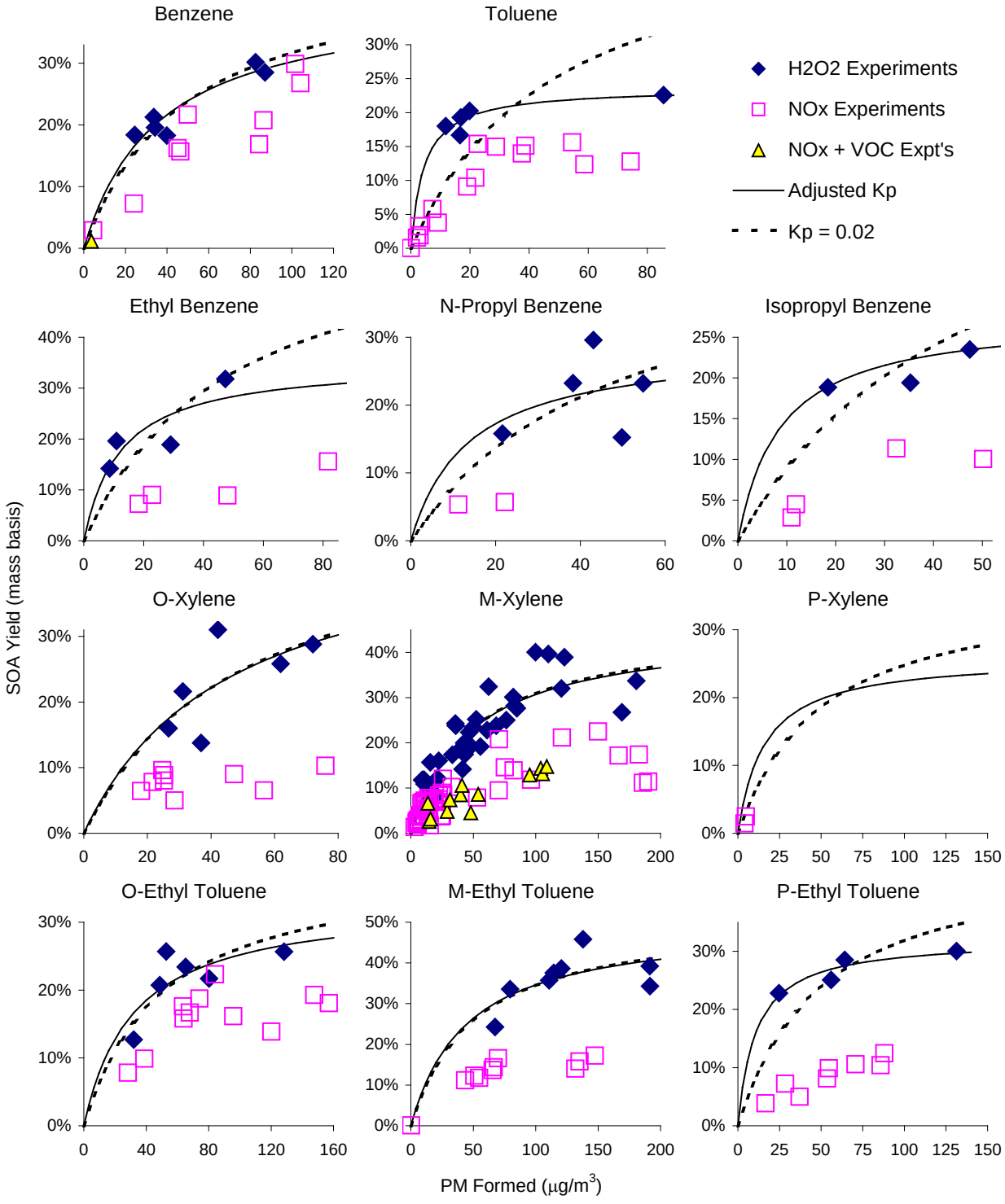

Figure 17. Plots of SOA yields for the mechanism evaluation experiments with the various aromatic compounds (set 1 of 2).

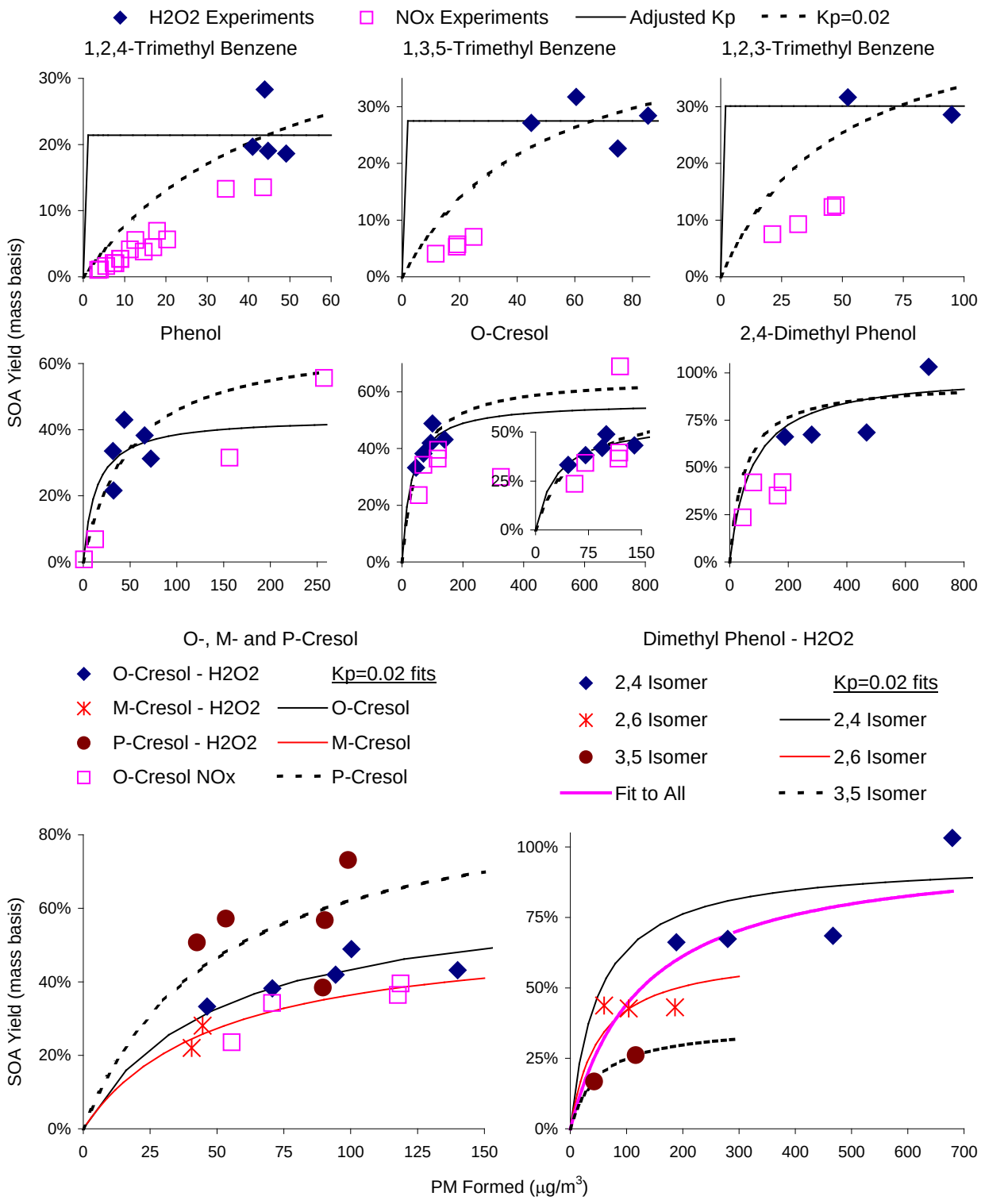

Figure 18. Plots of SOA yields for the mechanism evaluation experiments with the various aromatic compounds (set 2 of 2).

VOC data and therefore yield data are available for most of the experiments in the mechanism evaluation dataset.

As discussed by Odum et al (1996), and also discussed in the "Modeling PM Formation" section, above, if an equilibrium partitioning model is assumed then the SOA yields will depend on the amount of organic PM present in the experiment. The equilibrium partitioning model of Odum et al (1996) predicts that

$$Y = PMmassCorr \cdot \Sigma_i Y\infty_i \cdot Kp_i / (1 + PMmassCorr \cdot Kp_i) \quad (V)$$

where PMmassCorr is the PM volume corrected for wall loss in units of $\mu g/m^3$, the sum is over all the condensable products (i) formed in the experiment, $Y\infty_i$ is the yield of the condensable product i on a mass basis relative to the amount of aromatic reacting if it all goes into the particle phase, Kp_i is the equilibrium partitioning coefficient for product i in units of $m^3/\mu g$. Since we rarely know a-priori the nature, yields, and partitioning coefficients of all the products formed, often a "two-product" model is used to approximate the data, with four parameters, the yields and Kp values for each of the two products, adjusted to fit the data. However, the number of experiments and amount and scatter of the data in most cases are such that they cannot meaningfully be used to derive four parameter values, so instead we use a "one-product" model, where

$$Y \approx Y\infty \cdot PMmassCorr \cdot Kp / (1 + PMmassCorr \cdot Kp) \quad (VI)$$

and $Y\infty$ and Kp reflect the overall set of products formed, and are adjusted to fit the data. As indicated above for the few compounds, such as m-xylene, where there are sufficient data to use the two product model, the fits to the data were found not to be significantly better.

Figure 17 and Figure 18 show that in most cases the yields in the aromatic - NO_x experiments are much more variable and tend to be lower than those in the aromatic - H_2O_2 experiments where NO_x was absent, and the yields in the experiments where NO_x was present are not as well fit by the simple partitioning model as is the case when NO_x was absent. Because of this variability of the yields for the aromatic - NO_x experiments, only the data for the aromatic - H_2O_2 experiments were used to derive parameters for the 1-product model (Equation V). The parameters for the model where both $Y\infty$ and Kp were adjusted are summarized on Table 6, and the predictions of the model are shown as the solid lines on Figure 17 and Figure 18.

For a number of compounds the number of experiments and the range of PM levels are insufficient to derive the two parameters required in Equation (VI), and either the best fits are obtained assuming no dependence of the yield on PMmassCorr (i.e., that the product is non-volatile), or the fit parameters are unduly influenced by experimental scatter. However, there are enough data to obtain potentially meaningful $Y\infty$ and Kp values for m-xylene, and the parameters obtained for most other compounds are reasonably consistent with those derived for m-xylene. The compounds for which the one-product model appears to give consistent results indicate that one-product Kp values are on the order of 0.02 $m^3/\mu g$, and do not indicate any significant trend, at least for the aromatic hydrocarbons studied for this project. If the Kp value is specified, then Equation (VI) has only one parameter and meaningful fits can be obtained even for compounds with limited data. Table 6 gives the $Y\infty$ values derived for each compound assuming Kp = 0.02 $m^3/\mu g$, and the dotted lines on Figure 17 and Figure 18 show the fits for this one parameter model. With the possible exception of toluene, the fits assuming a compound-independent Kp value of 0.02 $m^3/\mu g$ does not give significantly worse fits to the no-NO_x SOA yield data than the models where the Kp values are optimized, considering the experimental scatter of the data. Even the SOA yields in the phenolic product experiments fit reasonably well with Kp value that was derived from the m-xylene data, as shown on Figure 18.

The k∞ values derived using the one-parameter model with a specified Kp of 0.02 $m^3/\mu g$ provides a means to place the yield data on a comparable basis with respect to the amount of PM present in the experiments. However, these Y∞ values are extrapolations that can be sensitive to the Kp value that is assumed and these in fact are expected to vary at least somewhat from compound to compound. The uncertainty is even greater when most experiments do not have very high PM levels. This extrapolation uncertainty can be reduced if the one-product model parameters are used to derive yield values for a given PM level that is within the range of PM levels for which there are experimental data, i.e.,

$$Yref = Y\infty \cdot PMref \cdot Kp / (1 + PMref \cdot Kp)$$

where PMref is the reference PM level and Yref is the yield computed for that level. If the PM level is representative of the range, then the yield value for the specified PM level is an interpolation not an extrapolation, and is not as sensitive to the Kp value that used when fitting the data. The Yref values can be used to compare the SOA yields adjusted to fit the data for the different compounds on an equal PM basis with less uncertainty due to extrapolation if PMref is chosen appropriately.

A comparison of the Y∞ values derived using Kp = 0.02 $m^3/\mu g$ and the PMref values calculated both with the fixed and adjusted Kp levels for the various compounds are shown on Figure 19. Yref values are calculated for a PMref of 50 $\mu g/m^3$, which is within the range of PM levels observed in the experiments for most of the compounds (see Table 6). The Yref values for a given compound agree reasonably well regardless of how Kp was derived, and as expected the Yref values correlates well with Y∞.

The trend in PM-adjusted SOA yields in the aromatic - H_2O_2 experiments shown on Figure 19 is different than what one might expect considering the molecular weights, though as expected in most cases they are higher for the phenolic compounds than the aromatic hydrocarbons. For the aromatic hydrocarbons, the highest yields are for ethylbenzene and the lowest are for p-xylene and o-ethyl toluene, but with the possible exception of these they are not significantly different for the various compounds. The variability is greater for the phenolic compounds, with the differences between the different isomers being greater than the differences between some of the compounds with different molecular weights. For example, the highest SOA yields are for 2,4-dimehtylphenol and the lowest are for its 3,5-isomer, and the yields for phenol, o-cresol and 2,6-dimethylphenol are not significantly different. The mechanistic implications of these results are uncertain, and suggest that the actual mechanisms are complex and the yields may be difficult to predict a-priori for aromatic compounds for which no data are available.

The SOA yields in the aromatic - NO_x experiments appear to depend on the NO_x level and possibly other factors as well as on the amount of SOA present. Because of this the data are not well fit by one-product partitioning models. Because the yields depend on the amount of PM present, a simple comparison of the observed yields with initial NO_x and other reactant conditions is not useful. However, the use of yields for a reference PM level provides a means for correcting for differences in PM levels when assessing effects of other reaction conditions on observed PM yields. Given a partitioning coefficient, Kp, and a reference PM level, PMref, a PM-adjusted yield, Yadj, can be calculated from the observed yield, Yobs, and the PM level in the experiment corrected for wall loss, PMmassCorr, as follows:

$$Yadj = Yobs \cdot \frac{(1 + Kp \cdot PMmassCorr)}{PMmassCorr} \cdot \frac{PMref}{(1 + Kp \cdot PMref)} \qquad \text{(VIII)}$$

This requires estimating a partitioning coefficient, but if the reference PM level is representative of the range of PM levels in the experiments, the correction should not be highly sensitive to this.

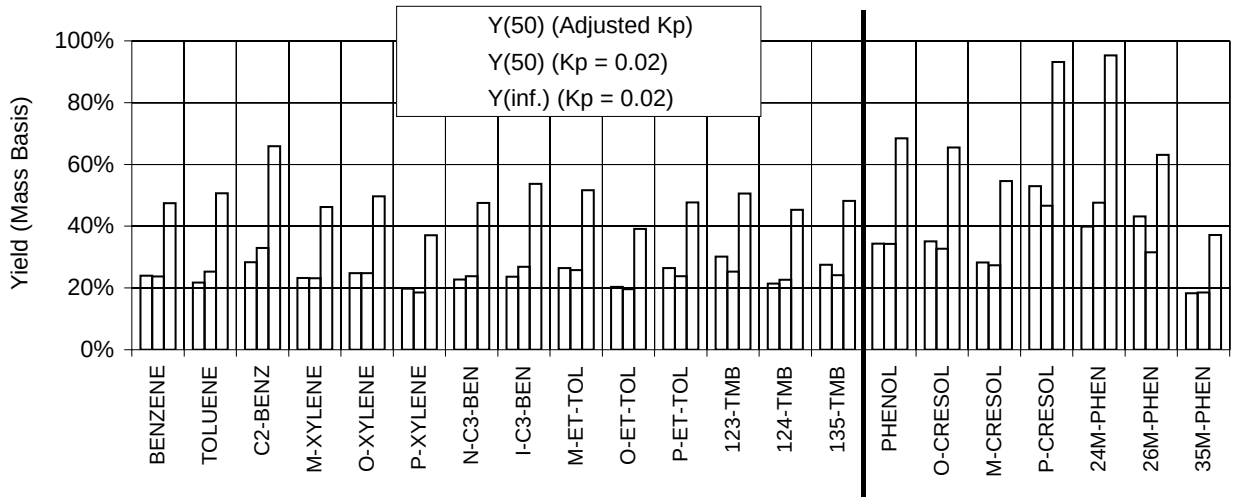

Figure 19. Plots of SOA yields derived from the data for the aromatic - H_2O_2 experiments at the limit of high PM [Y(inf)] and for PM levels of 50 μg/m^3 [Y(50)].

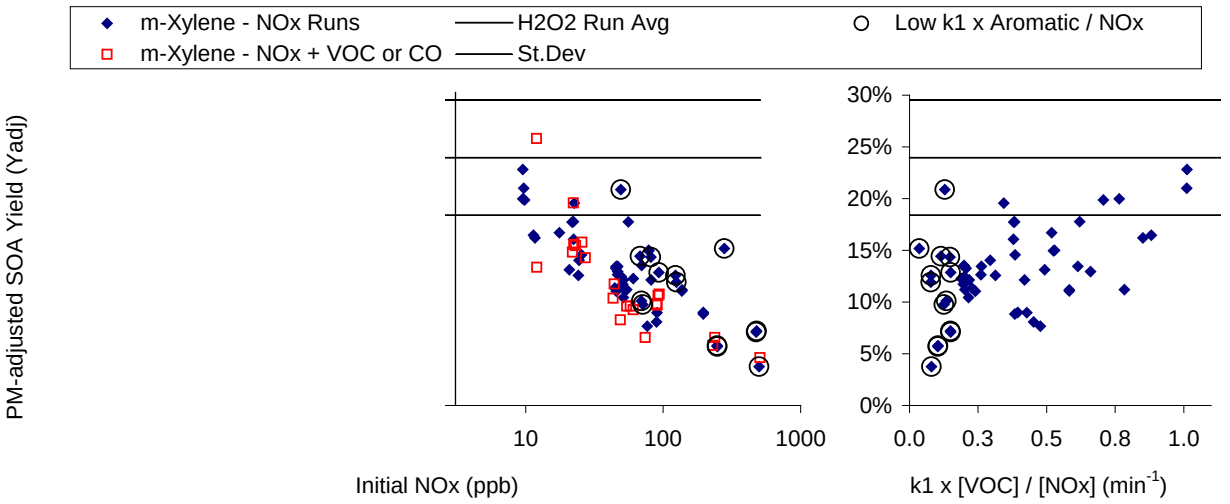

Figure 20. Plots of SOA yields in m-xylene - NO_x experiments against the initial NO_x levels, showing also the average yields for the H_2O_2 experiments. The yields are adjusted to correspond to a PM level of 50 μg/m^3 using a 1-product model with an assumed Kp of 0.02 m^3/μg.

Figure 20 shows plots of PM-adjusted SOA yields in the m-xylene - NO_x experiments against the initial NO_x levels and initial VOC/NO_x ratios (adjusted for differences in light intensity using the NO_2 photolysis rates assigned for the experiments). The yields are placed on an equal PM basis, using Equation (VIII) for PMref = 50 μg/m^3 and Kp = 0.02 m^3/μg, in order to assess the effects of NO_x or VOC/NO_x alone. The average and standard deviations for the Yref values for m-xylene - H_2O_2 experiments are also shown. It can be seen that the reduction in the SOA yields compared to the no-NO_x experiments corresponds quite well to the initial NO_x levels, especially when shown on a log scale, and

does not correlate as well with the reactivity in the experiment as measured by the light intensity-adjusted aromatic / NO_x ratio. However, the correlation is not perfect, suggesting that there are other factors besides the initial NO_x that influences SOA yields in these m-xylene - NO_x experiments. For example, note that the SOA yields tend to be lower in the experiments with added CO or other VOCs for a given NO_x level. This cannot be attributed to lower amounts of aromatic hydrocarbon reacted caused by the suppression of OH by the added VOC, because yields refer to SOA formed per amount of VOC reacted.

Figure 21 shows plots of PM-adjusted SOA yields in the aromatic - NO_x experiments for most of the other aromatics that were studied, with m-xylene also included for comparison. A few aromatic hydrocarbons are not shown but their results are similar to those for other isomers that are shown. In general, the trends are consistent with those shown for m-xylene, with the added VOC in the benzene and toluene experiments reducing the SOA yields similar to what was observed for m-xylene. The one exception is the phenol - NO_x experiments, where the yields are highly variable and have no apparent dependence on NO_x levels.

The implications of these SOA yield results and their dependence on reaction conditions on the mechanisms for SOA formation will be discussed in the section below that describes the results of the model simulations of these SOA mechanism evaluation experiments.

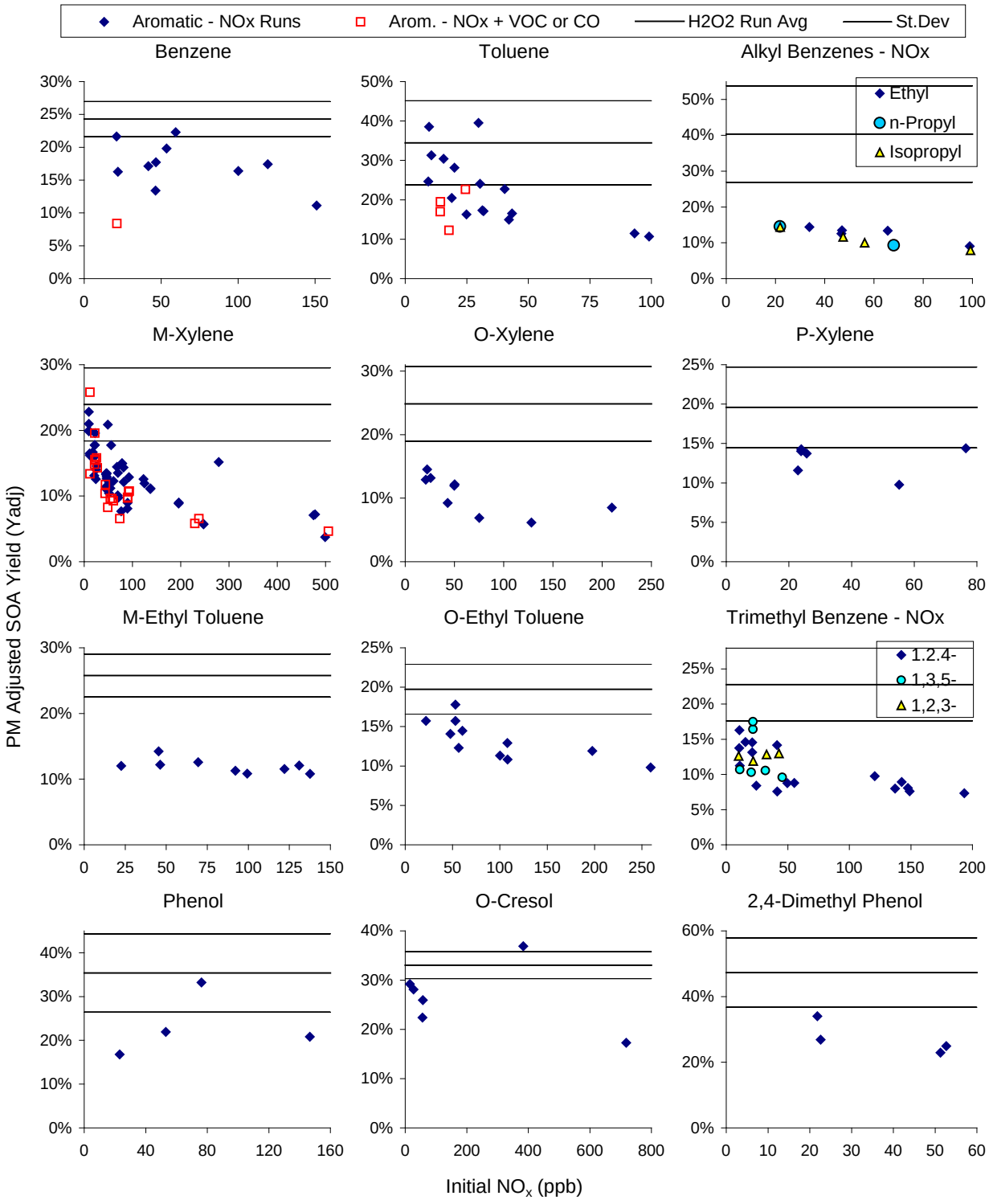

Figure 21. Plots of SOA yields in selected aromatic - NO_x experiments against the initial NO_x levels, showing also the average yields for the H_2O_2 experiments. The yields are adjusted to correspond to a PM level of 50 μg/m^3 using a 1-product model with an assumed Kp of 0.02 m^3/μg.

CHEMICAL MECHANISM

Gas-Phase Mechanism

The starting point for the SOA mechanism developed for this project was the SAPRC-11 aromatics mechanism, whose basis, development, evaluation and listing are documented comprehensively by Carter and Heo (2012). The major features of this gas-phase mechanism are summarized in the remainder of this section, though Carter and Heo (2012) should be consulted for details. The additions or revisions to this mechanism made for the purpose of aromatic SOA are then described in detail in the following section.

The starting point for the development of the SAPRC-11 aromatics mechanism is the SAPRC-07 mechanism documented by Carter (2010a,b). Since SAPRC-07 was developed, a large number of additional aromatic environmental chamber experiments were conducted, including experiments for additional compounds and many experiments at lower NO_x levels than previously available. These included, but are not limited to, many of the aromatic - NO_x experiments carried out to provide data to develop mechanisms for prediction of SOA formation from aromatics, as discussed in the previous section. However, they also included experiments in our chamber that could not be used for SOA evaluation but were otherwise suitable for gas-phase mechanism evaluations, and recent experiments from the CSIRO chamber in Australia (Hynes et al, 2005; White et al, 2010; White, 2010) that did not have SOA data. These new data indicate that the SAPRC-07 aromatics mechanisms do not give the best fits to the currently available chamber dataset, and need to be revised to take the new data into account.

Although a complete update of SAPRC-07 was not carried out, a number of updates and revisions were made. Almost all of the revisions concerned reactions of aromatics or aromatic oxidation products, with mechanisms updated for benzene, toluene, ethylbenzene, and all xylene, trimethylbenzene, ethyl toluene and propylbenzene isomers, as well as phenol, o-cresol, and 2,4-dimethylphenol. Mechanisms for other aromatics are derived based on those for these 17 representative compounds. Several revisions were made to make the mechanism more consistent with recent literature data, most concerning aromatics but a few concerning the base mechanism. The rate constants and yields of known oxidation products from the reactions of the aromatic hydrocarbons that are separately represented in the mechanism were updated to be consistent with current literature data. But the major changes concerned revisions made to improve model simulations of O_3 formation in the newer aromatic - NO_x environmental chamber experiments, many of which were carried out for this project. The quantum yields for radical formation from the model species representing unknown aromatic ring-opening products were adjusted to remove biases in model simulations of NO oxidation and O_3 formation rates in aromatic - NO_x experiments with NO_x levels lower than ~100 ppb. New mechanisms were derived for the reactions of the oxidation products phenol, cresols, and xylenols to improve model simulations of experiments with those compounds. In addition, new model species and reactions were added to SAPRC-11 for the purpose of predicting SOA formation from aromatic compounds as discussed in the following section.

Except as discussed below, the basic structure and level of chemical detail for the updated aromatic mechanisms are the same as that used for SAPRC-07. Figure 22 shows a schematic of the major features of the SAPRC-07 aromatics mechanisms, with additional processes considered when developing SAPRC-11 shown in the dashed-line box. As discussed by Carter (2010a,b), the major reaction of aromatic hydrocarbons is reaction with OH radicals, either by OH abstracting from the alkyl group off the ring (if present) (pathway 1 on Figure 22), or by adding to the ring forming an OH-aromatic adduct (pathway 2). The reactions following abstractions involve formation of an organic nitrate following the reactions of the peroxy radical with NO (pathway 3) or formation of an alkoxy radical that ultimately

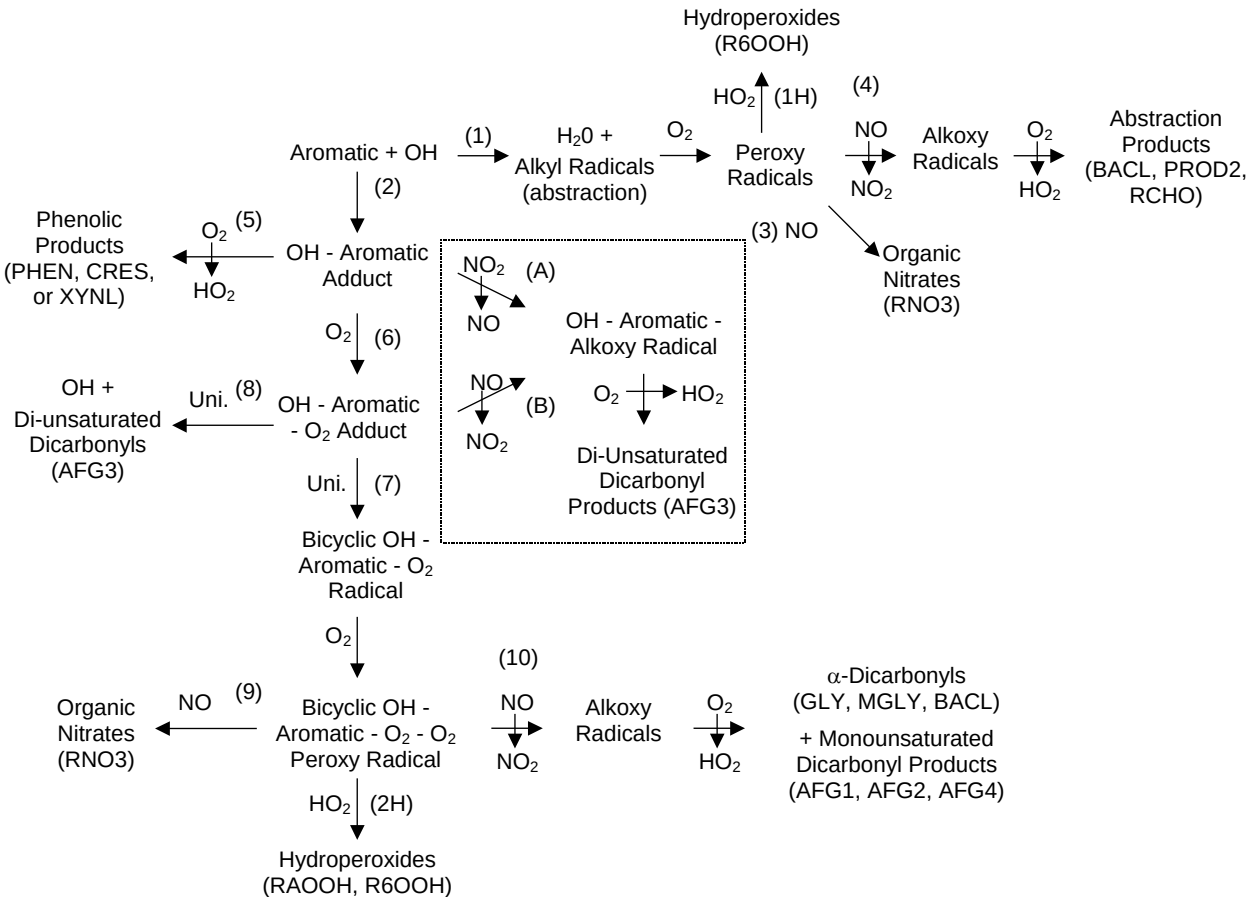

Figure 22. Schematic of major overall features of the initial reactions of alkylbenzenes in the presence of NO_x in the current SAPRC aromatics mechanisms. Processes not used in SAPRC-07 but considered for SAPRC-11 are shown in the dashed-line box. Model species used for reactive products are given in parentheses.

reacts to form HO_2 and various abstraction products (pathway 4). If the abstraction is from a methyl group, the product formed would be an aromatic aldehyde represented by the BALD model species; otherwise the product is either a ketone (represented by the PROD2 species) or an aldehyde with the carbonyl away from the aromatic group (represented by RCHO), depending on the location of the abstraction. This portion of the mechanism is not considered to be particularly uncertain and was not considered further in this mechanism update (see Carter, 2010a,b).

The most uncertain portion of the aromatics mechanism concerns the reactions following OH addition to the aromatic ring (pathway 2 on Figure 22). The OH-aromatic adduct is assumed to react with O_2 either by abstraction to form HO_2 and a phenolic compound (pathway 5), or by addition forming an OH-aromatic-O_2 adduct (pathway 6) that reacts further. The OH-aromatic-O_2 adduct is then assumed to undergo two competing unimolecular reactions, one (pathway 7) involving unimolecular cyclization by O_2 addition to an internal double bond to form a bicyclic radical that then reacts with O_2 to form a bicyclic peroxy radical, which then reacts with NO either to form an organic nitrate (pathways 9) or the corresponding alkoxy radical (pathway 10) that decomposes to ultimately form HO_2, an α-dicarbonyl such as glyoxal (GLY), methylglyoxal (MGLY) or biacetyl (BACL), and a mono-unsaturated dicarbonyl co-product represented by AFG1, AFG2, and (for the updated mechanism) AFG4 model species as

discussed by Carter and Heo (2012). These pathways and measured or estimated product yields are not sufficient to account for all the reaction routes, so it is necessary to assume that the OH-aromatic-O_2 adduct undergoes an additional unimolecular reaction, designated pathway 8 on Figure 22, competing with pathway 7. In SAPRC-07 pathway 8 is assumed to involve formation of OH and a di-unsaturated dicarbonyl product that is represented by the AFG3 model species. This assumption is retained in the updated version of the mechanism. Additional reactions, shown on Figure 22 as pathways A and B within the dashed-line box, were considered in various test calculations discussed by Carter and Heo (2012), but are not part of the final SAPRC-11 mechanism because they are not consistent with laboratory data on dependences of product yields on NO_x (Koch et al, 2007; Nishino et al, 2010 and references therein). This is almost certainly an oversimplification of the actual aromatic ring-opening mechanism and products formed (e.g., see Calvert et al, 2002), but given the current state of information and uncertainties in the mechanism this is considered appropriate for the level of detail and predictive capability of the current gas-phase mechanism. With the additions discussed in the following section, this is also considered sufficient for the predictions of SOA yields.

Figure 22 also shows the two pathways for formation of hydroperoxides from the reactions of peroxy radicals with HO_2 (pathways 1H and 2H). These pathways are not significant to predictions of O_3 formation and found not to be important in predictions of radical levels (unpublished results from this laboratory), but hydroperoxides formed from peroxy radicals formed following OH addition to the aromatic ring (pathway 2H) are believed to be important in predictions of aromatic SOA formation, and therefore need to be represented in the gas-phase mechanism. Hydroperoxide formation is not predicted to be important in the presence of NO_x because the competing reactions of the peroxy radicals with NO (Processes 4, 9 and 10) are believed to dominate, but it is predicted to be a major fate of peroxy radicals when NO_x is absent. As discussed in the following section and also above in the discussion of the SOA yields from the mechanism evaluation experiments, the SOA yields in the mechanism evaluation experiments tend to be higher in experiments carried out in the absence of NO_x, and significant SOA formation from these hydroperoxides is used as the main explanation for this finding. This is discussed further in the following section.

Major revisions were made to the mechanisms for the phenolic products because the SAPRC-07 mechanism, which was developed based on model simulations of a single relatively high concentration o-cresol - NO_x experiment carried out in the 1970's, performed very poorly in simulating the gas-phase reactivity results of all the experiments with the phenolic compounds carried out for this project. In particular, SAPRC-07, significantly underpredicted rates of NO oxidation, O_3 formation, and consumption of phenolic reactants. This is illustrated on Figure 23, which shows experimental and model calculation results for selected o-cresol - NO_x experiments. The results of the other o-cresol - NO_x experiments, and the NO_x experiments with other phenolic compounds, were similar to those shown on Figure 23 for the examples of the new cresol - NO_x runs. Much better simulations were obtained for all experiments except the old experiment EC281 when the yields of photoreactive products were increased and adjusted to fit the rates of NO oxidation and O_3 formation in the newer chamber data. Because of their importance in SOA formation, discussed in the following section, separate model species were derived for phenol (PHEN), cresols (CRES) and xylenols (XYNL), and parameters were optimized to fit the reactivity data in the relevant experiments. This resulted in much better fits to the simulations of the newer experiments with the updated mechanism, as shown on Figure 23, though the reactivity in the old o-cresol - NO_x experiment used to derive the earlier mechanisms was significantly overpredicted. The reason why the evaluation results are so different for the old EC experiment used to derive the previous mechanisms for the cresols is unknown.

The updated aromatics mechanisms were developed and evaluated by conducting model simulations of results of 410 aromatic - NO_x environmental chamber experiments carried out in 9 different environmental chambers at three different laboratories using five different types of light sources.

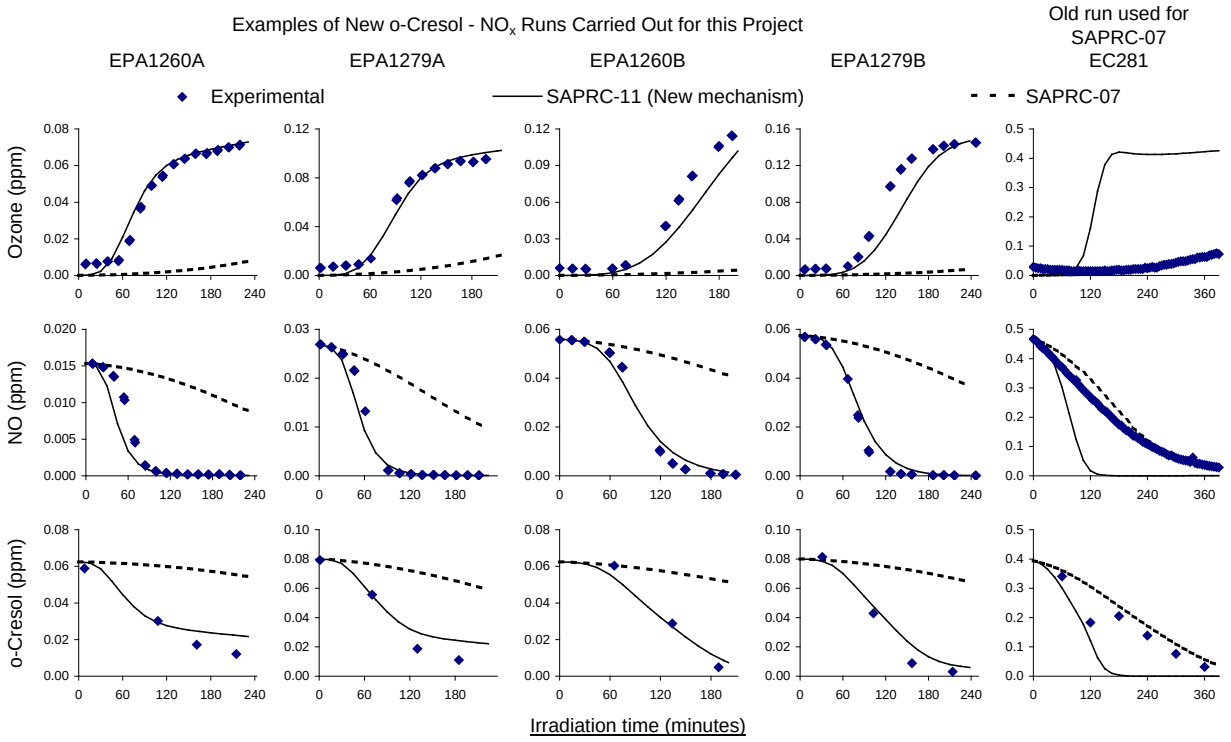

Figure 23. Experimental and calculated concentration-time plots for O_3, NO, and o-cresol for selected o-cresol - NO_x chamber experiments.

Approximately half were new experiments not used when developing SAPRC-07, including data at lower NO_x levels more representative of ambient conditions and involved new compounds, including phenolic products, which had not been experimentally studied previously. These included almost all of the aromatics - NO_x experiments used in this SOA mechanism evaluation study, plus additional aromatics - NO_x experiments that did not have suitable SOA data.

Besides the need to revise the mechanisms for the phenolic compounds, the most significant finding of the SAPRC-11 gas-phase mechanism development and evaluation is that it is not possible for the model to simulate the rates of NO oxidation and O_3 formation over the full range of available NO_x conditions for some important aromatic compounds without adding additional NO_x-dependent processes that were not previously considered in aromatics mechanisms used in airshed models. In order to simulate the data over the full range of NO_x conditions for these compounds, it is necessary to assume that the OH-aromatic adduct formed from compounds reacts with O_2 sufficiently slowly that reaction of the adduct with NO or NO_2 (e.g., processes "A" or "B" on Figure 22) can become competitive at the NO_x levels in the higher NO_x experiments, forming less reactive products. However, this is not consistent with laboratory data and with known dependences of aromatic product yields on NO_x levels (Koch et al, 2007; Nishino et al, 2010 and references therein). Therefore, either there is an inconsistency between the chamber data and the published laboratory results, or there is a different, unknown process that causes this additional NO_x dependence in the chamber experiments. This is applicable to benzene, toluene, ethylbenzene and p-xylene, but not to o- or m-xylene, the trimethylbenzenes and (probably) o-cresol. The data are not sufficient to determine whether it is applicable to the compounds studied.

The SAPRC-11 mechanism used as the basis for SOA modeling in this report does not incorporate these pathways ("A" or "B" in Figure 22) because they are not consistent with the laboratory data as discussed above. This means that this mechanism tends to overpredict rates of NO oxidation and O_3 formation in experiments or environments where NO_x levels exceed ~100 ppb. However, this is probably not a major concern for atmospheric modeling, since NO_x levels are generally lower than this. The SAPRC-11 mechanism gives good simulations not only for NO oxidation and O_3 formation rates at the lower NO_x levels (for which it was optimized), but also for maximum O_3 yields, for which it was not necessarily optimized. It represents a significant improvement over SAPRC-07, which tends to underpredict O_3 formation rates in many of the newer experiments, in this regard. This is probably also not a large concern in most of the SOA mechanism evaluation calculations carried out in this work, where OH radicals were adjusted so that the model would correctly simulate OH radical levels and amounts of aromatic consumption. This is because the occurrence of these additional NO_x-dependent reactions primarily affects predictions of overall radical levels, which are held fixed in most of the SOA yield evaluation calculations.

Although SAPRC-11 performs better than SAPRC-07 in simulating the available chamber experiments at atmospherically relevant NO_x levels, it still has model performance issues and does not satisfactorily simulate all of the results of the available experiments. The mechanisms still systematically underpredicts OH radical levels in the aromatic - NO_x experiments by about ~30% on the average, the model performance for O_3 predictions depends on the aromatic / NO_x ratios for many compounds, and the mechanism still tends to underpredict O_3 at lower reactive organic / NO_x levels in chamber experiments with ambient surrogate experiments, though to a somewhat lesser extent than SAPRC-07. Therefore, although model performance in simulating the available data has improved with this update, it is still not entirely satisfactory.

Test simulations were carried out to assess the effects of mechanism updates on ambient O_3 simulations, using the 1-day box model scenarios used to develop the Carter (1994) reactivity scales. SAPRC-11 was found to give predictions of somewhat higher O_3 concentrations in ambient simulations, with 3-15% higher O_3 in higher NO_x, maximum incremental reactivity (MIR) conditions and ~2% higher O_3 at lower NO_x levels. The ozone impacts under MIR conditions were not significantly affected for non-aromatic compounds, but MIR values for aromatic compounds increased by factors of ~2.5-4 for phenolic compounds, by over a factor of 2 for benzene, by 30-50% for toluene and other monoalkylbenzenes, and by lesser and more variable amounts for other aromatic hydrocarbons. However, use of 3-D models is necessary to completely evaluate the effect of the mechanism updates on ambient simulations.

Complete listings of the species, reactions, and rate parameters used in the gas-phase mechanism that was evaluated in this work are given in Table A-4 and Table A-5 in the Supplementary Materials. These listings also include model species and reactions added for the purpose of predicting aromatic SOA as discussed in the following section. Note that the changes made for predicting SOA did not change the predictions of gas-phase reactions and predictions of O_3, radical levels, NO_x, and other gas-phase species of interest, so in terms of gas-phase predictions this mechanism is substantially the same as that listed and documented by Carter and Heo (2012).

Aromatic SOA Mechanism

Overall Features and General Approach

The approach used to represent SOA formation and its overall level of detail followed that used in the gas-phase mechanism as described previously (Carter, 2010a,b, Carter and Heo, 2012). No attempt was made to explicitly represent all the individual reactions in the uncertain portions of the mechanism that may be important because many of the details are unknown, and such a mechanism would consist

largely of speculation and have more detail than necessary for predictive purposes. Such detail would also provide an illusion of mechanistic knowledge that does not actually exist. Furthermore, if a mechanism has a large number of uncertain parameters (e.g., rate constants, product yields or partitioning coefficients) that affect the SOA predictions of interest, then it would be unclear how to improve the mechanism if the number of parameters that need to be adjusted exceeds the number of parameters that is supported by the available data. It is necessary to make assumptions about relationships between the uncertain parameters that are functionally equivalent to using a condensed mechanism in the first place.

Therefore, the approach used in the SOA mechanism developed in this work is to use only the level of detail that is needed for predictive purposes, and that is supported by the available data and our current understanding of the overall processes involved. This involves employing lumped reactions representing the overall processes that are necessary to simulate the available data and that are consistent with our understanding or estimates of the actual processes that may occur. If two or more processes represented in the model give the same predictions of dependences on reaction conditions or extent of reaction, then they can either be lumped together or one can be used as a surrogate for the others. Processes or products are also lumped if they give similar predictions and there is insufficient information or data available to derive their relative importance.

Figure 24 shows a schematic of the aromatic mechanism showing the overall SOA formation processes that were considered for the mechanism developed for this project. This includes a maximum of 6 overall processes for each aromatic hydrocarbon plus a maximum of 8 for each model species used to represent phenolic products. Each of those lumped processes has up to two parameters that have to be derived or estimated: (1) the yield of the lumped model species representing the condensable product(s), and (2) the equilibrium partitioning coefficient (Kp) to be used for the model species. Ideally, separate model species should be used to represent the phenolic products from each aromatic hydrocarbon because each one forms a different distribution of such products. This would result in up to 14 processes and 28 parameters for each compound, or almost 400 parameters for the 14 different aromatic hydrocarbons studied. Our current knowledge and the available data clearly do not support deriving such many parameters, so further lumping and simplifications are necessary even with this highly lumped approach. Note that although partitioning coefficients in principle can be estimated, the estimates are too uncertain to be useful for predictive model development (e.g., Johnson et al, 2005; Healy et al, 2008), so they must be treated as adjustable parameters.

The various overall processes shown on Figure 24, and the types of reactions they represent, are discussed further below.

Process (p1): Condensable primary hydroperoxides. Either this process or its analogue in the phenolic system (process p1p and/or p1pN) is probably occurring to at least some extent because it is necessary to explain the suppression of SOA yields by NO_x in the chamber experiments. The presence of NO_x suppresses hydroperoxide formation because of the competing reactions of peroxy radicals with NO, but hydroperoxide formation is an important route in aromatic photooxidations when NO_x is absent. The SOA yield data shown on Figure 18 suggest that the SOA yields in the reactions of the phenolic products may not be as dependent on NO_x as is the case for the aromatic hydrocarbons as shown on Figure 17 and Figure 18, so it appears likely that Process p1 is the main reason for this suppression of SOA by NO_x. It is reasonable to assume that hydroperoxides formed in the reaction of HO_2 with aromatic + OH + O_2 + O_2 adduct peroxy radicals that are formed when OH adds to the aromatic ring. However, we assume that hydroperoxides (R6OOH on Figure 24) formed from the reaction of HO_2 with benzyl peroxy radicals (that in turn are formed when OH abstracts a hydrogen atom from the alkyl groups) are much more volatile and do not contribute to SOA formation. If this is assumed, and if it is assumed that all hydroperoxides formed from aromatic + OH + O_2 + O_2 adduct peroxy radicals are condensable, then the yields of the model species representing these hydroperoxides can be derived from the gas-phase

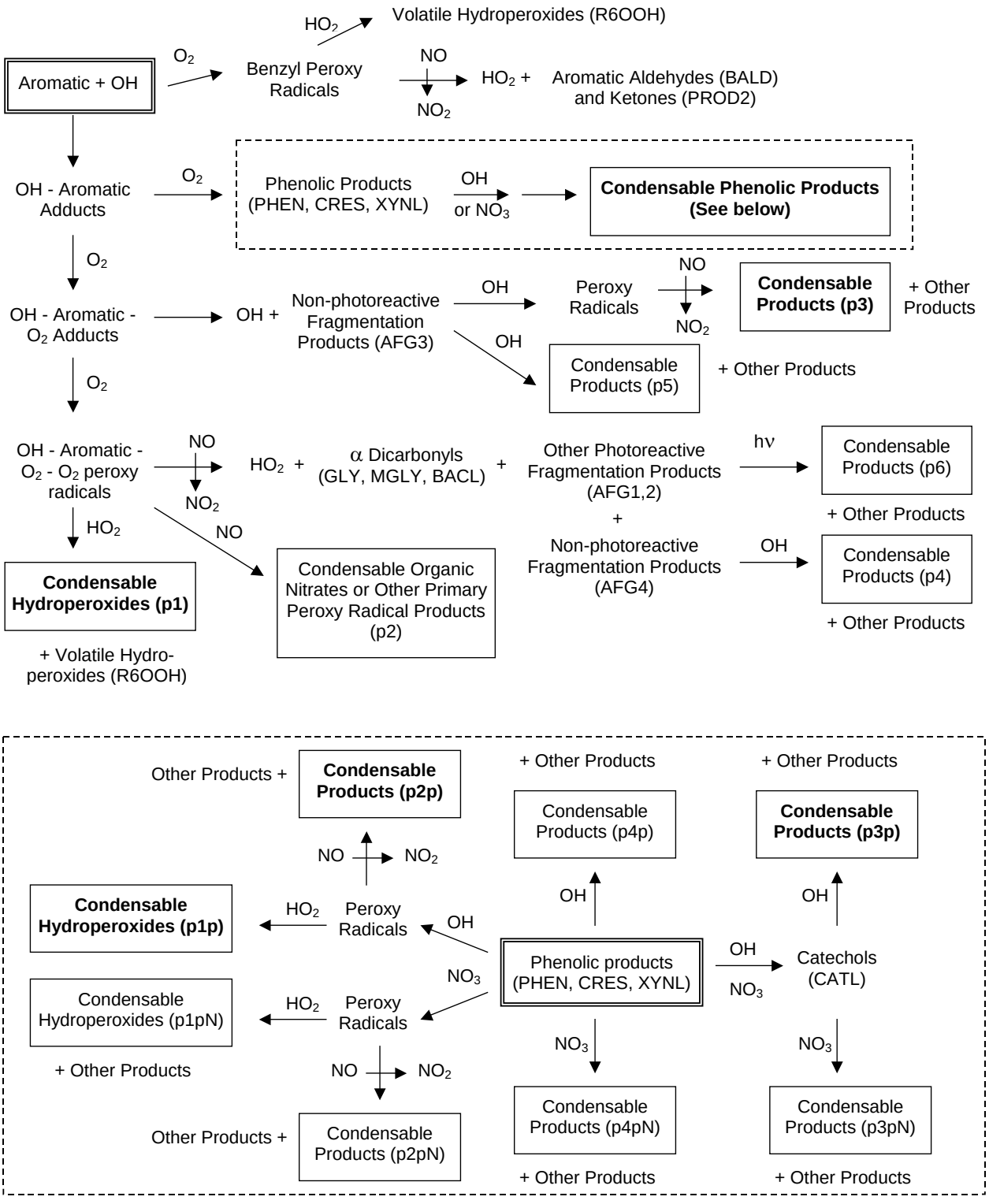

Figure 24. Overall processes considered for SOA formation in the aromatics mechanisms developed in this work. SOA-forming processes are shown in single-solid-line boxes and those that were included in the final version of the mechanism are shown in bold font.

mechanism. However, as discussed below, the mechanism evaluation data cannot be consistently simulated with models using this assumption, and we have to assume that at least some relatively more volatile hydroperoxides (represented by R6OOH in the model) are also formed from peroxy radicals formed following ring addition, and we use the condensable hydroperoxide (RAOOH) yield in process (p1) as an adjustable parameter.

Process (p2): Condensable products formed from primary peroxy radicals. This could represent the formation of condensable organic nitrates formed when the bicyclic aromatic + OH + O_2 + O_2 radical reacts with NO, or formation of other condensable compounds as primary products in the aromatic + OH reaction that involves the reaction of NO_x with peroxy radicals. It is possible that at least some organic nitrates formed from the bicyclic aromatic + OH + O_2 + O_2 adduct might be condensable because of the large number of oxygens on the molecule, as is the case for the hydroperoxide formed when this adduct reacts with HO_2 (process p1). It is also possible that other condensable products are formed as primary products involving the intermediacy of peroxy radicals. Note that this process requires the presence of NO_x to occur, so it differs from the other possibility discussed next. Note also that all the other non-hydroperoxide processes (p4-p6, p2p-p4p, and p2pN-p4pN) represent formation of condensable products as secondary or in some cases tertiary reactions of aromatic products, so SOA formation from this process would have a different dependence on extent of reaction than the others.

Condensable primary products whose formation do not depend on NO_x (not shown on Figure 24). Formation of condensable products in the reactions in the initial reactions of the aromatic hydrocarbons is also a possibility. Using this process in the model should give similar results as using process (p2), with somewhat lower yields for condensable hydroperoxide formation (process p1) needed to fit the data because this process, unlike (p2), also predicts SOA formation in the absence of NO_x. This process is not included in Figure 24 because it is expected that hydroperoxides and possibly organic nitrates would be the only potentially significant SOA-forming process in the initial reactions

Processes (p3) and (p4): Condensable products formed from peroxy radicals formed in secondary OH radical reactions of non-phenolic products. These processes represent possible formation of condensable products through reactions of peroxy radicals formed from reactions of second generation products other than phenolics. (Processes involving SOA formation from phenolics are represented separately as discussed below.) As with (p2), these require the presence of NO_x to occur. Processes (p3) and (p4) are similar in terms of predictions of effects of reaction conditions on SOA formation, since the overall processes for each involve the intermediacy of a peroxy radical. Process (p3) represents formation of SOA from peroxy radicals formed from reactions of oxidation products whose formation is independent of NO_x, such as compounds represented by the model species AFG3 in the mechanism. Process (p4) represents formation of SOA from NO_x-independent reactions of compounds whose formation involves the reaction of peroxy radicals with NO, such as those represented by the model species AFG4. Use of process (p3) with AFG3 as the intermediate is preferred because AFG3 is formed from all aromatics in the gas-phase mechanism used in this work (Carter and Heo, 2012), while AFG4 is only used in the mechanisms for 1,4-disubstitued benzenes such as p-xylene. Process (p3) is used in the baseline mechanism because as discussed below assuming that this is the major non-phenolic process forming SOA in the presence of NO_x gives somewhat better fits to some aspects of the mechanism evaluation data than assuming other processes of this type (i.e., p2, and p4-p6) dominate.

Process (p5): Condensable products formed in secondary reactions that are independent of NO_x. This could represent the formation of primary condensable products through NO_x-independent reactions of OH radicals with compounds whose formation does not depend on NO_x. This was considered as an alternative to process (p2) or (p3) in the mechanism, but was not adopted because assuming it is the major non-phenolic process involving SOA formation in the presence of NO_x results in overpredictions of SOA yields in the benzene - H_2O_2 experiments even if it is assumed that condensable hydroperoxide formation

from this compound is negligible. However, the data for m-xylene and most other aromatics could be fit equally well using this process in place of process (p2) or (p3).

Process (p6): Condensable products formed in the photolysis of photoreactive aromatic products. Significant formation of photoreactive products other than the observed α-dicarbonyls must be assumed in aromatic photooxidations since otherwise the models will significantly underpredict rates of NO oxidation and O_3 formation. This process represents the possible formation of condensable materials in these rapid photolysis reactions. This process was considered in preliminary sensitivity calculations where effects of various alternatives were examined, but results of model simulations were either very similar to, or not quite as good as, simulations using only process (p2) to represent SOA formation processes from reactions of non-phenolic products in the presence of NO_x. Therefore, this process was not considered further.

Condensable products formed in the reactions of O_3 with aromatic products (not shown on Figure 24). Some of the aromatic photooxidation products may also react with O_3 to some extent, so formation of condensable products from those reactions is also a possibility. This was considered in preliminary model simulations, but was rejected because assuming it is important did not give good fits to the data. For example, this process predicts higher SOA formation in experiments where CO or another reactive compound are added to aromatic - NO_x irradiations because of their higher ozone levels, which was opposite to what was found experimentally.

Representation and lumping of phenol model species. Experiments with the phenolic products indicate that secondary reactions of these products are very important SOA sources in the reactions of the aromatic hydrocarbons, though as discussed below they are not the only significant SOA precursors formed from non-phenolic aromatics. Therefore, SOA from phenolic products are represented separately and not lumped with the other processes discussed above. Although in principle separate model species should be used to represent the distribution of phenolic products from each aromatic hydrocarbon, this is not possible in practice because there are insufficient data to evaluate SOA forming mechanisms for all the relevant phenolic isomers. In addition, for some aromatic hydrocarbons the exact distributions of phenolic isomers formed are unknown or highly uncertain. Therefore, we lump all phenol isomers with the same molecular weights together based on the assumption that molecular weights should be a major factor affecting SOA formation from a homologous series of compounds that react similarly. Based on this, we represent phenol explicitly using the PHEN model species, use a CRES model species to represent all cresol isomers formed from toluene, and a XYNL model species to represent phenolic products from the xylenes and higher molecular weight aromatic hydrocarbons. There are no data to evaluate SOA mechanisms for C_{9+} phenols, so we use the XYNL species derived using data for C_8 phenols for C_{9+} phenols. Furthermore, we use the chamber data for 2,4-dimethylphenol, one of the two isomers formed in the highest yield for m-xylene (Calvert et al, 2002) and for which there are the most chamber data, to derive the mechanism used for the lumped XYNL species.

Process (p1p): Condensable hydroperoxides from reactions of OH radicals with phenols. The extent to which peroxy radicals are involved in the reactions of phenolic compounds is uncertain, and the highly simplified and parameterized mechanisms used to represent these reactions in SAPRC-11 provide no guidance in this regard. However, if peroxy radicals are involved then they would be expected to form hydroperoxides when they react with HO_2 radicals under low NO_x conditions, and if the hydroperoxides formed from the aromatic hydrocarbons have sufficiently low volatility to be condensable, one would expect the hydroperoxides formed in analogous reactions of the phenols, which have an additional OH group, to be even more condensable. Therefore, the possibility of condensable hydroperoxides formed in reactions of phenolic products is considered, with their yields and partitioning coefficients derived based on simulations of the chamber data.

Process (p3p): Formation of condensable products from the reactions of OH with catechols. Catechols (dihydroxybenzenes) are known products of these reactions of the reactions atmospheric reactions of phenolic compounds (Olariu et al, 2002; Berndt and Böge, 2003). It is also known that catechols react very rapidly with OH and NO_3 radicals (Olariu et al, 2000, 2004) and form high yields of SOA when they react with OH (Nakao et al, 2011a). For that reason, a catechol model species (CATL) was added to the SAPRC-11 aromatics mechanism (Carter and Heo, 2012), and formation of condensable products in its subsequent reactions with OH and NO_3 radicals is added to the aromatic SOA mechanism developed in this work. The yields of catechols in OH and NO_3 reactions have been measured but vary from compound to compound and for simplicity we assume the same yield regardless of the phenolic precursor and the same yield for both the OH and NO_3 reactions (Carter and Heo, 2012 A yield of 70% is assumed based on dihydroxybenzene yields reported by Olariu et al (2002) and Berndt and Böge (2003) for phenol and cresol isomers. The yields of the model species representing the condensable products in the catechol reactions are derived based on the model simulations of the chamber data as discussed below.

Processes (p2p and p4p): Condensable primary products from reactions of OH with phenols. These represent the possible formation of condensable products as primary products in the reactions of OH from phenols, rather than as secondary products through reactions of catechols. Process (p2p) involves the intermediacy of peroxy radicals and requires NO_x to be significant, while process (p4p) is independent of NO_x. However, the predictions of these two processes are not sufficiently different in terms of simulations of the available chamber experiments to allow us to distinguish between them, so we only consider process (p2p) for the mechanism primarily for convenience. (It is easier to derive its yield that best fits the data independently of the yield derived for condensable hydroperoxide formation p1p.) The effect of this process on SOA formation is also not sufficiently different from that of the process representing SOA formation from the catechols (p3p) if the optimization is being done for only a single compound. However, the SOA yields in the presence of NO_x are sufficiently different for phenol, o-cresol, and 2,4-dimethylphenol that it is not possible to use only process (p3p) without assuming that catechol yields from the different compounds vary in a way that is not consistent with the data of Olariu et al (2002). Therefore, we use both (p2p) and (p3p) to represent formation of SOA from the reactions of phenolics in the presence of NO_x, with (p3p) being adjusted to fit the data from the phenolic compound best fit with the lowest parameter values (phenol), and (p2p) being adjusted as needed to predict sufficient SOA from the other phenolic compounds.

Processes (p2pN, p3pN, and p4pN): Condensable products from reactions of NO_3 radicals with phenols or catechols. These correspond to processes (p2p) through (p4p) discussed above, except that they come from the reactions of the phenolic compounds or catechols with NO_3 radicals rather than with OH radicals. Because of lack of data to estimate SOA yields separately for the OH and NO_3 reactions, in initial versions of the mechanisms we assumed that yields of the SOA processes were equal for both reactions, However, as discussed below, this was found to result in consistent biases towards overpredicting SOA formation from aromatic - NO_x experiments where CO or a reactive non-aromatic VOC was added. Better fits to the data for those experiments are obtained if we assume that SOA formation from reactions of NO_3 with phenols or catechols are negligible.

Listing of SOA Model Species, Parameters, and Mechanism

A list of the model species used in the aromatic SOA mechanism developed in this work is given in Table 7. That table also has a discussion of the roles that the various model species have in SOA formation in the aromatics mechanisms, including those that were considered as SOA precursors but not represented as such in the final mechanism. These model species were used in a number of alternative SOA mechanisms that were considered in this work, with varying assumptions concerning which of the alternative processes discussed above account for SOA formation in the presence of NO_x, and varying assumptions concerning magnitudes of partitioning coefficients. The alternative mechanisms whose

Table 7. List of model species used in the SAPRC-11 gas-phase aromatics mechanism and the model species added to represent aromatic SOA formation.

Species	Represents	Discussion of role in SOA mechanism
Aromatic hydrocarbons		
BENZENE TOLUENE C2-BENZ M-XYLENE O-XYLENE P-XYLENE N-C3-BEN I-C3-BEN M-ET-TOL O-ET-TOL P-ET-TOL 123-TMB 124-TMB 135-TMB	Benzene Toluene Ethyl Benzene m-Xylene o-Xylene p-Xylene n-Propyl Benzene Isopropyl Benzene m-Ethyl Toluene o-Ethyl Toluene p-Ethyl Toluene 1,2,3-Trimethyl Benzene 1,2,4-Trimethyl Benzene 1,3,5-Trimethyl Benzene	These 14 aromatic hydrocarbons are those for which environmental chamber data were available to us to derive and evaluate aromatic SOA mechanisms. Each is represented separately in the model calculations described in this work, and each have their own assigned rate constants and product yield parameters, derived based on data available in the literature and adjustments to fit chamber data as documented by Carter and Heo (2012). The SAPRC-11 aromatic mechanism also includes separate representations and mechanistic parameters for other types of aromatic hydrocarbons, but SOA parameters were not derived for them in this work because of lack of suitable available data. Recommendations on how to represent SOA formation from lumped aromatic model species used in airshed models are discussed later in this report.
Aromatic oxidation products in gas-phase mechanism (See Carter and Heo, 2012, for documentation)		
BALD PROD2	Benzaldehyde, tolualdehydes and other aromatic aldehydes. Aromatic ketones such as methyl phenyl ketone. Also used for ketone products from non-aromatics	These model species are used to represent aromatic ring-retaining products formed when OH abstracts an H atom from alkyl groups off the aromatic rings. The reactions of these compounds may form SOA but this is assumed not to be important in the current mechanism
RNO3	Organic nitrates formed from peroxy + NO reactions (both aromatic and non-aromatic)	The organic nitrates formed in the reactions of the OH-aromatic-O_2-O_2 bicyclic peroxy radicals with NO might be expected to have low volatility, and this possibility is represented by process (p1) in Figure 24. However, as discussed below, assuming that this is an important SOA forming process in the presence of NO_x does not result in satisfactory simulations of the chamber data, so this is not represented as a SOA precursor in the present mechanism.
PHEN CRES XYNL	Phenol Cresols (o-, m- and p-) Xylenols and all C_{8+} phenols	Highly condensed and parameterized gas-phase mechanisms derived and adjusted to fit O_3 formation and other results of phenol, cresol, and xylenol - NO_x chamber experiments as described by Carter and Heo (2012). The reactions of these compounds are believed to be important SOA precursors, and products added to their reactions to represent SOA formation are discussed below.

Table 7 (continued)

Species	Represents	Discussion of role in SOA mechanism
CATL	Catechols (dihydroxybenzenes)	Represented as a separate model species because reactions of catechols are believed to be important in aromatic SOA formation. The way their reactions are represented in the model also affects gas-phase model simulations, so they are considered part of the gas-phase mechanism. Their simplified and highly parameterized mechanism was derived as discussed by Carter and Heo (2012).
NPHE	Nitrophenols and other nitrogen-containing and aromatic ring-retaining products.	Used to represent the primary products formed from phenoxy radicals in the presence of NO_x. Phenoxy radical formation is assumed in the parameterized mechanisms for the phenolic compounds (Carter and Heo, 2012), so these are important secondary products from phenols. Although their subsequent reactions may well involve SOA formation, SOA formation from NPHE is not represented in this mechanism. Any SOA formation that occurs from nitrophenols is represented by other processes.
GLY MGLY BACL	Glyoxal Methyl and other alkyl glyoxals Biacetyl and other α-diketones	Glyoxal and other α-dicarbonyls was proposed to be involved in SOA formation under humid conditions (Kalberer et al, 2004; Healy, 2008; Kamens et al, 2011). However, our recent study indicates SOA formation from glyoxal uptake was negligible in aromatic SOA formation even under humid conditions (RH less than 80%) in our experimental setup (Nakao et al., 2011b). Therefore, it is reasonable to assume these α-dicarbonyl species do not account for the SOA formation significantly, especially since all carried out under dry conditions.
AFG1 AFG2	Photoreactive monounsaturated dicarbonyl aromatic ring opening products and other unknown photoreactive aromatic ring opening products. AFG1 represents species whose photolysis forms radicals, while AFG2 represents those that photolyze to form non-radical products.	Total yields derived based on measured or estimated yields of their α-dicarbonyl co-products, with the AFG1/AFG2 yield ratios optimized based on model simulations of aromatic - NO_x chamber experiments, including the aromatic - NO_x experiments used in this project (Carter and Heo, 2012). The possibility of SOA formation from the reactions of these compounds is considered as process (p6) in Figure 24, but this process is not included in the final mechanism developed in this work. Instead, they are lumped with SOA formation from species represented by AFG3 (process p3).
AFG4	Monounsaturated 1,4-diketones.	Yield derived from measured or estimated yield of their α-dicarbonyl co-products. Assumed to be non-photoreactive. If their reactions form SOA precursors, they are lumped with SOA formation from products represented by AFG3.

Table 7 (continued)

Species	Represents	Discussion of role in SOA mechanism
AFG3	Di-unsaturated dicarbonyl ring opening products and/or other uncharacterized ring opening products that do not have α-dicarbonyl co-products. Assumed not to be photoreactive but to react rapidly with OH and non-negligibly with O_3.	Used to represent products formed in pathways other than abstraction from alkyl groups, formation of phenolic products, or ring-fragmentation to form α-dicarbonyls, so the total AFG3 yields depend on measured or estimated yields for all the other pathways, and are not adjusted. A separate model species, AFG3C, (discussed below) is used to represent only SOA formation from species represented by AFG3 in models where this is assumed.
R6OOH	Volatile hydroperoxides formed from peroxy + HO_2 reactions.	This is used to represent hydroperoxides that do not participate in SOA formation. Used in the gas-phase mechanism as developed by Carter and Heo (2012) to represent hydroperoxides formed from non-aromatic reactions and also from peroxy radicals formed following OH abstraction from alkyl groups of aromatics. However, as discussed below in this work it was found that assuming all hydroperoxides formed following addition of OH to the aromatic rings did not correctly simulate SOA formation in the chamber experiments, and it was necessary to assume that some hydroperoxides formed in these reactions did not form SOA. The mechanism was therefore revised to use the R6OOH model species to represent the non-SOA-forming fraction of the aromatic hydroperoxides, which was adjusted to fit the chamber data.
RAOOH	Condensable hydroperoxides formed in reactions of OH-aromatic-O_2-O_2 bicyclic peroxy radicals with HO_2.	The hydroperoxides formed following OH addition to the aromatic rings are represented by separate model species in the gas-phase mechanism because they are expected to be SOA precursors. Their yields are determined based on the measured or estimated yields of the α-dicarbonyls assumed to be formed when these peroxy radicals react in the presence of NO_x, and therefore strictly speaking should not be adjustable parameters. However, as discussed below, using RAOOH yields derived based on the gas-phase mechanism did not result in satisfactory simulations of SOA formation in the mechanism evaluation experiments, and it was necessary to use lower RAOOH yields to fit the SOA data if RAOOH is represented as condensable. The yields of R6OOH are increased in the model to offset the adjusted reduction of RAOOH yields.

Table 7 (continued)

Species	Represents	Discussion of role in SOA mechanism
<u>Steady state chemical operator species used in gas-phase mechanism</u> [a]		
xPROD (e.g., xBALD) yR6OOH yRAOOH zRNO3	Formation of the product when peroxy radicals react with NO or otherwise form the corresponding alkoxy radical Formation of a hydroperoxide when peroxy radicals react with HO_2. Formation of the organic nitrate model species when peroxy radicals react with NO.	These chemical operators are used in the SAPRC-07 mechanism to represent the net effects of peroxy radical reactions without having to add separate model species and peroxy + peroxy reactions for each type of peroxy radical that needs to be represented in the mechanism, and this approach is retained in the SAPRC-11 aromatics mechanism. See Carter (2010a,b) for a more complete discussion of this approach. For SOA predictions the primary utility is more accurate representation of SOA precursor yields under low NO_x conditions than the more condensed approach used for SAPRC-99 (Carter, 2000) and other mechanisms.
<u>Species added solely for SOA Predictions</u> [b]		
PMmass	Sum of all species in the condensed phase (see Table 2)	Total mass of species in the condensed phase. Calculated in units of $\mu g/m^3$. Equal to pmCNDp2p + pmCNDp2 + pmRAOOH + pmRAOOHp + pmCNDW converted to mass units.
CNDp2 pmCNDp2	Gas and particle phase forms of condensable compounds formed from reactions of aromatics hydrocarbons, or their non-phenolic products, in the presence of NO_x CNDp2 is used for the species in the gas phase, and pmCNDp2 is used for the species in the particle phase	These are used as the model species representing the condensable products formed in processes (p2-p7) on Figure 24. Only one set of condensable model species is needed for these because it is not possible to derive separate yields for all these processes, and only one process is used for all the others in the various alternative mechanisms that are considered in this work. The yields and approximate magnitude of the partitioning coefficient, KpCNDp2 are derived based on the simulations of the chamber data as discussed below. The yields vary from compound to compound and are given on Table 9. The simulations indicate that a KpCNDp2 value of 0.04 $m^3/\mu g$ is reasonably consistent with the data, and this is used in the model unless indicated otherwise. A molecular weight of 187.17 grams/mole, based on m-xylene + OH + 2 O_2, is used for the predictions of mass of PM formed. (See Note [c]) The gas-phase reactions of CNDp2 are neglected, so the formation of CNDp2 does not affect gas-phase predictions.
xCNDp2 [a]	Formation of CNDp2 following reactions of peroxy radicals with NO	This is needed for processes (p2), (p5), and (p6), which involves formation of SOA following reactions of peroxy radicals with NO. See Note [a].

Table 7 (continued)

Species	Represents	Discussion of role in SOA mechanism
AFG3C	Aromatic products that react with OH to form condensable products.	This is used to represent SOA formation from the reactions of AFG3 in model simulations representing processes (p4) or (p5) on Figure 24. It is used as a separate model species with 100% yield of the condensable species CNDp2 (for process p5) or its precursor xCNDp2 (for process p3) in the OH reaction. Its yield adjusted for each aromatic hydrocarbon, rather than adjusting the CNDp2 or xCNDp3 yield in the AFG3 reactions and requiring separate AFG3 species for each. AFG3C is representing as being consumed by gas-phase reactions with the same rates as AFG3 but with the reactions having no net effect other than formation of CNDp2 in either the OH reaction.
CNDp2p pmCNDp2p	Condensable compounds formed when phenolic compounds or catechols react with OH or NO_3 CNDp2p used for gas phase and pmCNDp2p used for particle phase forms.	Added to the mechanism for the purpose of SOA predictions from the reactions of phenolic compounds and catechols (processes p2p-p4p and p2p-p4pN on Figure 24). There are insufficient data to derive parameters for separate model species for each process, so this one set of species is used for all condensable products formed from phenolics in the presence of NO_x. The yields and approximate magnitude of the partitioning coefficient, KpCNDp2p are derived to simulate SOA formation in the experiments with phenol, o-cresol, and 2,4-dimethyl phenol as discussed in the text. The yields are given in Table 8. The model simulations indicate a KpCNDp2p of 0.03 $m^3/\mu g$ is reasonably consistent with the data, and this is used in the model unless indicated otherwise. A molecular weight of 157.19 grams/mole, based on m-xylene + 3 OH, is used for the predictions of mass of PM formed. (See Note [c]) The gas-phase reactions of CNDp2p are neglected, so the formation of CNDp2 does not affect gas-phase predictions.
RAOOH pmRAOOH	Gas and particle phase forms, respectively, of condensable hydroperoxides formed from aromatic hydrocarbons.	See above for a discussion of the use of RAOOH in the gas-phase mechanism. This is used to represent formation of condensable hydroperoxides in the reactions of aromatic hydrocarbons (processes p1 on Figure 24). The yields are adjusted for each aromatic hydrocarbon based on simulations of the chamber data as discussed below, and the yields derived are summarized on Table 9. As discussed in the section above on PM formation in the mechanism evaluation experiment,

Table 7 (continued)

Species	Represents	Discussion of role in SOA mechanism
		the SOA yields in the aromatic - H_2O_2 experiments indicate that the partitioning coefficient, KpRAOOH, should be 0.02 $m^3/\mu g$, and this is used in the primary SOA model developed in this work. However, as discussed below, models that assume that KpRAOOH is 0.1 $m^3/\mu g$ fit the data with less overall bias. A molecular weight of 188.18 grams/mole, based on that for m-xylene + OH + O_2 + HO_2, is used for calculation of PM mass (see Note [c]). The SAPRC-11 mechanisms, like SAPRC-07, include gas-phase reactions of RAOOH. These reactions are retained in the aromatic SOA mechanisms.
RAOOHp pmRAOOHp yRAOOHp	Gas and particle phase forms, respectively, of condensable hydroperoxides formed from phenolic products. Formation of RAOOHp when peroxy radicals react with HO_2 (see Note [a]).	Used to represent formation of condensable hydroperoxides for those phenolic products (process p1p on Figure 24). It is represented by a separate model species than RAOOH because the condensable hydroperoxides from the phenolic compounds are expected to be less volatile than those from the aromatic compounds, and also because it allows tracking the fraction of aromatic SOA that is due to reactions of the phenolic products. The yields are adjusted for each model species based on model simulations of SOA in the phenol, o-cresol, or 2,4-dimethyl phenol - H_2O_2 experiments, and are summarized in Table 8. It is assumed that these hydroperoxides are non-volatile since that gave satisfactory simulations of the data, the data are insufficient to derive a partitioning coefficient, and it is expected the these would be less volatile than the compounds represented by RAOOH A molecular weight of 205.19, based on that for m-xylene + 2 OH + O_2 + HO_2, is used for calculation of PM mass (see Note [c]). The gas-phase mechanism used for RAOOHp was the same as that for RAOOH, so the only difference is that the condensation reaction forms the model species pmRAOOHp rather than pmRAOOH, so they could be lumped together in the gas-phase mechanism.
CNDW pmCNDW	Gas and particle phase forms of condensable species formed from contaminants off-gassed from the chamber walls.	As discussed in the Characterization Results section, it is necessary to assume that condensable species are formed in the reactions of OH radicals from unknown contaminants off-gassed from the chamber walls, whose off-gassing rates are adjusted based on model simulations of background characterization experiments.

Table 7 (continued)

Species	Represents	Discussion of role in SOA mechanism
		The molecular weight is arbitrarily set at 200 grams/mole for calculation of background PM mass.

[a] See Carter (2010a,b) for a discussion of these chemical operators. It is recommended that the steady state approximation be used for these xPROD and yPROD species when the mechanism is implemented in models.

[b] The formation and reaction of these species do not affect predictions of other gas-phase species and can be removed from the mechanism if SOA predictions are not of interest.

[c] The most appropriate molecular weight is uncertain and would vary depending on the compound. However, errors in the molecular weights of the condensable model species are compensated for, at least in part, by opposite errors in yields that are adjusted to fit the PM volume (i.e., mass) data.

results are presented in this report, and the processes used to represent SOA formation in the presence of NO_x, are summarized in Table 8. In addition to the partitioning coefficients, Table 8 also shows the SOA yield parameters used for m-xylene, which was used for most of the calculations evaluating the alternative mechanisms because that compound was most comprehensively studied. (The parameters for the other aromatic hydrocarbons are given later in this section.) In addition, Table 9 gives the SOA formation parameters used in the alternative mechanisms examined for the phenolic species. The parameters derived for the baseline mechanism are assigned based on the results of the test calculations that are described in the Mechanism Evaluation Results section, below. A complete listing of all the model species and the aromatic reactions in baseline mechanisms are given in Table A-4 and Table A-5 in the Supplementary Materials section of this report. All the aromatic reactions and rate parameters that affect only gas-phase species, and all the reactions of the non-aromatic species, are based on those given by Carter and Heo (2012).

Summary of Alternative Mechanisms

Table 8 lists the alternative mechanisms that were examined whose calculation results are described in this report These were examined in test calculations with m-xylene and the selected representative phenolic compounds to evaluate which set of assumptions and partitioning coefficient (Kp) values was most consistent with the chamber data, and to determine what is the most appropriate for use for the baseline mechanism. These alternative mechanisms are summarized below.

Mechanism "A": Baseline mechanism. This is the mechanism selected as the recommended mechanism developed for this project because the alternatives examined either showed worse biases or other problems, or gave similar results. However, as discussed in the Mechanism Evaluation Results section, below, this mechanism is not without biases and problems, and clearly significant room for further improvement exists. Furthermore, as discussed below this mechanism did not have the lowest overall errors, though the mechanism with somewhat lower error was rejected because of greater bias problems (see the first section in the Mechanism Evaluation Results section for definitions of bias and error as used in this report). The yields and (in most cases) the partitioning coefficients for the model species representing SOA formation processes were derived based on results of test calculations for m-xylene and the representative phenolic compounds phenol, o-cresol, and 2,4-dimethylphenol as discussed below. The one exception to this was the partitioning coefficient for the condensable hydroperoxide formed from the phenolic compounds, RAOOHp, which was assumed to be non-volatile because of lack

Table 8. List of SOA mechanisms that are discussed in this report, their partitioning coefficients, and the yield parameters used in the sensitivity calculations.

ID	Description	Partitioning Coefficients ($m^3/\mu g$) [a]			Yield Parameters for m-Xylene [b]		
		(p1)	(p2, p3)	(p2p, p3p)	y^{rel}(p1)	y(p2)	y(p3)
A	Baseline Mechanism	0.1	0.04	0.03	32%	-	7.0%
B	Non-volatile CNDp2p	n/a [c]		Nvol		n/a [c]	
C	Low KpRAOOH	0.02	0.04	0.03	98%	-	7.3%
D	Non-volatile KpRAOOH	Nvol	0.04	0.03	12%	-	4.7%
E	Low KpCNDp2	0.1	0.02	0.03	17%	-	9.3%
F	High KpCNDp2	0.1	0.1	0.03	22%	-	3.3%
G	Process (p2) instead of (p3)	0.1	0.04	0.03	32%	6.0%	-
H	SOA from NO_3 (p2pN, p3pN)	0.1	0.04	0.03	32%	-	4.5%
I	Wall Absorption of Semi-Volatiles	0.1	0.04	0.03	28%	-	14.0%

[a] Processes indicated in Figure 24 that are affected by the partitioning coefficient are indicated in the column header. The affected model species are as follows: (p1): RAOOH, (p2 or p3): CNDp2; (p2p or p3p): CNDp2p. "NVol" means that the model species was treated as non-volatile in the simulations, or a Kp of 100 $m^3/\mu g$, which gives essentially the same result as non-volatile, was used. Note that RAOOHp, the model species used to represent process (p1p) on Figure 24, is assumed to be non-volatile in all the mechanisms, so it is not included on the table.

[b] Yield parameters shown are as follows, where the processes are as indicated in Figure 24: y^{rel}(p1): Yield of RAOOH that gives best fits of model to SOA data in the m-xylene experiments, relative to RAOOH yield in the gas-phase mechanism; y(p2): xCNDp2 yield in the OH + m-xylene reaction; y(p3): AFG3C yield in the m-xylene + OH reaction. These parameters were derived by minimizing average biases in model simulations of PM volume in the m-xylene - NO_x and m-xylene - H_2O_2 chamber experiments. Predictions of SOA formation in the m-xylene - H_2O_2 experiments were primarily sensitive to yrel(p1) but were also affected by y(p3) in the "C" and "D" mechanisms, while the SOA in the aromatic - NO_x runs were primarily affected by y(p2) and y(p3).

[c] Mechanism B was only used in simulations of experiments with phenolic compounds.

of data to derive a specific value and because this gave adequate simulations of the data for phenolic compounds. As shown on Table 8, the other partitioning coefficients used in the baseline mechanism were 0.1 $m^3/\mu g$ for RAOOH, 0.04 $m^3/\mu g$ for CNDp2 and 0.03 $m^3/\mu g$ for CNDp2p. All the other mechanisms discussed below use the same partitioning coefficients as this baseline mechanism except for the coefficient that was being varied, where applicable.

Mechanism "B": Baseline with non-volatile CNDp2p. This mechanism is used to show the effect of using a higher partitioning coefficient for the model species CNDp2p, which is used to represent SOA formation from phenolic compounds in the presence of NO_x. The results are not highly sensitive to this parameter, so an extreme assumption that CNDp2p is non-volatile is used for the purposes of showing the sensitivity of the results to alternative assumptions concerning this parameter.

Mechanisms "C" and "D": Baseline mechanism with varying hydroperoxide (RAOOH) partitioning coefficients. These mechanisms were used to determine the magnitude of KpRAOOH that gave the least bias in the simulations of the m-xylene - H_2O_2 experiments. Mechanism "C" used a low

Table 9. List of parameters used to represent SOA formation from the reactions of aromatic hydrocarbons.

Compound Yield and Process	Phenol (PHEN)	Cresols (CRES)	Xylenols (XYNL)	Catechols (CATL)
Baseline mechanisms (KpCNDp2p = 0.03 m3/mg) (Mechanisms A and C-G)				
Yield of yRAOOHp in the OH reactions (p1p)	2%	4%	21%	-
Yield of CNDp2p in the OH reactions (p3p)	-	-	-	33%
Yield of xCNDp2p in the OH reactions (p2p)	-	10%	12%	-
Mechanism with non-volatile CNDp2p (B)				
Yield of yRAOOHp in the OH reactions (p1p)	1%	4%	23%	-
Yield of CNDp2p in the OH reactions (p3p)	-	-	-	20%
Yield of xCNDp2p in the OH reactions (p2p)	-	10%	10%	-
Mechanism with SOA from Both OH and NO_3 + Phenols and Catechols (H)				
Yield of yRAOOHp in the OH, NO_3 reactions (p1p, p1pN)	4%	5%	20%	-
Yield of CNDp2p in the OH, NO_3 reactions (p3p, p3pN)	-	-	-	27%
Yield of xCNDp2p in the OH, NO_3 reactions (p2p, p2pN)	-	10%	14%	-
Mechanism with Wall Absorption of Semi-Volatiles (I)				
Yield of yRAOOHp in the OH reactions (p1p)	3%	3%	18%	-
Yield of CNDp2p in the OH reactions (p3p)	-	-	-	45%
Yield of xCNDp2p in the OH reactions (p2p)	-	9%	11%	-

[a] These yield parameters were derived by minimizing biases in model simulations of the phenol - NO_x, phenol - H_2O_2, o-cresol - NO_x, o-cresol - H_2O_2, 2,4-dimethylphenol - NO_x, and 2,4-dimethylphenol - H_2O_2 chamber experiments. The yield parameter for process (p3p) from catechols was derived from simulations of the phenol - H_2O_2 experiments because assuming any SOA from the other processes results in overprediction of SOA when modeling these runs in models with no biases in simulations of SOA from the phenol - NO_x experiments. The yields for (p1p) for the o-cresol and the 2,4-dimethylphenol were then increased as needed to simulate the SOA yields in the H_2O_2 experiments with these compounds, and the yields for (p2p) were then adjusted to simulate SOA in the phenolic - NO_x experiments.

value of 0.02 $m^3/\mu g$ for this parameter, which is the same as that derived using the 1-product analysis of the m-xylene - H_2O_2 experiments as discussed in the experimental results section, above. The yields of RAOOH from m-xylene that fit the SOA data are the same as predicted using the gas-phase mechanism, making this mechanism highly chemically reasonable, at least for m-xylene. However, this may not be the case for other VOCs, since as shown on Table 10, the RAOOH yields that fit the data in the baseline mechanism relative to the predicted gas-phase tended to be low for m-xylene compared to other aromatic hydrocarbons. An adjusted RAOOH yield that is higher than the predicted gas-phase value seems to be less chemically reasonable to us than one that is lower. In addition, using this low Kp value resulted in much more scatter and more biases in the simulations of the m-xylene experiments than was the case for the mechanism that used the higher Kp values for RAOOH. Mechanism "D" examined the other extreme and assumed that RAOOH is non-volatile[2]. As discussed below, this mechanism actually gives somewhat lower average model errors than the baseline mechanism, but it also has significantly larger biases, so it

[2] The calculations actually used a partitioning coefficient of 100 $m^3/\mu g$, which is sufficiently high that the it gave the same result. This is also applicable to Mechanism F.

was not adopted for this reason. It was found that using the Kp value of 0.1 $m^3/\mu g$ fit the data with smaller overall biases and only slightly larger average error than the non-volatile RAOOH mechanism, so this value was adopted for use in the baseline mechanism. However, the simulations were not highly sensitive to changes in this parameter, so the exact value used in the model is somewhat arbitrary.

Mechanisms "E" and "F": Mechanisms with varying KpCNDp2. These mechanisms are used to show the effects of using different partitioning coefficients for the CNDp2 model species that is used to represent SOA formation from aromatic hydrocarbons in the presence of NO_x that is not attributed to reactions of phenolic compounds. Mechanism "E" used a low value of 0.02 $m^3/\mu g$, while Mechanism "F" assumed that CNDp2 was non-volatile. Both of these mechanism had somewhat more biases than the mechanism using KpCNDp2 = 0.1 $m^3/\mu g$, so the latter was used for the baseline. However, as with KpRAOOH, the simulations were not highly sensitive to changes in this parameter so the most appropriate value is highly uncertain.

Mechanism "G": Process (p2) is used in place of process (p3). This alternative mechanism is used to examine use of a different type of process to account for SOA formation from aromatic hydrocarbons in the presence of NO_x that cannot be attributed to reactions of phenolic compounds. The baseline mechanism represents this using process (p3), which mechanism G represents this using process (p2). As discussed above, both represent SOA formation as a NO_x-dependent process, but (p2) represents this as a primary process, while (p3) represents this as secondary reaction of an aromatic ring-opening product. The same CNDp2 model species and the same Kp value are used for both alternatives because the test calculation results did not indicate that it needed to be re-optimized. The test calculations discussed below indicate that the two alternatives simulate the aromatic - NO_x and aromatic - H_2O_2 data about equally well, but using process (p3) instead of (p2) results in somewhat less bias in the simulations of SOA in the aromatic - NO_x experiments with added CO or other VOC. For this reason, process (p3) rather than (p2) is used in the baseline mechanism.

Mechanism "H": Processes (p2pN) and (p3pN), representing SOA formation from reactions of phenols and catechols with NO_3, also occur. This alternative mechanism assumes that the yields of SOA from the reactions of NO_3 radicals with the phenolic or catechol model species are the same as used in the baseline mechanism for the corresponding OH reaction. This differs from the baseline mechanism in that the baseline assumes that SOA from these NO_3 radical reactions is not important. The test calculations indicate that simulations of SOA formation in the phenolic - NO_x experiments are relatively insensitive to assumptions concerning these NO_3 reactions, with the yield parameters that fit the data for these experiments not being significantly different than those that fit the data using the baseline mechanism (see Table 9). However, Table 8 shows that the yield parameters that fit the data for the aromatic hydrocarbon - NO_x experiments are significantly affected, with the yield for process (p2) being ~36% lower for Mechanism H compared to the baseline mechanism. This is because the reactions of NO_x with phenolics are more important in the aromatic hydrocarbon experiments because of the higher levels of NO_3 radicals formed in most cases. Mechanism H fit the results of the aromatic - NO_x and aromatic - H_2O_2 experiments about as well as the baseline mechanism, but it consistently overpredicted SOA yields from the aromatic - NO_x experiments with added CO or other VOC, regardless of what assumptions are made concerning the partitioning coefficients or the other processes. For that reason, SOA formation from the phenolic + NO_3 reactions are not included in the baseline mechanism.

Mechanism "I": Wall absorption of semi-volatiles: This alternative mechanism used the same formulation and partitioning coefficients as the baseline mechanism (A), but differed from the baseline mechanism because a different chamber wall model was used when deriving the best fit yield parameters using the chamber data. As discussed above in the section on modeling methods and the treatment of absorption and desorption of organics from the chamber walls, the chamber model employed for most of the mechanism evaluation calculations in this work assumed that assumed that absorption of semi-

volatiles on the wall was not important. However, to assess the sensitivity of the mechanism and evaluation results to this assumption, mechanism "I" was optimized and evaluated using a chamber model assuming that wall absorption of low volatility compounds in the gas phase was non-negligible.

As discussed in the section on modeling PM formation, condensation of semi-volatiles on the walls is represented by the reaction

$$\text{CND1} \rightarrow \text{(CND1 on walls)} \qquad \text{k=WallCond} \quad (5)$$

where "CND1" represents any gas-phase condensable species and "WallCond" is a parameter specifying its rate constant, which is assumed to be zero in most of the chamber simulations in this work. However, the baseline chamber model does assume that particles go to the walls, as represented by

$$\text{pmCND1} \rightarrow \text{(CND1 on walls)} \qquad \text{k = PMwall} \quad (4)$$

where "pmCND1" represents the condensable species in the particle phase, and "PMwall" is the particle wall loss rate that is derived from the particle number data for each experiment. As discussed above, this particle wall loss rate is significant, averaging 4.2×10^{-3} min^{-1} (~25%/hour) for the mechanism evaluation experiments in this work. Mechanism "I" is optimized and evaluated based on assuming the absorption for condensation of condensable gas-phase species on the walls occurs at about the same rate as loss of particles on the walls, i.e., that WallCond = PMwall $\approx 4.2 \times 10^{-3}$ min^{-1}. Desorption of the species from the walls is assumed to be negligible in these calculations, and the same net loss rate is assumed for all condensable model species (RAOOH, CNDp1, RAOOHp, CNDp1p, and CNDW) regardless of partitioning coefficient. This is clearly a simplification, but is useful for the purpose of a preliminary assessment of the sensitivity of the mechanisms to alternative assumptions concerning wall condensation.

The evaluation results using this wall model are discussed in the following section. It was found that the final SOA yields in the experiments with the representative phenolic compounds and m-xylene could be simulated equally well with using this wall model, but it requires use of different SOA yield parameters to fit the data. The yield parameters so derived are shown on Table 9 for the phenols and on Table 8 for m-xylene (as parameters for Mechanism H), where they can be compared with those for the baseline mechanism (A). However, using this wall model also predicted that the PM volumes at the later stages in most experiments decline at much faster rates than the PM numbers, which is not consistent with the experimental data. Based on this, we conclude that if condensable species are being lost to the walls, it is must be at a slower rate than the loss of particles.

Other Mechanisms. These were not the only alternative mechanisms that were examined in this work, though calculations or effects of using other mechanisms are not shown either because they were very similar to the results shown below or the model performance was significantly worse. A number of additional calculations were done using different combinations of the parameters varied in the above mechanisms, but the results were generally similar to those discussed above.

SOA Yield Parameters and Predicted Process Contributions for the Baseline Mechanism

The SOA yield parameter for processes (p1) (the RAOOH yield) and (p3) (CNDp2 yield) for the baseline mechanism were derived for the 14 aromatic hydrocarbons studied. This was done by adjusting the yields for these two processes to minimize the average biases in the model simulations of the aromatic - NO_x runs and the aromatic - H_2O_2 experiments, in the same manner as employed for m-xylene in all the alternative mechanisms. Although in principle it would be possible to derive parameters to give zero average biases, in practice the optimization was stopped when the magnitude of the biases were less than 10%, since fine-tuning beyond this point was not judged to be meaningful given the run-to-run variability and the uncertainties in the mechanisms. Note that only the yield parameters for (p1) and (p3) were adjusted for the individual VOCs; the partitioning coefficients and the yield parameters for the phenolic

products (p1p), (p2p), and (p3p) were not changed. These were held constant at the values derived based on our analysis of the tests simulations conducted using the phenol, o-cresol, 2,4-dimethyl phenol, and m-xylene experiments.

The yield parameters in the baseline mechanism for the 14 aromatic hydrocarbons are given on Table 10, and they are also compared graphically on Figure 25. The condensable hydroperoxide (p1) yields ranged from a low of 18% for toluene and 20% for p-xylene to a high of 48% for ethylbenzene, with an average of 30±10%. Note, however, that condensable hydroperoxide yield parameter for toluene was highly uncertain because of limited and inconsistent data for the toluene - H_2O_2 experiments. The CNDp2 yield (p3) was more variable, ranging from a low of ~4% for p-ethyl toluene to ~10% for benzene and o-ethyl toluene, with an average of 7±2%. There was no obvious correlation with the size of the molecule, but except for the relatively low (p3) yield value for p-ethyl toluene, the parameters for isomeric compounds with similar structures were generally similar.

It should be pointed out that except for benzene the yield parameters were derived using the version of the mechanism where the OH levels were adjusted to force the model to predict the observed amount of aromatic reacting. This was necessary to avoid compensating errors because the gas-phase mechanism tends to underpredict OH levels when simulating aromatic - NO_x experiments. However, this adjustment was not done when deriving the parameters for benzene because benzene reacts too slowly for the OH radical levels to be determined with acceptable precision. Thus it is possible that the yield parameters for benzene, especially for the process (p3) that is important in affecting SOA in the presence of NO_x, may be biased low for this compound. Since the (p3) yield for benzene was in the high range of those for the other aromatics, this means that it may in fact be the highest.

Table 10 and Figure 25 also show the yields of the hydroperoxide predicted to be formed from the aromatic + OH + 2 O2 + HO_2 reactions in the gas-phase mechanism, which is presumed to be condensable. In all cases the RAOOH yield that fit the SOA data in the aromatic - H_2O_2 experiments was less than that predicted by the gas-phase mechanism, with the ratio of SOA-fit to gas-phase-predicted RAOOH ranging from a low of ~30% for m- and p-xylene, to a high of ~80-90% for toluene and ethylbenzene. The correlation between the SOA-fit and the gas-phase-predicted RAOOH values was only ~20%, and the ratios of these two were actually somewhat more variable than the SOA fit yields themselves. Therefore, the yield of RAOOH predicted by the gas-phase mechanism does not necessarily predict the yield that best fits the SOA data.

Figure 26 shows the average relative contributions to SOA formation of the various SOA forming processes in the baseline mechanisms for all the VOCs that were studied. Separate plots are given for the aromatic - NO_x, aromatic - H_2O_2 and aromatic - NO_x + added VOC runs (for those VOCs where there are more than one such run). Process (p3) is predicted to be the most important source of SOA in the aromatic - NO_x experiments, with primary hydroperoxide formation (p1) and SOA from phenolics being next most important, except for the trimethylbenzenes where the phenolics are not important because of their low yields in the gas-phase reactions. Although the formation of hydroperoxides (p1 and p1p) is suppressed by the presence of NO_x, it can be nonnegligible in the NO_x experiments with higher aromatic / NO_x ratios because most of the NO_x is consumed by the end of the experiments.

Hydroperoxide formation is predicted to be the major SOA forming process in the aromatic - H_2O_2 experiments, with primary hydroperoxides (p1) being more important than hydroperoxides from phenols (p1p) except for benzene. However, except for the trimethylbenzenes, SOA formation from the NO_x-independent reactions of the phenolics is also predicted to be non-negligible. The baseline mechanism assumes that these NO_x-independent reactions are all reactions of catechols (process p3p), though the possibility that much or all of this may come from other reactions of phenols (process p4p on Figure 24) cannot be ruled out, since assuming this should fit the data equally well.

Table 10. Summary of SOA yield parameters for all aromatic hydrocarbons studied for this project. The yield of RAOOH predicted by the gas-phase mechanism is also shown.

Compound or Species	Yield Parameters (molar) [a]			
	Gas-Phase RAOOH	SOA Fit RAOOH y(p1)	SOA / Pred. RAOOH, y^{rel}(p1)	SOA Fit CNDp2 y(p3) [b]
Benzene	34%	15%	44%	10.0%
Toluene	61%	18% [c]	30% [c]	9.0%
Ethyl Benzene	53%	51%	95%	3.1%
n-Propyl Benzene	38%	33%	88%	6.2%
Isopropyl Benzene	58%	32%	55%	4.5%
m-Xylene	65%	21%	32%	7.0%
o-Xylene	76%	29%	38%	4.9%
p-Xylene	66%	20%	30%	4.9%
m-Ethyl Toluene	63%	31%	49%	7.5%
o-Ethyl Toluene	70%	26%	38%	10.2%
p-Ethyl Toluene	64%	29%	45%	4.3%
1,2,3-Trimethyl Benzene	84%	48%	57%	7.5%
1,2,4-Trimethyl Benzene	66%	35%	53%	7.8%
1,3,5-Trimethyl Benzene	73%	37%	50%	5.7%
Lumped Species ARO1 [d]	57%	23%	41%	7.8%
Lumped Species ARO2 [d]	70%	30%	43%	6.4%

[a] "SOA Fit" parameters are those derived to minimize biases in model simulations of the aromatic - NO_x and aromatic - H_2O_2 experiments with those compound. The model species used in the mechanism and the process it corresponds to on Figure 24 are also shown. "Gas-Phase RAOOH" refers to RAOOH yield predicted by the gas-phase mechanism (Carter and Heo, 2012) if it is assumed that all of the hydroperoxides formed from the reaction of the aromatic + OH + 2 O_2 adduct peroxy radical with HO_2. "SOA/Pred. RAOOH is the ratio of the RAOOH yield that fits the SOA data to the yield predicted in the gas-phase mechanism.

[b] These are actually yields of the model species AFG3C, which reacts to form xCNDp2 (which forms CNDp2 in the presence of NO_x) with 100% yield in the aromatic + OH reaction.

[c] This is uncertain because of the limited number of the toluene - H_2O_2 experiments gave inconsistent results. In this case, the RAOOH yield parameter was derived to minimize biases on the toluene + NO_x + added VOC experiments, which are also sensitive to this parameter and gave more consistent results.

[d] Parameters for these lumped aromatic model species were derived as discussed in the "Condensed Mechanism for Airshed Models" section, below.

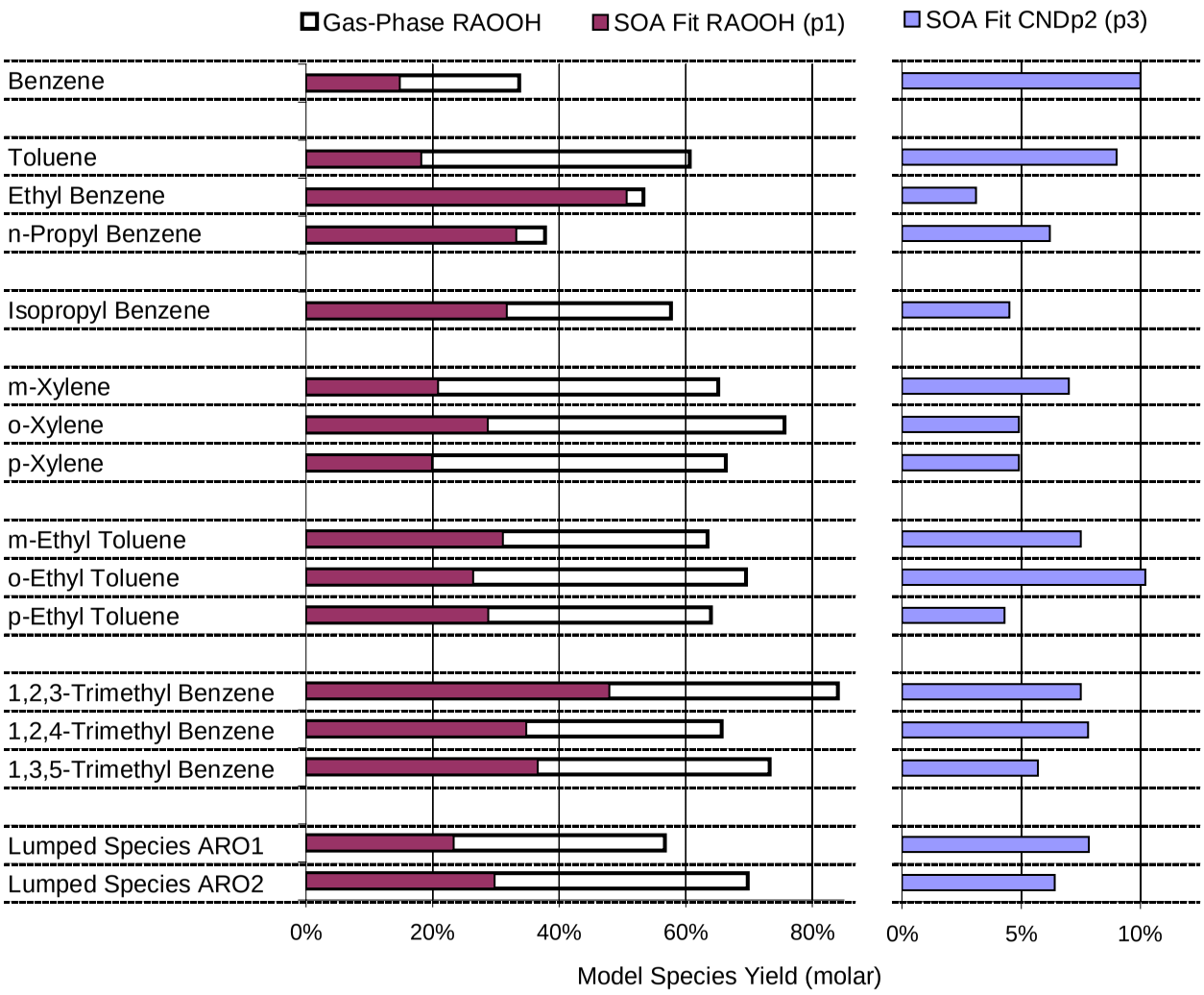

Figure 25. Comparison of RAOOH and CNDp2 model species yield parameters that fit the data for the various aromatic hydrocarbons using the baseline mechanism. Parameters derived for the lumped aromatic species for airshed models are also shown.

Figure 27 shows the relative contributions of SOA formation from the reactions of the phenolic products to SOA formation from the aromatic hydrocarbons. Note that this is phenol (PHEN) in the case of benzene, cresols (CRES) in the case of toluene, and xylenols (XYNL) in the case of the other compounds. The contributions of the phenols are on the order of 15-45% for most compounds except for benzene and the trimethylbenzenes, and tend to be similar in the NO_x and H_2O_2 experiments. In the case of benzene, which has a relatively high phenol yield, phenol contributes about 2/3 of the SOA yield in the H_2O_2 experiments, but its contribution in the NO_x experiments is similar to that for the mono and dialkyl benzenes. The contributions of phenolics are low in the trimethylbenzene experiments because of their low yields in the gas-phase mechanism. In any case, the baseline model predicts that while SOA formation from phenolic products is important for all VOCs studied except perhaps for the trimethylbenzenes, SOA formation from primary reactions or reactions of other aromatic products also must be taken into account.

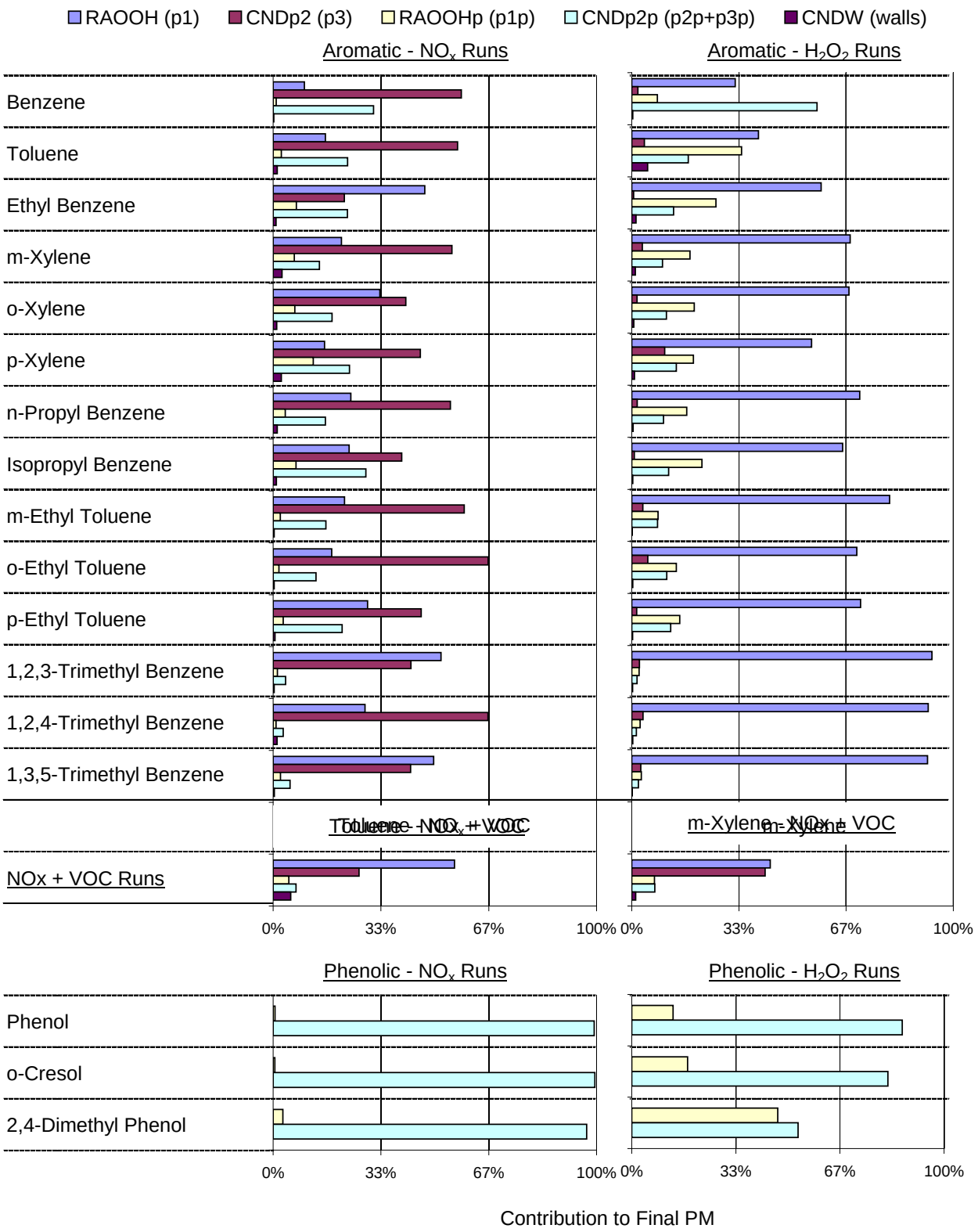

Figure 26. Average relative contributions of various SOA-forming model species in the model simulations of the various aromatic hydrocarbons with the baseline mechanism.

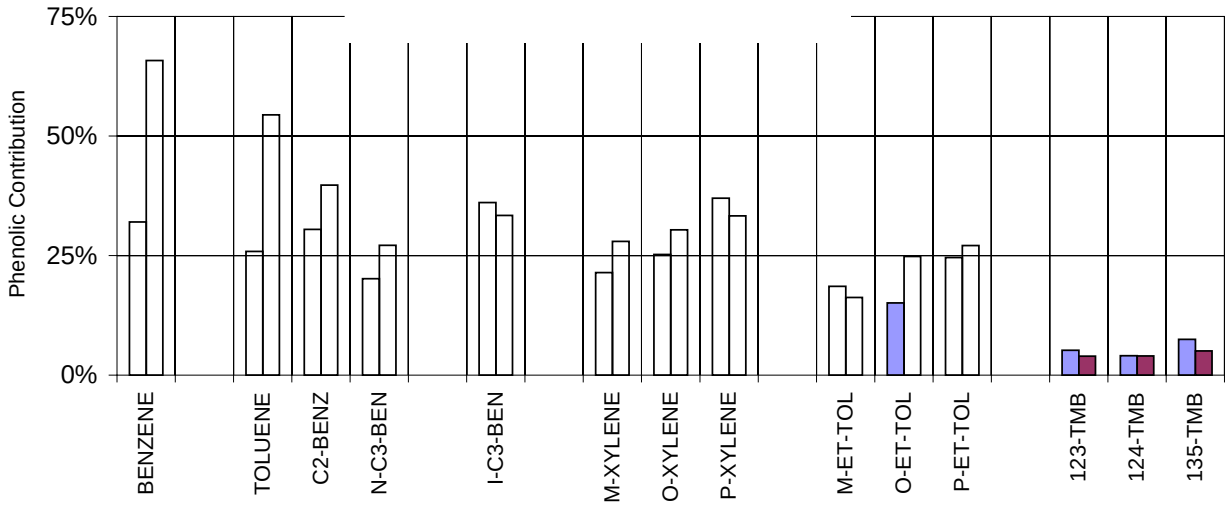

Figure 27. Relative contributions of reactions of the phenolic products to SOA formation from the aromatic hydrocarbons.

Figure 26 also shows the relative importance of the various SOA forming processes in the baseline mechanism to SOA formation calculated for the experiments with the phenols. Note that the baseline mechanism lumps primary SOA formation from the phenols themselves in the presence of NO_x (process p2p) with secondary SOA formation from the reactions of catechols in the presence or absence of NO_x (process p3p), so Figure 26 does not show the relative importance of these. However, since process (p2p) in the baseline mechanism assumes the SOA is from the reactions of peroxy radicals with NO, only process (p3p) would be important in the phenolic + H_2O_2 experiments.

Figure 26 also shows the contributions to SOA formation for the aromatic - NO_x experiments with added VOC for the two compounds, toluene and m-xylene, where more than one such experiment were carried out. In both cases, SOA formation from hydroperoxides (p1) is relatively more important and SOA formation from process (p3) is relatively less important than in the experiments without the added CO or VOC, though the difference is greater in the case of toluene. The relatively higher importance of the hydroperoxide formation can be attributed to added CO or VOC causing higher O_3 formation and NO_x consumption rates, which would reduce the overall NO level required for process (p3) and reduce the amount of time for NO_x to be consumed to levels where hydroperoxide formation becomes important.

Condensed Mechanisms for Airshed Models

Although the 14 aromatic hydrocarbons studied for this project represent all the possible C_6-C_9 isomers, they are only a subset of the many types of aromatic hydrocarbons that can be emitted into ambient atmospheres. These various types of hydrocarbons are not represented explicitly in most airshed models using the SAPRC mechanisms; instead they are represented using the lumped aromatic species ARO1 and ARO2. The model species ARO1 is used to represent all aromatic hydrocarbons that react with OH radicals with rate constants less than 2 x 10^4 ppm^{-1} min^{-1} (1.4 x 10^{-11} cm^3 $molec^{-1}$ s^{-1}) at ~300K, while ARO2 is used for those that react faster than that. ARO1 represents primarily monoalkyl benzenes such as toluene, ethylbenzene and propylbenzenes, while ARO2 represents primarily di- and poly-alkyl benzenes such as xylenes and trimethylbenzenes. The parameters for these lumped model species in the

gas-phase mechanism are derived from weighted averages of parameters for the specific compounds these lumped species represent in a representative ambient VOC mixture (Carter, 2010a, Carter and Heo, 2012). The representative mixture used for this purpose in the current mechanism is still the ambient mixture used when calculating the Carter (1994) reactivity scales, and is based on an analysis by Jeffries et al. (1989) of urban ambient air measurements made by Lonneman (1986). The compounds used to derive the ARO1 and ARO2 parameters, and their molar contributions to each, are listed on Table 11.

Table 11 shows that deriving SOA yield parameters for ARO1 and ARO2 requires SOA yield parameters for additional compounds beyond the 13 C_7-C_9 aromatics alkylbenzenes studied for these project, with carbon numbers up to C_{12}. Extrapolating the SOA yield parameters to compounds not studied for this project is highly uncertain because the parameters were found to vary from compound to compound, and no clear relationships were found between the molecular weight and structure of the compounds and their SOA yield parameters. In particular, one would expect that the SOA yields, and therefore the yield parameters used to derive them, would increase with the carbon number of the aromatic, though the parameters for the C_6-C_9 compounds listed on Table 10 indicate no such clear trend.

For the purpose for deriving at least highly approximate preliminary estimates of SOA yield parameters for ARO1 and ARO2, we estimate the yield parameters for the unstudied, higher molecular weight compounds, as follows:

- The yield parameters used for the monoalkylbenzenes (i.e, species lumped with ARO1) are the averages of $y^{rel}(p1)$ and y(p3) values listed on Table 10 for ethylbenzene and the two

Table 11. Relative contributions of the aromatic compounds used to derive the parameters for the lumped aromatic model species ARO1 and ARO2

Group and Compound	Mole Fract.	Group and Compound	Mole Fract.
Compounds Lumped as ARO1		ARO2 Compounds (continued)	
Toluene	75%	1,2,4-C10 trisubstituted benzenes	6%
Ethyl Benzene	10%	1,2,3-C10 trisubstituted benzenes	4%
C11 Monosubstituted Benzenes	5%	1,3,5-C10 trisubstituted benzenes	2%
n-Propyl Benzene	4%	m-C10 disubstituted benzenes	2%
C10 Monosubstituted Benzenes	3%	o-C10 disubstituted benzenes	2%
Isopropyl Benzene (cumene)	2%	p-C10 disubstituted benzenes	2%
t-Butyl Benzene	0.7%	1-methyl-4-isopropylbenzene	2%
C12 Monosubstituted Benzenes	0.2%	m-C11 disubstituted benzenes	0.4%
		1,3,5-C12 trisubstituted benzenes	0.3%
Compounds Lumped as ARO2		m-C12 disubstituted benzenes	0.2%
m-Xylene	13%	p-C12 disubstituted benzenes	0.2%
p-Xylene	13%	1,2,4-C11 trisubstituted benzenes	0.2%
o-Xylene	11%	1,2,3-C11 trisubstituted benzenes	0.2%
1,2,3-Trimethyl Benzene	9%	1,3,5-C11 trisubstituted benzenes	0.2%
1,3,5-Trimethyl Benzene	9%	1,2,4-C12 trisubstituted benzenes	0.12%
1,2,4-Trimethyl benzene	5%	1,2,3-C12 trisubstituted benzenes	0.12%
m-Ethyl Toluene	5%	o-C11 disubstituted benzenes	0.10%
o-Ethyl Toluene	5%	p-C11 disubstituted benzenes	0.10%
p-Ethyl Toluene	5%	o-C12 disubstituted benzenes	0.06%

propylbenzenes, each weighted equally, multiplied by a molecular weight factor derived as discussed below. The averages (without molecular weight factors) for these are 78±20% for y^{rel}(p1), and 1.8±0.6% for y(p3).

- The yield parameters used for the species lumped with ARO2 are the averages of those for all of the xylenes, ethylbenzenes, and trimethylbenzenes, each weighted equally, multiplied by a molecular weight factor derived as discussed below. The averages (without molecular weight factors) for these are 45±9% for y^{rel}(p1), and 3.3±1.8% for y(p2).
- For each compound the estimated yield is corrected by a molecular weight factor that is the ratio of the molecular weight of the compound to the average molecular weight of the compounds whose parameters were averaged to derive the estimates as discussed above. Although this linear correction obviously oversimplifies the dependence of SOA yields on the molecular weights of the compounds, at least it takes into account the fact that the higher molecular weights result in more mass of PM formed, even if the molar yields are the same. This type of correction is needed because the model uses the same model species for condensed products from all compounds, regardless of their molecular weights.

The SOA yield parameters derived using this method are included with the list of SOA yield parameters for the individual compounds studied in Table 10. Note that the y^{rel}(p1) values are higher than the averages for the compounds from which they were derived because of the use of the molecular weight factor. Nevertheless, the values of these parameters for ARO1 and ARO2 are within the range of those derived for the individual compounds listed on the table.

MECHANISM EVALUATION RESULTS

Summary of Evaluation Methods and Metrics

The performance of the mechanism in simulating SOA formation in the chamber experiments is evaluated by comparing experimental and calculated values of the PM volume measurements corrected for losses of particles on the walls. Therefore, unless indicated otherwise, whenever we reference "PM formed" or "SOA formed" in this section we mean PM volume corrected for wall losses[3]. The use of wall-loss-corrected PM values is considered appropriate because it represents the full amount of SOA formed as predicted by the model, because it is used as the basis for the Odum-type empirical models that are widely used, and because it simplifies evaluations because the final and maximum corrected concentrations are generally the same. The method used to correct for wall losses is discussed above in the subsection on particle wall loss characterization in the "Experimental and Characterization Results" section of this report. Note that using the uncorrected wall loss does not reduce the sensitivity of the evaluation results to the particle wall loss rates in the experiment – it just makes the model results sensitive to this parameter rather than the experimental data against which the model is compared.

In this work we compare experimental and calculated PM volume values by plotting them against each other, using tabulations or plots of model errors for individual experiments, or by using tabulations or plots of average biases or errors for groups of similar experiments. Unless indicated otherwise, the quantities used are the PM volume measured or calculated for the last hour of the experiment. For this purpose, the model bias, model error, average bias, and the average error are defined as follows:

$$\text{Model Bias} = (\text{Model} - \text{Experimental}) / \text{Average (Model, Experimental)} \quad \text{(IX)}$$

$$\text{Model Error} = \text{Abs (Model} - \text{Experimental)} / \text{Average (Model, Experimental)} \quad \text{(X)}$$

$$\text{Overall or Average Bias} = \text{Average over experiments (Model Bias in experiment)} \quad \text{(XI)}$$

$$\text{Overall or Average Error} = \text{Average over experiments (Model Error in experiment)} \quad \text{(XII)}$$

where "Abs" means absolute value. Note that this definition of model error is different than the more commonly used definition where the denominator is the experimentally measured quantity, not the average of the experimental and modeled results. The above definition is preferred here because it gives a symmetrical distribution of model errors in cases of extreme model underprediction or overprediction, which is critical if the average biases are to be used as a basis for mechanism adjustments. In particular, by this definition the model errors can range between ±200%, while by the more commonly used definition the model error ranges from -100% to +∞. The two definitions approach the same value when the magnitudes of the model errors are small. In both cases, a negative value means the model is underpredicting the quantity of interest, while a positive value means that the model is overpredicting it. However, for this work the model errors tend to be relatively large, so use of a symmetrical error quantification method is particularly important.

For the purpose of calculating average biases or errors or labeling plots of results of individual experiments, the experiments are grouped both by the aromatic or phenolic compound studied and also by the type of experiment. In most cases, the types of experiments are categorized as follows

[3] "PM" and "SOA" are used interchangeably because all the PM present in the experiments is attributed to SOA formation, though generally the term "PM" is used in the context of the conditions of the experiment while the term "SOA" is used in the context of the discussion of the mechanism.

NO_x Runs:	Aromatic - NO_x irradiations
H_2O_2 Runs:	Aromatic - H_2O_2 irradiations
NO_x + VOC Runs:	Aromatic - NO_x irradiations with added CO or other non-aromatic compound[4]

where "Aromatic" can be either an aromatic hydrocarbon such as m-xylene or a phenolic test compound such as o-cresol. This grouping is useful because as shown in Figure 26 different reactions are expected to be important in the aromatic - NO_x runs than in the aromatic - H_2O_2 runs, and also because different evaluation results were obtained in the aromatic - NO_x runs with added VOCs. The NO_x + VOC runs consisted primarily of m-xylene - NO_x irradiations with added CO, ethane, propane, n-butane, formaldehyde, or ethanol, but a few added VOC experiments were also carried out for benzene and toluene (see Table A-3 in the Supplementary Materials for the reactants in the individual experiments). The evaluation results were found not to depend significantly on which compound was added as long as a sufficient amount was added to have an effect on the system, so they are all grouped together for the purpose of presenting model errors or average biases or errors. A few aromatic - H_2O_2 experiments were carried out with CO added, but the evaluation results were essentially the same as the aromatic - H_2O_2 runs without added reactants, so they are all lumped together in the presentation of the results.

For presentation of the results of some of the test calculations using the m-xylene experiments, the experiments are also grouped according to the PM levels observed in the experiments. This is done in order to assess the extent to which average biases depend on the PM levels, since in some cases the plots of errors vs. PM had too much scatter for this dependence on PM level to be evident. The groupings are used such that there are approximately an equal number of experiments of a given type in each group. The groupings used are as follows:

Range	NO_x Runs		H_2O_2 Runs	
	PM Levels	Runs	PM Levels	Runs
Low PM	≤ 10 μg/m^3	17	≤ 28 μg/m^3	11
Mid PM	10 - 20 μg/m^3	14	28 - 45 μg/m^3	11
High PM	≥ 20 μg/m^3	19	≥ 45 μg/m^3	11

Evaluations of Alternative Mechanisms and Parameters

A series of test calculations with a variety of alternative mechanisms were carried out in order to determine the most appropriate model formulation and set of partitioning coefficient values to use for the full set of experiments and VOCs studied. These focused on the experiments with the representative aromatic hydrocarbon m-xylene because by far the largest number of experiments is available for this compound, and the experiments represented the widest range of conditions. It is assumed that mechanism formulations and sets of Kp values that simulated the m-xylene data with the lowest overall biases and errors would also be the most appropriate for the other aromatic hydrocarbons, though it would be expected that generally different yield parameters would be needed to fit the data for each compound. The alternative mechanisms and m-xylene parameters used are summarized on Table 8, above.

Test calculations were also carried out using alternative assumptions and Kp values for the model species used to represent the reactions of the phenolic products. The experiments with o-cresol and 2,4-dimethyl phenol were used to evaluate the cresol (CRES) and xylenol (XYNL) mechanisms, respectively, because these are considered as representative and had the largest number of experiments. The alternative phenolic mechanisms examined and the SOA parameters used are summarized on Table 9, above.

[4] Note that CO is considered to be a VOC for the purpose of this discussion because its reactions have a similar effect on the results as the addition of the other compounds that were added.

The results of the mechanism evaluation for the experiments with the other aromatic hydrocarbons and phenolic isomers are presented later in this report. These evaluations were done using the baseline mechanism that was derived based on the results of the test calculations discussed below.

Effects of Varying the Volatility of the Condensable Phenolic Products

Figure 28 has plots showing the performance of the mechanisms with different assumptions concerning the volatility of the CNDp2p model species that is used to represent condensable compounds formed when phenolic compounds or catechols react in the presence of NO_x. Model simulations of experiments with the representative compounds phenol, o-cresol, and 2,4-dimethylphenol are shown because these were used as the basis for the phenolic mechanism developed in this work. (Results of baseline model simulations of the limited number of experiments with the other phenolic isomers are discussed in a later section.) The mechanisms whose results are shown on Figure 28 include the baseline mechanism (A) that uses KpCNDp2p = 0.03 $m^3/\mu g$, and Mechanism B, which assumes that this model species is non-volatile. Note that Mechanisms C through G are the same as A in the simulations of these experiments, since they have the same mechanisms for phenolic species. The yield parameters affecting SOA formation from the phenolic compounds were derived to minimize errors in the simulations with the respective compounds, and are given in Table 9. As shown in Table 9, the yields that best fit the data are somewhat different between mechanism (A) and mechanism (B), though the hydroperoxide yields were similar because both mechanisms assume that the hydroperoxide model species (RAOOHp) is non-volatile.

Figure 28 shows that the two sets of mechanisms give very similar predictions in terms of final PM volume when the yield parameters are adjusted to minimize biases in the model simulations. Therefore, final SOA yields in the experiments with the phenols are not an adequate basis to assess the appropriate partitioning parameter to use. However, the mechanisms give different predictions of how model error varies with the duration of the simulation, with the mechanisms with the non-volatile CNDp2p model species having a greater tendency to overpredict SOA in the initial stages of the experiment, at least for phenol and o-cresol. Based on this, we use the higher volatility model for this model species in the baseline mechanism. However, the model simulations are not very sensitive to changes in this parameter, so the exact magnitude used is somewhat arbitrary. It may be that a somewhat lower KpCNDp2p value gives slightly less bias in the simulations of the early stages of the experiments, but the run-to-run scatter is such that further fine-tuning is probably not worthwhile. Further, when we consider relatively large uncertainty in processes related to nucleation and particle growth during the early stages of the experiments (see the "Modeling PM formation" subsection of the "Modeling Methods" section), further adjusting KpCNDp2p based on the performance in the early hours of the experiments may not be reliable.

As discussed above, we assume that the condensable hydroperoxides formed in the reactions of the phenolic compounds (RAOOHp) are non-volatile. We assumed that some condensable hydroperoxide formation (2-5%, depending on the compound and model) is necessary for the models to simulate SOA formation from phenol and o-cresol, and even more (18-23%) is necessary to fit SOA in the runs with 2,4-dimethylphenol (see Table 9). This results in the baseline mechanism predicting that ~1/6 of the SOA is from the hydroperoxide in the o-cresol - H_2O_2 experiments, and more than half of the SOA is from the hydroperoxide in the 2,4-dimethylphenol - H_2O_2 runs (see Figure 26). It may be that the SOA formation in the initial stages of these experiments would be simulated with somewhat less bias if a lower volatility model were used for RAOOHp, but given the other uncertainties and the fact that this reaction accounts for no more than half the SOA from the phenolics and much less than that for the aromatic hydrocarbons, this fine-tuning was not done.

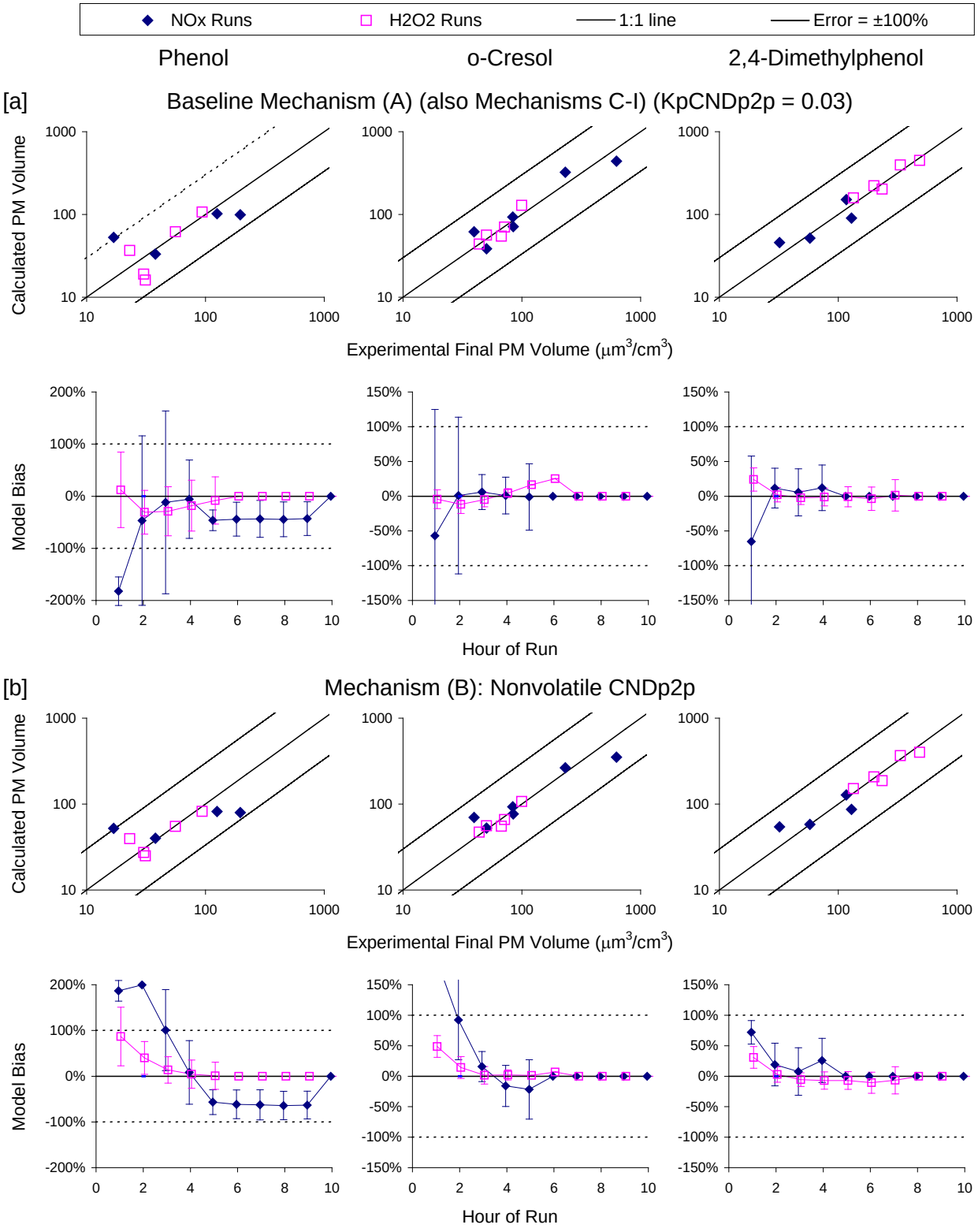

Figure 28. Plots comparing model performance of [a] baseline vs. [b] low-volatility CNDp2p mechanisms for SOA predictions for runs with phenol, o-cresol, and 2,4-dimethyl phenol.

Effects of Alternative Assumptions Concerning Hydroperoxide Volatility

Figure 29 and Figure 30 show the performance in simulating SOA formation in the m-xylene experiments with 3 versions of the baseline mechanism with varying values of the hydroperoxide partitioning coefficient (KpRAOOH): 0.1 $m^3/\mu g$ for baseline mechanism A, 0.02 $m^3/\mu g$ for mechanism C, and non-volatile RAOOH for mechanism B. Figure 29 gives plots of experimental vs. calculated and model biases for the individual experiments and also shows how model biases vary with the final PM volumes in the experiments. Figure 30 shows average model biases and errors for the various types of experiments, and also shows average model biases for experiments with varying PM levels. The PM level ranges used in Figure 30 are chosen so that there is approximately the same number of experiments in the various ranges, as discussed above. The m-xylene product yield parameters used for these various mechanisms are given in Table 8.

The mechanism with the lowest partitioning coefficient of 0.02 $m^3/\mu g$ appears to be the most reasonable *a priori*, both because that is the partitioning coefficient predicted by the 1-product model as discussed above in the section on the experimental results, and also because the hydroperoxide yield that fits the data is close to that predicted using the gas-phase mechanism. However, this mechanism does not give the best performance in simulating the SOA data in the m-xylene experiments. Figure 29 shows that this mechanism has the highest scatter in model performance in simulating the H_2O_2 experiments, and Figure 30 shows that it has the highest overall errors in simulating all the types of runs, and also shows that it tends to underpredict SOA in the H_2O_2 experiments with low PM levels, even though the hydroperoxide yield was adjusted to minimize the average bias for all the experiments.

In terms of ability to simulate the results of the m-xylene - H_2O_2 experiments, the mechanism with the least amount of error is the version that assumes that the hydroperoxides are non-volatile. Figure 29 shows that this model has the least amount of scatter in the simulations of these experiments, and Figure 30 shows that it has the lowest average errors. However, this mechanism does have greater biases than the other versions, with the model error in the simulations of the H_2O_2 experiments having a strong dependence on the PM formed in the experiment, as shown on Figure 29 and Figure 30. In addition, this mechanism has a higher bias towards overpredicting SOA in the experiments with added CO or other VOC, compared to the other two mechanisms. This dependence, i.e., a tendency to increasingly overpredict as the PM levels become low, is in the direction expected for models with partitioning coefficients that are too high.

The mechanism using a KpRAOOH value of 0.1 $m^3/\mu g$ appears to be a reasonable compromise considering the problems with the other alternatives shown. The average errors are between those for the low and high KpRAOOH alternatives, and the average model biases in the H_2O_2 experiments are approximately independent of the range of PM levels (Figure 30). Therefore, it is somewhat less biased and has a lower overall average model error than the low KpRAOOH option for the H_2O_2 experiments (Figure 30). For that reason, a KpRAOOH value of 0.1 $m^3/\mu g$ was adopted for the baseline mechanism used in this study.

Effects of Varying the Partitioning Coefficients for CNDp2

As discussed in Table 7, the model species CNDp2 is used to represent the condensable product formed in processes (p2) and (p3), which represent non-phenolic SOA sources that can occur in the presence of NO_x. Effects of using alternative values for the partitioning coefficient for this species are shown on Figure 31 and Figure 32, which are analogous to Figure 29 and Figure 30 discussed above but show the performance of models with different KpCNDp2 values: KpCNDp2 = 0.02 $m^3/\mu g$ (mechanism E), 0.04 $m^3/\mu g$ (baseline mechanism A), and 0.1 $m^3/\mu g$ (mechanism F). Although the differences in the model performance between these mechanisms are not large, the mechanism with KpCNDp2 of 0.04

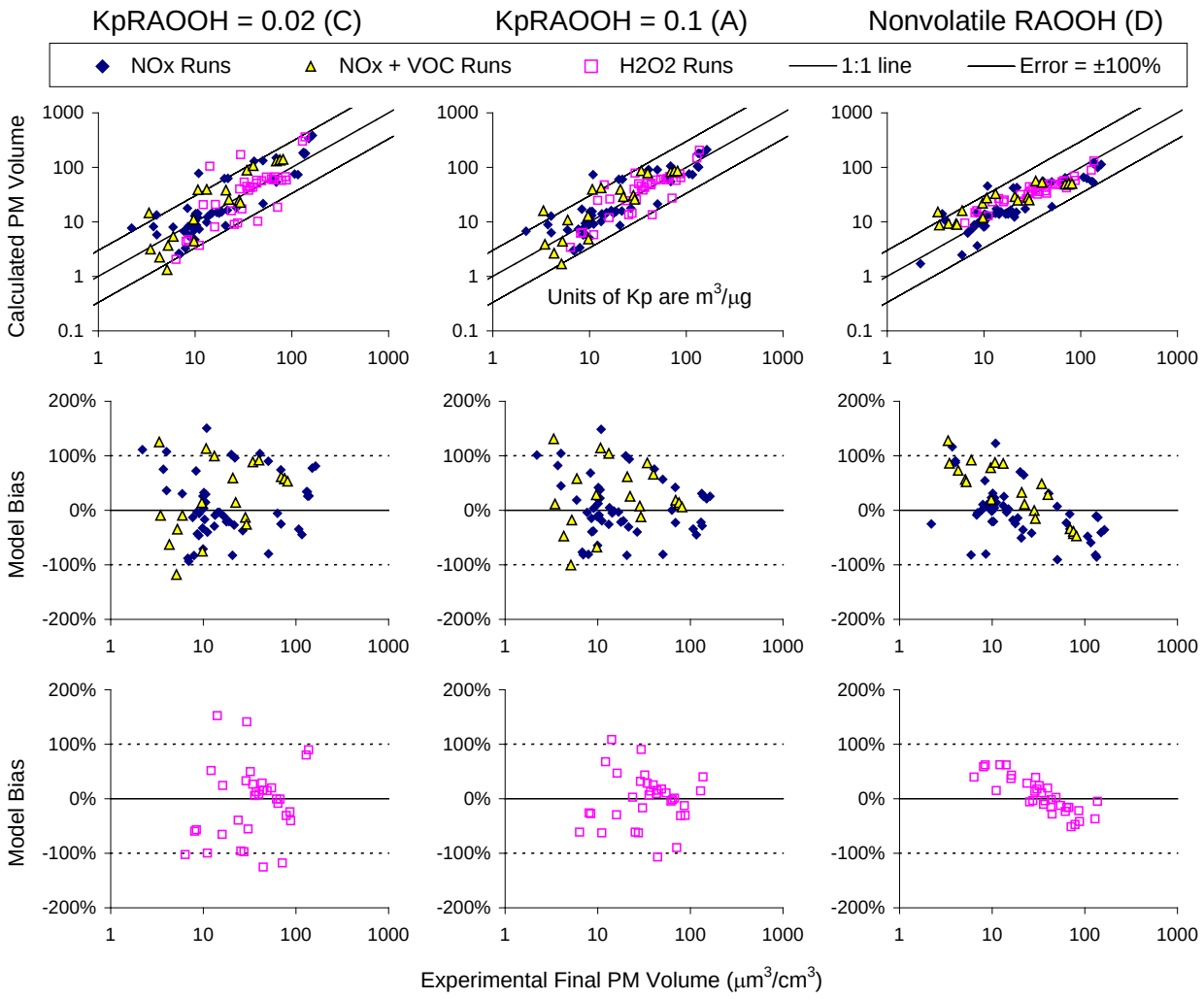

Figure 29. Plots comparing model performance of mechanisms with different KpRAOOH values for SOA predictions for the m-xylene experiments.

$m^3/\mu g$ had somewhat less biases than the other two. Both mechanisms E (with KpCNDp2 of 0.02 $m^3/\mu g$) and F (with KpCNDp2 of 0.1 $m^3/\mu g$) predicted a dependence of the model error on PM levels for the NO_x experiments, with the dependence being in the opposite direction as expected (see Figure 32). The low Kp mechanism (E) had somewhat higher errors in the simulations of the NO_x experiments, while the high Kp mechanism (F) had the lowest model errors for these experiments (see Figure 31), but the difference between the mechanisms using KpCNDp2 of 0.04 $m^3/\mu g$ and KpCNDp2 of 0.1 $m^3/\mu g$ was not large. The mechanism with Kp of 0.04 $m^3/\mu g$ also had lower biases towards overpredicting SOA in the experiments with added CO or other VOC than those with the higher or lower Kp's. Therefore, despite the slightly larger average model errors compared to the high KpCNDp2 mechanism, the KpCNDp2 of 0.04 $m^3/\mu g$ was selected for use in the baseline mechanism.

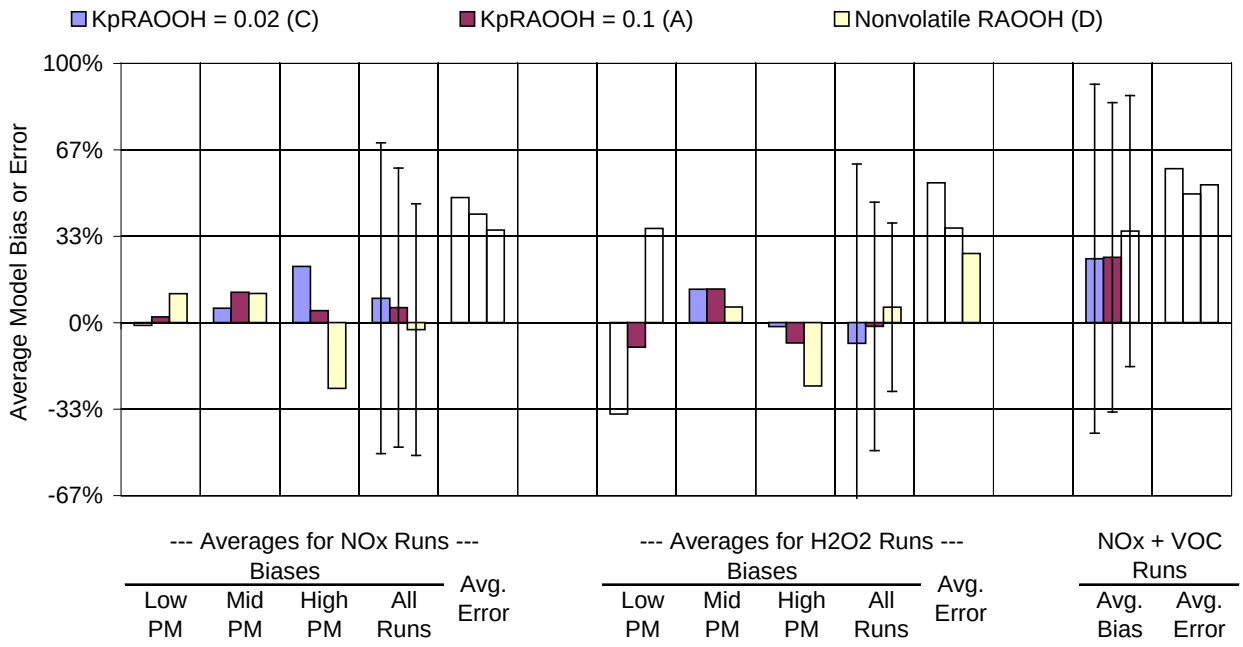

Figure 30. Plots of average model biases and errors for SOA predictions for m-xylene experiments for model simulations with varying values of KpRAOOH.

Effects of Alternative Mechanisms for Aromatic SOA Formation in the Presence of NO_x

Figure 33 and Figure 34 show the effects of using two alternative mechanisms concerning SOA formation in the presence of NO_x, compared to the baseline mechanism. Mechanism (G) uses process (p2) instead of (p3) for representing SOA formation from non-phenolic processes in the presence of NO_x, and shows the effects of assuming that this NO_x-dependent, non-phenolic SOA source is due to a primary rather than a secondary reaction. Mechanism (H) differs from the baseline mechanism in that it assumes that SOA formation comes from the reactions of phenolic compounds with NO_3 in equal yields as their reactions with OH radicals, while the baseline mechanism assumes that SOA only comes from their OH reactions.

The two alternative mechanisms give essentially the same results as the baseline mechanism in simulating the results of the m-xylene - NO_x and m-xylene - H_2O_2 experiments, as shown on both figures. Therefore, modeling these experiments is not useful as a basis for choosing between these alternatives. However, the results of the simulations of the m-xylene - NO_x experiments with added CO or other VOC are significantly different with these alternatives, with SOA formation in these experiments being overpredicted to a much greater extent by the alternatives compared to the baseline. This is shown most clearly with the average bias plots on Figure 34. Although the baseline mechanism has a tendency to somewhat overpredict SOA in these experiments, with an average bias of 25±60%, the average bias is within the run-to-run scatter of the results. The average biases for the mechanism using process (p2) rather than (p3) is higher at ~48±58%, which is still within the scatter of the data but more significant statistically. For this reason, process (p3) is used instead of (p2) in the baseline mechanism. The average bias for the mechanism with SOA formation from phenolic + NO_3 reactions is much higher at ~64±46%, and similar biases are seen in other alternative mechanisms assuming that SOA formation comes from these reactions. This is a significant bias that is well outside the scatter of the data. For this reason, SOA formation from the NO_3 reactions is assumed to be insignificant in the baseline mechanism.

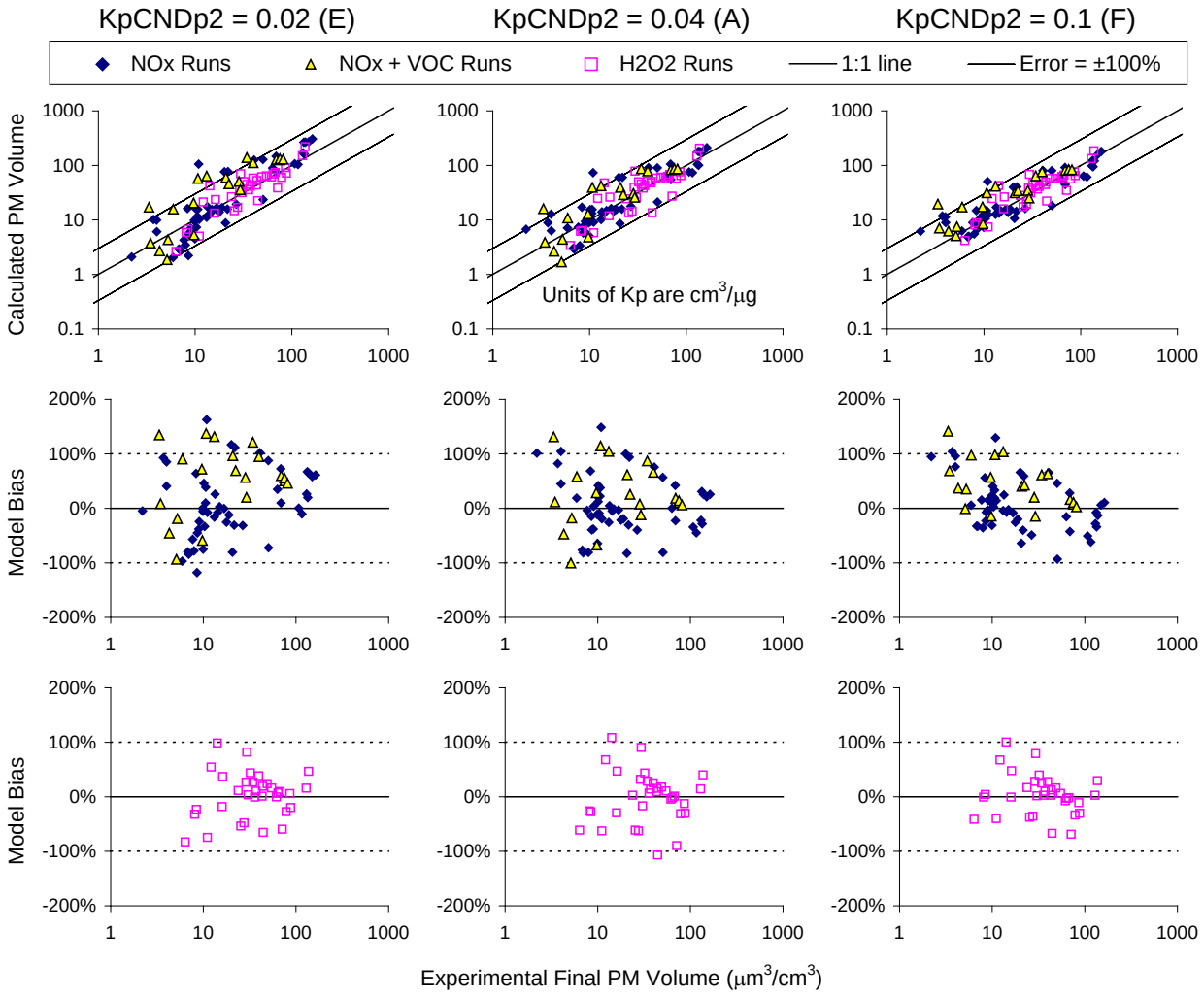

Figure 31. Plots comparing model performance of baseline mechanisms with varying values of KpCNDp2 for SOA predictions for the m-xylene experiments.

Evaluation of Possible Effects of Wall Absorption of Semi-Volatiles

The best fit parameters for the baseline and alternative mechanisms were derived by fitting the model simulations to the data with the model assuming that absorption of gas-phase semi-volatile species on the walls is negligible. Since the validity of this assumption is uncertain, Mechanism (I) was developed using the same processes and partitioning coefficients as used in the baseline mechanism, but with the best fit yield parameters were derived assuming gas-phase condensable species are absorbed on the walls as rapidly as the wall loss rates for particles. Table 8 and Table 9 shows that this resulted in different values for some of the yield parameters, with the largest change being the yields for process (p3) (SOA formation from reactions of non-phenolic products in the presence of NO_x) increasing by a factor of two, and the yield for process (p3p) (NO_x-independent formation of SOA from catechols) increasing by 36%. However, once the yield parameters are re-adjusted, the resulting calculations of final SOA levels on the experiments, using the same wall models as used to derive the parameters, are relatively little affected. This is shown on Figure 35, which shows plots of final PM volume levels calculated using

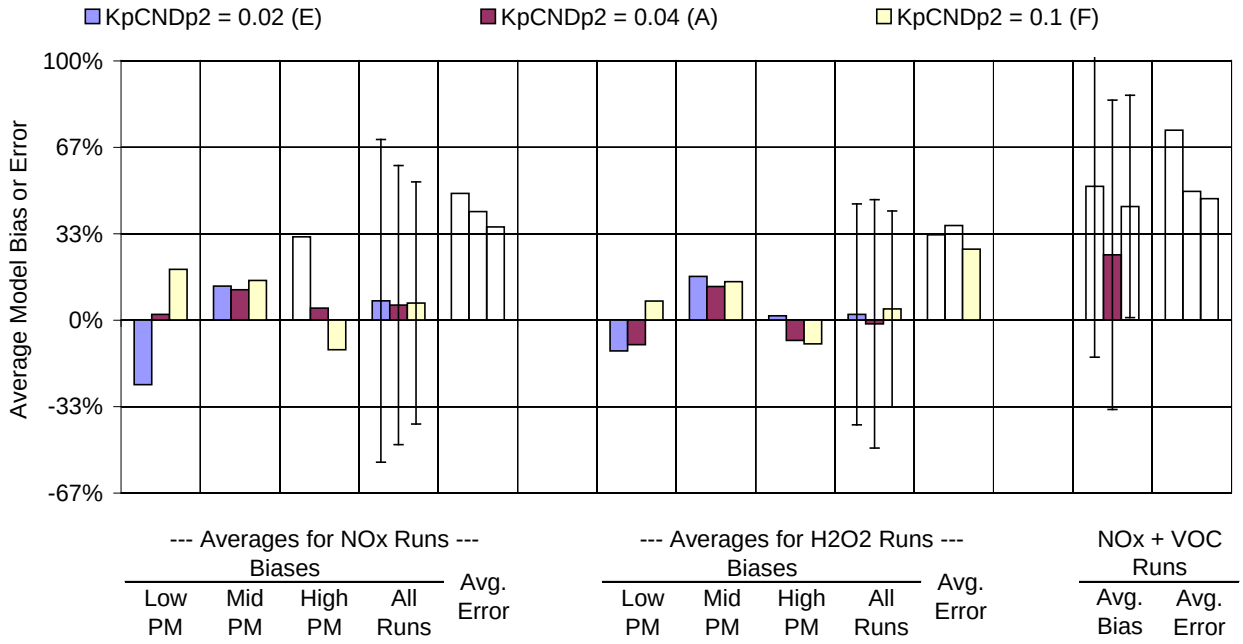

Figure 32. Plots of average model biases and errors for SOA predictions for m-xylene experiments for model simulations with varying values of KpCNDp2.

Mechanism (I) against those calculated using the baseline mechanism. There is relatively little difference except for some of the experiments with PM volume levels lower than ~10 $\mu g/m^3$.

Despite the fact that the evaluation results are nearly the same, assuming wall absorption of the gas-phase condensable species clearly has an effect on the simulations because the optimized yield parameters are significantly different in some cases, as shown on Table 8 and Table 9. The importance of the wall condensation for this model is also shown on Figure 35, which shows the ratios of condensable materials calculated to go onto the walls due to gas-wall partitioning to the total amount of calculated condensed materials in the walls or the suspended particle phase. A clear relationship exists between this fraction and the calculated amount of PM present (Figure 35), though the relationship is somewhat different for the m-xylene - H_2O_2 experiments compared to the other types of runs. Partitioning of gas-phase condensables onto the walls is calculated to be the major fate of SOA formed for the lower PM experiments, and only becomes minor for experiments with final PM volume levels greater than about 100 $\mu m^3/cm^3$.

Although the mechanism derived assuming wall absorption of condensable gas-phase species can simulate the final SOA yields, it does not give good simulations of the evolution of PM over time. This is shown on Figure 36, which shows experimental and calculated time plots for PM volume data for several representative m-xylene - NO_x experiments. The calculations assuming wall absorption may give approximately the same final PM levels as the baseline calculations, but predict much faster consumption of PM volume with time. Note that the particle wall loss correction is calculated using PM number data, which should not be affected by the growth or evaporation of particles once the nucleation

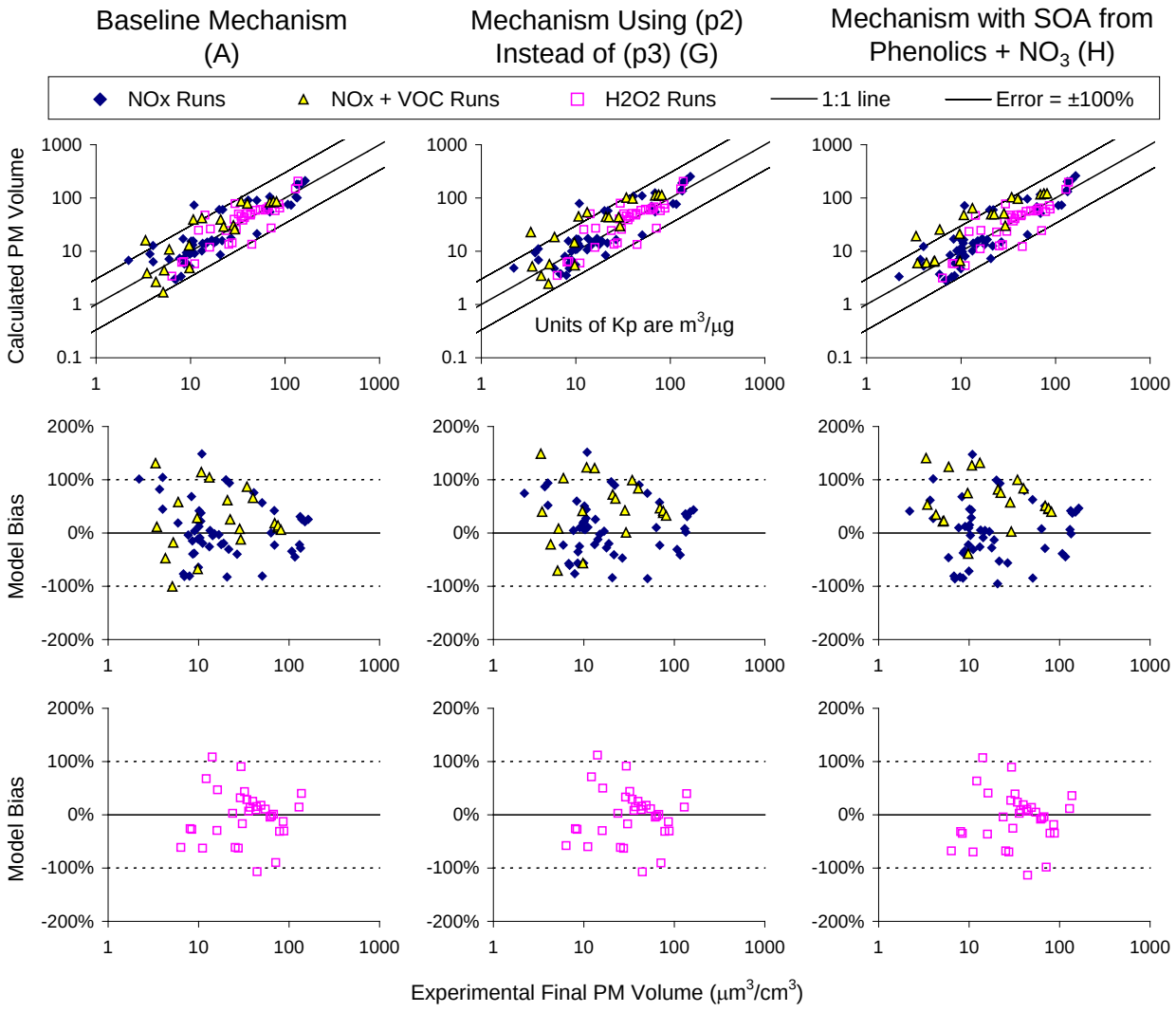

Figure 33. Plots comparing model performance of baseline mechanisms with different assumptions on SOA formation from non-phenolic processes in the presence of NO_x for the m-xylene experiments.

process is complete. If no wall losses of gas-phase species are assumed then the PM volume corrected for particle wall losses would be expected to become constant during the later stages of the experiments, or at least not decline with time. Any evaporation from the particles that occurs is countered by re-absorption. This is reasonably consistent with the experimental data. The model assuming wall losses of gas-phase species predict much faster declines of PM volume with time, caused by wall absorption of evaporated semi-volatiles competing with their re-condensation on the particles. The rate of PM volume consumption predicted by assuming that wall losses of semi-volatiles occur at the same rate as for particles is clearly much faster than experimentally observed. This means that if wall absorption of gas-phase species is occurring, it must be at a much lower rate than the wall loss rate of particles.

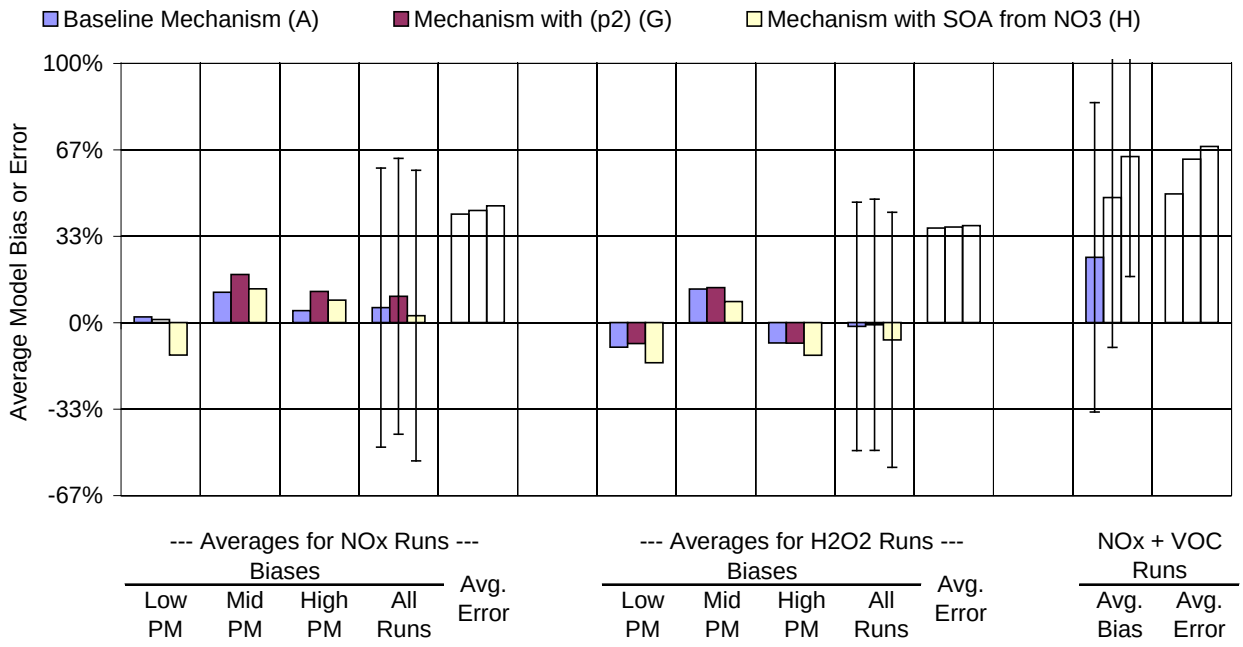

Figure 34. Plots of average model biases and errors for SOA predictions for m-xylene experiments for model simulations with varying assumptions about processes (p2) and (p3).

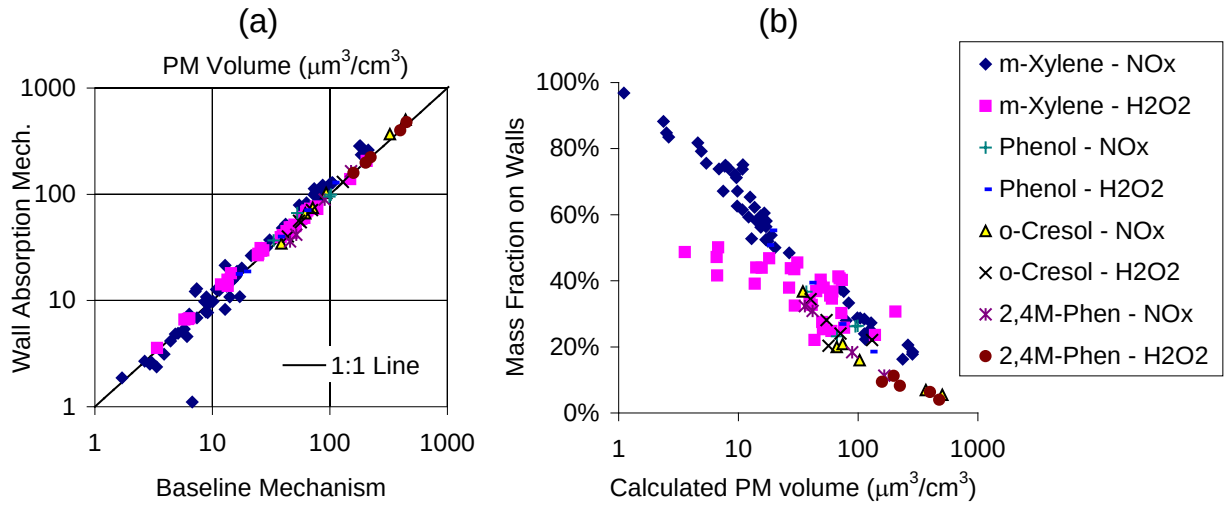

Figure 35. (a) Plots of final PM volume calculated using the wall absorption mechanism (I) against the baseline mechanism. (b) Fractions of condensable material calculated using Mechanism (I) to go on the walls due to absorption of gas-phase condensables, relative to the total final PM volume on the walls or the suspended particle phase.

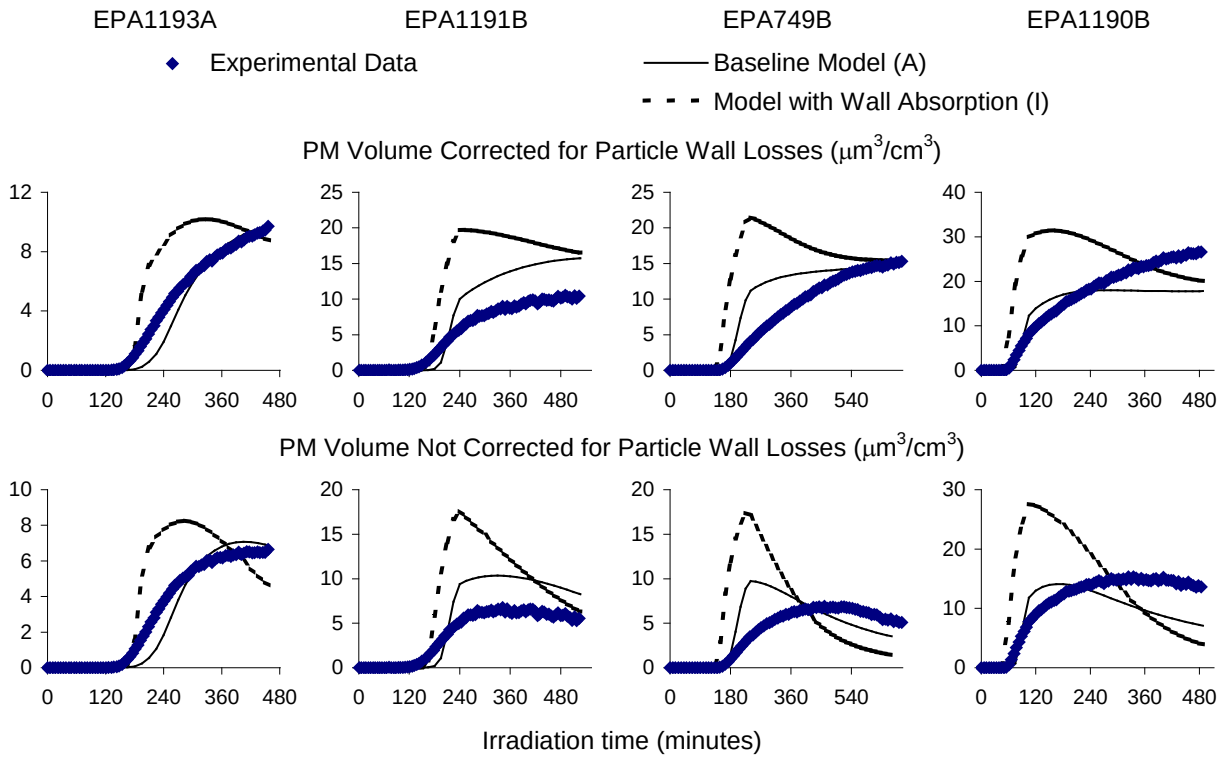

Figure 36. Experimental and calculated time series plots for PM volume, showing calculations using the baseline mechanism and the mechanism assuming wall absorption of gas-phase semi-volatiles.

Effects of Varying Particle Size Parameters

As discussed in the Modeling Methods section, above, results of model simulations of PM formation are affected by parameters in the model used to calculate rates of absorption or condensation of gas-phase condensable species onto particles. The most uncertain parameter is probably the particle radius, which varies from run to run and with time during a run. Because this is not calculated by the model, we use an empirical fit to derive the representative particle radius at each hour since start of irradiation from the total corrected amount of PM formed. The PM radius values predicted from this empirical relationship are compared with the experimentally measured values on Figure 4, where it can be seen that many experiments have much higher or lower radius values than predicted by this relationship.

Figure 37 shows the relative changes in the calculated final PM volume concentrations (corrected for wall loses) resulting from using the "low limit" and "high limit" curves on Figure 4 to calculate the particle sizes from the calculated PM volumes. These reflect the lower and upper limits for particle sizes, respectively; so the relative changes reflect the effects of varying the particle sizes within the experimentally observed range. It can be seen that the sensitivity to particle size is greatest for the experiments with lower levels of PM formation, though the sensitivity does not decrease as the PM volume levels are reduced below 10 $\mu m^3/cm^3$. However, even for the lowest PM experiments, the changes are less than ±10% in most cases. These are relatively small changes compared to the other uncertainties, and indicate that the results of the calculations are not highly sensitive to the methods used to estimate particle sizes, as long as they give particle sizes in the range observed in the experiments.

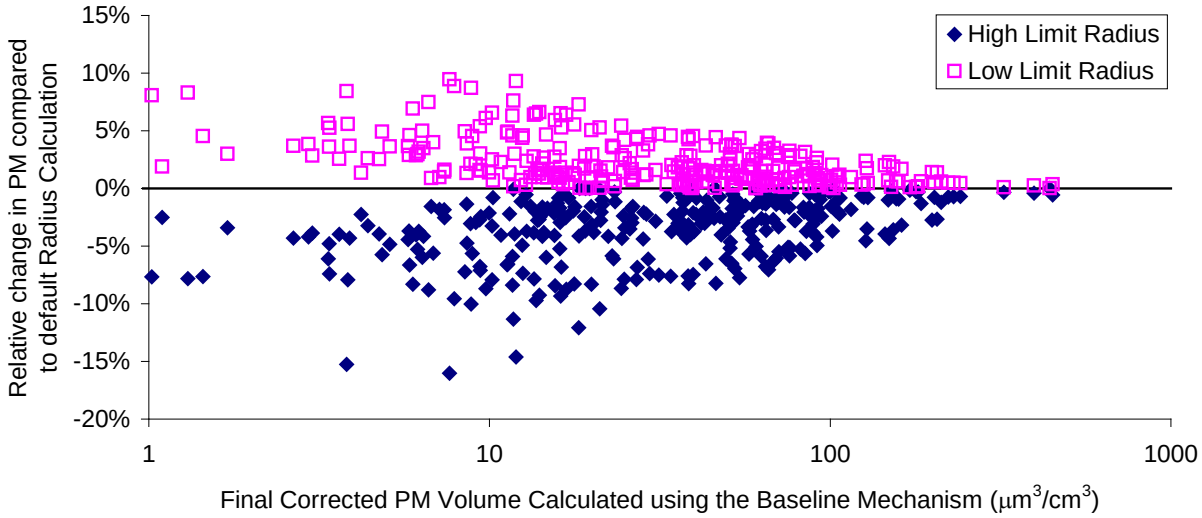

Figure 37. Changes in final PM concentrations calculated using the high and low limit PM radius relationship relative to those using the default PM radius model for all the mechanism evaluation experiments used in this work.

Effects of Varying Nucleation Rates

As also discussed in the Modeling Methods section, above, results of model simulations of PM formation are also affected by the nucleation rates used in the model. The simplified nucleation model used in this work represents nucleation as bimolecular reactions between the condensable model species, with rate constants that depend on the equilibrium partitioning coefficient (Kp) values assigned for the model species. For non-volatile model species, the nucleation rates are assumed to be a maximum value of ~10^3 ppm^{-1} min^{-1} (~6 x 10^{-13} cm^3 $molec^{-1}$ s^{-1}). For the others, the nucleation rates are determined by the ratio of Kp to the parameter MaxNucM. This parameter specifies the Kp value where the nucleation rate factor is 50% of the value for non-volatile species (see the discussion of the NC_CND parameters in Table 2). The default value of MaxNucM, used in all calculations in this work unless indicated otherwise, is 10 $m^3/\mu g$, based on the objective of obtaining sufficiently high nucleation rates to promote PM formation, but not too high to perturb the gas-particle equilibrium. Table 12 shows the bimolecular self-reaction nucleation rates for the various model species calculated using the various values of MaxNucM. For the default model, the bimolecular self-reaction nucleation rates for the volatile species range from 0.009 to 0.1 ppm^{-1} min^{-1}.

Effects of changing the nucleation rate parameters in the model simulations discussed in this work are shown on Figure 38, which gives relative changes in final corrected PM levels using various MaxNucM values, relative to using the default value of 10 $m^3/\mu g$. Figure 38 indicates that the results are very sensitive to changes in MaxNucM when it is decreased below the default value of 10, i.e., when nucleation rate constants are increased (as shown on Table 12). The sensitivity to nucleation decreases as the amount of PM formation increases, but if the nucleation rates are high enough (i.e., as when MaxNucM $\leq$ 1 $m^3/\mu g$), then even runs with relatively high PM levels are sensitive to nucleation rates. This is attributed to the nucleation reaction perturbing the equilibrium partitioning when the nucleation rate constants are sufficiently high. On the other hand, the calculations become relatively

Table 12. Nucleation rates calculated for the condensable model species in the baseline mechanism for various values of the MaxNucM parameter.

Model Species	Process	Kp ($m^3/\mu g$)	Self-reaction nucleation rate constants (ppm^{-1} min^{-1}) for various values of the MaxNucM parameter ($m^3/\mu g$)				
			1	3	10 (default)	30	100
RAOOH	(p1)	0.1	8.3	1.0	0.10	0.011	1.0e-3
CNDp2	(p3)	0.04	1.5	0.17	0.016	1.8e-3	1.6e-4
RAOOHp	(p1p)	Non-volatile	1000	1000	1000	1000	1000
CNDp2P	(p2p,p3p)	0.03	0.85	0.10	0.009	1.0e-3	9.0e-5
CNDW	Walls	Non-volatile	1000	1000	1000	1000	1000

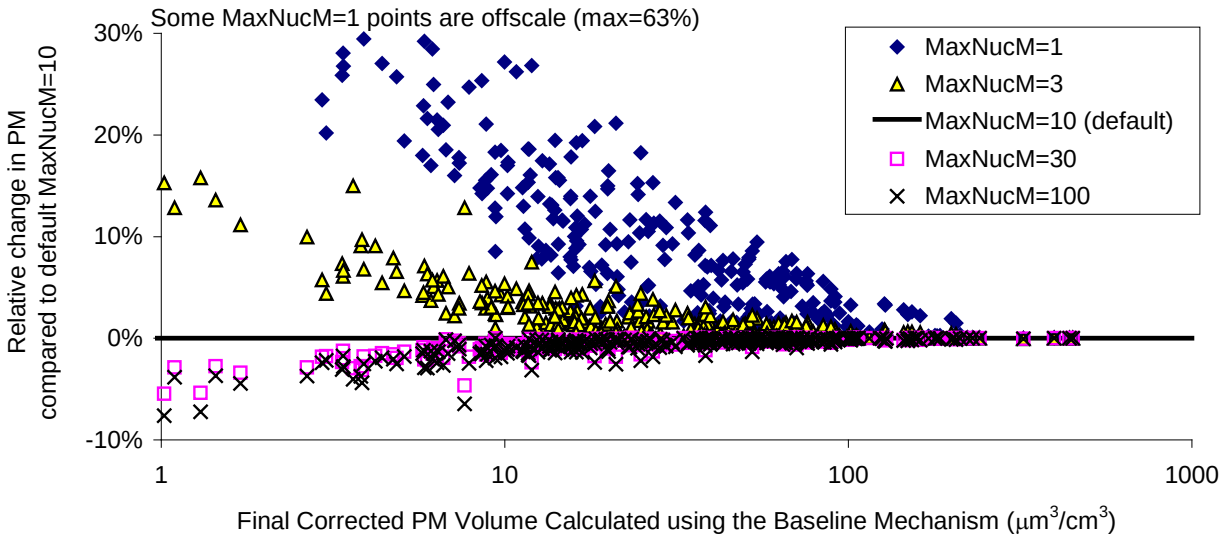

Figure 38. Changes in calculated final PM concentrations calculated using various values of the MaxNucM parameter relative to those calculated using the default nucleation model for all the mechanism evaluation experiments used in this work.

insensitive to nucleation rates when they are decreased below the default value, as long as they are sufficiently high for particle formation to begin.

The sensitivities to nucleation rates shown on Figure 38 are consistent with the objective of using nucleation rate parameters that are not so high that they appear to perturb the partitioning equilibrium but are sufficiently high that the results of the calculations are not highly sensitive to the nucleation parameters used. The low sensitivity to MaxNucM for MaxNucM values greater than the default (i.e., lower nucleation rate constants for semi-volatile species) comes from the fact that when MaxNucM is sufficiently high that all the nucleation is from non-volatile species, including background PM attributed to the walls, and the nucleation rates for non-volatile species are not sensitive to MaxNucM. Although

Figure 38 shows relatively low sensitivities when MaxNucM is varied around the default value, the appropriateness of the methods used to estimate the nucleation rate constants in this work, and therefore the nucleation rates that are calculated, is highly uncertain.

Performance of Baseline SOA Mechanisms for the Individual Compounds

The average model biases and errors for the baseline model predictions of SOA formation in the aromatic - NO_x and aromatic - H_2O_2 mechanism evaluation experiments are shown on Table 13 and Figure 39, and plots of selected mechanism evaluation results for the individual VOCs are shown on Figure A-3 through Figure A-13 in the Supplementary Materials. Note that the average biases for the aromatic - NO_x and aromatic - H_2O_2 experiments are low for most of the compounds because the SOA yield parameters were optimized to minimize these biases. However, the parameters were not optimized for m- and p-cresol or for 2,6- or 3.5-xylenol or for the experiments where CO or a second VOC was added. The standard deviations of the biases and the average errors give an indication of the overall ability of the model to predict SOA formation in these experiments. The plots shown on Figure A-3 through Figure A-13, which show the quality of the fits for the individual experiments, also give indications of the overall performance of the mechanism and potential biases.

Overall, the model simulates SOA in most of the experiments within a factor of two, and the average errors for most VOCs are on the order of 50%. The averages of the average errors for the various compounds are 41±17% for the NO_x runs and 40±18% for the H_2O_2 runs, so they are nearly the same for each type of run. The biases for the experiments with added CO or non-aromatic VOC are an independent test of the mechanism, and indicate that although the xylene runs of this type are simulated with relatively little bias, SOA is underpredicted in the benzene + CO experiment and significantly overpredicted in the toluene + ethane or propene experiments. The discrepancy for the benzene + CO experiment may not be significant because it is only one experiment, but consistent results are observed for the four toluene experiments with two different added VOCs.

In general, there are no compounds where the average fit statistics are significantly better or worse than the rest of the group, except for the cresol and dimethylphenol isomers for which the yield parameters were not optimized. However, the plots shown on Figure A-3 through Figure A-13 indicate that there are differences among the VOCs studied in terms of overall model performance and biases for the various experiments, which in some cases may be due to run to run variability or problems with individual runs. The model performance issues and special considerations (where applicable) for the various individual compounds are discussed below.

m-Xylene. We discuss m-xylene first because the largest number of experiments has been carried out using this compound and because it was used in the initial evaluations of the alternative mechanisms as discussed above. The model performance of the baseline mechanism in simulating the individual experiments has been shown previously in Figure 29 through Figure 34, and in the top plots of Figure A-6. In general, the baseline model simulates the m-xylene data overall with relatively small biases, primarily because the yield and partitioning coefficient parameters have been adjusted to minimize these biases. Also, the model calculated yield vs PM formed plots are reasonably consistent with the experimental yield data, particularly for the H_2O_2 experiments. However, the model calculated yields as a function of PM formed for the NO_x experiments are much less variable than are the experimental data, suggesting that the model may not be accounting for all the factors affecting the variability of SOA formation in the presence of NO_x. There is significant run-to-run scatter overall, much more than is seen when evaluating mechanisms for predictions of ozone (see for example, Carter and Heo, 2012), but this run-to-run scatter in PM fits is about the same for all the aromatics studied.

Table 13. Summary of average model biases and errors for predictions of final corrected PM volumes for the simulations of the mechanism evaluation experiments using the baseline mechanism.

Compound	NO_x Runs		H_2O_2 Runs		Notes
	Bias	Error	Bias	Error	[a]
Benzene	3% ± 47%	31%	0% ± 30%	22%	1
Toluene	-3% ± 50%	36%	-132% ± 86%	140%	2
Ethyl Benzene	0% ± 39%	30%	-1% ± 79%	68%	
n-Propyl Benzene	6% ± 39%	28%	-2% ± 63%	47%	
Isopropyl Benzene	4% ± 34%	26%	-8% ± 48%	41%	
o-Xylene	6% ± 52%	42%	-1% ± 62%	42%	
m-Xylene	6% ± 54%	42%	-2% ± 48%	36%	
p-Xylene	2% ± 71%	55%	-6% ± 50%	41%	
o-Ethyl Toluene	6% ± 33%	27%	8% ± 40%	35%	
m-Ethyl Toluene	7% ± 47%	25%	5% ± 30%	22%	
p-Ethyl Toluene	7% ± 25%	22%	-4% ± 43%	37%	
1,2,3-Trimethyl Benzene	-1% ± 60%	49%	2% ± 84%	60%	
1,2,4-Trimethyl Benzene	7% ± 73%	58%	1% ± 87%	65%	
1,3,5-Trimethyl Benzene	2% ± 66%	53%	3% ± 46%	39%	
Phenol	1% ± 72%	51%	-8% ± 45%	36%	3
o-Cresol	1% ± 32%	28%	3% ± 17%	12%	1
m-Cresol			33% ± 16%	33%	4,5
p-Cresol			-34% ± 25%	34%	4,5
2,4-Dimethyl Phenol	4% ± 33%	27%	4% ± 15%	13%	1
2,6-Dimethyl Phenol			66% ± 8%	66%	4,6
3,5-Dimethyl Phenol			114% ± 8%	114%	4,6
Benzene + CO	-58%	58%			4,7
Toluene + 2nd VOC	-3% ± 110%	88%			4
m-Xylene + CO or VOC	25% ± 60%	50%			4

[a] Notes are as follows:

1 The evaluations were carried out without adjusting the model for experimental OH levels

2 This high negative bias is due to the three toluene - H_2O_2 experiments that had relatively low PM formation, and that were not used in the optimization because their results were inconsistent with the toluene - H_2O_2 experiment with PM levels in the normal range and with the toluene - NO_x + added VOC experiments. See the discussion of the results for the toluene experiments.

3 The evaluations using the phenol - NO_x experiments were carried out without adjusting the model for experimental OH levels.

4 The parameters were not optimized to minimize biases for these experiments.

5 Mechanism based on that optimized for o-cresol

6 Mechanism based on that optimized for 2,4-dimethyl phenol.

7 Only a single experiment of this type was carried out.

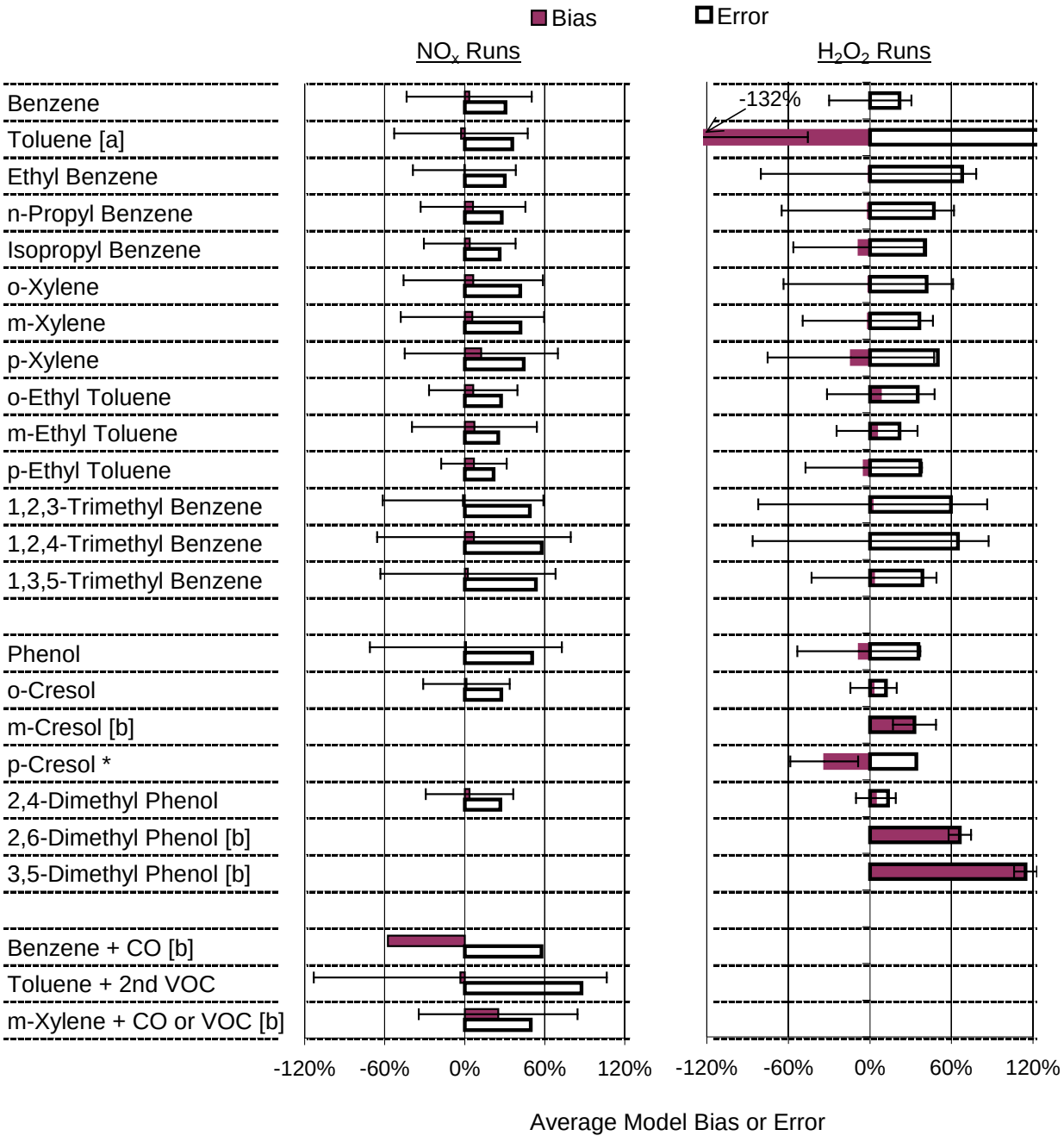

[a] Parameters not optimized to minimize biases for all the H_2O_2 experiments (see text)

[b] Parameters not optimized to minimize biases for these experiments

Figure 39. Average biases and errors for the baseline model simulations of SOA formation in the aromatic - NO_x and aromatic - H_2O_2 experiments.

Benzene. The model performance for the individual benzene experiments are shown on the top set of plots on Figure A-3. Overall the quality of the fits is comparable to that shown and discussed above for m-xylene, except that the scatter in the model calculated yields as a function of PM formed in the NO_x experiments is comparable to that seen in the experimental data. The plots of model biases and yields vs. PM formed suggest that the model may be using too low partitioning coefficients for the H_2O_2 experiments, but this may not be the case for the NO_x experiments. Note that benzene differs from the other aromatic hydrocarbons in that the model simulation did not use adjusted OH levels to force the model to correctly predict the amount of benzene reacted because benzene reacts too slowly for this approach to be appropriate. This would not necessarily cause greater model errors, but could cause compensating errors in the SOA parameters that were derived. This is discussed further below.

Toluene. The model performance for the toluene experiments are shown on the bottom set of plots on Figure A-3. The quality of the fits for toluene is not as good as those for the other VOCs that were studied for which yield parameters were separately derived, despite the fact that the 2nd largest number of experiments were carried out with this compound. The main problem with the toluene experiments is the limited and inconsistent results for the toluene - H_2O_2 experiments. Although 5 toluene - H_2O_2 experiments were carried out, 4 of those experiments had relatively low PM formation (~12-14 $\mu m^3/cm^3$), much lower than the PM levels in the other aromatic - H_2O_2 experiments used for mechanism evaluation. The amounts of PM formed in those other aromatic - H_2O_2 experiments could only be fit using yield parameters that significantly overpredicted the amounts of PM formed in the toluene - H_2O_2 experiment with the higher PM levels, and also significantly overpredicted PM in all the toluene - NO_x + added VOC experiments. Because of the greater uncertainty in modeling SOA in low PM runs, the 4 toluene - H_2O_2 experiments were not taken into account when deriving the yield parameters for toluene, and the higher PM toluene - H_2O_2 experiment and the toluene - NO_x + VOC experiments were used instead. These parameters resulted in significant underprediction of PM in the low PM toluene - H_2O_2 experiments, which is why these toluene - H_2O_2 experiments have such a large negative average bias (Table 13 and Figure 39). Note, however, that the toluene - NO_x + VOC experiments also had low PM, so modeling these experiments is also uncertain.

Because of this inconsistency with the toluene - H_2O_2 experiments and the limited number of such experiments with significant PM formation (well above 10 $\mu m^3/cm^3$), the yield parameters for toluene, especially the condensable hydroperoxide (p1) yield, are significantly more uncertain than for the other VOCs. Additional toluene - H_2O_2 experiments with higher toluene levels need to be carried out to reduce this uncertainty.

Other Monoalkylbenzenes. The model performances for the C_8 and C_9 alkylbenzene compounds are shown on Figure A-4 for ethylbenzene and n-propyl benzene and on the top set of plots on Figure A-5 for isopropyl benzenes. There is a relatively small number of experiments for these compounds compared to those discussed above, but the time dependence of the model errors for these compounds suggest that the Kp values affecting the NO_x experiments may be too low for these compounds. Other than that, the data available do not clearly suggest that the overall model performances for these compounds are qualitatively different than that for m-xylene.

o- and p-Xylenes. The model performance for o-xylene is shown on the bottom set of plots on Figure A-5 and that for p-xylene is shown on the bottom set of plots of Figure A-6. There may be a dependence of the model bias in the p-xylene - NO_x runs on the amount of PM formed, but this may be just run-to-run variability. Otherwise, the data available do not suggest model performance issues for these compounds that are different than those for m-xylene and the C_{8+} monoalkylbenzenes discussed above.

Ethyl Toluenes. The model performances for the ethyl toluene isomers are shown on Figure A-7 for the o- and m- isomer, and on the top plots of Figure A-8 for p-ethyl toluene. Except for one possibly anomalous m-ethyl toluene - NO_x run, the data available do not suggest model performance issues for these compounds that are different than those for most other compounds discussed above.

Trimethylbenzenes. The model performances for the trimethylbenzenes are shown on the bottom plots of Figure A-8 and on Figure A-9. Although the number of runs and in some cases the range of conditions are relatively limited and there is some scatter, overall the model performance is comparable to that seen for most of the other aromatic hydrocarbons, and no obvious biases are seen.

Phenol. The performance of the baseline mechanism in simulating the phenol experiments was shown in the top left plots on Figure 28, above, and more plots are shown on the top plots of Figure A-10. Although the number of experiments is limited and there is variability in the results, there does not appear to be large biases in the model predictions. There is a greater tendency for the model to underpredict SOA in the initial stages of he NO_x experiments, and the final PM in some NO_x experiments with lower PM, suggesting that the partitioning coefficients used in the model might be somewhat low.

Cresols. Most of the cresol experiments were conducted using o-cresol, though several H_2O_2 experiments with m- and p-cresol were also carried out. The parameters in the mechanism were adjusted to fit only the o-cresol experiments, so the simulations of the experiments with the other cresol isomers provide a test of the assumption that these isomers have similar SOA forming potentials. The performance of the baseline mechanism in simulating the o-cresol experiments was shown in the top middle plots on Figure 28 and more plots are shown on the bottom plots of Figure A-10. The model performance in simulating the o-cresol experiments is reasonably good and there is no indication of significant biases. The model performance for the simulations of the H_2O_2 experiments with the other cresol isomers is shown on Figure A-11. The model tends to overpredict SOA in the m-cresol - H_2O_2 experiments and underpredict SOA in the experiments with p-cresol by about the same amount. The biases for the m- and p-isomers are within the range of variability and the overall errors in the simulations of the o-cresol experiments. If a single model species is to be used for all cresols, the fact that the biases for o-cresol are in the middle of those found for the other isomers suggests that an o-cresol mechanism may be an appropriate surrogate for the cresols overall.

Xylenols. Most of the xylenol experiments were conducted using 2,4-dimethylphenol, though several H_2O_2 experiments with the 2,6- and 3,5- isomers were also carried out. The parameters in the mechanism were adjusted to fit only the experiments with the 2,4- isomers, so the simulations of the experiments with the other isomers provide an independent test of the mechanism. The performance of the baseline mechanism in simulating the 2,4-dimethylphenol experiments was shown in the top right plots on Figure 28 and more plots are shown on the top plots of Figure A-12. As with o-cresol, the baseline mechanism simulates SOA formation in the experiments with 2,4-dimethylphenol reasonably well. However, a mechanism adjusted to fit the data for the 2,4- isomer may not be a good surrogate for the other two xylenol isomers because the model significantly overpredicts SOA in the H_2O_2 experiments with the other isomers, as shown on Figure 39 and on the bottom plots of Figure A-12 (for 2,6-dimethylphenol) and on Figure A-13 (for the 3,5-dimethylphenol). Therefore, it is possible that the lumped xylenol (XYNL) model species may be predicting too much SOA in the absence of NO_x for the xylenols overall.

Effects of Adjusting OH Radical Levels on Mechanism Evaluation Results

As discussed above, except for benzene the SOA mechanism evaluation calculations for the experiments with the aromatic hydrocarbons were done by adjusting OH levels to force the model to predict the correct amount of the test aromatic reacting during the experiment. This is necessary to avoid

compensating errors because gas-phase mechanism tends to underpredict OH levels in aromatic - NO_x experiments, and therefore the amounts of aromatic reacting to form SOA. Figure 40 shows the average model biases and errors in the simulations of SOA formation for these compounds in model calculations where the OH radical levels are not adjusted. As expected, the tendency of the model to underpredict amounts of aromatic reacting in the aromatic - NO_x experiments causes the model to significantly underpredict PM levels in these experiments when the OH radicals are not adjusted. However, this is not a problem with the aromatic - H_2O_2 experiments, because the OH levels are determined primarily by the amount of injected H_2O_2, whose photolysis serves as the major radical source in these experiments. Although the initial H_2O_2 concentration is not measured and had to be inferred based on the calculated amounts injected, the low biases seen on Figure 40 suggest that the initial H_2O_2 estimates used in the model calculations are reasonably accurate, at least on the average.

These results suggest that if the gas-phase mechanism also underpredicts OH levels in benzene experiments, then optimizing the SOA parameters for benzene using the unadjusted model will result in SOA yields for benzene relative to amounts of benzene reacted that are too high. The importance of this source of bias is difficult to assess because the magnitude of the OH underprediction in simulations of benzene experiments is unknown.

The OH adjustment was also not done for most of the experiments with the phenolic compounds because they can also be consumed to a non-negligible extent by reactions with NO_3 radicals, at least in experiments where NO_x is present. Figure 41 shows plots of model biases in simulations of the amounts

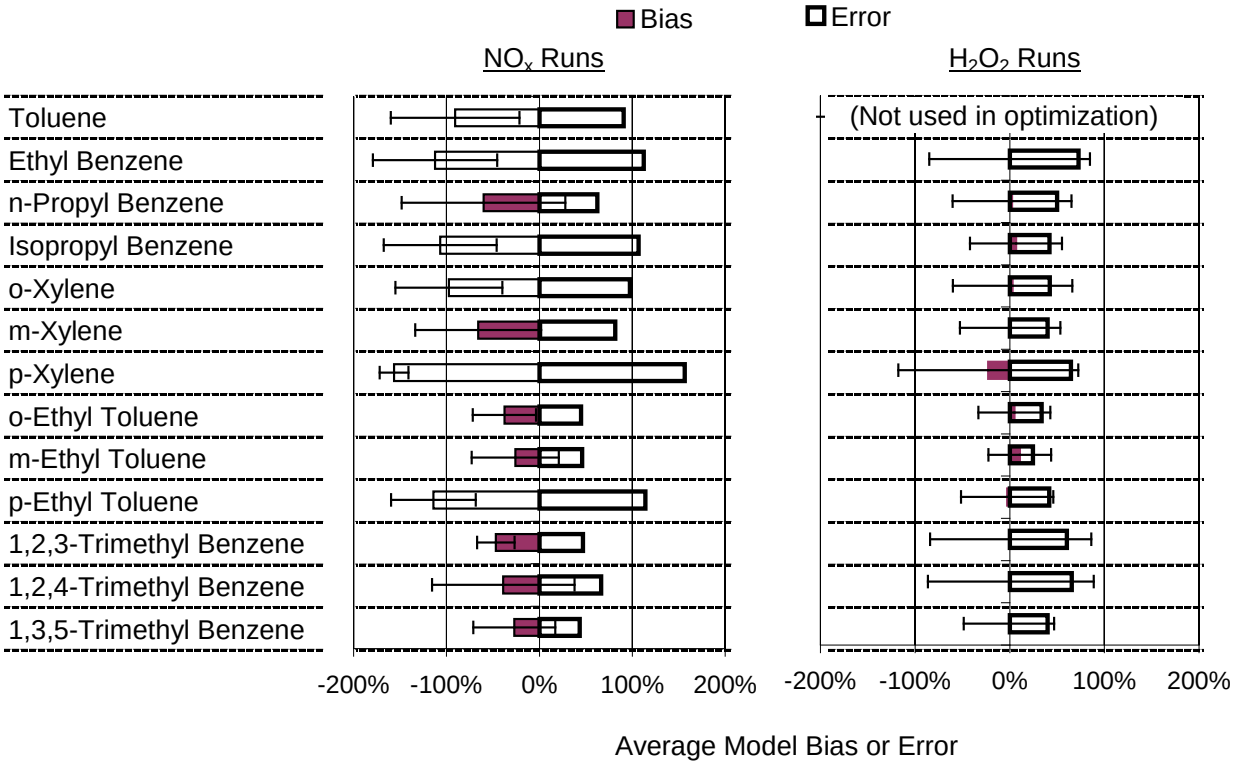

Figure 40. Average biases and errors for the unadjusted baseline model simulations of SOA formation in the aromatic hydrocarbon - NO_x and H_2O_2 experiments where the unadjusted OH model was used.

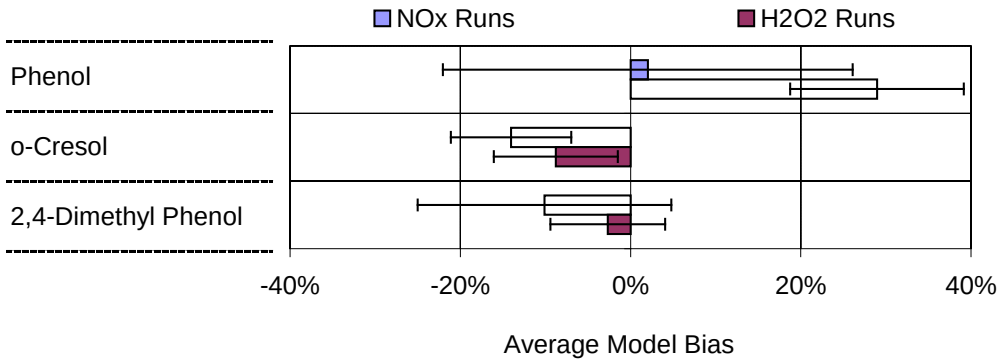

Figure 41. Average model errors for unadjusted model simulations of amount of phenolic reactant reacted in the phenol, o-cresol, and 2,4-dimethylphenol experiments.

of phenolic reacted in the experiments with the phenolic compounds that were used for SOA mechanism evaluation. It can be seen that except for the phenol - H_2O_2 experiments where the amount of phenol reacted is overpredicted by ~30%, the biases in the simulations of the amounts of phenolic compound reacted were relatively small, being less than 15%. This means that use of the unadjusted model to derive the SOA parameters should not be a large problem for those experiments. It is unknown why the model would tend to overpredict the amount of phenol reacted in the phenol - H_2O_2 experiments, given the reasonably good simulations of amounts reacted in most of the other aromatic - H_2O_2 experiments. Because of this, and because consumption by reaction with NO_3 would not be important in the absence of NO_x, the adjusted model was also used in the mechanism evaluation simulations of the phenol - H_2O_2 experiments. This had an effect on the SOA parameters both for phenol and for benzene, where at least half of the SOA formed is predicted to come from reactions of phenol (see Figure 27). It does not affect the predictions of SOA formation from the other compounds of which phenol is not a product in the mechanism.

DISCUSSION AND CONCLUSIONS

Discussion

Summary Project Accomplishments

This project made significant progress in addressing the objective of improving models for predicting SOA formation from the reactions of aromatic hydrocarbons in the atmosphere. Addressing this required work in a number of areas, and the accomplishments of this project are summarized below.

- A total of 158 dual reactor environmental chamber experiments were carried out to provide data needed for aromatic SOA mechanism development for this project, using the state-of-the-science UCR-EPA environmental chamber at our laboratories. Of these 316 separate reactor irradiations, 40 (13%) were analyzed or modeled for chamber characterization purposes, 217 (69%) were judged to be useful for SOA mechanism evaluation, and the rest were judged not to be useful for various reasons. The aromatic compounds studied included benzene all 13 of the C_7-C_9 alkylbenzene isomers, and several representative phenolic aromatic oxidation products.
- The results of the mechanism evaluation and characterization experiments were combined with results of experiments conducted previously in our chamber, and their data and characterization quality were screened for all runs to judge their suitability for mechanism evaluation. This effort yielded a combined dataset of inputs and results for 315 well-characterized and quality-assured reactor irradiations useful for SOA mechanism evaluation and associated characterization runs.
- The results of the 315 mechanism evaluation experiments provided experimental data on SOA yields from the 14 aromatic hydrocarbons and 3 representative phenolic compounds in both the presence and absence of NO_x, with additional data for 4 additional phenolic compounds in the absence of NO_x. These provide a dataset that can be used to develop and evaluate empirical models for describing SOA formation from aromatics.
- The characterization data were examined to develop the characterization input and chamber effects models that are needed when evaluating mechanisms by conducting model simulations of chamber data. We have previously developed characterization procedures and chamber effects models for gas-phase mechanism evaluation, but suitable methods for characterizing SOA-related chamber effects had to be developed and evaluated for this project. This included characterizing losses of particles to the walls, background particle formation, and assessing reproducibility of particle formation. The possibility of absorption and desorption of condensable gas-phase species on the walls was also considered.
- Methods for modeling particle formation in chamber experiments were developed and evaluated, and their uncertainties were assessed. We adopted a kinetic approach to calculate rates of condensation of gas-phase species onto existing particles and to estimate rates of nucleation, and an equilibrium approach was used to calculate rates of evaporation from particles using equilibrium partitioning coefficients for condensable species, which have to be specified as part of the mechanism. Test calculations were conducted to assess the potential importance of uncertainties in these approaches.
- The recently-developed SAPRC-11 gas-phase aromatics mechanism (Carter and Heo, 2012) was used as the starting point to develop a mechanism formulation for predicting SOA formation from aromatics. The model to represent SOA formation was developed in this study by using a level of detail similar to that used for the gas-phase mechanism, and using the minimum number of SOA-

related parameters required to represent the major types of SOA-forming processes expected and how they depend on conditions. The resulting mechanism has five different SOA formation processes, represented using 11 new model species, for which yields and partitioning coefficients had to be estimated or derived based on simulations of the chamber data. Two of these processes and their corresponding parameters are associated with each of the 14 aromatic hydrocarbons studied and three are associated with each of the three model species used to represent reactions of phenolic products.

- Various alternative mechanism formulations, different values of partition coefficients for the model species representing the five SOA forming processes, and alternative assumptions concerning absorption of gas-phase species on the walls were examined in test calculations simulating the experiments with selected representative compounds that had the most comprehensive chamber data. The results of the evaluation allowed us to select a baseline mechanism that seemed to be chemically reasonable and to fit the available data with the least bias.

- The baseline mechanism was used as the basis for optimization of the two SOA yield parameters that were adjusted separately for all of the aromatic hydrocarbons and three representative phenolic compounds that were studied. These were used as the basis for estimating SOA-related parameters for lumped aromatic model species for use in airshed models.

- The baseline mechanism with the optimized SOA parameters was evaluated by conducting model simulations of the full set of SOA mechanism evaluation experiments developed for this and previous projects. The model simulated the data from the aromatic - NO_x and aromatic - H_2O_2 runs without overall biases because they were optimized to minimize these biases. More run-to-run variability in model performance was seen in the evaluation results than is generally seen in ozone mechanism evaluations, and some potentially significant biases were seen for some compounds. However, the biases did not appear to be significant for most of the compounds, including m-xylene, the compound that was the most extensively studied, and whose mechanism was used as the basis for the formulation of the mechanisms for the other compounds.

Although the progress and accomplishments of this project are significant, it is clear that this is just the beginning of the process of developing reliable predictive mechanisms to model SOA formation, and additional work is needed. The scope of the project is limited to SOA formation from aromatic hydrocarbons under dry conditions at a single temperature and without other sources of PM or SOA present other than a small amount of background PM due to wall effects. Clearly there are other sources of SOA in the atmosphere, and effects of temperature, humidity, and interactions with other PM sources also need to be taken into account in atmospheric models. In addition, there are significant uncertainties in the mechanism and the methods used to characterize and model PM formation in the chambers, and the performance of the mechanism developed in this work is not satisfactory in some areas. These areas are discussed further below.

Chemical Mechanism and Mechanism Uncertainties

Overall Mechanism Uncertainty. The validity and predictive capability of the gas-phase mechanism is critical to modeling SOA formation because it represents the processes that account for the formation of the condensable species that constitute SOA. Despite progress in recent years in our understanding of the gas-phase atmospheric chemistry of aromatics (Calvert et al, 2002, and references therein), and significant recent improvements in our ability to model O_3 formation from aromatics in a comprehensive environmental chamber database (Carter and Heo, 2012), there remain significant uncertainties in the current aromatics mechanisms and potentially significant problems with its ability to simulate some aspects of the environmental chamber data. The identities and reactions of the most reactive aromatic photooxidation products are uncertain and current models may not be appropriately

representing their reactions or their formation processes. Evidence of problems with the gas-phase mechanism comes from the fact that it does not correctly predict the dependence of the rate of O_3 formation on the absolute NO_x level when the NO_x level exceeds about 100 ppb, and, perhaps more significantly in the context of this project, the fact that mechanisms adjusted to fit O_3 formation tend to underpredict OH radical levels in aromatic - NO_x experiments.

Since the processes expected to be responsible for SOA formation are expected to be even more complex and uncertain than those responsible for O_3 formation, this means that developing scientifically valid and predictive mechanisms for SOA formation will be even more difficult than doing this for ozone formation. However, despite their uncertainties and problems, the mechanisms predict O_3 reasonably well in aromatic experiments and atmospheric simulations, and much progress has been made in recent years in improving our understanding of SOA formation processes and our ability to model atmospheric SOA formation (Kanakidou et al, 2005; Kroll and Seinfeld, 2008; Hallquist et al, 2009) Therefore, although difficult, significant progress has already been made prior to this project (Johnson et al, 2004, 2005; Hu et al, 2007; Carlton et al, 2010; Derwent et al, 2010; Kelly et al, 2010; Kamens et al, 2011; Zhou et al, 2011). This project provides the additional experimental data and mechanism development work that is needed to ultimately achieve this goal, utilizing the approach that have been used over many years to successfully develop mechanisms for predicting O_3 formation.

Aromatic SOA Mechanism. As with the gas-phase mechanism upon which it is based, the aromatic SOA mechanism developed in this work is chemically detailed in that it represents each reactant aromatic hydrocarbon explicitly but is condensed in that it lumps together or combines the various reaction routes and reactive products formed using a limited number of reactions and model species representing various overall processes involved in formation of the secondary pollutants of interest. Although development of fully explicit mechanisms or near-explicit mechanisms such as the Master Chemical Mechanism (MCM, e.g., see Bloss et al, 2005) is a worthwhile scientific goal, it does not appear to us to be an optimal approach for developing predictive models for regulatory applications. This is particularly so for aromatics, given the uncertainties involved. Therefore, as with our development of the gas-phase aromatics mechanism, no attempt was made to explicitly represent all the individual SOA-forming reactions involved. This is not only because their details are highly uncertain. Any attempt to represent them explicitly would be largely speculation and give a misleading impression of our understanding of the system, and the number of unknown parameters that would have to be optimized to fit the data would be far greater than supported by the data that are currently available.

Based on our assessments of the likely processes involved in aromatic SOA formation and the results of test calculations with alternative mechanisms, the mechanism developed in this work assumes that five overall processes are involved in aromatic SOA formation. Two of these are involved in the primary reactions of the aromatic hydrocarbons, and three are involved with secondary reactions of the phenolic compounds formed when the aromatic hydrocarbons react. Two of these involve the formation of bicyclic hydroperoxides from the reactions of bicyclic peroxy radicals with HO_2, which is assumed to allow the model to account for the finding that the SOA formation yield is generally higher in the absence of NO_x, whose reactions compete with HO_2 over bicyclic peroxy radicals. However, SOA formation also occurs when NO_x is sufficiently high that bicyclic hydroperoxides cannot constitute a major fraction of SOA formed. Therefore, three additional processes are included to represent SOA from aromatic compounds in the presence of NO_x; one for each hydrocarbon, one for each phenolic model species, and one for the species used to represent the catechols formed from the phenolic products.

Developing separate SOA mechanisms for phenolic compounds and catechols is important because results of previous work (Grosjean, 1984, 1985; Johnson et al, 2004, 2005; Henry et al, 2008; Coeur-Tourneur et al, 2010; Nakao et al, 2011a) indicate that these reactions are important, and may even be dominant, to aromatic SOA formation. Therefore, a number of phenolic - NO_x and phenolic - H_2O_2

experiments were conducted for this project, and the results were used to derive and optimize mechanisms for predicting SOA formation from reactions of phenols. Experiments with catechols were attempted but could not be used for mechanism evaluation because the amounts injected could not be reliably quantified. The yields of condensable materials from catechols were adjusted primarily based on model simulations of phenol - NO_x experiments, based in turn on assuming that reactions of catechols were the major source of SOA. This was not sufficient to account for SOA formation in the cresol - NO_x and xylenol - NO_x experiments if the same catechols yields are assumed for cresols and xylenols as is assumed for phenol (based on the data of Olariu et al, 2002), so an additional process for SOA formation from phenols in the presence of NO_x was added to the mechanism. Finally, in order to account for higher SOA yields in the absence of NO_x, SOA formation from hydroperoxides formed from the phenolic compounds also had to be assumed. The hydroperoxide yields that fit the data were respectively 5%, 7%, and 23% for phenol, o-cresol, and 2,4-dimethylphenol respectively, though these are based on assuming that the hydroperoxide is non-volatile, so the actual yields may be higher.

The details of the gas-phase reaction mechanisms of the phenolic compounds are even more uncertain than those for the non-phenolic aromatic hydrocarbons, and the current mechanism uses highly simplified and parameterized lumped reactions for their gas-phase reactions. Phenolic compounds react to a significant extent with NO_3 as well as with OH radicals, and, because of lack of data, the gas-phase mechanism assumes the overall processes for both are similar. The validity of this assumption is highly uncertain. With regard to SOA modeling, the major issue is how these reactions differ in their SOA yields. SOA formation in the experiments with the phenolic compounds themselves could be equally well simulated by models assuming that SOA formation is equal in both types of reactions and models assuming that SOA only comes from the OH radical reactions. This was also true for the simulations of the experiments with the non-phenolic aromatic hydrocarbons in the absence of other reactants besides NO_x or H_2O_2. However, we found that assuming the same SOA yields for both the OH and NO_3 reactions led to significantly overpredicted PM levels in m-xylene - NO_x experiments with added CO or non-aromatic VOC, so the baseline mechanism assumes that no SOA formation comes from the reactions of phenols or catechols with NO_3. This is probably an oversimplification, but was necessary to obtain acceptable simulations of these added CO or VOC experiments.

The mechanisms developed for the phenolic compounds were based on model simulations of the experiments for phenol, o-cresol, and 2,4-dimethylphenol. o-Cresol was taken as representative of all the cresol isomers and 2,4-dimethylphenol was taken as representative of all the xylenols and higher phenolic compounds. Experiments were also carried out in the absence of NO_x using m-cresol and p-cresol, and 2,6-dimethylphenol and 3,5-dimethylphenol. The results for cresols indicated that the o-cresol mechanism appears to be a good representative of the other isomers at least with respect to predicting SOA in the absence of NO_x. However, the results for dimethylphenols (xylenols) indicated that the 2,4-dimethylphenol mechanism overpredicts SOA from the other two isomers in the absence of NO_x. Nevertheless, the mechanism developed using the data for 2,4-dimethylphenol was taken as representative because there were more data available for this compound, and there is insufficient data for the other isomers. The representativeness of this mechanism for the C9+ phenolic compounds such as those formed from ethyl toluenes is even more uncertain because no such phenolic compounds were studied.

In any case, the SOA predicted to be formed from the reactions of the phenolic compounds was not sufficient to account for the SOA measured in the experiments with the non-phenolic aromatic hydrocarbons, so additional processes representing SOA formation from non-phenolic processes had to be included in the mechanism. The contributions of the phenols are on the order of 20-30% for most compounds except for benzene (where it is up to 60% in the absence of NO_x due to the relatively high phenol yield for the reaction of benzene with OH) and the trimethylbenzenes (where it is low because of the low yields of phenols from the trimethylbenzenes). This is true for experiments both in the presence and absence of NO_x. Therefore, primary SOA-forming processes in the reactions of aromatic

hydrocarbons, and/or secondary SOA-forming processes involving the reactions of aromatic oxidation products other than phenols, have to be included in the mechanism.

It is assumed that formation of condensable hydroperoxides as primary products in the aromatic reactions is a significant SOA source for the model to simulate the SOA yields in the aromatic experiments in the absence of NO_x. Least biased fits of simulations to these experiments were obtained if the model used a partitioning coefficient of 0.1 $m^3/\mu g$ for the condensable hydroperoxide model species, which is higher than the 0.02 $m^3/\mu g$ predicted by the empirical analysis of the PM yields in the aromatic - H_2O_2 environmental chamber experiments using the Odum one-product model. The reason for this difference is unclear but suggests that this type of empirical model may not be sufficient to represent the complexity of this system, where other SOA forming processes such as SOA formation from reactions of the phenolic compounds are also occurring. (Note that the two-product model did not fit the data any better) The condensable hydroperoxide yields that fit the SOA mechanism evaluation data ranged from 30% to 90% of the potentially condensable hydroperoxide yields predicted by the gas-phase mechanism if it is assumed to be from reactions of HO_2 with aromatic + OH + O_2 + O_2 adduct peroxy radicals. The variability of the predicted potentially condensable hydroperoxide yield in the gas-phase mechanism did not account for the variability of the condensable hydroperoxide yield that fits the SOA data, and no obvious relationship between the yield that fits the SOA data and the structure and size of the molecule could be found. However, generally similar isomers had similar values for this yield parameter.

The processes responsible for SOA formation from aromatic hydrocarbons in the presence of NO_x that is not attributable to the phenolic products are uncertain because there are a number of possibilities, and the data are not sufficient to distinguish among them. Formation of condensable organic nitrates from the reactions of aromatic + OH + O_2 + O_2 adduct peroxy radicals and NO is a chemically reasonable possibility, but mechanisms assuming that the major SOA forming process in the presence of NO_x is a primary reaction tend to overpredict SOA formation in experiments where CO or a 2nd VOC was added to aromatic - NO_x irradiations. Somewhat better fits to the data are obtained if it is assumed that SOA formation in the presence of NO_x comes mainly from reactions of aromatic oxidation products. This is represented as coming from the reactions of the model species used to represent di-unsaturated dicarbonyls formed in the pathway that does not form α-dicarbonyls as co-products, but other possibilities could probably fit the data about as well. Least biased fits to the data are obtained if the model species used to represent this product has a partitioning coefficient of 0.04 $m^3/\mu g$, lower than that used for the model species representing the hydroperoxide products. The yields of this product that fit the SOA data are 7±2% if that partitioning coefficient is used, with no obvious correlation with the size or structure of the molecule. This ~30% compound-to-compound variability[5] is comparable to the compound-to-compound variability in the primary condensable hydroperoxide yields that fit the data.

Because the current aromatic photooxidation mechanisms tend to underpredict OH levels, and therefore the amount of aromatic compound reacting; in aromatic - NO_x experiments, the SOA yield parameters for the aromatic hydrocarbons were derived by adjusting OH levels in the model to force the model to correctly predict the amount of aromatic reacting in the SOA mechanism evaluation calculations. This was necessary to avoid compensating errors when evaluating mechanisms for PM formation, with overly high SOA yields compensating for underpredictions of the amount of consumption of aromatic reacting. However, this was not possible for the simulations of the experiments with benzene because benzene reacts too slowly to reliably derive OH levels; nor was it possible for the experiments with the phenolic compounds in the presence of NO_x because they also react with NO_3 radicals. This turned out not to be a problem for the phenolic compounds because the unadjusted mechanism predicted the amount of phenolic reacting reasonably well; except for phenol in the experiments with NO_x absent, where the OH-adjusted mechanism could be used. However, this is a potential problem for benzene, and

[5] As measured by the standard deviation of the averages of the yields in Table 10 divided by the average.

it is likely that the model may overestimate the SOA yield from benzene in the presence of NO_x. No attempt was made to correct for this, but probably a correction should be made in simulations where SOA formation from benzene may be important. Fortunately, benzene is relatively unreactive and its levels are not as high as other aromatics (such as toluene) in urban atmospheres, so this potential source of bias may not have a large effect on practical airshed model applications.

Equilibrium Partitioning Coefficients. The partitioning coefficients that specify the equilibrium between condensable species in the gas and aerosol phases are inputs to the model that impact predictions of how SOA formation is affected by overall PM levels in the environment. Therefore, these are important components of any SOA formation mechanism. Theoretically estimated values of these parameters tend to underpredict measured values, in some cases by orders of magnitude (e.g., Healy et al, 2008), so they need to be derived experimentally. Since the identities of the condensable products are uncertain and in any case authentic samples are not available, they need to be derived by modeling the available chamber data. Although approximate magnitudes of these partitioning coefficients can be estimated by looking at biases in test simulations using the alternative mechanisms, the results are not highly sensitive to changes in these parameters and therefore the exact values used in the baseline model are somewhat arbitrary. This causes an uncertainty in the yield parameters that fit the data, at least in terms of their absolute magnitudes, because errors in partitioning coefficients used can often be compensated by errors in the yields of the condensable species when evaluating the mechanism against the chamber data.

This is a particular concern for compounds for which there are limited data concerning levels of PM that is formed in the evaluation experiments. Although there are data at different PM levels for most compounds, only for m-xylene are the data sufficiently varied that they can be reasonably used for evaluating at least approximate magnitudes of the partitioning coefficients. For this reason, the model uses the same partitioning coefficients for the model species, namely, those derived using the m-xylene data, regardless of which compound is being modeled. In fact, one would expect that the volatility of the condensable products (such as bicyclic hydroperoxides or whatever species contribute to SOA formation in the presence of NO_x) to vary from compound to compound. Errors in this regard can be compensated at least to some extent by opposite errors in the yield parameters for the model species, though this compromises the ability of the model to be extended to beyond the PM ranges where it was evaluated. To some extent, the apparent variability in the yield parameters for the different compounds may actually be due to variability in the volatility of the condensable oxidation products they form.

Note that the partitioning coefficients would be major factors affecting how SOA formation is affected by temperature, since they are expected to be highly temperature-dependent parameters. Temperature effects were not assessed in this study, so this aspect of the mechanism could not be evaluated. The current mechanism does not represent the temperature dependence of the partitioning coefficients, and it would have to be modified to include temperature dependence estimates before it can be used to assess effects of temperature on PM formation.

Mechanism Performance Issues. A number of uncertain parameters in the SOA mechanisms developed in this work were optimized to minimize overall biases in the model simulations of the available environmental chamber data. In that sense, the evaluations against the same dataset do not provide an independent test of the mechanism. However, the variability of the quality of the fits of the model simulations to the results of the individual experiments, i.e., the overall model error as opposed to the model bias, does provide a useful test of the overall predictive capability of the mechanism. If the variability is so great that the model predicts the results about as well as random chance, then its predictive capability is minimal even if it gives the correct results on the average. In addition, the dataset did include some types of experiments that were not used in the parameter optimizations, and modeling those did provide an independent test of the mechanism.

Figure 42 shows the distribution of model biases in the model simulations of SOA formation in all the experiments used for mechanism development and evaluation, with separate distributions shown for the experiments used to optimize the parameters in the mechanism and for those just used for evaluations. The distribution plots of model biases in the model simulations of ozone formation for the chamber experiments used by Carter and Heo (2012) for gas-phase aromatic mechanism evaluation are also shown on Figure 42 for comparison. Note that most of the runs were used for the optimizations so the runs that were not used did not significantly affect the overall distribution. As expected, the distribution is around zero for the runs used for the optimizations because the optimizations were designed to minimize average biases. The average errors in the simulations of these runs and all runs were on the order of 50%, with about 40% of the runs fitting the data to within ±25%, half the runs fitting to within ±50%, and 92% of the runs fitting the data by ±100%, as measured by the model error as defined in Equation (X)[6]. Note that by this definition, an error of 50% means that the model disagrees with the experiment by a factor of ~1.7.

The quality of fits seen in the simulations of SOA formation in this work is not nearly as good as the quality of fits typically seen in evaluating mechanisms for ozone formation, as can be seen on Figure 42. This higher degree of scatter could indicate problems with the mechanism, though if this were the primary factor one might expect to see better correlations of errors with experimental conditions. The scatter could be due to problems of reproducibility of SOA formation in the experiments, though the replicate experiments suggest a reproducibility of ±30% or better, which is less than the scatter of the model fits. However, this reproducibility in SOA formation is not nearly as good as generally seen in ozone formation in replicate experiments. It could also be due to problems with characterization of experimental conditions or to problems of modeling the dynamics of SOA formation in chamber experiments, which have uncertainties unrelated to the gas-phase chemical mechanism relevant to ozone formation. These possibilities are discussed further below.

As expected, the distribution of errors for the runs not used for the optimizations were not quite as good, with the model performing differently with different types of runs. Given the scatter of the fits to the runs used for the optimizations, the performance was generally acceptable for the benzene or m-xylene - NO_x experiments with added CO or other VOC, with the average bias being +13% for these experiments, and similar errors as seen for the other types of runs. As discussed above, the model also gave reasonably good fits for the cresol isomers not used in the optimizations, though tended to underpredict SOA in the runs with the other dimethylphenol isomers. The worst performance was for the toluene + H_2O_2 experiments, where the results of the four experiments with relatively low PM formation (≈ 12-14 $\mu m^3/cm^3$) were inconsistent with the experiment with the PM level in the normal range for the other aromatics. We derived the condensable hydroperoxide yield parameters based on the results of the higher PM toluene - H_2O_2 experiment and the toluene - NO_x + added VOC experiments, since modeling uncertainties in higher PM experiments are generally less, and those two types of experiments were generally consistent. However, the PM levels in the toluene - NO_x + added VOC experiments were also relatively low, so using these data for parameter optimization is also uncertain. Until data from additional toluene - H_2O_2 experiments are available, the condensable hydroperoxide yield parameter for toluene must be considered to be much more uncertain than for the other VOCs.

Heterogeneous Reactions. The mechanism and modeling methods used in this work assumes that most of the semi-volatile material condensed onto the particle phase will also evaporate with a rate that is controlled by an equilibrium partitioning coefficient that is specified in the mechanism. This is the case

[6] Absolute value of (model - experiment) / average (model, experiment)

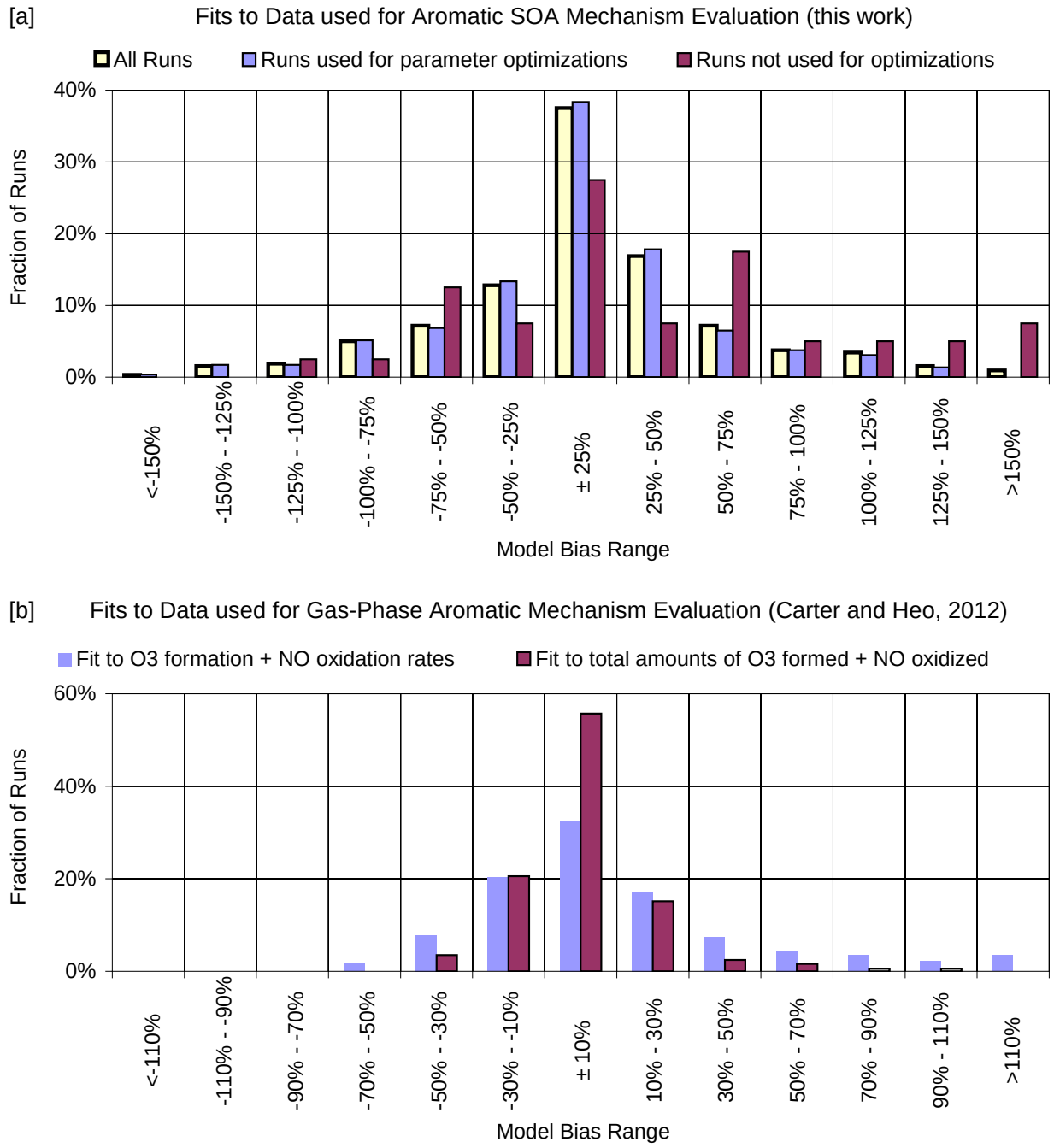

Figure 42. Distribution of model biases in the model simulations of [a] SOA formation and [b] measures of O_3 formation in all the experiments used to develop the respective mechanisms. Note the different scales used for the model bias ranges.

for most of the SOA predicted to be formed by our mechanism, except for that represented by the model species representing hydroperoxides from phenolic reactions, which (somewhat arbitrarily) are assumed to be non-volatile, and as shown on Figure 26 represents a relatively small fraction (less than 25% in all cases) of the total predicted SOA. This ignores the possibility that these species can react in the condensed phase and form oligomers or other species that are much less volatile. Such reactions are known or suspected to be important in many chemical systems involving SOA formation (Jang et al, 2002; Claeys et al, 2004; Johnson et al, 2004, 2005; Volkamer et al, 2009; Galloway et al, 2009, 2011; Kamens et al, 2011; Zhou et al, 2011). However, if such heterogeneous reactions dominated for compounds represented by a particular model species, then the model could adequately represent this simply by representing the model species as non-volatile. The data are not as well fit by assuming most of these model species are non-volatile; less biased fits to much of the data are obtained if relatively low partitioning coefficients in the range of 0.03 - 0.1 $m^3/\mu g$ are used. This indicates that if heterogeneous reactions occur, they do not dominate over evaporation, and if they occur to some non-negligible extent then they are represented in effect by using a net higher partitioning coefficient than would be appropriate for evaporation alone. But if they are non-negligible, then using an equilibrium model to determine rates of evaporation may not be appropriate, and may result in incorrect predictions when the model is applied beyond the range of conditions where the partitioning coefficients were adjusted to fit the environmental chamber data.

It is important to recognize that all the experiments for this project were carried out under dry conditions. Since heterogeneous reactions are expected to be more favored when water is present (Claeys et al, 2004; Volkamer et al, 2009; Galloway et al, 2009, 2011; Kamens et al, 2011; Zhou et al, 2011), use of higher net partitioning coefficients or non-volatile model species, or including some representation of heterogeneous reactions, may be necessary when modeling humidified experiments or ambient atmospheres. These heterogeneous reactions may also be affected by factors such as acidity and the presence of inorganics in the particle phase. This will need to be assessed when the mechanism is evaluated using experiments carried out under humidified conditions and with other aerosols present.

Mechanisms for Ambient Modeling. This project has focused primarily on modeling SOA formation from individual aromatic hydrocarbons in environmental chamber experiments. However, the ultimate goal of this effort (and the primary reason it was funded) was to develop mechanisms that can be used in airshed models to predict SOA formation in ambient atmospheres. The mechanisms developed in this work were used to derive SOA yield parameters for the lumped aromatic model species (ARO1 and ARO2) that are used in airshed models with SAPRC mechanisms to represent reactions of aromatics. Estimates had to be made for SOA parameters for higher molecular weight aromatics contained in ambient mixtures that were not studied, and these estimates are highly uncertain. However, it turns out that the individual compounds studied for this project comprise respectively ~95% and ~75% of the compounds used to derive parameters for ARO1 and ARO2 in the ambient mixture that were used to derive lumped parameters for SAPRC-07. This mixture is out of date and needs to be updated, but it is expected that the compounds studied will still comprise an important fraction of aromatic hydrocarbons in the atmosphere.

Of greater concern for using this mechanism for ambient modeling is the limited scope of the mechanism developed for this project. It covers only SOA formation from aromatics, and only under dry conditions and at a single temperature. Despite those limitations, this is an important and necessary starting point. However, this is clearly not the ending point to developing reliable SOA mechanisms for ambient modeling, and additional work is needed. This is discussed further in the "Conclusions and Recommendations" section of this report.

SOA Modeling Methods and Uncertainties

As is the case with predicting SOA formation in the atmosphere, predicting SOA formation under chamber conditions also requires SOA mechanisms to appropriately model rates of particle growth from condensable species formed in the gas phase. This requires (1) predicting the rates of condensation of gas-phase species onto particles, (2) predicting rates of nucleation and creation of new particles, and (3) predicting rates of evaporation of semi-volatiles off the particles back into the gas phase. Each of these has uncertainties, as discussed below.

Evaporation. The model used in this work incorporates the assumption that the rates of evaporation of a condensable species off the particles can be calculated from the rate of condensation given the equilibrium partitioning coefficients (Kp's) that are specified with the mechanism. This is based on absorption-based partitioning theory (Pankow, 1994a,b), which has limitation (e.g., Shiraiwa et al, 2011; Perraud et al, 2012). Although the Kp's are uncertain as discussed above, they are specified as part of the mechanism and therefore their uncertainty is not considered as a modeling methods issue that is relevant to the discussion in this section. The assumption that an equilibrium-based approach can be employed may lead to incorrect predictions if heterogeneous reactions are competitive with evaporation[7], but this is also a chemical mechanism issue. On the other hand, the assumption that all the PM present is organic material that affects this equilibrium is an issue concerning the environment that is being modeled and not the chemical mechanism. This assumption is probably reasonable when modeling these chamber experiments, since condensable inorganics are not expected to be present. Therefore, this is not considered a significant uncertainty issue in this mechanism evaluation work. However, this assumption is probably not valid when modeling ambient atmospheres where inorganics constitute a significant fraction of the PM present (Zhang et al, 2007; Jimenez et al, 2009).

Condensation. Theories and methods exist to predict rates of condensation of gas-phase materials onto particles, though they depend on assumptions about particle shapes and sizes, which are difficult to predict in the model. Test calculations carried out in this work show that the results of model simulations of PM formation in the experiments are affected by the condensation rates that are used in the model, and indicate that it is not appropriate to assume that condensation is so fast that a simple equilibrium model can be employed. The experiments with lower PM levels and models using relatively low partitioning coefficients (as is the case with the mechanism developed for this project) are most sensitive to assumptions affecting calculated condensation rates. The model we used does not include a method to predict how particle sizes evolve over time, and simply uses an empirical relationship between particle sizes and amounts of PM material formed that may not be applicable to all conditions. This introduces uncertainties in the model simulations, particularly for experiments where PM levels are predicted to be relatively low. It may be that evaluating SOA mechanisms may require use of more sophisticated model for how particles are formed and grow than was employed in this work. This is also applicable to nucleation, as discussed below.

Nucleation. The method used to represent condensation of condensable gas-phase species onto particles requires the existence of particles that condensable species can condense onto. Since the experiments modeled in this project did not have seed aerosol present initially, the model needed to have some representation of creation of new particles, or nucleation. The model used in this work has a highly simplified representation of nucleation. It was assumed that nucleation was as relatively fast, but not so fast that it would perturb the equilibrium when measurable amounts of particles are present. Sensitivity calculations indicate that assumptions we make concerning how to model nucleation rates in this range may affect SOA predictions in experiments where relatively low amounts of PM are formed and where

[7] If heterogeneous reactions dominate over evaporation then the system can be adequately modeled simply by assuming that evaporation does not occur, i.e., that the relevant model species is non-volatile.

partitioning coefficients are relatively low. This is also an area of uncertainty where use of a more sophisticated model may be appropriate, at least for screening purposes.

The uncertainties concerning to condensation and nucleation (though probably not evaporation) may well be contributing to some of the variability of the mechanism performance that was discussed above. This is a particular concern when the final PM level is low (e.g., less than 10 $\mu g/m^3$). It is consistent with Bowman et al (1997) and Kroll et al (2007). However, as the PM level increases above ~10 $\mu g/m^3$, the impact of these uncertainties may become less important.

Uncertainties Due to Chamber Effects

Using environmental chamber data to develop and evaluate mechanisms requires an appropriate representation of chamber effects when modeling chamber experiments. This is known to be important when evaluating gas-phase mechanisms (e.g., see Jeffries et al, 1992; Carter et al, 2005b), and is probably even more important for evaluating SOA mechanisms. Known or possible SOA-related chamber effects include background particle formation, loss of particles to the walls, and possibly absorption and evaporation of semi-volatile materials on the walls. These issues are discussed below.

Background Particle Formation. Background particle formation in our chamber is observed in pure air irradiations but not in the dark and not in experiments where reactants suppress OH radical levels. This can be modeled by assuming that contaminants evaporate from the walls then react with OH radicals to form non-volatile materials, with the rate of evaporation being adjusted to fit PM levels measured in pure irradiation characterization experiments. This apparent contamination evaporation rate is variable, and could be a factor affecting mechanism evaluation results if the background particle formation is a significant fraction of the total calculated PM for the experiment. To assess this, model simulations were carried out with all mechanism evaluation experiments assuming no background particle formation. The effect of removing the background particle formation was relatively small for most experiments, with the calculated PM being reduced by less than ~10% for 85% of the experiments. However, the background particle formation was calculated to reduce PM levels by 40% or more for 19 experiments of the experiments in the evaluation dataset. This is considered to be an unacceptable degree of sensitivity to this highly variable parameter so these 19 experiments were removed from the evaluation dataset. However, background particle formation may be a factor affecting evaluation results at least to some extent for a number of other experiments. The most affected experiments would be runs with relatively low PM levels but relatively high levels of OH radicals to react with the chamber background PM precursor.

Particle Wall Losses. Particles are lost to the walls at rates of ~30%/hour, though the rates are highly variable from run to run. They can be characterized reasonably well for each experiment by fitting the loss of particle numbers after the time of maximum PM number to a unimolecular decay rate, so estimating them is not a large uncertainty. But the variability from run to run is a concern and may be contributing to the variability of the evaluation results. However, there is essentially no correlation between the particle wall loss rates and the model errors of the evaluation experiments. One might expect particle wall loss rates to depend on particle sizes, which also vary from run to run, but there is also no correlation. The reasons for this variability in wall losses, and the implications concerning uncertainties in mechanism evaluations, are unknown at the present time.

Absorption and Evaporation of Gas-Phase Species on the Walls. Another chamber effect that needs to be considered is the absorption and possible evaporation of condensable species formed in the gas phase onto the chamber walls. Matsunaga and Ziemann (2010) showed that this does occur in chambers made of the same Teflon material as used for the walls of our chamber, though the chamber they employed was somewhat smaller. They argue that the total mass of organic materials on the walls is

orders of magnitude higher than suspended in the particle phase in normal experiments, so in long run (i.e., in equilibrium) all the equilibrium materials would be on the walls. On the other hand, the rate of absorption or condensation onto particles is faster than absorption on the walls, though the time scales of wall absorption they measured in their chamber were well within the time scales of our experiments. We assume that wall absorption is not significant in our mechanism evaluation calculations, though we do not have any data to directly support this assumption. Evidence that it is not highly important comes from the fact that PM volume measurements in our chamber corrected for particle wall loss rates calculated using particle number decay rates do not decline at the end of the experiments. If wall absorption of gas-phase semi-volatiles were sufficiently important, i.e., on the order of particle wall loss rates, then the particle volumes would decline at the end of the experiments faster than the particle numbers because of wall losses of semi-volatiles evaporating from the particles. However, calculations assuming that absorption of gas-phase species is non-negligible can fit the final SOA volume data as well as the models assuming that wall absorption is not important, and the results give significantly higher values for some SOA yield parameters that fit the model to the data. Therefore, if wall absorption is not negligible, it may mean that the SOA yield parameters derived in this work may be too low. More information is needed concerning wall absorption rates of gas-phase species in our chamber to determine if this needs to be taken into account in the wall model, and if so what absorption and evaporation rates should be used.

Environmental Chamber Database

New Data from this Project. The experiments carried out for this project represent a significant expansion of the database of environmental chamber experiments for evaluating mechanisms for SOA formation. The new experiments include a total of 217 separate experiments suitable for aromatic SOA mechanism evaluation, and results in approximately a factor of three increase in the number of such experiments from our environmental chamber facility. The new experiments expand the number of aromatic compounds that have SOA evaluation data from 6 to over 20, most of which were studied in both the presence and absence of NO_x. Most of the new experiments with NO_x present are also suitable for gas-phase mechanism evaluation, and in fact were an important subset to the experiments used when developing and evaluating the gas-phase aromatics mechanism that was used as the starting point for the SOA mechanism developed for this project (Carter and Heo, 2012).

The experiments were conducted for the purpose of evaluating predictive mechanistic models, but the results can also be used to expand the existing database of chamber experiments suitable for deriving SOA yield parameters using empirical models (Carlton et al, 2010). Although the data from this study confirmed pervious results that Odum-type models cannot fit yield data obtained from aromatic - NO_x experiments because of the dependence of SOA formation processes on NO_x, these data could well be used to support development of more sophisticated empirical models that may take this NO_x dependence into account. Developing such models was beyond the scope of the present project. On the other hand, the results of the aromatic - H_2O_2 experiments could be relatively reasonably fit using the Odum 1-product model (Ng et al, 2007; Henze et al, 2008), though not all of the experiments had enough experiments to derive both parameters needed for this model.

Available Data from Other Laboratories. Because of limitations in resources and data availability, the SOA mechanism evaluation database used in this study was restricted to experiments carried out in our environmental chamber, though it did include experiments carried out in our laboratory prior to this project. A number of chamber experiments carried out in other chambers have been used for SOA mechanisms evaluations (e.g., Johnson et al, 2005; Hu and Kamens, 2007), and some of them may well be suitable for the purposes of this study. However, obtaining data and necessary characterization conditions from other laboratories is not always practical, in many cases the characterization information and control of conditions do not meet the standards we require for this purpose, or the experiments were carried out under conditions that are beyond the scope of this present study. For example, because of

variability of lighting and temperature conditions, we do not consider data from outdoor chamber experiments particularly useful for deriving mechanistic parameters that fit chamber data, though they will be useful in the future to evaluate mechanisms for suitability in ambient conditions. In addition, at this phase of the project we are restricting the evaluation to experiments with single compounds or very simple mixtures carried out under dry conditions at a single temperature without added aerosols from other sources, because this is a necessary first step in the mechanism development process.

However, chamber data from other laboratories should not be ignored, just as is the case for the data obtained from our chamber. A comprehensive mechanism evaluation database needs to include well-documented and suitably characterized data from as many laboratories as possible. The Eurochamp project (see http://www.eurochamp.org/), which is aimed integrating atmospheric simulation data from multiple European laboratories, provides a good model for data integration in general, and the possibility of incorporating our data, as well as data from chambers in other non-European countries, into this project should be explored. In addition to providing a more comprehensive evaluation database, there needs to be an evaluation of consistency of SOA data obtained from different laboratories, especially considering the greater characterization uncertainties for SOA-related chamber effects. As far as we are aware, no such inter-laboratory comparison of SOA data designed for mechanism evaluation has been carried out.

In any case, the SOA mechanism evaluation database used in this work is insufficient to develop SOA mechanisms for use in air quality models because it concerns only aromatics, has data only for single mixtures, and includes only experiments carried out under dry conditions at a single temperature and without added aerosols from other sources. Data do exist for other compounds and mixtures and from experiments carried out under more varied conditions both at our laboratory and elsewhere, and these would need to be incorporated into the database used in any follow-up projects for further SOA mechanism development and evaluation. This would involve surveying data from different laboratories for relevance, availability to outside groups, and examinations of data quality, adequacy of control of conditions, and adequacy of characterization information, including availability of data from necessary control and characterization experiments. It would also require setting up the data for modeling and simulating the results with existing mechanisms (e.g., see Carter, 2004; Yarwood et al, 2012), which in our experience has proven to be a valuable method for assessing data quality and characterization, even if the mechanism used does not perform well in simulating the results.

Data Needs. Although the availability and suitability of existing data for SOA mechanism evaluation needs to be surveyed before designing any new experimental projects, it is clear that the available data are not sufficient to addressing the data needs for developing valid and reliable mechanisms for predicting SOA formation under ambient conditions. Ideally we need well-characterized SOA mechanism evaluation data for a variety of representative compounds and under a variety of relevant conditions. This would include the following types of experiments.

- Additional experiments with toluene, particularly toluene - H_2O_2 experiments where higher levels of PM are formed, are needed to reduce the significant uncertainty in the SOA yield parameters for this important compound.
- Different types of SOA forming compounds need to be studied. There are already a variety of experiments with biogenic compounds, but more types of anthropogenic compounds, including some with lower but non-negligible SOA forming potentials, need to be studied.
- The chemical systems studied should range from single compounds and simple mixtures such as used in this study through complex ambient mixtures. This will allow the mechanisms to be evaluated in a stepwise manner, with effects of incremental changes being used to isolate sources of mechanism errors as they are found. The aromatic experiments with added CO or VOC proved useful to this project and more such experiments are needed, including especially such

experiments with phenolic compounds, which would be useful not only for evaluating the important phenolic SOA mechanisms under a wider range of conditions, but to make the conditions of the phenolic experiments more representative of ambient conditions. Experiments with two different SOA-producing compounds of the same and different types (e.g., an aromatic compound with a terpene) need to be studied before moving to complex ambient mixtures. Note that the ambient surrogate mixtures presently used in chamber experiments may not be suitable for SOA evaluation because they may not include higher molecular weight compounds present in ambient mixtures that do not contribute much to O_3 reactivity because of relatively low levels but may have a disproportionate effect on SOA formation.

- The effects of humidity need to be studied since this may affect heterogeneous reactions on the particles that may affect partitioning and the validity of models based on the absorption-based partitioning theory (Pankow, 1994a,b). Previous studies indicate that humidity may enhance SOA formation from aromatic hydrocarbons (Kamens et al., 2011; Nakao et al., 2011b); though our recent work (Nakao et al. 2011b) suggests that glyoxal uptake plays a minor role in aromatic SOA formation. Further investigation is necessary to probe the mechanism of enhanced SOA formation under humid conditions, such as studies of aqueous reaction of phenolic compounds (Sun et al., 2010). Humidity effects may be quite different for different types of compounds, and also for mixtures of different types of SOA-forming VOCs, so this needs to be studied as well.

- Temperature is expected to be very important in affecting SOA formation, if only because volatility and partitioning coefficients are known to be highly temperature-dependent. Our chamber is one of the few available chambers that have been characterized for mechanism evaluation work where temperature can be controlled in a systematic manner, though unfortunately repairs to the arc light system, or a method to isolate the blacklights from the temperature in the reactors[8], are needed before it can be used for systematic temperature effects studies. Temperature effect studies may also be useful in evaluating whether the mechanisms have appropriate partitioning coefficient parameters, as well as providing needed data to evaluate model representations of how these parameters vary with temperature.

- Mechanism evaluation experiments are also needed to assess the effects of seed aerosol on SOA formation. Kroll et al. (2007) suggested that chamber experiments carried out without inorganic seeds would underestimate SOA yield due to loss of semi-volatiles to the chamber surface. However, we do not observe the seed effect proposed by Kroll; this may be the result of the large reactor size, small surface area to volume ratio, and additional controls on this environmental chamber system. (Warren et al, 2008b). The presence of an organic seed should reduce the sensitivity of the experiments to uncertainties regarding nucleation, and may be useful in assessing whether assumptions we make in this regard may be affecting parameters in the mechanisms that are adjusted to fit chamber data.

- Because of problems with the light source employed in our chamber, most of the mechanism evaluation experiments used in this study were carried out using a blacklight light source. Blacklights give a good representation of the solar spectrum in the UV range which affects most of the photolysis reactions involved in atmospheric chemistry, but their spectrum is poor in the longer wavelength region that affects photolysis of NO_3 radicals and some aromatic photooxidation products. However, no significant differences between black lights and arc lights were seen when evaluating aromatic mechanisms for ozone formation (Carter and Heo, 2012), so we do not think this is a major issue with this evaluation. But some mechanism developers prefer not to use blacklights when evaluating mechanisms (e.g., Whitten et al, 2010), so more data using arc light sources, which provide a more realistic spectrum, are needed to improve the credibility

[8] The output of blacklights is affected by temperature, so changing the temperature of blacklights would change the light intensity.

of the evaluation, and to verify the utility of the large database developed for this project. In addition, ozone formation results of early smog chamber experiments with cresols carried out using arc lights, such as the run EC281 o-cresol - NO_x run shown on Figure 23, are not consistent with ozone formation results in the cresol experiments carried out using blacklights for this project. Although SOA was not measured in run EC281, clearly the lower reactivity seen in that experiment would mean lower SOA formation. Therefore, carrying out arc light experiments with phenolic compounds is clearly a near-term priority.

Carrying out a comprehensive set of experiments with all of these factors examined would be a multi-year effort involving hundreds if not thousands of experiments and is not likely to be funded in the near or even mid-term. Priorities for additional studies should be based on the current stage of mechanism development and to determine effects of various factors to guide priorities for additional experiments. The experiments with the single compounds, single temperature, dry conditions and no seed aerosol that were used in this study were appropriate for the needs for the first stage of systematic mechanism development, but now additional factors need to be studied. The priorities for additional experiments needed for the next stage of SOA mechanism development are discussed in the following section.

Conclusions

Regulatory agencies such as the California ARB need scientifically valid and reliable models for predicting SOA formation in the atmosphere. Unfortunately, this need may not be fully addressed in the near term because of the complexity of the problem and the considerable amount of work that is still required. The current stage of SOA mechanism development reminds some of us of the situation in gas-phase atmospheric mechanism development in the late 1970's, when the process of developing useable chemical kinetic mechanisms for airshed models was just beginning. Hopefully it won't take more than 10 years to reach the stage on SOA modeling as it did to go from that stage in the late 1970's to the development of the CB4 (Gery et al, 1988), RADM (Stockwell et al, 1990) and SAPRC-90 (Carter, 1990) gas-phase mechanisms in the late 1980's, but is a possibility given the greater complexity of the problem. The mechanism developed in this work may be an improvement over the empirical add-in models currently used for SOA in airshed models, but its scope is limited to aromatics, it does not provide for temperature or humidity effects, and it has not been evaluated over the range of conditions that it needs to cover.

Nevertheless, this work represents what we believe was necessary at this stage in the process of adapting gas-phase mechanisms to predicting SOA formation in the atmosphere, and we believe it represents significant progress. A mechanism with our condensable model species representing five types of SOA forming processes was developed that could simulate the available data reasonably well, or at least without large obvious biases, in environmental chamber experiments with 14 different types of aromatic hydrocarbons and a number of representative phenolic compounds and with a variety of reactant concentrations and NO_x levels. A large part of this project was to carry out the environmental chamber experiments necessary to support this development and evaluation. There were mechanism evaluation issues such as greater scatter in the fits to the data than seen when evaluating gas-phase mechanisms and clearly many uncertainties exist in the mechanism as well as the modeling methods and chamber effects model, but this reflects the current state of the science.

The areas of uncertainty concerning the mechanism developed for this project have been discussed above. The gas-phase mechanism itself is uncertain and this clearly causes uncertainties in the overall mechanism for SOA formation. For example, because the gas phase mechanism tends to underpredict amounts of aromatic consumed in aromatic - NO_x experiments, it is necessary to adjust the OH radical levels in the SOA mechanism evaluation calculations to force the model to calculate the correct amounts of aromatic reacting to avoid compensating errors. The available data are not sufficient to

determine exactly which of the various possible types of SOA-forming processes are actually the most important for aromatics, though the five processes represented by the current model species should reflect the major overall features of the possible processes concerning how SOA formation depends on reaction conditions. The validity of the absorptive partitioning assumptions and the appropriateness of neglecting heterogeneous reactions in this mechanism are also uncertain. A number of parameters in the mechanisms had to be derived by adjustments to fit the chamber data, and uncertainties in the chamber effects model or the methods used to estimate condensation, evaporation or nucleation rates will affect the values of the parameters that are derived. But this represents our best estimate of the mechanism given our current state of knowledge.

With regard to implementation of an improved SOA mechanism in airshed models, the greatest limitation of this work is not necessarily the many uncertainties (which will always be present) but the limitation in the scope and applicability of the mechanism and its evaluation. The SOA-forming reactions in the mechanism developed in this work could well be added to the aromatic reactions in models that presently use SAPRC mechanisms (once they are updated to SAPRC-11 based on the work of Carter and Heo, 2012), and it would be a significant improvement over the present models. However, this would not account for SOA formation from other types of emitted VOCs (e.g., biogenics), would not account for effects of temperature that are expected to be important, and may not give correct predictions in the presence of humidity or in the presence of the other aerosol species that are present in real atmospheres. At least these aspects of the mechanism need to be enhanced before this mechanism is really ready for use in airshed models.

The additional work needed to develop a fully model-ready mechanism could not be carried out with the time and resources available to this project. The number of useable experiments conducted for this project actually exceeded the number promised in the proposal, and the person-hours used for analysis and mechanism development also exceeded the budgeted amount. The following section gives our recommendations for additional work that is needed in the near- and mid-term, both for a follow-up project from our laboratories but for needed research in general.

Recommendations

The recommendations discussed below will be given in approximate order of priority in terms of near-term and longer-term work necessary to address the needs of the CARB and other regulatory agencies for modeling SOA formation in the lower troposphere. This does not mean that the longer-term work further down the list is lower priority and should not be supported now, but just means that it may take longer to get the benefits that the CARB needs for its near-term regulatory activities. But in the long run the benefits of supporting this longer-term work will be well worth the resources required, and the sooner the work starts the sooner the CARB and others will get the benefits from them.

As discussed above, additional near-term work is needed before the mechanism developed for airshed models will be ready for implementation in airshed models. At a minimum it needs to be expanded to cover at least the classes of VOCs whose SOA formation is already represented in airshed models. For example, in addition to representing SOA from aromatics hydrocarbons, the CMAQ model has representations for SOA formation from isoprene, terpenes, and alkanes (e.g., see Carlton et al, 2010). Although these are based on parameterized models whose validity and applicability are uncertain, having these representations is better than ignoring SOA from these species, particularly terpenes. Therefore, for the nearest term the mechanism developed in this work could replace the existing representations of aromatics hydrocarbons and phenols, but the representations for the other classes of VOCs would have to be retained for the time being.

With regard to improving the representations for the other classes of VOCs in the near term, the first priority is probably to evaluate and if necessary improve the methods used in existing models to predict SOA formation from terpenes and isoprene. This is the priority for practical modeling applications because SOA from terpenes is probably more important than SOA from aromatics in many situations. A large body of chamber data on SOA from terpenes and isoprene exists, including data from our chamber, that could be used to evaluate and if necessary improve existing SOA mechanisms, provided that data from a sufficient number of experiments are available and the experiments were carried out under sufficiently well controlled and characterized conditions for modeling. Targeted additional experiments may be needed if the results of a review of available data indicate that there are data gaps or that there are inconsistencies between laboratories.

With regard to improving representations for anthropogenic VOCs, we believe that additional improvements to the aromatic mechanisms is probably a higher priority than improving the SOA mechanisms for anthropogenic alkenes and alkanes, because the aromatics are believed to be more important SOA sources, and because of the limitations of the aromatics mechanism developed in this work. As discussed above, the priorities for improving the aromatics SOA mechanism include the following:

- Determine the extent to which the present mechanism can predict SOA from aromatics in humidified experiments and modify it as needed to predict humidity effects.
- Develop and evaluate methods to predict how temperature affects SOA formation. Experimental studies of temperature effects should also reduce uncertainties concerning partitioning coefficients, and provide data concerning whether their magnitudes as used in the model are appropriate and how they vary with temperature.
- Determine if inorganic and organic seed aerosols, and the presence of other SOA-forming VOCs affect the predictive capabilities of the mechanism and adjust it as needed. The partitioning behavior of condensable species may depend on the aerosols present and the additional aerosol species may affect heterogeneous reactions and humidity effects.
- Conduct additional targeted experiments to fill data gaps and improve the predictive capability of the mechanism. This would include experiments using an arc light source (with phenolics being a priority), phenolic - NO_x experiments with added VOCs, and additional experiments for toluene, an important aromatic where the current database has problems.

With regard to other types of anthropogenic VOCs, the priority is probably collecting and evaluating available data concerning relative SOA formation potentials of individual compounds, and determining the priorities for further studies concerning how to best evaluate SOA formation potentials for previously unstudied compounds and represent their effects on SOA formation in models. Existing empirical data may be adequate for at least potentially the most important compounds, but probably a standard experimental approach, perhaps analogous to the incremental reactivity experiments used to develop mechanisms for ozone reactivity scales (see Carter, 2010a and references therein), will need to be developed for screening SOA formation potentials and, if necessary, developing and evaluating mechanisms in the model for calculating SOA formation potentials. We recommend an initial screening study to evaluate available data and models and recommend how best to proceed. Ideally it could include resources for experiments to investigate experimental approaches, though this could be reserved to a second phase for this project. The next phase would be to use the recommended methods to develop and improve SOA mechanisms for VOCs in emissions inventories that are known or suspected to contribute to atmospheric SOA.

How to seamlessly link gas-phase chemistry and SOA formation without demanding an unacceptable amount of computational resources is another issue that needs to be addressed. The lumping

approach used in current SAPRC and other mechanisms are probably not optimum for SOA modeling, and additional model species and less lumping of emitted VOCs is needed. However, beyond a certain point the additional model species and mechanistic detail just add complexity and computing time without significantly improving model accuracy, especially considering the many other uncertainties involved. Mechanisms with varying levels of detail need to be implemented in the 3-D models used by regulatory agencies and their predictions need to be compared. This would give us at least an idea of the point of diminishing returns with regard to mechanism detail, and guide mechanism developers on the appropriate level of detail for airshed model applications. Note that this would require developing more detailed versions of the existing mechanisms to serve as the standard against which the more condensed mechanisms can be compared. Of course, these detailed mechanisms would need to be at least as consistent with the available data as the condensed mechanism developed for this project, and the condensed mechanisms whose predictions are compared with the detailed versions need to be derived from those detailed mechanisms in a chemically consistent manner. Otherwise, the comparisons of model outputs would be looking at effects of using different chemistries, not looking at effects of condensations.

Uncertainties in SOA-related chamber effects, and concerning the best way to represent absorption and nucleation processes when modeling chamber experiments, affect SOA mechanisms that are derived from chamber data to an extent that is difficult to determine. The large variability on quality of model fits when simulating multiple experiments is a concern, and it may be due to chamber characterization or modeling methods problems. The approach used in this work to represent absorption and nucleation processes and wall effects needs to be independently reviewed by experts in the physics of particle formation, and have them either approve or make recommendations for how to improve our modeling methods, and to recommend what types of experiments might be useful to test the approach we use and to better understand the uncertainties and how to reduce them.

Intercomparisons of *well-characterized* experiments carried out at different laboratories are needed to further assess the potential importance of chamber artifacts of possible experimental methodology problems at different laboratories. This would include conducting needed control and characterization experiments as well as representative experiments used for SOA mechanism development. The causes of the variability of the SOA data need to be better understood, and results of such intercomparisons may be revealing.

Because of the importance of gas-particle partitioning in modeling SOA formation, the scientific soundness and appropriateness of the absorptive partitioning assumptions need to be further evaluated both experimentally and theoretically. In addition, more accessible and scientifically sound methods for deriving or estimating partitioning coefficients, and how they vary with temperature and other environmental factors, are needed. This may require developing improved methods for actually measuring gas-particle partitioning coefficients, and certainly will require improved theoretical or empirical methods. Estimation procedures that are off by orders of magnitude are not useful and need to be modified or replaced, using empirically derived parameters if needed.

Finally, work needs to continue in chamber and laboratory studies to characterize the chemical identity and properties of SOA formed from aromatics and other compounds to determine the details of the reaction mechanism actually responsible for their formation. For aromatics, further chemical characterization and mechanistic and product studies are still needed concerning the gas-phase mechanism. Deriving condensed and semi-empirical mechanisms with parameters adjusted to fit chamber may be necessary to develop the predictive mechanisms that airshed model users need now, but in the long run we need to understand the details of the actual chemical processes so that we can model them predictively with a mechanism based on this understanding. This may take many years, but eventually the improved scientific validity and predictive accuracy of the models and the other benefits of the scientific knowledge we obtain, such as knowing the actual fates of the emitted compounds and how they impact

the environment and public health, will be well worth the effort. In the meantime, the insights obtained as such studies proceed should result in improved condensed mechanisms and parameterizations that have better predictive capability and less uncertainty when used in atmospheric models.

REFERENCES

Atkinson, R. and J. Arey (2003): "Atmospheric Degradation of Volatile Organic Compounds," Chem. Rev. 103, 4605-4638.

Atkinson, R., C. N. Plum, W. P. L. Carter, A. M. Winer, and J. N. Pitts, Jr. (1984): "Rate Constants for the Gas-Phase Reactions of Nitrate Radicals with a Series of Organics in Air at 298 +/- 1 K," J. Phys. Chem. 88, 1210-1215.

Bertram, T. H., R. C. Cohen, W. J. Thorn III, and P. M. Chu (2005): "Consistency of Ozone and Nitrogen Oxides Standards at Tropospherically Relevant Mixing Ratios," J. Air & Waste Manage. Assoc. 55(10), 1473-1479.

Berndt, T. and O. Böge (2003): "Gas-Phase Reaction of OH Radicals with Phenol," Phys. Chem. Chem. Phys. 5, 342-350.

Bloss, C., V. Wagner, A. Bonzanini, M. E. Jenkin, K.Wirtz, M. Martin-Reviejo, and M. J. Pilling (2005): "Evaluation of Detailed Aromatic Mechanisms (MCMv3 and MCMv3.1) against Environmental Chamber Data," Atmos. Chem. Phys. 5, 623–639.

Bowman, F. M., J. R. Odum, J. H. Seinfeld, and S. N. Pandis (1997): "Mathematical Model for Gas-Particle Partitioning of Secondary Organic Aerosols," Atmos. Environ. 31(23), 3921-3931.

Carlton, A. G., Bhave, P. V., Napelenok, S. L., Edney, E. O., Sarwar, G., Pinder, R. W., Pouliot, G. A., and M. Houyoux (2010): "Model Representation of Secondary Organic Aerosol in CMAQv4.7," Environ. Sci. Technol. 44, 8553-8560.

Carter, W. P. L. (1990): "A Detailed Mechanism for the Gas-Phase Atmospheric Reactions of Organic Compounds," Atmos. Environ. 24A, 481-518.

Carter, W. P. L. (1994a): "Development of Ozone Reactivity Scales for Volatile Organic Compounds," J. Air & Waste Manage. Assoc., 44, 881-899.

Carter, W. P. L. (1994b): "Calculation of Reactivity Scales Using an Updated Carbon Bond IV Mechanism," Report Prepared for Systems Applications International Under Funding from the Auto/Oil Air Quality Improvement Research Program, April 12.

Carter, W. P. L. (2000a): "Documentation of the SAPRC-99 Chemical Mechanism for VOC Reactivity Assessment," Report to the California Air Resources Board, Contracts 92-329 and 95-308, May 8. Available at http://www.cert.ucr.edu/~carter/absts.htm#saprc99 and http://www.cert.ucr.edu/~carter/reactdat.htm.

Carter, W. P. L. (2000b): "Implementation of the SAPRC-99 Chemical Mechanism into the Models-3 Framework," Report to the United States Environmental Protection Agency, January 29. Available at http://www.cert.ucr.edu/~carter/absts.htm#s99mod3.

Carter, W. P. L. (2002): "Development of a Next Generation Environmental Chamber Facility for Chemical Mechanism and VOC Reactivity Research," Draft Research Plan and First Progress Report to the United States Environmental Protection Agency Cooperative Agreement CR 827331-01-0, January 3. Available at http://www.cert.ucr.edu/~carter/epacham.

Carter, W. P. L. (2004): Evaluation of a Gas-Phase Atmospheric Reaction Mechanism for Low NO_x Conditions," Final Report to California Air Resources Board Contract No. 01-305, May 5. Available at http://www.cert.ucr.edu/~carter/absts.htm#lnoxrptf.

Carter, W. P. L. (2008). "Reactivity Estimates for Selected Consumer Product Compounds," Final Report to the California Air Resources Board Contract 06-408, February 19. Available at http://www.cert.ucr.edu/~carter/absts.htm#aminrep.

Carter, W. P. L. (2009a): "Investigation of Atmospheric Ozone Impacts of Trans 1,3,3,3-Tetrafluoropropene," Final Report to Honeywell International Inc, February 9.

Carter, W. P. L. (2009b): "Investigation of Atmospheric Ozone Impacts of 2,3,3,3-Tetrafluoropropene," Final Report to Honeywell International Inc, June 2.

Carter, W. P. L. (2009c): "Investigation of Atmospheric Ozone Impacts of 1-Chloro-3,3,3-Trifluoropropene," Final Report to Honeywell International Inc, June 8.

Carter, W. P. L. (2010a): "Development of the SAPRC-07 Chemical Mechanism and Updated Ozone Reactivity Scales," Revised Final report to the California Air Resources Board Contract No. 03-318. January 27. Available at www.cert.ucr.edu/~carter/SAPRC. See also Carter, W. P. L. (2010): "Development of the SAPRC-07 Chemical Mechanism," Atmospheric Environment, 44, 5324-5335.

Carter, W. P. L (2010b): "Updated Maximum Incremental Reactivity Scale and Hydrocarbon Bin Reactivities for Regulatory Applications," Report to the California Air Resources Board, Contract 07-339, January 28, available at http://www.cert.ucr.edu/~carter/SAPRC/MIR10.pdf.

Carter, W. P. L. (2011): "Environmental Chamber Studies of Ozone Impacts of Coatings VOCs," Final Report to the California Air Resources Board, Contract 07-339, March 11. Available at http://www.cert.ucr.edu/~carter/pubs/coatrpt2.pdf.

Carter, W. P. L. (2012): Reports available at "Downloadable Documents by William P. L. Carter," http://www.cert.ucr.edu/~carter/pubs. Last updated May 11.

Carter, W. P. L., J. A. Pierce, and I. L. Malkina (1992): "Investigation of the Ozone Formation Potential of Selected Volatile Silicone Compounds," Final report to Dow-Corning Corporation, November.

Carter, W. P. L., D. Luo, I. L. Malkina, and D. Fitz (1995): "The University of California, Riverside Environmental Chamber Data Base for Evaluating Oxidant Mechanism. Indoor Chamber Experiments through 1993," Report submitted to the U. S. Environmental Protection Agency, EPA/AREAL, Research Triangle Park, NC, March 20. Available at http://www.cert.ucr.edu/~carter/absts.htm#databas.

Carter, W. P. L., J. H. Seinfeld, D. R. Fitz, and G. S. Tonnesen (1999): "Development of a Next-Generation Environmental Chamber Facility for Chemical Mechanism and VOC Reactivity Evaluation," Proposal to the U. S. Environmental Protection Agency, February 22. Available at http://www.cert.ucr.edu/~carter/epacham.

Carter, W. P. L. and I. L. Malkina (2005): "Evaluation of Atmospheric Impacts of Selected Coatings VOC Emissions," Final report to the California Air Resources Board Contract No. 00-333, March 21. Available at http://www.cert.ucr.edu/~carter/absts.htm#coatrpt.

Carter, W. P. L., D. R. Fitz, D. Cocker, III, I. L. Malkina, K. Bumiller, C. G. Sauer, J. T. Pisano, C. Bufalino, and Chen Song (2005a): "Development of a Next-Generation Environmental Chamber Facility for Chemical Mechanism and VOC Reactivity Research," Final Report to the United States Environmental Protection Agency Cooperative Agreement CR 827331-01-0. June 27. Available at http://www.engr.ucr.edu/~carter/epacham/chamrpt.pdf.

Carter, W. P. L., D. R. Cocker III, D. R. Fitz, I. L. Malkina, K. Bumiller, C. G. Sauer, J. T. Pisano, C. Bufalino, and C. Song (2005b): "A New Environmental Chamber for Evaluation of Gas-Phase Chemical Mechanisms and Secondary Aerosol Formation," Atmos. Environ. 39 7768-7788.

Carter, W. P. L., I. L. Malkina, D. R. Cocker III, and C. Song (2005c): "Environmental Chamber Studies of VOC Species in Architectural Coatings and Mobile Source Emissions," Final Report to the South Coast Air Quality Management District Contract No. 03468, July 5. Available at http://www.cert.ucr.edu/~carter/absts.htm#scaqcham.

Carter, W. P. L. and I. L. Malkina (2007): "Investigation of the Atmospheric Impacts of Selected Pesticides," Final Report to the California Air Resources Board Contract 04-334, January 10. Available at http://www.cert.ucr.edu/~carter/absts.htm#pestrep.

Carter W. P. L, W. S. Goliff, R. Atkinson, J. Arey, and S. M. Aschmann (2010): "Investigation of Atmospheric Ozone Impacts of 3-Methoxy-3-Methyl-1-Butanol," Final Report to the Kuraray Co. Ltd, July 8. Available at http://www.cert.ucr.edu/~carter/absts.htm#MMBrept.

Carter, W. P. L. and G. Heo (2012): "Development of Revised SAPRC Aromatics Mechanisms," Report to the California Air Resources Board Contracts No. 07-730 and 08-326, April 12, 2012. Available at http://www.cert.ucr.edu/~carter/absts.htm#saprc11.

Chen, J., H. Mao, R.W. Talbot, and R.J. Griffin (2006), Application of the CACM and MPMPO Modules Using the CMAQ Model for the Eastern United States, J. Geophys. Res. *111*, D23S25, doi:10.1029/2006JD007603.

Claeys, M., W. Wang, A. C. Ion, I. Kourtchev, A. Gelencsér, and W. Maenhaut (2004): "Formation of Secondary Organic Aerosols from Isoprene and its Gas-Phase Oxidation Products through Reaction with Hydrogen Peroxide," Atmos. Environ. 38, 4093-4098

Cocker, D.R, R.C. Flagan, and J. H. Seinfeld (2001): "State-of-the-Art Chamber Facility for Studying Atmospheric Aerosol Chemistry," Environ. Sci. Technol. 35(12), 2594-2601.

Coeur-Tourneur, C., V. Foulon, and M. Laréal (2010) : "Determination of Aerosol Yields from 3-Methylcatechol and 4-Methylcatechol Ozonolysis in a Simulation Chamber," Atmos. Environ. 44, 852-857.

Derwent, R. G., Jenkin, M. E., Utembe, S. R., Shallcross, D. E., Murrells, T. P., Passant, N. R, (2010): "Secondary Organic Aerosol Formation from a Large Number of Reactive Man-Made Organic Compounds," Sci. Total Environ. 408, 3374-3381.

Finlayson-Pitts, B. J., and J. N. Pitts, Jr. (1999): "Chemistry of the Upper and Lower Atmosphere: Theory, Experiments, and Applications," Academic Press, San Diego.

Fried, A, and J. Hodgeson (1982): "Laser Photoacoustic Detection of Nitrogen Dioxide in the Gas-Phase Titration of Nitric Oxide with Ozone," Anal. Chem. 54 (2), 278–282.

Galloway, M. M., Chhabra, P., Chan, A. W. H., Surratt, J. D., Flagan, R. C., Seinfeld, J. H., Keutsch, F. N. (2009): "Glyoxal Uptake on Ammonium Sulphate Seed Aerosol: Reaction Products and Reversibility of Uptake under Dark and Irradiated Conditions," Atmos. Chem. Phys. 9, 3331-3345.

Galloway, M. M., C. L. Loza, P. S. Chhabra, A. W. H. Chan, L. D. Yee, J. H. Seinfeld, and F. N. Keutsch (2011): "Analysis of Photochemical and Dark Glyoxal Uptake: Implications for SOA Formation," Geophys. Res. Lett. 38(17), L17811.

Gery, M. W., G. Z. Whitten, and J. P. Killus (1988): "Development and Testing of the CBM-IV for Urban and Regional Modeling," EPA-600/ 3-88-012, January.

Griffin, R.J., D. R. Cocker, R. C. Flagan, and J. H. Seinfeld (1999): "Organic Aerosol Formation from the Oxidation of Biogenic Hydrocarbons," J. Geophys. Res. 104, 3555-3567.

Grosjean, D. (1984): "Atmospheric Reactions of Ortho Cresol: Gas Phase and Aerosol Products," Atmos. Environ. 18(8), 1641-1652.

Grosjean, D. (1985): "Reactions of *o*-Cresol and Nitrocresol with NO_x in Sunlight and with Ozone-Nitrogen Dioxide Mixtures in the Dark," Environ. Sci. Technol. 19(10), 968-974.

Hallquist, M., J. C. Wenger, U. Baltensperger, Y. Rudich, D. Simpson, M. Claeys, J. Dommen, N. M. Donahue, C. George, A. H. Goldstein, J. F. Hamilton, H. Herrmann, T. Hoffmann, Y. Iinuma, M. Jang, M. Jenkin, J. L. Jimenes, A. Kiendler-Scharr, W. Maenhaut, G. McFiggans, Th. F. Mentel, A. Monod, A. S. Prévót, J. H. Seinfeld, J. D. Surratt, R. Szmigielski, and J. Willdt (2009): "The Formation, Properties and Impact of Secondary Organic Aerosol: Current and Emerging Issues," Atmos. Chem. Phys. 9, 5155-5236.

Hargrove, J. and J. Zhang (2008): "Measurements of NOx, Acyl Peroxynitrates, and NOy with Automatic Interference Corrections Using a NO_2 Analyzer and Gas Phase Titration," Rev. Sci. Instrum. 79, 046109.

Healy, R. M., J. C. Wenger, A. Metzger, J. Duplissy, M. Kalberer, and J. Dommen (2008): "Gas/Particle Partitioning of Carbonyls in the Photooxidation of Isoprene and 1,3,5-Trimethylbenzene," Atmos. Chem. Phys. 8, 3215-3230. Available at http://www.atmos-chem-phys.net/8/3215/2008.

Henry, F., C. Coeur-Tourneur, F. Ledoux, A. Tomas, and D. Menu (2008) : "Secondary Organic Aerosol Formation from the Gas Phase Reaction of Hydroxyl Radicals with m-, o- and p-Cresol," Atmos. Environ. 42, 3035-3045.

Henze, D. K., J. H. Seinfeld, N. L. Ng, J. H. Kroll, T.-M. Fu, D. J. Jacob, and C. L. Heald (2008): “Global Modeling of Secondary Organic Aerosol Formation from Aromatic Hydrocarbons: High- vs. Low-Yield Pathways,” Atmos. Chem. Phys. 8, 2405-2421. Available at http://www.atmos-chem-phys.net/8/2405/2008/.

Hurley, M.D., O. Sokolov, T. J. Wallington, H. Takekawa, M. Karasawa, B. Klotz, I. Barnes, and K. H. Becker (2001): "Organic Aerosol Formation during the Atmospheric Degradation of Toluene," Environ. Sci. Technol. 35(7), 1358-1366.

Hu, D., M. Tolocka, Q. Li, and R. M. Kamens (2007): "A Kinetic Mechanism for Predicting Secondary Organic Aerosol Formation from Toluene Oxidation in the Presence of NOx and Natural Sunlight," Atmos. Environ. 41, 6478-6496.

Hu, D. and R. M. Kamens (2007): "Evaluation of the UNC Toluene-SOA Mechanism with Respect to Other Chamber Studies and Key Model Parameters," Atmos. Environ. 41, 6465-6477.

Hynes, R. G., D. E. Angove, S, M. Saunders, V. Haverd, and M. Azzi (2005): “Evaluation of Two MCM v3.1 Alkene Mechanisms Using Indoor Environmental Chamber Data,” Atmos. Environ., 39, 7251-7262.

Izumi, K., and T. Fukuyama (1990), "Photochemical Aerosol Formation from Aromatic-Hydrocarbons in the Presence of NOx," Atmos. Environ. 24(6), 1433-1441.

Jang, M.S., and R. M. Kamens (2001), "Characterization of Secondary Aerosol from the Photooxidation of Toluene in the Presence of NOx and 1-Propene," Environ. Sci. Technol. 35(18), 3626-3639.

Jang, M., N. M. Czoschke, S. Lee, R. M. Kamens (2002): "Heterogeneous Atmospheric Aerosol Production by Acid-Catalyzed Particle-Phase Reaction," Science 298, 814-817.

Jeffries, H. E., K. G. Sexton, J. R. Arnold, and T. L. Kale (1989): "Validation Testing of New Mechanisms with Outdoor Chamber Data. Volume 2: Analysis of VOC Data for the CB4 and CAL Photochemical Mechanisms," Final Report, EPA-600/3-89-010b.

Jeffries, H. E., M. W. Gery, and W. P. L. Carter (1992): “Protocol for Evaluating Oxidant Mechanisms for Urban and Regional Models,” Report for U.S. Environmental Protection Agency Cooperative Agreement No. 815779, Atmospheric Research and Exposure Assessment Laboratory, Research Triangle Park, NC. Available at http://www.cert.ucr.edu/~carter/absts.htm#mechprot.

Jimenez, J. L., Canagaratna, M. R., Donahue, N. M., Prevot, A. S. H., Zhang, Q., Kroll, J. H., DeCarlo, P. F., Allan, J. D., Coe, H., Ng, N. L., Aiken, A. C., Docherty, K. S., Ulbrich, I. M., Grieshop, A. P., Robinson, A. L., Duplissy, J., Smith, J. D., Wilson, K. R., Lanz, V. A., Hueglin, C., Sun, Y. L., Tian, J., Laaksonen, A., Raatikainen, T., Vaattovaara, P., Ehn, M., Kulmala, M., Tomlinson, J. M., Collins, D. R., Cubison, M. J., Dunlea, E. J., Huffman, J. A., Onasch, T. B., Alfarra, M. R., Williams, P. I., Bower, K., Kondo, Y., Schneider, J., Drewnick, F., Borrmann, S., Weimer, S., Demerjian, K., Salcedo, D., Cottrell, L., Griffin, R. J., Takami, A., Miyoshi, T., Hatakeyama, S., Shimono, A., Sun, J. Y., Zhang, Y. M., Dzepina, K., Kimmel, J. R., Sueper, D., Jayne, J. T., Herndon, S. C., Trimborn, A. M., Williams, L. R., Wood, E. C., Middlebrook, A. M., Kolb, C. E., Baltensperger, U., Worsnop, D. R. (2009): "Evolution of organic aerosols in the atmosphere," Science 326, 1525-1529.

Johnson, D., M. E. Jenkin, K. Wirtz, and M. Martin-Reviejo (2004): "Simulating the Formation of Secondary Organic Aerosol from the Photooxidation of Toluene," Environ. Chem. 1, 150-165.

Johnson, D., M. E. Jenkin, K. Wirtz, and M. Martin-Reviejo. (2005): "Simulating the Formation of Secondary Organic Aerosol from the Photooxidation of Aromatic Hydrocarbons," Environ. Chem. 2(1), 35-48.

Kalberer, M., D. Paulsen, M. Sax, M. Steinbacher, J. Dommen, A. S. H. Prevot, R. Fisseha, E. Weingartner, V. Frankevich, R. Zenobi, U. Baltensperger (2004): "Identification of Polymers as Major Components of Atmospheric Organic Aerosols," Science 303, 1659-1662.

Kamens, R., J. Odum, and Z.-H. Fan (1995): "Some Observations on Times to Equilibrium for Semi-volatile Polycyclic Aromatic Hydrocarbons," Environ. Sci. Technol. 29, 43-50.

Kamens, R., M. Jang, C.-J. Chien, and K. Leach (1999): "Aerosol Formation from the Reaction of α-Pinene and Ozone Using a Gas-Phase Kinetics-Aerosol Partitioning Model," Environ. Sci. Technol. 33(9), 1430-1438.

Kamens, R. M., H. Zhang, E. H. Chen, Y. Zhou, H. M. Parikh, R. L. Wilson, K. E. Galloway, and E. P. Rosen (2011): "Secondary Organic Aerosol Formation from Toluene in an Atmospheric Hydrocarbon Mixture: Water and Particle Seed Effects," Atmos. Environ. 45(13), 2324-2334.

Kanakidou, M., J. H. Seinfeld, S. N. Pandis, I. Barnes, F. J. Dentener, M. C. Facchini, R. Van Dingenen, B. Ervens, A. Nenes, C. J. Nielsen, E. Swietlicki, J. P. Putaud, Y. Balkanski, and J. Wilson (2005): "Organic Aerosol and Global Climate Modelling: A Review," Atmos. Chem. and Phys. 5, 1053-1123.

Kelly, J. L., D. V. Michelangeli, P. A. Makar, D. R. Hastie, M. Mozurkewich, and J. Auld (2010): "Aerosol Speciation and Mass Prediction from Toluene Oxidation under High NO_x Conditions," Atmos. Environ. 44, 361-369.

Kroll, J. H., A. W. H. Chan, N. L. Ng, R. C. Flagan, and J. H. Seinfeld (2007): "Reactions of Semi-volatile Organics and Their Effects on Secondary Organic Aerosol Formation," Environ. Sci. Technol. 41(10), 3545-3550.

Kroll, J. H., and J. H. Seinfeld (2008): "Chemistry of Secondary Organic Aerosol: Formation and Evolution of Low-Volatility Organics in the Atmosphere," Atmos. Environ. 42, 3593-3624.

Lonneman, W. A. (1986): "Comparison of 0600-0900 AM Hydrocarbon Compositions Obtained from 29 Cities," Proceedings APCA/U.S. EPA Symposium on Measurements of Toxic Air Pollutants, Raleigh, NC.

Loza, C. L., A. W. H. Chan, M. M. Galloway, F. N. Keutsch, R. C. Flagan, and J. H. Seinfeld (2010): "Characterization of Vapor Wall Loss in Laboratory Chambers," Environ. Sci. Technol. 44: 5074-5078.

Malloy, Q. G. J., S. Nakao, L. Qi, R. Austin, C. Stothers, H. Hagino, and D. R. Cocker, III (2009): "Real-Time Aerosol Density Determination Utilizing a Modified Scanning Mobility Particle Sizer-Aerosol Particle Mass Analyzer System," Aerosol Sci. Technol. 43(7), 673-678.

Matsunaga, A. and P. J. Ziemann (2010): "Gas-Wall Partitioning of Organic Compounds in a Teflon Film Chamber and Potential Effects on Reaction Product and Aerosol Yield Measurements," Aerosol Sci. Technol. 44, 881-892.

McMurry, P. H. and D. Grosjean (1985): "Gas and Aerosol Wall Losses in Teflon Film Smog Chambers," Environ. Sci. Technol. 19(12), 1176-1182.

Nakao, S., C. Clark, P. Tang, K. Sato, and D. Cocker, III (2011a): "Secondary Organic Aerosol Formation from Phenolic Compounds in the Absence of NOx," Atmos. Chem. Phys., 11, 10649-10660, 10.5194/acp-11-10649-2011.

Nakao, S., Y. Liu P. Tang, C. L. Chen, J. Zhang, D. Cocker III (2011b): "Role of Glyoxal in SOA Formation from Aromatic Hydrocarbons: Gas-Phase Reaction Trumps Reactive Uptake," Atmos. Chem. Phys. Discuss. 11(11), 30599-30625

Ng, N. L., J. H. Kroll, A. W. H. Chan, P. S. Chhabra, R. C. Flagan, and J. H. Seinfeld (2007): "Secondary Organic Aerosol Formation from *m*-Xylene, Toluene, and Benzene," Atmos. Chem. Phys. 7, 3909-3922. Available at http://www.atmos-chem-phys.net/7/3909/2007/.

Nishino, N., Arey, J., Atkinson, R. (2010): " Formation Yields of Glyoxal and Methylglyoxal from the Gas-Phase OH Radical-Initiated Reactions of Toluene, Xylenes, and Trimethylbenzenes as a Function of NO_2 Concentration," J. Phys. Chem. A 114, 10140-10147.

Odum, J. R., T. Hoffmann, F. Bowmann, D. Collins, R. C. Flagan, and J. H. Seinfeld (1996): "Gas/Particle Partitioning and Secondary Organic Aerosol Yields," Environ. Sci. Technol. 30, 2580-2586.

Odum, J. R., T. P. W. Jungkamp, R. J. Griffin, R. C. Flagan, and J. H. Seinfeld (1997): "The Atmospheric Aerosol-Forming Potential of Whole Gasoline Vapor," Science 276, 96-99.

Olariu, R. I., I. Barnes, K. H. Becker, and B. Klotz (2000): "Rate Coefficients for the Gas-Phase Reaction of OH Radicals with Selected Dihydorxybenzenes and Benzoquinones," Int. J. Chem. Kinet. 32, 696-702.

Olariu, R. I., B. Klotz, I. Barnes, K.H. Becker, and R. Mocanu (2002): "FT-IR Study of the Ring-Retaining Products from the Reaction of OH Radicals with Phenol, o-, m-, and p-Cresol," Atmos. Environ. 36, 3685-3697.

Olariu, R. I., I. Bejan, I. Barnes, B. Klotz, K. H. Becker, and K. Wirtz (2004): "Rate Coefficients for the Gas-Phase Reaction of NO_3 Radicals with Selected Dihydorxybenzenes" Int. J. Chem. Kinet. 32, 577-583.

Qi, L., S. Nakao, Q. Malloy, B. Warren, and D. R. Cocker, III (2010a): "Can Secondary Organic Aerosol Formed in an Atmospheric Simulation Chamber Continuously Age?" Atmos. Environ. 44, 2990-2996.

Qi, L., S. Nakao, P. Tang, and D. R. Cocker, III (2010b): "Temperature Effect on Physical and Chemical Properties of Secondary Organic Aerosol from m-Xylene Photooxidation," Atmos. Chem. Phys. 10(8), 3847-3854.

Pankow, J. F. (1994a): "An Absorption-Model of Gas-Particle Partitioning of Organic Compounds in the Atmosphere," Atmos. Environ. 28, 185-188.

Pankow, J. F. (1994b): "An Absorption-Model of the Gas Aerosol Partitioning Involved in the Formation of Secondary Organic Aerosol," Atmos. Environ. 28, 189-193.

Pierce, J. R., G. Engelhart, L. Hildebrandt, E. A. Weitkamp, R. K. Pathak, N. M. Donahue, A. L. Robinson, P. J. Adams, and S. N. Pandis (2008): "Constraining Particle Evolution from Wall Losses, Coagulation, and Condensation-Evaporation in Smog-Chamber Experiments: Optimal Estimation Based on Size Distribution Measurements," Aerosol Sci. Technol. 42, 1001-1015.

Perraud, V., E. A. Bruns, M. J. Ezell, S. N. Johnson, Y. Yu, M. L. Alexander, A. Zelenyuk, D. Imre, W. L. Chang, D. Babdub, J. F. Pankow, and B. J. Finlayson-Pitts (2012): "Nonequilibrium Atmospheric Secondary Organic Aerosol Formation and Growth," Proc. Natl. Acad. Sci. USA 109(8), 2836-2841. Available at http://www.pnas.org/cgi/doi/10.1073/pnas.1119909109.

Shiraiwa, M., M. Ammann, T. Koop, and U. Pöschl (2011): "Gas Uptake and Chemical Aging of Semisolid Organic Aerosol Particles. Proc. Natl. Acad. Sci. USA 108(27), 11003-11008. Available at http://www.pnas.org/cgi/doi/10.1073/pnas.1103045108.

Singh, T, R. F. Sawyer, E. S. Starkman, and L. S. Caretto (1968): "Rapid Continuous Determination of Nitric Oxide Concentration in Exhaust Gases," Journal of the Air Pollution Control Association 18(2), 102-105.

Song, C., K. Na, and D.R. Cocker III (2005): "Impact of the Hydrocarbon to NO_x Ratio on Secondary Organic Aerosol Formation," Environ. Sci. Technol. 39, 3143-3149.

Song, C, Na., B. Warren, Q. Malloy, and D. R. Cocker, III (2007): "Secondary Organic Aerosol Formation from m-Xylene in the Absence of NO_x," Environ. Sci. Technol. 41, 7409-7416.

Stockwell, W. R., P. Middleton, J. S. Chang, and X. Tang (1990): "The Second Generation Regional Acid Deposition Model Chemical Mechanism for Regional Air Quality Modeling," J. Geophys. Res. 95, 16343-16376.

Stroud, C. A., P. A. Makar, D. V. Michelangli, M. Mozurkewich, D. R. Hastie, A. Barbu and J. Humble (2004): "Simulating Organic Formation during the Photooxidation of Toluene/NOx Mixtures: Comparing the Equilibrium and Kinetic Assumption," Environ. Sci. Technol. 38, 1471-1479.

Sun, Y. L., Q. Zhang, C. Anastasio, and J. Sun (2010): "Insights into Secondary Organic Aerosol Formed via Aqueous-Phase Reactions of Phenolic Compounds Based on High Resolution Mass Spectrometry," Atmos. Chem. Phys. 10, 4809-4822.

Volkamer, R., J. L. Jimenez, F. San Martini, K. Dzepina, Q. Zhang, D. Salcedo, L.T. Molina, D. R.Worsnop, and M. J. Molina (2006): "Secondary Organic Aerosol Formation from Anthropogenic Air Pollution: Rapid and Higher than Expected," Geophys. Res. Letters *33*, L16804, doi:10.1029/2006GL026310.

Volkamer, R., P. J. Ziemann, and L. T. Molina (2009): "Secondary Organic Aerosol Formation from Acetylene (C_2H_2): Seed Effect on SOA Yields Due to Organic Photochemistry in the Aerosol Aqueous Phase," Atmos. Chem. Phys. 9, 1907-1928.

Warren, B., D. R. Cocker, C. Song, and W. P. L. Carter (2007): "Predicting Secondary Organic Aerosol Formation from Aromatics: m-Xylene Case Study," Presented at the 26th Annual Conference of the American Association for Aerosol Research, Grand Sierra Resort and Casino, Reno, Nevada, September 24-28.

Warren, B., Song, C., Carter, W.P.L., Cocker, D.R. (2008a) "Predicting Secondary Organic Aerosol Formation: PM-SAPRC08," Presented at the 27th Annual Conference of the American Association for Aerosol Research, Orlando, Florida, Oct. 24-28.

Warren, B., C. Song, and D. R. Cocker, III (2008b): "Light Intensity and Light Source Influence on Secondary Organic Aerosol Formation for the m-Xylene/NOx Photooxidation System," Environ. Sci. Technol. 42, 5461-5466.

White, S. J. (2010): Stephen. J. White, Commonwealth Scientific and Industrial Research Organisation, Personal Communication.

White, S.J., M. Azzi, D. E. Angove, and I. M. Jamie (2010): “Modelling the Photooxidation of ULP, E5 and E1 in the CSIRO Smog Chamber,” Atmos. Environ. 44(14), 1707-1713.

Whitten, G. Z., G. Heo, Y. Kimura, E. McDonald-Buller, D. T. Allen, W. P. L. Carter, and G. Yarwood (2010): “A New Condensed Toluene Mechanism for Carbon Bond: CB05-TU,” Atmos. Environ. 44, 5346-5355.

Yarwood, G., G. Heo, W. P. L. Carter, and G. Z. Whitten (2012): “Environmental Chamber Experiments to Evaluate NOx Sinks and Recycling in Atmospheric Chemical Mechanisms,” Final Report, Prepared for Dr. Elena C. McDonald-Buller, Texas Air Quality Research Program, The University of Texas at Austin, AQRP Project 10-042, February 17. Available at http://aqrp.ceer.utexas.edu/projectinfo/10-042/10-042%20Final%20Report.pdf.

Zafonte, L., P. L. Rieger, and J. R. Holmes (1977): "Nitrogen Dioxide Photolysis in the Los Angeles Atmosphere," Environ. Sci. Technol. 11, 483-487.

Zhang, Q., Jimenez, J. L., Canagaratna, M. R., Allan, J. D., Coe, H., Ulbrich, I., Alfarra, M. R., Takami, A., Middlebrook, A. M., Sun, Y. L., Dzepina, K., Dunlea, E., Docherty, K., DeCarlo, P. F., Salcedo, d., Onasch, T., Jayne, J. T., Miyoshi, T., Shimono, A., Hatakeyama, S., Takegawa, N., Kondo, Y., Schneider, J., Drewnich, F., Borrmann, S., Weimer, S., Demerjian, K., Williams, P., Bower, K., Bahreini, R., Cottrell, L., Griffin, R. J., Rautiainen, J., Sun, J. Y., Zhang, Y. M., Worsnop, D. R. (2007): "Ubiquity and Dominance of Oxygenated Species in Organic Aerosols in Anthropogenically-Influenced Northern Hemisphere Midlatitudes," Geophys. Res. Lett. 32(L13801), doi:10.1029/2007GL029979.

Zhou, Y., H. Zhang, H. M. Parikh, E. H. Chen, W. Rattanavaraha, E. P. Rosen, , W. Wang, and R. M. Kamens (2011): "Secondary Organic Aerosol Formation from Xylenes and Mixtures of Toluene and Xylenes in an Atmospheric Urban Hydrocarbon Mixture: Water and Particle Seed Effects (II)," Atmos. Environ. 45, 3882-3890.

APPENDIX A. SUPPLEMENTARY MATERIALS

Table A-1. Summary of environmental chamber experiments carried out for this project.

Date	Run No.	Side A (see below for codes)		Side B	
		Code	Description	Code	Description
5/16/09	1013	0	CO - Air	0	CO - Air
5/25/09	1017	0	Pure Air	0	Pure Air
6/6/09	1024	1	26M-PHEN - H2O2	1	M-XYLENE - H2O2
8/30/09		Reactors Changed			
9/1/09	1033	0	Pure Air	0	Pure Air
1/5/10	1091	1	M-XYLENE - NOx	1	M-XYLENE - NOx
1/6/10	1092	1	M-XYLENE - NOx	1	M-XYLENE - NOx
1/12/10	1095	4	TOLUENE - NOx	4	TOLUENE - NOx
1/13/10	1096	4	TOLUENE - NOx	4	TOLUENE - NOx
1/14/10	1097	1	M-XYLENE - NOx	1	M-XYLENE - NOx
1/15/10	1098	1	TOLUENE - NOx	1	TOLUENE - NOx
1/17/10	1099	4	TOLUENE - NOx	7	TOLUENE - NOx
1/19/10	1100	4	TOLUENE - NOx - CO	4	TOLUENE - NOx - CO
1/20/10	1101	1	TOLUENE - NOx	1	TOLUENE - NOx
1/21/10	1102	1	TOLUENE - NOx	1	TOLUENE - NOx
1/22/10	1103	0	CO - NOx	0	CO - NOx
1/26/10	1105	4	M-XYLENE - NOx	1	M-XYLENE - NOx
1/27/10	1106	7	TOLUENE - NOx	7	TOLUENE - NOx
1/28/10	1107	7	TOLUENE - NOx	7	TOLUENE - NOx
1/30/10	1109	0	Pure Air	0	Pure Air
1/31/10	1110	0	Pure Air	0	Pure Air
2/7/10	1117	1	124-TMB - NOx	1	124-TMB - NOx
2/9/10	1119	1	124-TMB - NOx	1	124-TMB - NOx
2/18/10	1123	1	124-TMB - NOx	1	124-TMB - NOx
2/19/10	1124	0	CO - Air	0	CO - Air
2/21/10	1126	1	124-TMB - NOx	1	124-TMB - NOx
2/25/10	1129	7	124-TMB - NOx	7	124-TMB - NOx
3/6/10	1134	1	24M-PHEN - H2O2	1	M-XYLENE - H2O2
3/7/10	1135	1	124-TMB - NOx - H2O2	1	124-TMB - NOx - H2O2
3/13/10	1141	1	BENZENE - H2O2	1	TOLUENE - H2O2
3/14/10	1142	1	C2-BENZ - NOx	7	C2-BENZ - NOx
3/16/10	1144	0	Pure Air	0	Pure Air
3/18/10	1146	5	C2-BENZ - NOx	1	C2-BENZ - NOx
3/19/10	1147	1	C2-BENZ - NOx	1	C2-BENZ - NOx
3/21/10	1149	1	BENZENE - H2O2	1	TOLUENE - H2O2
3/23/10	1151	1	M-ET-TOL - NOx	4	M-ET-TOL - NOx
3/25/10	1153	1	135-TMB - NOx	1	135-TMB - NOx
3/26/10	1154	1	135-TMB - H2O2	1	135-TMB - H2O2
3/27/10	1155	4	135-TMB - H2O2	4	135-TMB - H2O2
3/28/10	1156	1	135-TMB - NOx	1	135-TMB - NOx
3/31/10	1158	1	123-TMB - NOx	1	123-TMB - NOx
4/3/10	1161	1	BENZENE - H2O2	1	BENZENE - H2O2

Table A-1 (continued)

Date	Run No.	Side A (see below for codes)		Side B	
		Code	Description	Code	Description
4/4/10	1162	1	123-TMB - NOx	1	123-TMB - NOx
4/7/10	1165	0	CO - NOx	0	CO - NOx
4/8/10	1166	0	Pure Air	0	Pure Air
4/10/10	1168	2	Butylamine - H2O2	1	O-ET-TOL - NOx
4/11/10	1169	0	Pure Air	0	Pure Air
4/12/10	1170	0	Pure Air	0	Pure Air
5/1/10			Reactors Changed		
5/2/10	1173	0	Pure Air	0	Pure Air
5/5/10	1175	1	M-XYLENE - NOx	1	M-XYLENE - NOx
5/9/10	1179	1	O-ET-TOL - NOx	1	O-ET-TOL - NOx
5/10/10	1180	1	24M-PHEN - H2O2	1	M-XYLENE - H2O2
5/19/10	1185	0	Pure Air	0	Pure Air
6/4/10	1189	0	H2O2 - Air	0	H2O2 - Air
6/5/10	1190	1	M-XYLENE - NOx	1	M-XYLENE - NOx
6/6/10	1191	1	M-XYLENE - NOx	1	M-XYLENE - NOx
6/7/10	1192	1	M-XYLENE - NOx	1	M-XYLENE - NOx
6/9/10	1193	1	M-XYLENE - NOx	1	M-XYLENE - NOx
6/10/10	1194	1	P-ET-TOL - NOx	1	P-ET-TOL - NOx
6/11/10	1195	1	BENZENE - NOx - H2O2	1	BENZENE - NOx
6/14/10	1197	1	P-ET-TOL - NOx	1	P-ET-TOL - NOx
6/16/10	1199	1	M-ET-TOL - NOx	1	M-ET-TOL - NOx
6/20/10	1202	1	O-ET-TOL - NOx	1	O-ET-TOL - NOx
6/25/10	1205	1	M-ET-TOL - H2O2	1	M-ET-TOL - H2O2
6/26/10	1206	1	PHENOL - H2O2	1	PHENOL - H2O2
6/29/10	1209	1	M-XYLENE - H2O2	3	M-XYLENE - H2O2
7/1/10	1211	1	M-ET-TOL - H2O2	1	M-ET-TOL - H2O2
7/2/10	1212	1	M-XYLENE - H2O2	1	M-XYLENE - H2O2
7/6/10	1214	1	P-ET-TOL - NOx	1	P-ET-TOL - NOx
7/7/10	1215	1	O-ET-TOL - NOx	1	O-ET-TOL - NOx
7/9/10	1217	1	PHENOL - H2O2	1	PHENOL - H2O2
7/10/10	1218	1	M-ET-TOL - H2O2	1	M-ET-TOL - H2O2
7/11/10	1219	1	PHENOL - NOx	1	PHENOL - NOx
7/14/10	1222	1	M-ET-TOL - NOx	1	M-ET-TOL - NOx
7/15/10	1223	1	BENZENE - NOx	1	BENZENE - NOx
7/18/10	1225	1	BENZENE - H2O2	1	BENZENE - H2O2
7/19/10	1226	1	M-ET-TOL - NOx	1	M-ET-TOL - NOx
7/20/10	1227	1	P-ET-TOL - H2O2	1	P-ET-TOL - H2O2
7/22/10	1229	1	P-ET-TOL - NOx	1	P-ET-TOL - NOx
7/24/10	1230	0	H2O2 - Air	0	H2O2 - Air
7/25/10	1231	1	BENZENE - NOx	4	BENZENE - NOx
7/26/10	1232	1	M-ET-TOL - NOx	4	M-ET-TOL - NOx
7/27/10	1233	1	O-ET-TOL - NOx	1	O-ET-TOL - NOx
7/31/10	1236	1	BENZENE - NOx	1	BENZENE - NOx
8/1/10	1237	1	BENZENE - NOx	1	BENZENE - NOx
8/2/10	1238	1	24M-PHEN - H2O2	1	24M-PHEN - H2O2
8/3/10	1239	1	P-ET-TOL - H2O2	1	P-ET-TOL - H2O2
8/4/10	1240	1	26M-PHEN - H2O2	1	26M-PHEN - H2O2

Table A-1 (continued)

Date	Run No.	Side A (see below for codes)		Side B	
		Code	Description	Code	Description
8/7/10	1242	1	O-ET-TOL - H2O2	1	O-ET-TOL - H2O2
8/8/10	1243	1	35M-PHEN - H2O2	1	35M-PHEN - H2O2
8/9/10	1244	1	M-XYLENE - H2O2	4	M-XYLENE - H2O2
8/10/10	1245	1	N-C3-BEN - NOx	4	N-C3-BEN - NOx
8/12/10	1246	1	N-C3-BEN - NOx	6	N-C3-BEN - NOx
8/13/10	1247	1	I-C3-BEN - NOx	1	I-C3-BEN - NOx
8/14/10	1248	1	M-XYLENE - H2O2	1	M-XYLENE - H2O2
8/18/10	1250	4	I-C3-BEN - NOx	4	I-C3-BEN - NOx
8/19/10	1251	1	O-CRESOL - H2O2	1	TOLUENE - H2O2
8/21/10	1252	1	O-CRESOL - H2O2	1	O-CRESOL - H2O2
8/22/10	1253	1	I-C3-BEN - NOx	1	I-C3-BEN - NOx
8/26/10	1255	1	M-CRESOL - H2O2	1	M-CRESOL - H2O2
8/26/10	1256	1	N-C3-BEN - H2O2	1	N-C3-BEN - H2O2
8/28/10	1258	1	P-CRESOL - H2O2	1	P-CRESOL - H2O2
8/29/10	1259	4	Pure Air	4	Pure Air
8/30/10	1260	1	O-CRESOL - NOx	1	O-CRESOL - NOx
9/4/10	1265	1	I-C3-BEN - H2O2	1	I-C3-BEN - H2O2
9/5/10	1266	1	TOLUENE - H2O2	1	O-CRESOL - H2O2
9/8/10	1269	1	N-C3-BEN - H2O2	1	N-C3-BEN - H2O2
9/12/10	1273	1	PHENOL - NOx	1	PHENOL - NOx
9/13/10	1274	1	I-C3-BEN - H2O2	1	I-C3-BEN - H2O2
9/14/10	1275	1	24M-PHEN - NOx	1	24M-PHEN - NOx
9/16/10	1277	1	24M-PHEN - NOx	1	24M-PHEN - NOx
9/17/10	1278	1	124-TMB - H2O2	1	124-TMB - H2O2
9/18/10	1279	1	O-CRESOL - NOx	1	O-CRESOL - NOx
9/29/10	1284	0	H2O2 - air	0	H2O2 - Air
10/1/10	1285	0	H2O2 - air	0	H2O2 - Air
10/3/10	1287	1	123-TMB - H2O2	1	123-TMB - H2O2
10/5/10	1289	2	PHENOL - N2O5	5	PHENOL - NOx
10/6/10	1290	1	P-CRESOL - H2O2	1	TOLUENE - H2O2
10/8/10	1292	1	124-TMB - H2O2	1	124-TMB - H2O2
10/9/10	1293	4	CATECHOL - H2O2	4	CATECHOL - H2O2
10/10/10	1294	1	C2-BENZ - H2O2	1	C2-BENZ - H2O2
10/12/10	1296	1	C2-BENZ - H2O2	1	C2-BENZ - H2O2
10/14/10	1298	1	135-TMB - H2O2	1	135-TMB - H2O2
10/18/10	1301	4	P-XYLENE - H2O2	4	P-XYLENE - H2O2
10/21/10	1304	1	P-XYLENE - H2O2	1	P-XYLENE - H2O2
11/1/10	1308	1	P-XYLENE - NOx	1	P-XYLENE - NOx
11/2/10	1309	4	Pure Air	4	Pure Air
11/3/10	1310	1	O-XYLENE - H2O2	1	O-XYLENE - H2O2
11/6/10	1312	1	P-CRESOL - H2O2	1	P-CRESOL - H2O2
11/7/10	1313	1	O-XYLENE - H2O2	1	O-XYLENE - H2O2
11/8/10	1314	1	CATECHOL - H2O2	1	CATECHOL - H2O2
11/9/10	1315	1	O-XYLENE - NOx	1	O-XYLENE - NOx
11/14/10	1320	4	O-XYLENE - NOx	4	O-XYLENE - NOx
11/16/10	1321	4	O-XYLENE - NOx	4	O-XYLENE - NOx
11/18/10	1323	0	Pure Air	0	Pure Air
11/23/10	1326	1	O-ET-TOL - H2O2	1	O-ET-TOL - H2O2

Table A-1 (continued)

Date	Run No.	Side A (see below for codes)		Side B	
		Code	Description	Code	Description
11/29/10	1329	4	135-TMB - NOx	4	135-TMB - NOx
11/30/10	1330	4	123-TMB - NOx	4	123-TMB - NOx
12/5/10	1333	8	BENZENE - H2O2	8	BENZENE - H2O2
1/6/11	1350	1	O-CRESOL - NOx	1	O-CRESOL - NOx
1/8/11	1351	0	CO - NOx	0	CO - NOx
1/9/11	1352	1	124-TMB - NOx	1	124-TMB - NOx
1/11/11	1354	4	124-TMB - NOx	4	124-TMB - NOx
1/13/11	1356	1	124-TMB - NOx	1	124-TMB - NOx
3/2/11	1374	1	124-TMB - NOx	1	124-TMB - NOx
3/10/11	1380	8	124-TMB - NOx	1	124-TMB - NOx
3/12/11	1381	8	123-TMB - NOx	8	123-TMB - NOx
3/21/11	1389	4	O-XYLENE - H2O2	1	O-XYLENE - H2O2
3/25/11	1390	4	H2O2 - Air	4	H2O2 - Air
4/10/11	1406	1	O-ET-TOL - H2O2	1	O-ET-TOL - H2O2
4/16/11	1412	1	24M-PHEN - H2O2	8	M-XYLENE - H2O2
4/17/11	1413	1	O-ET-TOL - NOx	1	O-ET-TOL - NOx
4/20/11	1416	1	M-ET-TOL - H2O2	1	M-ET-TOL - H2O2
4/25/11	1421	1	M-ET-TOL - NOx	1	M-ET-TOL - NOx
4/28/11	1424	1	PHENOL - H2O2	1	M-XYLENE - H2O2
4/30/11	1426	1	N-C3-BEN - H2O2	1	N-C3-BEN - H2O2
5/1/11	1427	1	O-CRESOL - H2O2	8	M-XYLENE - H2O2
5/6/11	1432	1	P-XYLENE - NOx	1	P-XYLENE - NOx
5/11/11	1437	1	O-XYLENE - NOx	1	O-XYLENE - NOx

Notes: All experiments are irradiation experiments. Following codes indicate if and how the experiments were used for mechanism evaluation, or why they were not used, if applicable.

Code Description

0 Modeled as a characterization experiment. See discussion of "Characterization Results" later in this section.

1 Used for mechanism evaluation. See the discussion of the mechanism evaluation experiments in the following section, and the section on Mechanism Evaluation Results later in this report.

2 This run was not modeled either because it is not relevant to this project or modeling this type of experiment is beyond the scope of the present mechanism evaluation.

3 This run was not modeled because the results were similar to another run that was judged to have higher data quality.

4 The results for both reactors were rejected for modeling because of instrumental or operational problems or missing data.

5 This run was not used for mechanism evaluation because the experiment had atypical PM data compared to most other runs of this type

6 This run was not used for SOA mechanism evaluation because the PM yields were too low to determine wall loss rates and all of the other runs with this type had data needed to compute wall loss rates.

7 This run was not used for mechanism evaluation because the model calculated that background PM formed from apparent offgasing of PM precursors from the chamber walls contributed unduly to the total PM formed in the experiment. In particular, the PM calculated by assuming no

Table A-1 (continued)

background PM from wall effects (i.e., WallPMparm=0) was lower than 60% of the PM calculated using the standard wall model.

8 This run was not used for the final mechanism evaluation because a sufficient number of similar experiments were judged to be suitable for mechanism evaluation and the preliminary evaluation results for this experiment were sufficiently atypical of evaluation results for similar experiments that experimental or characterization problems are suspected.

Table A-2. List of all characterization experiments whose data were used to develop or evaluate the chamber characterization model for this project.

Run	Type	Initial Concentration (ppm)				Best Fit (ppt) [a]	
		NO_x	H_2O_2	CO	Acetald.	RN-I	WallPMparm
First set of reactors used for SOA evaluation experiments							
EPA087A	CO - Air			75		17.0	
EPA087B	CO - Air			75		11.0	
EPA103A	CO - NOx	0.026		46		27.0	
EPA103B	CO - NOx	0.027		46		17.0	
EPA112A	CO - Air			100		25.0	
EPA112B	CO - Air			101		8.0	
EPA140A	CO - NOx	0.023		44		15.0	
EPA140B	CO - NOx	0.023		44		11.0	
EPA160A	CO - Air			95		18.0	
EPA160B	CO - Air			95		12.0	
EPA172A	Pure Air					1.9	12.7
EPA172B	Pure Air						1.3
EPA173A	CO - Air			45		10.0	
EPA173B	CO - Air			42		8.5	
EPA174A	CO - NOx	0.023		47		12.0	
EPA174B	CO - NOx	0.023		47		8.0	
EPA184A	CO - NOx	0.012		23		23.0	
EPA184B	CO - NOx	0.012		24		18.0	
EPA185A	Pure Air					17.8	5.7
EPA185B	Pure Air					16.0	1.1
EPA205A	CO - Air			44		10.0	
EPA205B	CO - Air			45		7.0	
EPA221A	Pure Air					21.6	3.1
EPA221B	Pure Air					20.5	0.9
EPA228A	CO - NOx	0.025		46		8.5	
EPA228B	CO - NOx	0.025		46		6.0	
EPA234A	CO - NOx	0.025		45		7.5	
EPA234B	CO - NOx	0.026		45		5.0	
EPA251A	CO - Air			45		15.0	
EPA251B	CO - Air			45		10.0	
EPA285A	CO - Air			47		12.5	
EPA285B	CO - Air			48		8.0	
EPA295A	Pure Air					21.3	2.7
EPA295B	Pure Air					3.3	0.8
EPA306A	CO - NOx	0.022		47		9.0	
EPA306B	CO - NOx	0.022		47		4.5	
EPA307A	Pure Air					19.1	2.2
EPA307B	Pure Air					10.0	0.9
EPA311A	Pure Air					7.6	3.3
EPA311B	Pure Air					10.0	1.3
EPA312A	Pure Air					2.7	4.0
EPA312B	Pure Air					1.9	0.3
EPA317A	Pure Air					4.8	4.1

Table A-2 (continued)

Run	Type	Initial Concentration (ppm)				Best Fit (ppt) [a]	
		NO_x	H_2O_2	CO	Acetald.	RN-I	WallPMparm
EPA317B	Pure Air					4.9	0.2
EPA327B	Pure Air					16.0	0.3
EPA336A	Pure Air					2.4	4.7
EPA336B	Pure Air						0.5
		Reactors Replaced					
EPA338A	Pure Air					3.4	3.7
EPA338B	Pure Air					1.8	0.8
EPA339A	Pure Air					2.4	2.1
EPA339B	Pure Air					1.8	0.5
EPA340A	Pure Air						0.6
EPA344A	CO - Air			49		1.0	
EPA344B	CO - Air			55		2.0	
EPA345A	CO - NOx	0.027		48		3.3	
EPA345B	CO - NOx	0.028		48		2.3	
EPA346A	CO - NOx	0.027		46		3.3	
EPA346B	CO - NOx	0.027		48		3.3	
EPA347B	Pure Air					4.8	0.1
EPA362A	CO - NOx	0.021		33		8.0	
EPA362B	CO - NOx	0.021		33		5.7	
EPA384A	Pure Air					6.3	5.5
EPA384B	Pure Air					8.7	0.5
EPA401A	CO - NOx	0.029		49		8.0	
EPA401B	CO - NOx	0.029		50		5.0	
EPA405A	CO - Air			83		5.0	
EPA405B	CO - Air			83		8.0	
EPA407A	Pure Air					10.0	2.6
EPA407B	Pure Air					4.7	0.3
EPA411A	CO - NOx	0.027		50		25.0	
EPA411B	CO - NOx	0.027		50		15.0	
EPA437A	CO - NOx	0.028		42		5.0	
EPA437B	CO - NOx	0.029		42		3.0	
		Reactors Replaced					
EPA523A	Pure Air					16.0	2.8
EPA537A	CO - NOx	0.015		35		6.0	
EPA537B	CO - NOx	0.015		36		5.0	
EPA578A	Pure Air						0.0
EPA578B	Pure Air						0.0
EPA582A	Pure Air					5.2	4.3
EPA582B	Pure Air					4.9	5.2
EPA585A	CO - NOx	0.024		50		8.0	
EPA585B	CO - NOx	0.025		51		10.0	
EPA601A	CO - Air			49		9.0	
EPA601B	CO - Air			50		10.0	
		Reactors Replaced					
EPA719A	CO - Air			57		20.0	
EPA719B	CO - Air			58		20.0	
EPA729A	CO - NOx	0.024		42		12.0	

Table A-2 (continued)

Run	Type	Initial Concentration (ppm)				Best Fit (ppt) [a]	
		NO_x	H_2O_2	CO	Acetald.	RN-I	WallPMparm
EPA729B	CO - NOx	0.024		42		12.0	
EPA730A	Pure Air					10.0	0.8
EPA730B	Pure Air					13.8	0.1
EPA739A	Pure Air						3.8
EPA739B	Pure Air						5.7
EPA740A	Pure Air						3.3
EPA740B	Pure Air						1.9
EPA741A	CO - NOx	0.024		63		6.0	
EPA741B	CO - NOx	0.025		64		8.0	
EPA744A	Pure Air						2.9
EPA744B	Pure Air						2.4
EPA745A	Pure Air						1.0
EPA745B	Pure Air						1.4
EPA746A	Pure Air						3.0
EPA746B	Pure Air						3.0
EPA747A	Pure Air						2.0
EPA747B	Pure Air						2.1
EPA777A	CO - NOx	0.025		49		17.0	
EPA777B	CO - NOx	0.025		50		11.0	
EPA778A	Pure Air					16.0	0.3
EPA778B	Pure Air					16.0	0.2
EPA786A	CO - Air			49		20.0	
EPA786B	CO - Air			50		18.0	
EPA787B	Pure Air						0.1
EPA788B	Pure Air					18.8	0.2
EPA801B	Pure Air					16.0	0.6
EPA802A	Pure Air					28.0	1.4
EPA802B	Pure Air					13.0	0.9
EPA808A	CO - NOx	0.023		62		22.0	
EPA809A	Pure Air					21.1	0.4
EPA809B	Pure Air					6.3	0.5
EPA810A	Pure Air					19.2	1.1
EPA810B	Pure Air					6.3	0.2
EPA811A	Pure Air					3.5	1.0
EPA811B	Pure Air						0.3
EPA846A	Pure Air						4.6
EPA846B	Pure Air						5.6
EPA848A	Pure Air						6.0
EPA848B	Pure Air					28.8	1.1
			Reactors Replaced				
EPA861A	Pure Air						2.2
EPA861B	Pure Air						1.1
EPA862A	Pure Air					1.7	2.3
EPA862B	Pure Air					2.4	2.0
EPA863A	CO - Air			51		5.0	
EPA863B	CO - Air			51		5.0	
EPA864A	Pure Air					1.2	0.3
EPA864B	Pure Air					2.0	0.2

Table A-2 (continued)

Run	Type	Initial Concentration (ppm)				Best Fit (ppt) [a]	
		NO_x	H_2O_2	CO	Acetald.	RN-I	WallPMparm
EPA865A	Pure Air					16.0	1.5
EPA865B	Pure Air					3.7	0.6
EPA874A	Pure Air						0.3
EPA874B	Pure Air					30.4	0.4
EPA886A	CO - NOx	0.022		42		15.0	
EPA886B	CO - NOx	0.023		44		15.0	
EPA935A	Pure Air					7.5	1.4
EPA935B	Pure Air					13.4	1.1
EPA945A	CO - NOx	0.026		48		10.0	
EPA945B	CO - NOx	0.026		49		10.0	
EPA946A	CO - Air			39		15.0	
EPA946B	CO - Air			40		15.0	
EPA971A	CO - NOx	0.022		39		1.0	
EPA971B	CO - NOx	0.022		36		2.0	
EPA979A	Pure Air					4.9	0.1
EPA979B	Pure Air					3.9	0.2
EPA982A	CO - Air			36		10.0	
EPA982B	CO - Air			36		10.0	
EPA1004A	CO - NOx	0.022		42		6.0	
EPA1004B	CO - NOx	0.021		42		8.0	
EPA1013A	CO - Air			47		10.0	
EPA1013B	CO - Air			46		10.0	
EPA1017A	Pure Air					16.0	0.9
EPA1017B	Pure Air					10.0	0.5
EPA1033A	Pure Air					2.0	0.3
EPA1033B	Pure Air					3.1	0.3
		Reactors Replaced					
EPA1076A	CO - Air			55		25.0	
EPA1076B	CO - Air			55		15.0	
EPA1103A	CO - NOx	0.022		40		21.0	
EPA1103B	CO - NOx	0.023		40		14.0	
EPA1109A	Pure Air					31.6	0.2
EPA1109B	Pure Air					19.4	0.2
EPA1110A	Pure Air					32.2	0.1
EPA1110B	Pure Air					20.4	0.1
EPA1124A	CO - Air			31		8.0	
EPA1124B	CO - Air			31		8.0	
EPA1144A	Pure Air					16.0	2.3
EPA1144B	Pure Air					10.0	0.9
EPA1165A	CO - NOx	0.024		36		15.0	
EPA1165B	CO - NOx	0.024		36		10.0	
EPA1166A	Pure Air					6.3	0.2
EPA1166B	Pure Air					5.0	0.1
EPA1169A	Pure Air					5.0	0.7
EPA1169B	Pure Air					22.0	0.1
EPA1170A	Pure Air					4.8	0.2
EPA1170B	Pure Air					10.0	0.0

Table A-2 (continued)

Run	Type	Initial Concentration (ppm)				Best Fit (ppt) [a]	
		NO_x	H_2O_2	CO	Acetald.	RN-I	WallPMparm
			Reactors Replaced				
EPA1172A	Pure Air					1.3	0.8
EPA1172B	Pure Air					2.0	0.6
EPA1173A	Pure Air						0.3
EPA1173B	Pure Air					1.2	0.3
EPA1185A	Pure Air						4.3
EPA1185B	Pure Air						3.8
EPA1187A	Pure Air					4.8	0.8
EPA1187B	Pure Air					6.3	0.9
EPA1188A	Pure Air					4.8	0.6
EPA1188B	Pure Air					4.8	0.8
EPA1189A	H2O2 - Air		2.0			2.9	0.5
EPA1189B	H2O2 - Air		2.0			3.5	0.5
EPA1230A	H2O2 - Air		0.5			12.0	0.2
EPA1230A	H2O2 - Air		0.5			12.0	0.2
EPA1230B	H2O2 - Air		0.5			11.0	0.1
EPA1230B	H2O2 - Air		0.5			11.0	0.1
EPA1284A	H2O2 - Air		1.0			4.6	0.2
EPA1284B	H2O2 - Air		1.0			3.5	0.8
EPA1285A	H2O2 - Air		1.0			2.9	0.1
EPA1285B	H2O2 - Air		1.0			3.1	0.2
EPA1323A	Pure Air					10.0	0.0
EPA1323B	Pure Air					10.0	0.0
EPA1390A	H2O2 - Air		3.0			5.0	
EPA1390B	H2O2 - Air		1.5			5.0	
EPA1429A	H2O2 - CO		0.5	45		3.0	
EPA1429B	H2O2 - CO		0.5	45		3.0	
EPA1431A	H2O2 - CO		0.5	49		2.0	
EPA1431B	H2O2 - CO		0.5	49		2.5	
EPA1434A	Acetald. - H2O2		0.5		0.52	3.0	
EPA1434B	Acetald. - H2O2		0.5		0.52	4.0	
EPA1447B	Acetald. - H2O2		0.5		0.40	10.0	
EPA1456A	CO - NOx	0.016		49		13.0	
EPA1456B	CO - NOx	0.015		50		7.0	

[a] Values of chamber wall characterization parameters that best fit the data. The "RN-I" parameter is the ratio of the HONO offgasing rate to the NO_2 photolysis rate that is adjusted to fit the rate of NO oxidation and O_3 formation in radical source characterization experiments or the amount of O_3 formation in the NO_x offgasing experiments. The "WallPMparm" parameter is the rate of background SOP precursor relative to the NO_2 photolysis rate. See the "Characterization Results" section for a more complete discussion of these parameters and how they were derived and used.

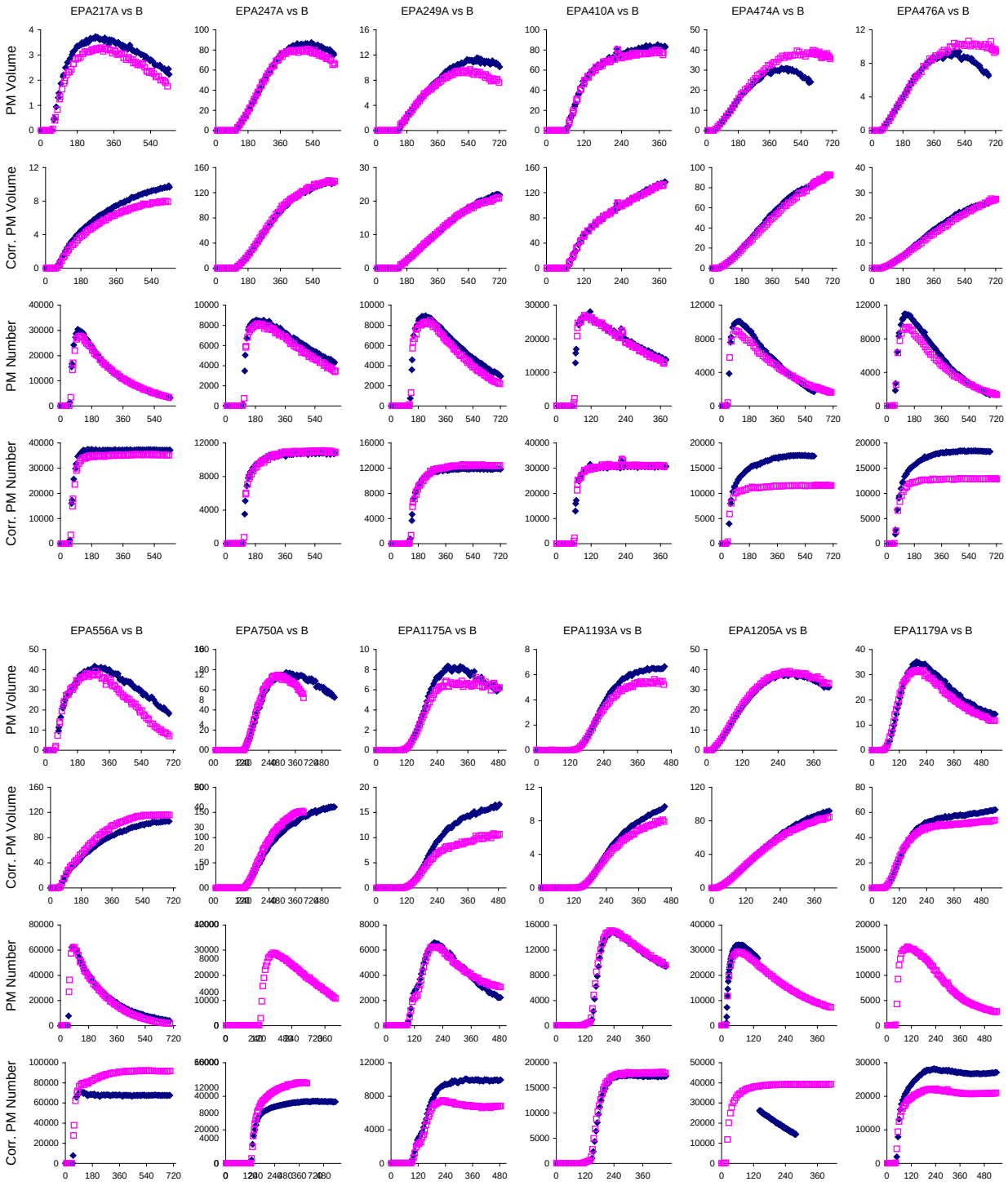

Figure A-1. Plots of corrected and uncorrected PM volume ($\mu m^3/cm^3$) and number (cm^{-3}) data for the replicate or near-replicate experiments (part 1 of 2)

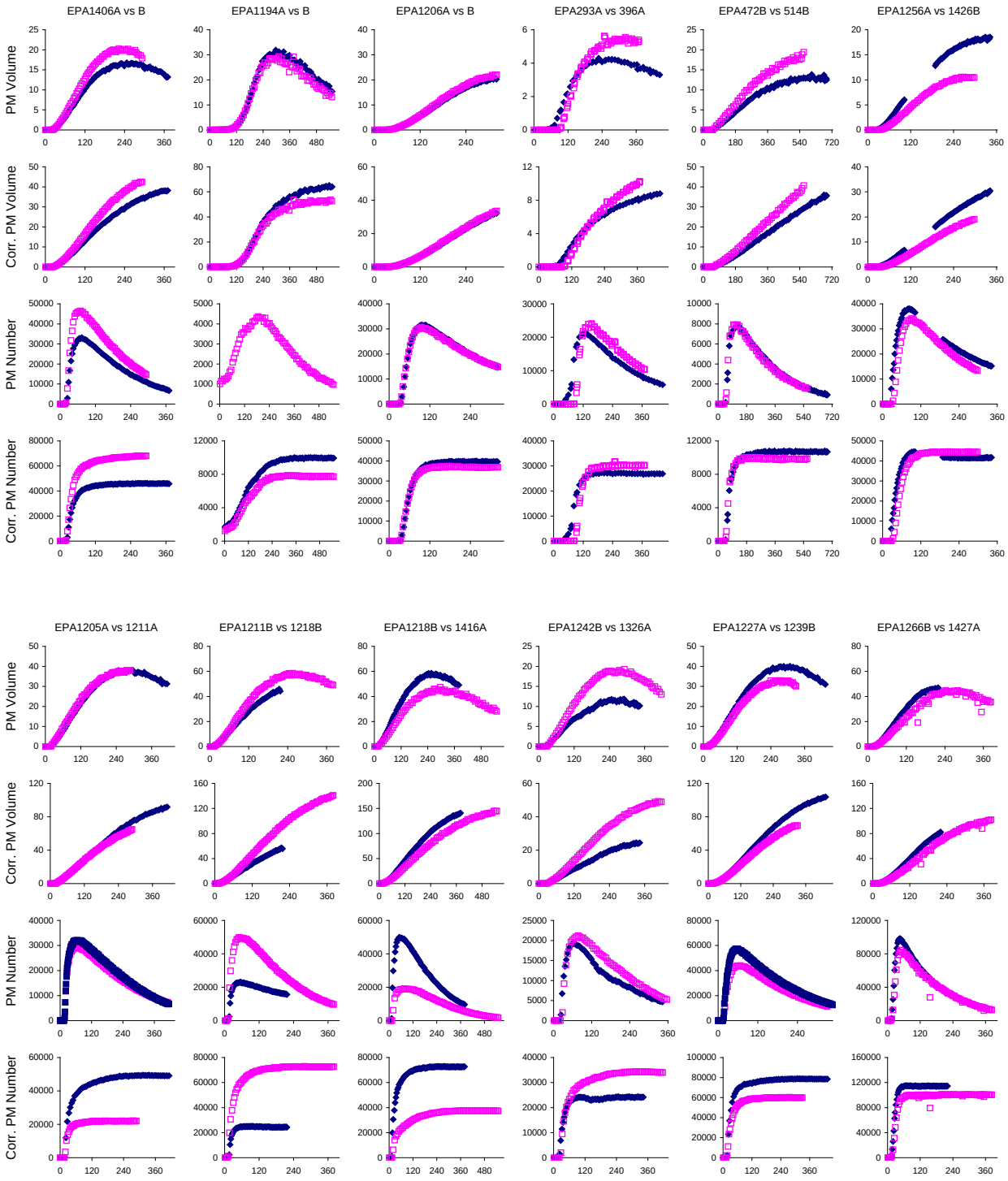

Figure A-2. Plots of corrected and uncorrected PM volume ($\mu m^3/cm^3$) and number (cm^{-3}) data for the replicate or near-replicate experiments (part 2 of 2)

Table A-3. List of experiments used for SOA mechanism evaluation in this work.

Run	Type	Reactants added (ppm)				Light	Char	Hours	Final
		Arom.	NO_x	H_2O_2	Other	[a]	[b]	Run	PM [c]
				Benzene					
EPA1236B	NOx	0.93	0.151			Bl-2	9	6	17
EPA1237A	NOx	0.44	0.042			Bl-2	9	7	32
EPA1237B	NOx	0.45	0.021			Bl-2	9	6	36
EPA412B	NOx	2.93	0.022			Bl-1	4	6	38
EPA1223B	NOx	0.97	0.119			Bl-2	9	5	59
EPA1195B	NOx	1.01	0.046			Bl-2	9	6	60
EPA1231A	NOx	0.95	0.100			Bl-2	9	6	69
EPA1236A	NOx	0.93	0.054			Bl-2	9	6	74
EPA1223A	NOx	0.97	0.059			Bl-2	9	6	89
EPA1195A	NOx - H2O2	1.01	0.047	0.20		Bl-2	9	8	95
EPA1161B	H2O2	0.53		5.1		Bl-2	8	4	17
EPA1141A	H2O2	0.49		1.50		Bl-2	8	7	24
EPA1149A	H2O2	0.49		5.0		Bl-2	8	6	24
EPA1225B	H2O2	0.96		1.02		Bl-2	9	5	28
EPA1225A	H2O2	0.96		2.0		Bl-2	9	6	59
EPA1161A	H2O2	1.03		5.1		Bl-2	8	6	62
EPA412A	NOx - CO	2.93			26	Bl-1	4	5	3
				Toluene					
EPA1098B	NOx	0.084	0.030			Bl-1	8	6	3
EPA1098A	NOx	0.084	0.016			Bl-1	8	9	8
EPA1102A	NOx	0.076	0.043			Bl-2	8	7	15
EPA1102B	NOx	0.076	0.032			Bl-2	8	7	16
EPA1101B	NOx	0.079	0.009			Bl-2	8	6	16
EPA1101A	NOx	0.079	0.019			Bl-2	8	8	21
EPA289B	NOx	0.22	0.025			Bl-1	3	7	27
EPA443A	NOx	0.170	0.031			Arc	4	6	32
EPA210B	NOx	0.26	0.093			Arc	3	6	42
EPA210A	NOx	0.26	0.042			Arc	3	6	44
EPA443B	NOx	0.36	0.099			Arc	4	5	53
EPA1251B	H2O2	0.084		1.02		Bl-2	9	4	12
EPA1266A	H2O2	0.104		1.02		Bl-2	9	4	12
EPA1149B	H2O2	0.082		5.0		Bl-2	8	3	12
EPA1141B	H2O2	0.085		1.50		Bl-2	8	4	14
EPA1290B	H2O2	0.43		1.02		Bl-2	9	6	61
EPA289A	NOx - Ethane	0.22			25	Bl-1	3	8	6
EPA1436A	NOx - Propene	0.39			0.43	Bl-2	9	5	1.5
EPA1407A	NOx - Ethene	0.34			0.84	Bl-2	9	6	2
EPA1443A	NOx - Propene	0.41			0.31	Bl-2	9	7	7
				Ethyl Benzene					
EPA1142A	NOx	0.100	0.047			Bl-2	8	6	15
EPA1146B	NOx	0.100	0.034			Bl-2	8	6	16
EPA1147A	NOx	0.34	0.099			Bl-2	8	5	53
EPA1147B	NOx	0.34	0.047			Bl-2	8	5	58
EPA1294B	H2O2	0.045		1.02		Bl-2	9	6	15

Table A-3 (continued)

Run	Type	Reactants added (ppm)				Light [a]	Char [b]	Hours Run	Final PM [c]
		Arom.	NO_x	H_2O_2	Other				
EPA1296B	H2O2	0.046		2.0		Bl-2	9	5	20
EPA1294A	H2O2	0.100		1.02		Bl-2	9	6	23
EPA1296A	H2O2	0.100		2.0		Bl-2	9	6	38
			m-Xylene						
EPA222B	NOx	0.054	0.125			Bl-1	3	10	2
EPA1091B	NOx	0.058	0.024			Bl-1	8	6	4
EPA764B	NOx	0.068	0.071			Bl-1	6	10	4
EPA1091A	NOx	0.055	0.024			Bl-1	8	6	4
EPA186B	NOx	0.054	0.093			Arc	3	5	6
EPA219A	NOx	0.054	0.010			Bl-1	3	6	7
EPA219B	NOx	0.055	0.010			Bl-1	3	6	7
EPA1193B	NOx	0.070	0.045			Bl-1	9	7	8
EPA217B	NOx	0.039	0.010			Bl-1	3	10	8
EPA764A	NOx	0.071	0.069			Bl-1	6	17	8
EPA365B	NOx	0.053	0.070			Arc	4	5	9
EPA293A	NOx	0.051	0.022			Bl-1	3	7	9
EPA288A	NOx	0.055	0.018			Bl-1	3	8	9
EPA1193A	NOx	0.071	0.045			Bl-1	9	7	9
EPA758B	NOx	0.076	0.012			Bl-1	6	10	10
EPA154B	NOx	0.063	0.061			Bl-1	3	7	10
EPA396A	NOx	0.053	0.022			Bl-1	4	6	10
EPA1192B	NOx	0.077	0.044			Bl-1	9	7	10
EPA1191B	NOx	0.084	0.046			Bl-1	9	8	10
EPA1192A	NOx	0.077	0.042			Bl-1	9	7	10
EPA1191A	NOx	0.080	0.052			Bl-1	9	8	11
EPA1175B	NOx	0.084	0.051			Bl-1	9	8	11
EPA419A	NOx	0.26	0.499			Bl-1	4	9	11
EPA758A	NOx	0.077	0.011			Bl-1	6	10	11
EPA290A	NOx	0.059	0.026			Bl-1	3	10	13
EPA820A	NOx	0.078	0.021			Bl-1	6	14	13
EPA164B	NOx	0.068	0.047			Bl-1	3	8	14
EPA749B	NOx	0.076	0.051			Bl-1	6	11	15
EPA1175A	NOx	0.085	0.051			Bl-1	9	8	17
EPA164A	NOx	0.068	0.047			Bl-1	3	8	18
EPA749A	NOx	0.076	0.050			Bl-1	6	13	19
EPA249B	NOx	0.155	0.247			Bl-1	3	11	20
EPA365A	NOx	0.053	0.022			Arc	4	6	21
EPA1190A	NOx	0.070	0.046			Bl-2	9	8	22
EPA249A	NOx	0.155	0.246			Bl-1	3	12	22
EPA1190B	NOx	0.077	0.047			Bl-2	9	8	27
EPA983A	NOx	0.28	0.077			Bl-1	7	7	41
EPA1092B	NOx	0.31	0.090			Bl-1	8	6	50
EPA149A	NOx	0.082	0.056			Arc	3	7	50
EPA149B	NOx	0.164	0.054			Arc	3	8	63
EPA1092A	NOx	0.29	0.090			Bl-1	8	9	69
EPA558A	NOx	0.132	0.082			Arc	5	8	69
EPA556A	NOx	0.160	0.078			Arc	5	11	107

Table A-3 (continued)

Run	Type	Reactants added (ppm)				Light	Char	Hours	Final
		Arom.	NO_x	H_2O_2	Other	[a]	[b]	Run	PM [c]
EPA556B	NOx	0.159	0.079			Arc	5	11	116
EPA410B	NOx	0.52	0.137			Bl-1	4	6	131
EPA247A	NOx	0.40	0.475			Bl-1	3	10	133
EPA410A	NOx	0.52	0.137			Bl-1	4	6	134
EPA247B	NOx	0.40	0.478			Bl-1	3	11	138
EPA1097B	NOx	0.59	0.196			Bl-1	8	6	150
EPA1097A	NOx	0.57	0.196			Bl-1	8	9	163
EPA469B	H2O2	0.051		0.30		Bl-1	4	6	6
EPA510B	H2O2 - CO	0.041		1.71		Bl-1	5	10	8
EPA510A	H2O2	0.041		0.57		Bl-1	5	10	8
EPA469A	H2O2	0.053		0.30		Bl-1	4	8	11
EPA471A	H2O2	0.106		0.50		Bl-1	4	11	12
EPA1248A	H2O2	0.32		1.02		Bl-2	9	2	14
EPA526B	H2O2	0.050		1.71		Bl-1	5	10	16
EPA471B	H2O2	0.102		0.50		Bl-1	4	12	16
EPA750B	H2O2	0.071		1.17		Bl-1	6	10	24
EPA476A	H2O2	0.054		1.00		Bl-1	4	11	25
EPA476B	H2O2	0.055		1.00		Bl-1	4	12	28
EPA513B	H2O2	0.113		0.85		Bl-1	5	8	29
EPA1024B	H2O2	0.23		4.0		Bl-1	7	5	30
EPA750A	H2O2	0.069		1.17		Bl-1	6	14	31
EPA472A	H2O2	0.116		1.00		Bl-1	4	11	32
EPA472B	H2O2	0.111		1.00		Bl-1	4	11	34
EPA514A	H2O2	0.110		1.00		Bl-1	5	9	36
EPA514B	H2O2	0.111		1.00		Bl-1	5	9	37
EPA1424B	H2O2	0.103		1.02		Bl-2	9	5	40
EPA513A	H2O2 - CO	0.112		3.3		Bl-1	5	9	43
EPA1248B	H2O2	0.115		1.02		Bl-2	9	4	44
EPA1212B	H2O2	0.052		2.0		Bl-2	9	5	44
EPA521A	H2O2	0.106		2.3		Bl-1	5	10	49
EPA1244A	H2O2	0.124		1.00		Bl-2	9	5	55
EPA473A	H2O2	0.110		2.0		Bl-1	4	11	62
EPA473B	H2O2	0.108		2.0		Bl-1	4	12	64
EPA520A	H2O2	0.113		1.71		Bl-1	5	11	67
EPA1134B	H2O2	0.078		1.10		Bl-2	8	7	71
EPA474A	H2O2	0.106		4.0		Bl-1	4	9	79
EPA1212A	H2O2	0.114		2.0		Bl-2	9	5	86
EPA474B	H2O2	0.106		4.0		Bl-1	4	11	88
EPA1180B	H2O2	0.23		4.1		Bl-2	9	4	129
EPA1209A	H2O2	0.23		2.0		Bl-2	9	6	137
EPA442A	NOx - Propene	0.161			0.36	Bl-1	4	12	3
EPA391B	NOx - Ethanol	0.060			0.29	Bl-1	4	8	3
EPA378B	NOx - Propene	0.058			0.06	Bl-1	4	9	4
EPA290B	NOx - Propene	0.060			0.13	Bl-1	3	10	5
EPA391A	NOx - Ethanol	0.060			0.29	Bl-1	4	9	5
EPA303A	NOx - CO	0.105			39	Bl-1	3	8	6
EPA1105B	NOx - CO	0.084			8.33	Bl-2	8	8	10
EPA293B	NOx - HCHO	0.054			0.10	Bl-1	3	7	10

Table A-3 (continued)

Run	Type	Reactants added (ppm)				Light	Char	Hours	Final
		Arom.	NO_x	H_2O_2	Other	[a]	[b]	Run	PM [c]
EPA424A	NOx - CO	0.144			25	Bl-1	4	11	11
EPA516B	NOx - CO	0.161			26	Bl-1	5	10	13
EPA424B	NOx - Propene	0.149			0.16	Bl-1	4	11	21
EPA442B	NOx - Propene	0.165			0.37	Bl-1	4	12	22
EPA429B	NOx - Propene	0.152			0.18	Bl-1	4	12	28
EPA303B	NOx - HCHO	0.106			0.03	Bl-1	3	8	29
EPA419B	NOx - Propene	0.27			0.23	Bl-1	4	12	34
EPA296B	NOx - Propene	0.24			0.26	Bl-1	3	12	40
EPA447A	NOx - Propene	0.32			0.27	Bl-1	4	11	69
EPA453A	NOx - Propene	0.31			0.28	Bl-1	4	11	75
EPA447B	NOx - Propene	0.32			0.26	Bl-1	4	11	75
EPA453B	NOx - Propene	0.32			0.28	Bl-1	4	11	81
			o-Xylene						
EPA1437B	NOx	0.079	0.050			Bl-2	9	4	13
EPA517B	NOx	0.101	0.021			Bl-1	5	10	15
EPA1315B	NOx	0.078	0.022			Bl-2	9	5	18
EPA1315A	NOx	0.082	0.050			Bl-2	9	5	18
EPA1437A	NOx	0.080	0.026			Bl-2	9	8	18
EPA503A	NOx	0.170	0.075			Bl-1	5	11	20
EPA518B	NOx	0.20	0.043			Bl-1	5	11	38
EPA504A	NOx	0.26	0.128			Bl-1	5	11	40
EPA518A	NOx	0.20	0.210			Bl-1	5	11	54
EPA1310B	H2O2	0.065		1.02		Bl-2	9	5	19
EPA1389B	H2O2	0.076		1.02		Bl-2	9	4	22
EPA1310A	H2O2	0.120		1.02		Bl-2	9	5	26
EPA1313B	H2O2	0.051		1.02		Bl-2	9	6	33
EPA1313A	H2O2	0.100		1.02		Bl-2	9	6	48
EPA512B	H2O2	0.120		4.6		Bl-1	5	11	51
			p-Xylene						
EPA1308A	NOx	0.079	0.055			Bl-2	9	4	3
EPA422B	NOx	0.100	0.024			Bl-1	4	6	5
EPA1308B	NOx	0.078	0.023			Bl-2	9	5	7
EPA1432B	NOx	0.064	0.024			Bl-2	9	6	8
EPA1432A	NOx	0.062	0.026			Bl-2	9	7	8
EPA503B	NOx	0.146	0.076			Bl-1	5	11	55
EPA511B	H2O2	0.118		2.3		Bl-1	5	11	18
EPA1304B	H2O2	0.070		1.02		Bl-2	9	5	28
EPA1304A	H2O2	0.120		1.02		Bl-2	9	5	39
EPA512A	H2O2	0.111		4.6		Bl-1	5	10	44
EPA504B	H2O2	0.26				Bl-1	5	11	96
			n-Propyl Benzene						
EPA1245A	NOx	0.101	0.022			Bl-2	9	7	8
EPA1246A	NOx	0.20	0.068			Bl-2	9	6	16
EPA1426B	H2O2	0.100		1.02		Bl-2	9	5	19
EPA1256A	H2O2	0.100		1.02		Bl-2	9	5	27
EPA1269A	H2O2	0.100		2.0		Bl-2	9	4	31
EPA1426A	H2O2	0.28		1.02		Bl-2	9	6	41

Table A-3 (continued)

Run	Type	Reactants added (ppm)				Light	Char	Hours	Final
		Arom.	NO_x	H_2O_2	Other	[a]	[b]	Run	PM [c]
EPA1269B	H2O2	0.20		2.0		Bl-2	9	3	43
EPA1256B	H2O2	0.21		1.02		Bl-2	9	5	48
			Isopropyl Benzene						
EPA1253B	NOx	0.20	0.099			Bl-2	9	5	8
EPA1247B	NOx	0.099	0.048			Bl-2	9	6	12
EPA1247A	NOx	0.100	0.022			Bl-2	9	7	23
EPA1253A	NOx	0.20	0.056			Bl-2	9	5	36
EPA1265A	H2O2	0.083		1.02		Bl-2	9	4	17
EPA1274A	H2O2	0.115		2.0		Bl-2	9	4	33
EPA1265B	H2O2	0.20		1.02		Bl-2	9	4	33
EPA1274B	H2O2	0.185		2.0		Bl-2	9	4	44
			m-Ethyl Toluene						
EPA1151A	NOx	0.087	0.099			Bl-2	8	4	5
EPA1421A	NOx	0.100	0.023			Bl-2	9	8	33
EPA1421B	NOx	0.099	0.046			Bl-2	9	5	39
EPA1199B	NOx	0.100	0.092			Bl-2	9	6	39
EPA1222B	NOx	0.100	0.069			Bl-2	9	5	47
EPA1222A	NOx	0.099	0.131			Bl-2	9	7	49
EPA1199A	NOx	0.100	0.045			Bl-2	9	7	50
EPA1226A	NOx	0.20	0.251			Bl-2	9	7	95
EPA1226B	NOx	0.20	0.138			Bl-2	9	5	97
EPA1232A	NOx	0.20	0.122			Bl-2	9	6	105
EPA1211B	H2O2	0.20		1.02		Bl-2	9	3	48
EPA1211A	H2O2	0.100		1.02		Bl-2	9	4	57
EPA1205B	H2O2	0.100		1.02		Bl-2	9	6	79
EPA1205A	H2O2	0.100		1.02		Bl-2	9	6	86
EPA1416B	H2O2	0.107		1.02		Bl-2	9	6	90
EPA1218A	H2O2	0.090		1.02		Bl-2	9	7	104
EPA1218B	H2O2	0.20		1.02		Bl-2	9	6	137
EPA1416A	H2O2	0.20		1.02		Bl-2	9	9	142
			o-Ethyl Toluene						
EPA1202B	NOx	0.100	0.108			Bl-2	9	5	20
EPA1168B	NOx	0.100	0.100			Bl-2	8	6	31
EPA1413A	NOx	0.100	0.022			Bl-2	9	8	45
EPA1413B	NOx	0.099	0.048			Bl-2	9	6	46
EPA1202A	NOx	0.099	0.060			Bl-2	9	7	49
EPA1179B	NOx	0.093	0.053			Bl-2	9	9	54
EPA1179A	NOx	0.092	0.053			Bl-2	9	9	62
EPA1215B	NOx	0.21	0.057			Bl-2	9	4	68
EPA1233B	NOx	0.20	0.259			Bl-2	9	6	86
EPA1215A	NOx	0.21	0.108			Bl-2	9	5	105
EPA1233A	NOx	0.20	0.198			Bl-2	9	7	113
EPA1242B	H2O2	0.101		1.02		Bl-2	9	5	23
EPA1406B	H2O2	0.096		1.02		Bl-2	9	4	38
EPA1406A	H2O2	0.096		1.02		Bl-2	9	6	38
EPA1326A	H2O2	0.102		1.02		Bl-2	9	6	47
EPA1326B	H2O2	0.20		1.02		Bl-2	9	5	57

Table A-3 (continued)

Run	Type	Reactants added (ppm)				Light	Char	Hours	Final
		Arom.	NO_x	H_2O_2	Other	[a]	[b]	Run	PM [c]
EPA1242A	H2O2	0.25		1.02		Bl-2	9	7	97
		p-Ethyl Toluene							
EPA1214A	NOx	0.101	0.104			Bl-2	9	6	12
EPA1214B	NOx	0.102	0.053			Bl-2	9	5	20
EPA1229B	NOx	0.20	0.258			Bl-2	9	6	27
EPA1197B	NOx	0.192	0.099			Bl-2	9	6	38
EPA1197A	NOx	0.192	0.056			Bl-2	9	7	45
EPA1194B	NOx	0.20	0.089			Bl-2	9	7	50
EPA1229A	NOx	0.20	0.192			Bl-2	9	8	63
EPA1194A	NOx	0.20	0.091			Bl-2	9	9	64
EPA1227B	H2O2	0.083		1.02		Bl-2	9	5	46
EPA1239A	H2O2	0.093		1.02		Bl-2	9	6	59
EPA1239B	H2O2	0.20		1.02		Bl-2	9	5	66
EPA1227A	H2O2	0.20		1.02		Bl-2	9	7	103
		1,2,3-Trimethyl Benzene							
EPA1158A	NOx	0.080	0.010			Bl-2	8	7	16
EPA1158B	NOx	0.080	0.022			Bl-2	8	5	23
EPA1162A	NOx	0.080	0.033			Bl-2	8	6	33
EPA1162B	NOx	0.080	0.043			Bl-2	8	5	34
EPA1287B	H2O2	0.037		1.02		Bl-2	9	7	38
EPA1287A	H2O2	0.080		1.02		Bl-2	9	7	68
		1,2,4-Trimethyl Benzene							
EPA1352A	NOx	0.079	0.193			Bl-2	9	7	4
EPA1352B	NOx	0.079	0.137			Bl-2	9	7	6
EPA1123A	NOx	0.080	0.010			Bl-2	8	6	7
EPA1126A	NOx	0.079	0.011			Bl-2	8	6	8
EPA1117A	NOx	0.060	0.011			Bl-2	8	8	9
EPA1123B	NOx	0.080	0.023			Bl-2	8	6	10
EPA1126B	NOx	0.081	0.024			Bl-2	8	6	10
EPA1356B	NOx	0.079	0.149			Bl-2	9	8	11
EPA1374A	NOx	0.077	0.143			Bl-2	9	8	11
EPA1380B	NOx	0.079	0.055			Bl-2	9	5	12
EPA1119B	NOx	0.079	0.041			Bl-2	8	7	13
EPA1117B	NOx	0.060	0.021			Bl-2	8	8	13
EPA1119A	NOx	0.078	0.050			Bl-2	8	7	14
EPA1356A	NOx	0.079	0.121			Bl-2	9	7	15
EPA1374B	NOx	0.077	0.148			Bl-2	9	8	15
EPA1135B	NOx	0.075	0.021	2.0		Bl-2	8	7	43
EPA1135A	NOx	0.075	0.011	2.0		Bl-2	8	7	54
EPA1278B	H2O2	0.060		1.02		Bl-2	9	4	29
EPA1278A	H2O2	0.070		1.02		Bl-2	9	4	32
EPA1292B	H2O2	0.040		1.02		Bl-2	9	6	35
EPA1292A	H2O2	0.079		1.02		Bl-2	9	5	40
		1,3,5-Trimethyl Benzene							
EPA1153A	NOx	0.079	0.011			Bl-2	8	6	8
EPA1156B	NOx	0.080	0.045			Bl-2	8	5	14
EPA1153B	NOx	0.080	0.020			Bl-2	8	5	14

Table A-3 (continued)

Run	Type	Reactants added (ppm)				Light	Char	Hours	Final
		Arom.	NO_x	H_2O_2	Other	[a]	[b]	Run	PM [c]
EPA1156A	NOx	0.080	0.032			Bl-2	8	7	18
EPA1154B	H2O2	0.039		0.80		Bl-2	8	4	32
EPA1298B	H2O2	0.040		1.02		Bl-2	9	6	43
EPA1154A	H2O2	0.079		0.80		Bl-2	8	6	53
EPA1298A	H2O2	0.071		1.02		Bl-2	9	6	64
			Phenol						
EPA1273B	NOx	0.106	0.053			Bl-2	9	4	17
EPA1273A	NOx	0.106	0.023			Bl-2	9	4	38
EPA1219A	NOx	0.140	0.147			Bl-2	9	9	125
EPA1219B	NOx	0.140	0.076			Bl-2	9	9	196
EPA1424A	H2O2	0.065		1.02		Bl-2	9	5	23
EPA1206A	H2O2	0.051		1.02		Bl-2	9	5	30
EPA1206B	H2O2	0.052		1.02		Bl-2	9	5	31
EPA1217B	H2O2	0.076		2.0		Bl-2	9	5	56
EPA1217A	H2O2	0.138		2.0		Bl-2	9	5	94
			m-Cresol						
EPA1255A	H2O2	0.067		1.02		Bl-2	9	3	29
EPA1255B	H2O2	0.055		1.02		Bl-2	9	3	32
			p-Cresol						
EPA1258B	H2O2	0.028		1.02		Bl-2	9	3	30
EPA1312B	H2O2	0.025		1.02		Bl-2	9	5	43
EPA1258A	H2O2	0.068		1.02		Bl-2	9	4	64
EPA1312A	H2O2	0.044		1.02		Bl-2	9	5	65
EPA1290A	H2O2	0.033		1.02		Bl-2	9	6	74
			o-Cresol						
EPA1260B	NOx	0.062	0.056			Bl-2	9	3	40
EPA1260A	NOx	0.062	0.015			Bl-2	9	3	50
EPA1279B	NOx	0.080	0.057			Bl-2	9	3	84
EPA1279A	NOx	0.080	0.027			Bl-2	9	3	85
EPA1350A	NOx	0.31	0.718			Bl-2	9	5	233
EPA1350B	NOx	0.30	0.384			Bl-2	9	5	627
EPA1252B	H2O2	0.042		1.02		Bl-2	9	4	44
EPA1252A	H2O2	0.055		1.02		Bl-2	9	4	51
EPA1266B	H2O2	0.101		1.02		Bl-2	9	3	67
EPA1251A	H2O2	0.075		1.02		Bl-2	9	4	72
EPA1427A	H2O2	0.105		1.02		Bl-2	9	6	100
			2,4-Dimethyl Phenol						
EPA1275B	NOx	0.040	0.053			Bl-2	9	4	32
EPA1275A	NOx	0.040	0.022			Bl-2	9	4	58
EPA1277B	NOx	0.094	0.051			Bl-2	9	3	117
EPA1277A	NOx	0.094	0.023			Bl-2	9	3	129
EPA1238B	H2O2	0.062		1.02		Bl-2	9	4	135
EPA1238A	H2O2	0.084		1.02		Bl-2	9	5	200
EPA1134A	H2O2	0.072		1.10		Bl-2	8	7	234
EPA1412A	H2O2	0.183		1.02		Bl-2	9	7	334
EPA1180A	H2O2	0.150		4.1		Bl-2	9	4	485

Table A-3 (continued)

Run	Type	Reactants added (ppm)				Light [a]	Char [b]	Hours Run	Final PM [c]
		Arom.	NO_x	H_2O_2	Other				
				2,6-Dimethyl Phenol					
EPA1024A	H2O2	0.040		4.0		Bl-1	7	5	43
EPA1240B	H2O2	0.049		1.02		Bl-2	9	5	74
EPA1240A	H2O2	0.098		1.02		Bl-2	9	5	133
				3,5-Dimethyl Phenol					
EPA1243B	H2O2	0.060		1.02		Bl-2	9	4	30
EPA1243A	H2O2	0.090		1.02		Bl-2	9	5	83
				Catechol					
EPA1314B	H2O2	0.038		1.02		Bl-2	9	5	65
EPA1314A	H2O2	0.085		1.02		Bl-2	9	5	125

[a] Codes for light sources: "Arc" = arc light, NO_2 photolysis rate = 0.26 min^{-1}; "Bl-1": original blacklights, NO_2 photolysis rate = 0.13 - 0.18 min^{-1}; "Bl-2": enhanced blacklights, NO_2 photolysis rate = 0.4 min^{-1}.

[b] Characterization set that is used to determine chamber-dependent parameters as discussed in the "Characterization Results" section.

[b] Final PM formation, corrected for wall loss, in units of $\mu g/m^3$.

Table A-4. Listing of all model species used in the baseline mechanism that was evaluated in this work

Type and Name	Description
Constant Species.	
O2	Oxygen
M	Air
H2O	Water
H2	Hydrogen Molecules
HV	Light
Active Inorganic Species.	
O3	Ozone
NO	Nitric Oxide
NO2	Nitrogen Dioxide
NO3	Nitrate Radical
N2O5	Nitrogen Pentoxide
HONO	Nitrous Acid
HNO3	Nitric Acid
HNO4	Peroxynitric Acid
HO2H	Hydrogen Peroxide
CO	Carbon Monoxide
SO2	Sulfur Dioxide
Active Radical Species and Operators.	
OH	Hydroxyl Radicals
HO2	Hydroperoxide Radicals
MEO2	Methyl Peroxy Radicals
RO2C	Peroxy Radical Operator representing NO to NO2 and NO3 to NO2 conversions, and the effects of peroxy radical reactions on acyl peroxy and other peroxy radicals.
RO2XC	Peroxy Radical Operator representing NO consumption (used in conjunction with organic nitrate formation), and the effects of peroxy radical reactions on NO3, acyl peroxy radicals, and other peroxy radicals.
MECO3	Acetyl Peroxy Radicals
RCO3	Peroxy Propionyl and higher peroxy acyl Radicals
BZCO3	Peroxyacyl radical formed from Aromatic Aldehydes
MACO3	Peroxyacyl radicals formed from methacrolein and other acroleins.
Steady State Radical Species	
O3P	Ground State Oxygen Atoms
O1D	Excited Oxygen Atoms
TBUO	t-Butoxy Radicals
BZO	Phenoxy Radicals
HCOCO3	HC(O)C(O)OO Radicals
PAN and PAN Analogues	
PAN	Peroxy Acetyl Nitrate

Table A-4 (continued)

Type and Name	Description
PAN2	PPN and other higher alkyl PAN analogues
PBZN	PAN analogues formed from Aromatic Aldehydes
MAPAN	PAN analogue formed from Methacrolein
Explicit and Lumped Molecule Reactive Organic Product Species	
HCHO	Formaldehyde
CCHO	Acetaldehyde
RCHO	Lumped C3+ Aldehydes (mechanism based on propionaldehyde)
ACET	Acetone
MEK	Ketones and other non-aldehyde oxygenated products which react with OH radicals faster than 5 x 10-13 but slower than 5 x 10-12 cm3 molec-2 sec-1. (Based on mechanism for methyl ethyl ketone).
MEOH	Methanol
HCOOH	Formic Acid
CCOOH	Acetic Acid. Also used for peroxyacetic acid.
RCOOH	Higher organic acids and peroxy acids (mechanism based on propionic acid).
COOH	Methyl Hydroperoxide
ROOH	Lumped organic hydroperoxides with 2-4 carbons. Mechanism based on that estimated for n-propyl hydroperoxide.
R6OOH	Lumped organic hydroperoxides with 5 or more carbons (other than those formed following OH addition to aromatic rings, which is reprsented separately). Mechanism based on that estimated for 3-hexyl hydroperoxide.
GLY	Glyoxal
MGLY	Methyl Glyoxal
BACL	Biacetyl
PHEN	Phenol
CRES	Cresols
XYNL	Xylenols and higher alkyl phenols
CATL	Catechols
NPHE	Nitrophenols
BALD	Aromatic aldehydes (e.g., benzaldehyde)
MACR	Methacrolein
MVK	Methyl Vinyl Ketone
IPRD	Lumped isoprene product species
Aromatic unsaturated ring fragmentation products	
AFG1	Monounsaturated dialdehydes or aldehyde-ketones formed from aromatics. - Most photoreactive
AFG2	Monounsaturated dialdehydes or aldehyde-ketones formed from aromatics. - Least photoreactive
AFG3	Diunsaturatred dicarbonyl aromatic fragmentation products that are assumed not to photolyze rapidly
AFG4	3-hexene-2,5-dione and other monounsaturated diketone aromatic products.
Lumped Parameter Products	
PROD2	Ketones and other non-aldehyde oxygenated products which react with OH radicals faster than 5 x 10-12 cm3 molec-2 sec-1.
RNO3	Lumped Organic Nitrates

Table A-4 (continued)

Type and Name	Description

Model species used for SOA formation only. See Table 7 for details

RAOOH	Condensable hydroperoxides formed in reactions of aromatics with OH radicals. (process p1 on Figure 24).
RAOOHp	Condensable hydroperoxides formed in reactions of aromatics with OH or NO_3 radicals. With phenols (process p1 on Figure 24).
AFG3C	Used to represent formation of CNDp2 from AFG3 with different yields from each aromatic hydrocarbon without having to add a separate AFG3 model species for each.
CNDp2	Condensable non-hydroperoxide products formed from aromatic + OH reactions (process p2 on Figure 24).
CNDp2p	Condensable non-hydroperoxide products formed reactions of reactions of phenols or catechols (process p2p and p3p on Figure 24)
CNDW	Condensable compounds formed from reactions of species off-gassed from the chamber walls.
pmRAOOH pmRAOOHp	pmCNDp2 pmCNDp2p pmCNDW Particle-phase forms of the species listed above.

Steady state operators used to represent radical or product formation in peroxy radical reactions.

xHO2	xTBUO	xPROD2	xAFG4	Formation of HO2 or other products from the reactions of alkoxy radicals formed in peroxy radical reactions with NO and NO3 (100% yields) and RO2 (50% yields)
xOH	xCO	xBALD	xMACR	
xNO2	xHCHO	xGLY	xMVK	
xMEO2	xCCHO	xMGLY	xIPRD	
xMECO3	xRCHO	xBACL	xRNO3	
xRCO3	xACET	xAFG1	xCNDp2	
xMACO3	xMEK	xAFG2	xCNDp2p	

zRNO3	Formation of RNO3 in the RO2 + NO, reaction, or formation of corresponding non-nitrate products (represented by PROD2) formed from alkoxy radicals formed in RO2 + NO3 and (in 50% yields) RO2 + RO2 reactions.
yROOH yR6OOH yRAOOH yRAOOHp	Formation of the corresponding hydroperoxide model species following RO2 + HO2 reactions, or formation of H-shift disproportionation products (represented by MEK) in the RO2 + RCO3 and (in 50% yields) RO2 + RO2 reactions.

Non-Reacting Species

CO2	Carbon Dioxide
SULF	Sulfates (SO3 or H2SO4)
XC	Lost Carbon or carbon in unreactive products
XN	Lost Nitrogen or nitrogen in unreactive products

Primary Organics Represented explicitly

CH4	Methane
ETHENE	Ethene
ISOPRENE	Isoprene
ACETYLEN	Acetylene

Non-aromatic compounds represented explicitly in chamber simulations

ETHANE	Ethane
N-C4	n-Butane
PROPENE	Propene
ETOH	Ethanol

Table A-4 (continued)

Type and Name	Description
N-C6F14	Perfluorohexane
Aromatic compounds represented explicitly in chamber simulations	
BENZENE	Benzene
TOLUENE	Toluene
C2-BENZ	Ethyl Benzene
N-C3-BEN	n-Propyl Benzene
I-C3-BEN	Isopropyl Benzene
M-XYLENE	m-Xylene
O-XYLENE	o-Xylene
P-XYLENE	p-Xylene
M-ET-TOL	m-Ethyl toluene
O-ET-TOL	o-Ethyl toluene
P-ET-TOL	p-Ethyl toluene
123-TMB	1,2,3-trimethylbenzene
124-TMB	1,2,4-trimethylbenzene
135-TMB	1,3,5-trimethylbenzene
Lumped Aromatic Species for Airshed Models	
ARO1	Aromatic compounds with OH radical rate constants $\leq 1 \times 10^4$ ppm^{-1} min^{-1}.
ARO2	Aromatic compounds with OH radical rate constants $> 1 \times 10^4$ ppm^{-1} min^{-1}.

Table A-5. Listing of aromatic reactions and rate parameters of the baseline aromatic SOA mechanism that was developed in this work. See Carter and Heo (2012) for a listing of the other reactions in the mechanism, which were not changed in this work.

Label	Reaction and Products [a]	Rate Parameters [b]				Notes [a]
		k(300)	A	Ea	B	
	Initial Reactions of Aromatic Hydrocarbons					
BENZ	BENZENE + OH = #.027 RO2XC + #.31 RO2C + #.57 HO2 + #.31 xHO2 + #.027 zRNO3 + #.189 yR6OOH + #.57 PHEN + #.31 xGLY + #.189 xAFG1 + #.121 xAFG2 + #.148 yRAOOH + #.093 OH + #.093 AFG3 + #.1 AFG3C	1.22e-12	2.33e-12	0.384		1,2
TOLU	TOLUENE + OH = #.074 RO2XC + #.605 RO2C + #.18 HO2 + #.605 xHO2 + #.074 zRNO3 + #.2 yR6OOH + #.065 xBALD + #.18 CRES + #.29 xGLY + #.25 xMGLY + #.324 xAFG1 + #.216 xAFG2 + #.182 yRAOOH + #.141 OH + #.141 AFG3 + #.09 AFG3C	5.58e-12	1.81e-12	-0.672		1,2
C2BN	C2-BENZ + OH = #.105 RO2XC + #.642 RO2C + #.153 HO2 + #.642 xHO2 + #.105 zRNO3 + #.266 yR6OOH + #.161 xPROD2 + #.023 xRCHO + #.153 XYNL + #.246 xGLY + #.212 xMGLY + #.183 xAFG1 + #.275 xAFG2 + #.507 yRAOOH + #.101 OH + #.101 AFG3 + #.031 AFG3C	6.50e-12				1,2
MXYL	M-XYLENE + OH = #.098 RO2XC + #.6 RO2C + #.11 HO2 + #.6 xHO2 + #.098 zRNO3 + #.489 yR6OOH + #.04 xBALD + #.11 XYNL + #.11 xGLY + #.45 xMGLY + #.319 xAFG1 + #.241 xAFG2 + #.208 yRAOOH + #.192 OH + #.192 AFG3 + #.07 AFG3C	2.31e-11				1,2
OXYL	O-XYLENE + OH = #.114 RO2XC + #.695 RO2C + #.11 HO2 + #.695 xHO2 + #.114 zRNO3 + #.522 yR6OOH + #.045 xBALD + #.11 XYNL + #.13 xGLY + #.33 xMGLY + #.19 xBACL + #.293 xAFG1 + #.358 xAFG2 + #.287 yRAOOH + #.081 OH + #.081 AFG3 + #.049 AFG3C	1.36e-11				1,2
PXYL	P-XYLENE + OH = #.107 RO2XC + #.655 RO2C + #.13 HO2 + #.655 xHO2 + #.107 zRNO3 + #.563 yR6OOH + #.085 xBALD + #.13 XYNL + #.37 xGLY + #.2 xMGLY + #.37 xAFG4 + #.178 xAFG1 + #.022 xAFG2 + #.199 yRAOOH + #.108 OH + #.108 AFG3 + #.049 AFG3C	1.43e-11				1,2

Table A-5 (continued

Label	Reaction and Products [a]	Rate Parameters [b]				Notes [a]
		k(300)	A	Ea	B	
NC3B	N-C3-BEN + OH = #.14 RO2XC + #.698 RO2C + #.105 HO2 + #.698 xHO2 + #.14 zRNO3 + #.506 yR6OOH + #.36 xPROD2 + #.023 xRCHO + #.105 XYNL + #.169 xGLY + #.146 xMGLY + #.179 xAFG1 + #.135 xAFG2 + #.332 yRAOOH + #.057 OH + #.057 AFG3 + #.062 AFG3C	6.13e-12				1,2
IC3B	I-C3-BEN + OH = #.126 RO2XC + #.627 RO2C + #.16 HO2 + #.526 xHO2 + #.126 zRNO3 + #.435 yR6OOH + #.1 xMEO2 + #.1 xPROD2 + #.046 xRCHO + #.16 XYNL + #.258 xGLY + #.222 xMGLY + #.182 xAFG1 + #.298 xAFG2 + #.317 yRAOOH + #.088 OH + #.088 AFG3 + #.045 AFG3C	6.20e-12				1,2
METL	M-ET-TOL + OH = #.123 RO2XC + #.612 RO2C + #.104 HO2 + #.612 xHO2 + #.123 zRNO3 + #.424 yR6OOH + #.021 xBALD + #.054 xPROD2 + #.008 xRCHO + #.104 XYNL + #.104 xGLY + #.425 xMGLY + #.354 xAFG1 + #.174 xAFG2 + #.311 yRAOOH + #.162 OH + #.162 AFG3 + #.075 AFG3C	1.86e-11				1,2
OETL	O-ET-TOL + OH = #.142 RO2XC + #.709 RO2C + #.098 HO2 + #.709 xHO2 + #.142 zRNO3 + #.587 yR6OOH + #.033 xBALD + #.085 xPROD2 + #.012 xRCHO + #.098 XYNL + #.116 xGLY + #.294 xMGLY + #.169 xBACL + #.318 xAFG1 + #.261 xAFG2 + #.264 yRAOOH + #.05 OH + #.05 AFG3 + #.102 AFG3C	1.19e-11				1,2
PETL	P-ET-TOL + OH = #.133 RO2XC + #.664 RO2C + #.122 HO2 + #.664 xHO2 + #.133 zRNO3 + #.51 yR6OOH + #.033 xBALD + #.086 xPROD2 + #.012 xRCHO + #.122 XYNL + #.346 xGLY + #.187 xMGLY + #.346 xAFG4 + #.187 xAFG1 + #.288 yRAOOH + #.081 OH + #.081 AFG3 + #.043 AFG3C	1.18e-11				1,2
B123	123-TMB + OH = #.148 RO2XC + #.736 RO2C + #.031 HO2 + #.736 xHO2 + #.148 zRNO3 + #.405 yR6OOH + #.036 xBALD + #.031 XYNL + #.06 xGLY + #.17 xMGLY + #.47 xBACL + #.28 xAFG1 + #.42 xAFG2 + #.479 yRAOOH + #.085 OH + #.085 AFG3 + #.075 AFG3C	3.27e-11				1,2

Table A-5 (continued

Label	Reaction and Products [a]	Rate Parameters [b]				Notes [a]
		k(300)	A	Ea	B	
B124	124-TMB + OH = #.117 RO2XC + #.581 RO2C + #.022 HO2 + #.581 xHO2 + #.117 zRNO3 + #.349 yR6OOH + #.034 xBALD + #.022 XYNL + #.077 xGLY + #.36 xMGLY + #.11 xBACL + #.167 xAFG4 + #.182 xAFG1 + #.198 xAFG2 + #.348 yRAOOH + #.281 OH + #.281 AFG3 + #.078 AFG3C	3.25e-11				1,2
B135	135-TMB + OH = #.128 RO2XC + #.638 RO2C + #.04 HO2 + #.638 xHO2 + #.128 zRNO3 + #.4 yR6OOH + #.028 xBALD + #.04 XYNL + #.61 xMGLY + #.238 xAFG1 + #.372 xAFG2 + #.366 yRAOOH + #.194 OH + #.194 AFG3 + #.057 AFG3C	5.67e-11				1,2
	Reactions of Phenolic Products					
BP83	PHEN + OH = #.7 HO2 + #.1 BZO + #.11 xHO2 + #.09 OH + #.11 RO2C + #.7 CATL + #.09 AFG3 + #.055 xAFG1 + #.055 xAFG2 + #.11 xGLY + #.09 yR6OOH + #.020 yRAOOHp	2.74e-11	4.70e-13	-2.42		1,3
BP84	PHEN + NO3 = #.1 HNO3 + #.9 XN + #.7 HO2 + #.1 BZO + #.11 xHO2 + #.09 OH + #.11 RO2C + #.7 CATL + #.09 AFG3 + #.055 xAFG1 + #.055 xAFG2 + #.11 xGLY + #.090 yR6OOH	3.80e-12				1,3
BP38	CRES + OH = #.7 HO2 + #.1 BZO + #.17 xHO2 + #.03 OH + #.17 RO2C + #.7 CATL + #.03 AFG3 + #.085 xAFG1 + #.085 xAFG2 + #.085 xGLY + #.085 xMGLY + #.1 xCNDp2p + #.13 yR6OOH + #.040 yRAOOHp	4.06e-11	1.60e-12	-1.93		1,3
BP39	CRES + NO3 = #.1 HNO3 + #.9 XN + #.7 HO2 + #.1 BZO + #.17 xHO2 + #.03 OH + #.17 RO2C + #.7 CATL + #.03 AFG3 + #.085 xAFG1 + #.085 xAFG2 + #.085 xGLY + #.085 xMGLY + #.130 yR6OOH	1.40e-11				1,3
BP85	XYNL + OH = #.7 HO2 + #.1 BZO + #.21 xHO2 + #.21 RO2C + #.7 CATL + #.105 xAFG1 + #.105 xAFG2 + #.105 xGLY + #.105 xMGLY + #.12 xCNDp2p + #.21 yRAOOHp	7.38e-11				1,3
BP86	XYNL + NO3 = #.1 HNO3 + #.9 XN + #.7 HO2 + #.1 BZO + #.21 xHO2 + #.210 RO2C + #.7 CATL + #.105 xAFG1 + #.105 xAFG2 + #.105 xGLY + #.105 xMGLY	3.06e-11				1,3

Table A-5 (continued

Label	Reaction and Products [a]	Rate Parameters [b]				Notes [a]
		k(300)	A	Ea	B	
BP87	CATL + OH = #.4 HO2 + #.2 BZO + #.2 xHO2 + #.2 OH + #.2 RO2C + #.2 AFG3 + #.1 xAFG1 + #.1 xAFG2 + #.1 xGLY + #.1 xMGLY + #.33 CNDp2p + #.2 yR6OOH	2.00e-10				1,4
BP88	CATL + NO3 = #.2 HNO3 + #.8 XN + #.4 HO2 + #.2 BZO + #.2 xHO2 + #.2 OH + #.2 RO2C + #.2 AFG3 + #.1 xAFG1 + #.1 xAFG2 + #.1 xGLY + #.1 xMGLY + #.2 yR6OOH	1.70e-10				1,4
	Reactions of Condensable Species					
BP28	RAOOH + OH = #.139 OH + #.148 HO2 + #.589 RO2C + #.124 RO2XC + #.124 zRNO3 + #.074 PROD2 + #.147 MGLY + #.139 IPRD + #.565 xHO2 + #.024 xOH + #.448 xRCHO + #.026 xGLY + #.030 xMEK + #.252 xMGLY + #.073 xAFG1 + #.073 xAFG2 + #.713 yR6OOH	1.41e-10				1
BP29	RAOOH + HV = OH + HO2 + #.5 {GLY + MGLY + AFG1 + AFG2}	Phot Set= COOH				1
nOOH	RAOOH + PMmass = pmRAOOH + #(1+fOOH) PMmass	See Note 5. (Depends on Mw, T, and PMrad)				5
vOOH	pmRAOOH = RAOOH + #-fOOH PMmass	See Note 6. (Depends on kP)				5,6
cOOH	RAOOH + RAOOH = #2 pmRAOOH + #2*fOOH PMmass	See Note 7. (Depends on Kp)				7
nCAP	CNDp2 + PMmass = pmCNDp2 + #(1+fCNDp2) PMmass	See Note 5. (Depends on Mw, T, and PMrad)				5
vCAP	pmCNDp2 = CNDp2 + #-fCNDp2	See Note 6. (Depends on kP)				5,6
cCAP	CNDp2 + CNDp2 = #2 pmCNDp2 + #2*fCNDp2 PMmass	See Note 7. (Depends on Kp)				7
BP90	RAOOHp + OH = #.139 OH + #.148 HO2 + #.589 RO2C + #.124 RO2XC + #.124 zRNO3 + #.074 PROD2 + #.147 MGLY + #.139 IPRD + #.565 xHO2 + #.024 xOH + #.448 xRCHO + #.026 xGLY + #.030 xMEK + #.252 xMGLY + #.073 xAFG1 + #.073 xAFG2 + #.713 yR6OOH	1.41e-10				8
BP91	RAOOHp + HV = OH + HO2 + #.5 {GLY + MGLY + AFG1 + AFG2}	Phot Set= COOH				1
nO2H	RAOOHp + PMmass = pmRAOOHp + #(1+fOOHp) PMmass	See Note 5. (Depends on Mw, T, and PMrad)				5
vO2H	pmRAOOHp = RAOOHp + #-fOOHp PMmass	Assumed negligible				9
cO2H	RAOOHp + RAOOHp = #2 pmRAOOHp + #2*fRAOOHp PMmass	See Note 7 (Coef = NCrateI)				7,9
nCCA	CNDp2p + PMmass = pmCNDp2p + #(1+fCNDp2p) PMmass	See Note 5. (Depends on Mw, T, and PMrad)				5
vCCA	pmCNDp2p = CNDp2p + #-fCNDp2p	See Note 6. (Depends on kP)				5,6

Table A-5 (continued

Label	Reaction and Products [a]	Rate Parameters [b]				Notes [a]
		k(300)	A	Ea	B	
cCCA	CNDp2p + CNDp2p = #2 pmCNDp2p + #2*fCNDp2p PMmass	See Note 7. (Depends on Kp)				7
cn02	RAOOH + CNDp2 = pmRAOOH + pmCNDp2 + #(fRAOOH+fCNDp2) PMmass	See Note 7 and 10 (Depends on Kp's)				7, 10
cn09	RAOOH + RAOOHp = pmRAOOH + pmRAOOHp + #(fRAOOH+fRAOOHp) PMmass	See Note 7 and 10 (Depends on Kp's)				7, 10
cn03	RAOOH + CNDp2p = pmRAOOH + pmCNDp2p + #(fRAOOH+fCNDp2) PMmass	See Note 7 and 10 (Depends on Kp's)				7, 10
cn08	CNDp2 + RAOOHp = pmCNDp2 + pmRAOOHp + #(fCNDp2+fRAOOHp) PMmass	See Note 7 and 10 (Depends on Kp's)				7, 10
cn01	CNDp2 + CNDp2p = pmCNDp2 + pmCNDp2p + #(fCNDp2 +fCNDp2p) PMmass	See Note 7 and 10 (Depends on Kp's)				7, 10
cn07	RAOOHp + CNDp2p = pmRAOOHp + pmCNDp2p + #(fRAOOHp+fCNDp2) PMmass	See Note 7 and 10 (Depends on Kp's)				7, 10
	Reactions of other aromatic products in the gas-phase mechanism					
BP26	R6OOH + OH = #.84 OH + #.222 RO2C + #.029 RO2XC + #.029 zRNO3 + #.84 PROD2 + #.09 xHO2 + #.041 xOH + #.02 xCCHO + #.075 xRCHO + #.084 xPROD2 + #.16 yROOH	5.60e-11				1
BP27	R6OOH + HV = OH + #.142 HO2 + #.782 RO2C + #.077 RO2XC + #.077 zRNO3 + #.085 RCHO + #.142 PROD2 + #.782 xHO2 + #.026 xCCHO + #.058 xRCHO + #.698 xPROD2 + #.858 yR6OOH	Phot Set= COOH				1
BP68	PROD2 + OH = #.472 HO2 + #.379 xHO2 + #.029 xMECO3 + #.049 xRCO3 + #.473 RO2C + #.071 RO2XC + #.071 zRNO3 + #.002 HCHO + #.211 xHCHO + #.001 CCHO + #.083 xCCHO + #.143 RCHO + #.402 xRCHO + #.115 xMEK + #.329 PROD2 + #.007 xPROD2 + #.528 yR6OOH	1.55e-11				1
BP69	PROD2 + HV = #.913 xHO2 + #.4 MECO3 + #.6 RCO3 + #1.59 RO2C + #.087 RO2XC + #.087 zRNO3 + #.303 xHCHO + #.163 xCCHO + #.78 xRCHO + yR6OOH	Phot Set= MEK-06, qy= 4.86e-3				1
BP70	RNO3 + OH = #.189 HO2 + #.305 xHO2 + #.019 NO2 + #.313 xNO2 + #.976 RO2C + #.175 RO2XC + #.175 zRNO3 + #.011 xHCHO + #.429 xCCHO + #.001 RCHO + #.036 xRCHO + #.004 xACET + #.01 MEK + #.17 xMEK + #.008 PROD2 + #.031 xPROD2 + #.189 RNO3 + #.305 xRNO3 + #.157 yROOH + #.636 yR6OOH	7.20e-12				1

Table A-5 (continued

Label	Reaction and Products [a]	Rate Parameters [b]				Notes [a]
		k(300)	A	Ea	B	
BP71	RNO3 + HV = #.344 HO2 + #.554 xHO2 + NO2 + #.721 RO2C + #.102 RO2XC + #.102 zRNO3 + #.074 HCHO + #.061 xHCHO + #.214 CCHO + #.23 xCCHO + #.074 RCHO + #.063 xRCHO + #.008 xACET + #.124 MEK + #.083 xMEK + #.19 PROD2 + #.261 xPROD2 + #.066 yROOH + #.591 yR6OOH	Phot Set= IC3ONO2				1
BP30	GLY + HV = #2 {CO + HO2}	Phot Set= GLY-07R				1
BP31	GLY + HV = HCHO + CO	Phot Set= GLY-07M				1
BP32	GLY + OH = #.7 HO2 + #1.4 CO + #.3 HCOCO3	9.63e-12	3.10e-12	-0.68		1
BP33	GLY + NO3 = HNO3 + #.7 HO2 + #1.4 CO + #.3 HCOCO3	1.02e-15	2.80e-12	4.72		1
BP80	HCOCO3 + NO = HO2 + CO + CO2 + NO2	2.08e-11	6.70e-12	-0.68		1
BP81	HCOCO3 + NO2 = HO2 + CO + CO2 + NO3	1.21e-11	1.21e-11	0.00	-1.07	1
BP82	HCOCO3 + HO2 = #.44 {OH + HO2 + CO + CO2} + #.56 GLY + #.15 O3	1.36e-11	5.20e-13	-1.95		1
BP34	MGLY + HV = HO2 + CO + MECO3	Phot Set= MGLY-06				1
BP35	MGLY + OH = CO + MECO3	1.50e-11				1
BP36	MGLY + NO3 = HNO3 + CO + MECO3	2.53e-15	1.40e-12	3.77		1
BP37	BACL + HV = #2 MECO3	Phot Set= BACL-07				1
BP40	NPHE + OH = BZO + XN	3.50e-12				1
BP41	NPHE + HV = HONO	Phot Set= NO2-06, qy= 1.5e-3				1
BP42	NPHE + HV =	Phot Set= NO2-06, qy= 1.5e-2				1
BP43	BALD + OH = BZCO3	1.20e-11				1
BP44	BALD + HV =	Phot Set= BALD-06, qy= 0.06				1
BP45	BALD + NO3 = HNO3 + BZCO3	2.73e-15	1.34e-12	3.70		1
BP46	AFG1 + OH = #.217 MACO3 + #.723 RO2C + #.060 {RO2XC + zRNO3} + #.521 xHO2 + #.201 xMECO3 + #.334 xCO + #.407 xRCHO + #.129 xMEK + #.107 xGLY + #.267 xMGLY + #.783 yR6OOH	7.40e-11				1
BP48	AFG1 + HV = #1.023 HO2 + #.173 MEO2 + #.305 MECO3 + #.500 MACO3 + #.695 CO + #.195 GLY + #.305 MGLY	Phot Set= AFG1				1
BP49	AFG2 + OH = #.217 MACO3 + #.723 RO2C + #.060 {RO2XC + zRNO3} + #.521 xHO2 + #.201 xMECO3 + #.334 xCO + #.407 xRCHO + #.129 xMEK + #.107 xGLY + #.267 xMGLY + #.783 yR6OOH	7.40e-11				1
BP51	AFG2 + HV = PROD2	Phot Set= AFG1				1

Table A-5 (continued

Label	Reaction and Products [a]	Rate Parameters [b]				Notes [a]
		k(300)	A	Ea	B	
BP52	AFG3 + OH = #.206 MACO3 + #.733 RO2C + #.117 {RO2XC + zRNO3} + #.561 xHO2 + #.117 xMECO3 + #.114 xCO + #.274 xGLY + #.153 xMGLY + #.019 xBACL + #.195 xAFG1 + #.195 xAFG2 + #.231 xIPRD + #.794 yR6OOH	9.35e-11				1
BP53	AFG3 + O3 = #.471 OH + #.554 HO2 + #.013 MECO3 + #.258 RO2C + #.007 {RO2XC + zRNO3} + #.580 CO + #.190 CO2 + #.366 GLY + #.184 MGLY + #.350 AFG1 + #.350 AFG2 + #.139 AFG3 + #.003 MACR + #.004 MVK + #.003 IPRD + #.095 xHO2 + #.163 xRCO3 + #.163 xHCHO + #.095 xMGLY + #.264 yR6OOH	1.43e-17				1
BP89	AFG4 + OH = #.902 RO2C + #.098 RO2XC + #.098 zRNO3 + #.902 xMECO3 + #.902 xRCHO + yROOH	6.30e-11				1
	Other Reaction forming Condensable Species from Non-Phenolic products					
TS03	AFG3C + OH = xCNDp2	Same K as Rxn BP52				11
TS04	AFG3C + O3 =	Same K as Rxn BP53				11
TS05	xCNDp2 = CNDp2	k is variable parameter: RO2RO				12
TS06	xCNDp2 =	k is variable parameter: RO2XRO				12
	PM wall reactions					
PMMW	PMmass =	Coef = PMwall				13
wCAP	pmCNDp2 =	Coef = PMwall				13
wOOH	pmRAOOH =	Coef = PMwall				13
wCCA	pmCNDp2p =	Coef = PMwall				13
PPMW	HV = CNDWPRE	Phot Set= NO2-06, qy= PPM-I				14
PPOH	CNDWPRE + OH = OH + CNDW	1.00e-11				14
cnCW	CNDW + PMmass = pmCNDW + #(1+fCNDW) PMmass	See Note 5. (Depends on Mw, T, and PMrad)				5,14
	pmCNDW = CNDW + #-fCNDW PMmass	Assumed negligible				14
ncCW	CNDW + CNDW = #2 pmCNDW + #2*fCNDW PMmass	See Note 7 (Coef = NCrateI)				7,14
nc06	CNDW + RAOOH = pmCNDW + pmRAOOH + #(fCNDW+fRAOOH) PMmass	See Note 7 and 10 (Depends on Kp's)				7, 10
nc04	CNDW + CNDp2 = pmCNDW + pmCNDp2 + #(fCNDW+fCNDp2) PMmass	See Note 7 and 10 (Depends on Kp's)				7, 10
nc10	CNDW + RAOOHp = pmCNDW + pmRAOOHp + #(fCNDW+fRAOOHp) PMmass	See Note 7 and 10 (Coef = NCrateI)				7, 9, 10,14
nc05	CNDW + CNDp2p = pmCNDW + pmCNDp2p + #(fCNDW+fCNDp2p) PMmass	See Note 7 and 10 (Depends on Kp's)				7, 14

Table A-5 (continued

Label	Reaction and Products [a]	Rate Parameters [b]				Notes [a]
		k(300)	A	Ea	B	
	Lumped reactions for airshed models					
BL14	ARO1 + OH = #.089 RO2XC + #.622 RO2C + #.167 HO2 + #.612 xHO2 + #.089 zRNO3 + #.474 yR6OOH + #.007 xMEO2 + #.049 xBALD + #.064 xPROD2 + #.003 xCCHO + #.006 xRCHO + #.135 CRES + #.032 XYNL + #.268 xGLY + #.231 xMGLY + #.283 xAFG1 + #.216 xAFG2 + #.233 yRAOOH + #.126 OH + #.126 AFG3 + #.078 AFG3C	6.07e-12	1.97e-12	-0.672		15
BL15	ARO2 + OH = #.126 RO2XC + #.651 RO2C + #.083 HO2 + #.649 xHO2 + #.126 zRNO3 + #.479 yR6OOH + #.002 xMEO2 + #.038 xBALD + #.025 xPROD2 + #.004 xRCHO + #.083 XYNL + #.14 xGLY + #.336 xMGLY + #.109 xBACL + #.093 xAFG4 + #.252 xAFG1 + #.24 xAFG2 + #.298 yRAOOH + #.14 OH + #.14 AFG3 + #.064 AFG3C	2.60e-11				15

[a] Format of reaction listing: "=" separates reactants from products; "*#number or formula*" indicates stoichiometric coefficient, "*#coefficient* {*product list*}" means that the stoichiometric coefficient is applied to all the products listed.

[b] Except as indicated, the rate constants are given by $k(T) = A \cdot (T/300)^B \cdot e^{-Ea/RT}$, where the units of k and A are cm^3 $molec^{-1}$ s^{-1}, Ea are kcal mol^{-1}, T is ^oK, and R=0.0019872 kcal mol^{-1} deg^{-1}. The following special rate parameter expressions are used:

Phot Set = *name*: The absorption cross sections and (if applicable) quantum yields for the photolysis reaction are given by Carter (2010a), where "*name*" indicates the photolysis set used. If a "qy=*number or coefficient name*" notation is given, the number or coefficient gives the overall quantum yield, which is assumed to be wavelength independent.

Coef = *name*: The rate constant is given by the coefficient value. The names and values or methods used to calculate coefficients related to SOA formation are given in Table 2.

Same K as Rxn xxxx: This reaction has the same rate constant as the reaction whose label is given.

K is variable parameter RO2RO (or RO2XRO): See Carter (2010a) for a discussion of these xPROD operators and how their rate constants are calculated. The parameter RO2RO is calculated from rates of reactions of the peroxy radicals that form alkoxy radicals, primarily reactions with NO but to some extent reactions with other peroxy radicals, while RO2XRO is calculated from the rates of reactions that form other species, primarily reactions with HO_2 and also to some extent with other peroxy radicals. These parameters are updated at each time step of the simulation based on calculated peroxy radical concentrations.

Depends on Mw, T, and PMrad: The method used to calculate the rates of the condensation reactions, which depend on the molecular weight assigned to the PM model species, the temperature, and the average particle size, is given on Table 2.

Depends on Kp's: The rate constant from this nucleation reaction is calculated as given in Equations (I) or (II) in the section on modeling PM formation and nucleation. It depends on the parameters NCrateI, MaxNucM, and the partitioning coefficients of the reacting species. If both of the species are non-volatile, then it is given by NCrateI. If only one of the species is non-volatile, it is

Table A-5 (continued

calculated using NCrateI / (1 + [MaxNucM / Kp]), where Kp is the partitioning coefficient of the more volatile species.

[c] Footnotes discussing the source of the reaction and rate constants used are as follows:

1 The gas-phase mechanism is that given by Carter and Heo (2012) except as indicated in other footnotes. A second footnote, if present, indicates that SOA-forming products have been added, but these additions will not affect the gas-phase predictions.

2 The yields of yRAOOH and xCNDp2 have been adjusted to fit the PM data in the experiments with this compound. If yRAOOH is reduced less than the value used in the gas-phase mechanism, the yield of yR6OOH is increased to keep the total hydroperoxide yields the same. (There are no cases where the yRAOOH yield that fit the SOA data exceeded that predicted by the gas-phase mechanism.)

3 The yields of yRAOOHp and xCNDp2p are adjusted based on model simulations of experiments with phenolic compounds as discussed in the text. The yield of yR6OOH in the gas-phase mechanism is not modified.

4 The yield of CNDp2p in the OH reaction is adjusted based on model simulations of the experiments with the phenolic compounds as discussed in the text. Condensable hydroperoxide formation is assumed not to be significant.

5 See Table 2 and the discussion in the section on modeling PM formation for the methods used to calculate rates of reactions representing condensation, evaporation, and nucleation of condensable species. The first reaction represents condensation and its rate constant depends on the temperature, molecular weight, temperature and PM radius but not the partitioning coefficient. The second reaction represents evaporation and is assumed to be negligible for non-volatile compounds. If non-negligible it is calculated from the rate constant for the condensation reaction and the partitioning coefficient assigned for the model species, which is given in Table 8. The third and subsequent reactions represent nucleation and their rate constants depend on the nucleation parameters discussed in Table 2 and the partitioning coefficient as discussed in the text.

6 Rate constant derived from the rate constant for the condensation reaction and the partitioning coefficient as discussed in the text. The partitioning coefficients are given in Table 8 and were derived fit the chamber data as discussed in the text. The adjusted values are highly approximate and the data could probably be fit approximately as well using different coefficients and yields if the partitioning coefficient is within approximately an order of magnitude of the values given on Table 8.

7 These reactions are used to representation nucleation and their rate constants are derived as discussed in Table 2 and the discussion of the section on modeling PM formation. The rate constant depends on the Kp values of the nucleating species except for those that are assumed to be non-volatile. If both nucleating species are non-volatile, then the nucleation rate constant is the maximum value of NCrateI (see Table 2).

8 The same gas-phase reactions are used for the model species representing condensable hydroperoxides formed from the phenols as used gas-phase mechanism for the model species (RAOOH) representing condensable hydroperoxides from aromatic hydrocarbons (Carter, 2010a,b; Carter and Heo, 2012).

9 The SOA data are simulated reasonably well if the condensable species represented by RAOOHp species are assumed to be non-volatile, so they are treated as non-volatile in the mechanism for simplicity.

9 These reactions represent loss of PM to the chamber walls. The rate constant, PMwall, is derived for each experiment based on analysis of the PM number data as discussed in the section on

Table A-5 (continued

particle wall loss characterization and corrections in the Experimental and Characterization Results section of this report.

10 These represent nucleation reactions involving interactions of different condensable model species. The rate constant depends on the Kp values for the individual species as discussed in Table 2.

11 This is used to represent CNDp2 formation (following reactions of peroxy radicals) from the reactions of the model species AFG3. To avoid having separate AFG3 model species in the mechanisms with different CNDp2 yields for each aromatic, a separate model species, AFG3C, which forms CNDp2 with 100% yields and whose yields are adjusted separately for each aromatic hydrocarbon, is used for this purpose. Its rate constants are the same as those used for the corresponding reaction of AFG3

13 This represents loss of particles on the chamber walls. The rate constant parameter, PMwall, is derived for each experiment from the particle number data as discussed in the Experimental and Characterization Results section of this report.

14 These reactions are added to represent background PM formation as discussed in the section on background PM formation in the Experimental and Characterization Results section of this report. The model species CNDWPRE represents the compound that is off-gassed from the walls with a rate constant given by the NO_2 photolysis rate · the PM offgasing rate parameter PPM-I. The latter is derived based on PPM-I values that best fit results of pure air and H_2O_2-air characterization experiments as discussed in the text. The rate constant for the reactions of CNDWPRE with OH is estimated. The model species CNDW and pmCNDW represent the gas- and pm-phase condensable species formed from CNDWPRE and it is assumed to be non-volatile for simplicity and because it gives adequate simulations of the data. The molecular weight is arbitrarily assigned 200 gm/mole; using different values would change the PPM-I values that fit the data by a constant factor but not the results of the model simulations using the PPM-I values adjusted to fit the data.

15 Mechanisms derived by averaging parameters estimated for the compounds listed on Table 11 as discussed in the section on lumped mechanisms for airshed models.

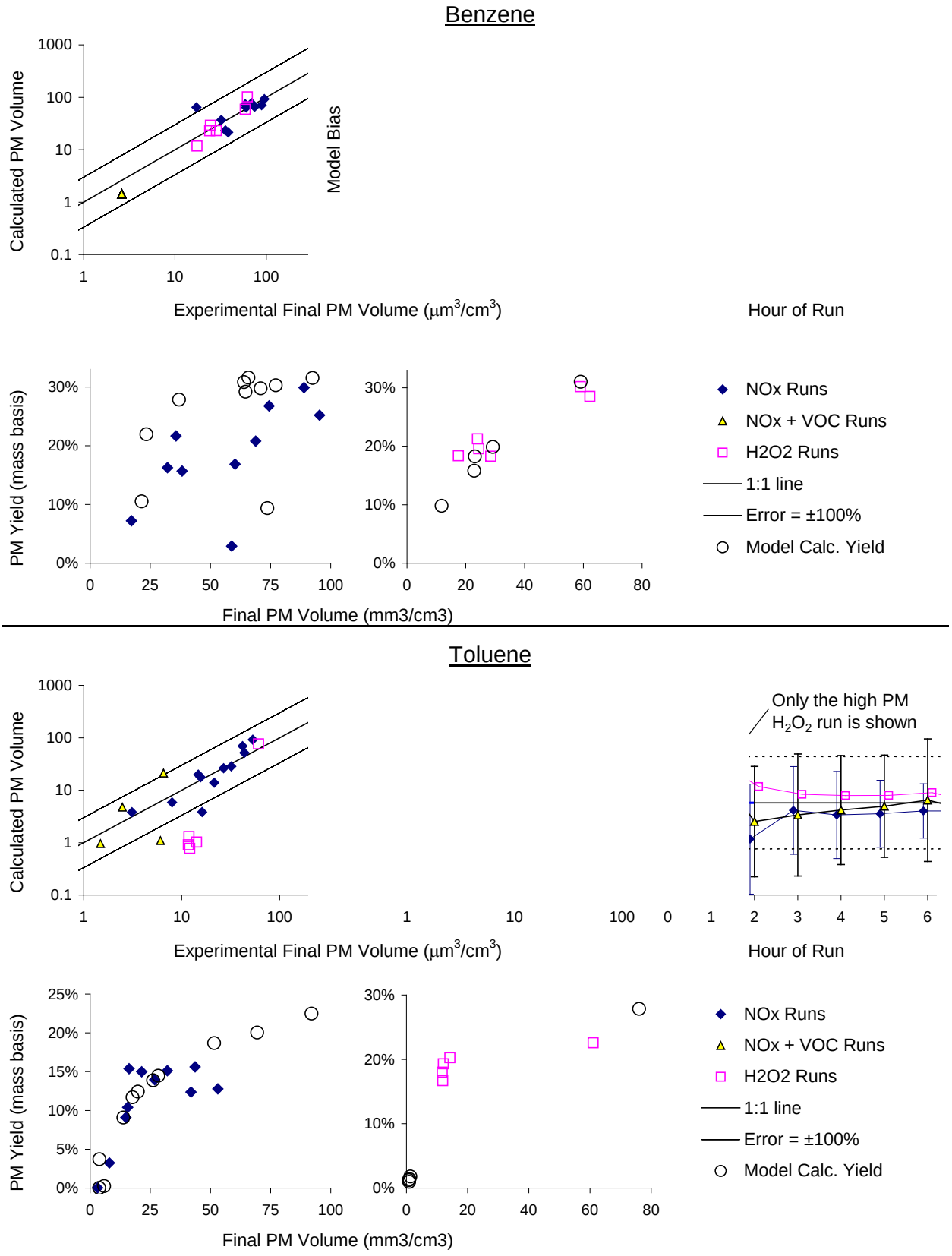

Figure A-3. Plots of SOA mechanism evaluation results for benzene and toluene.

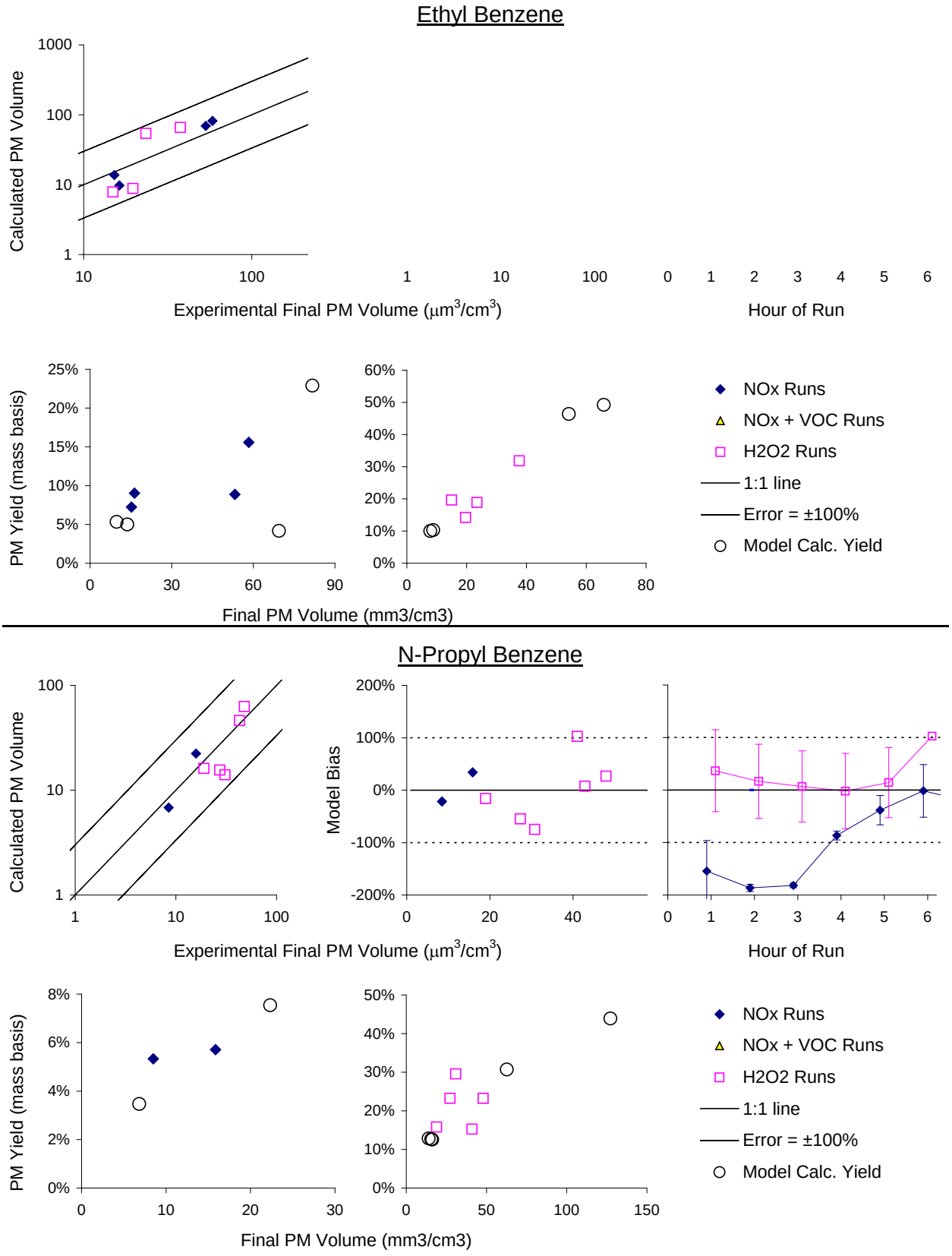

Figure A-4. Plots of SOA mechanism evaluation results for ethyl and n-propyl benzenes.

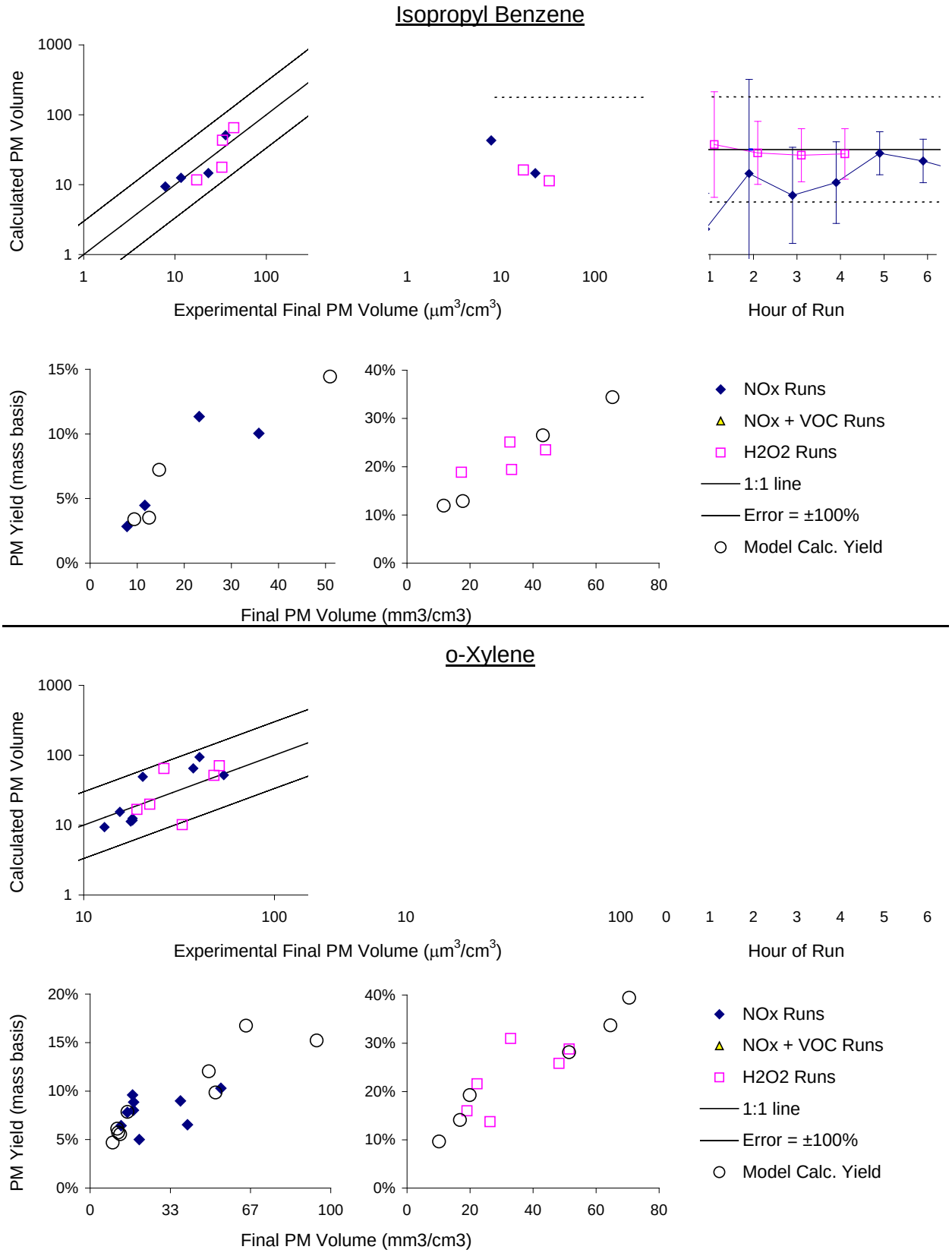

Figure A-5. Plots of SOA mechanism evaluation results for isopropyl benzene and o-xylene.

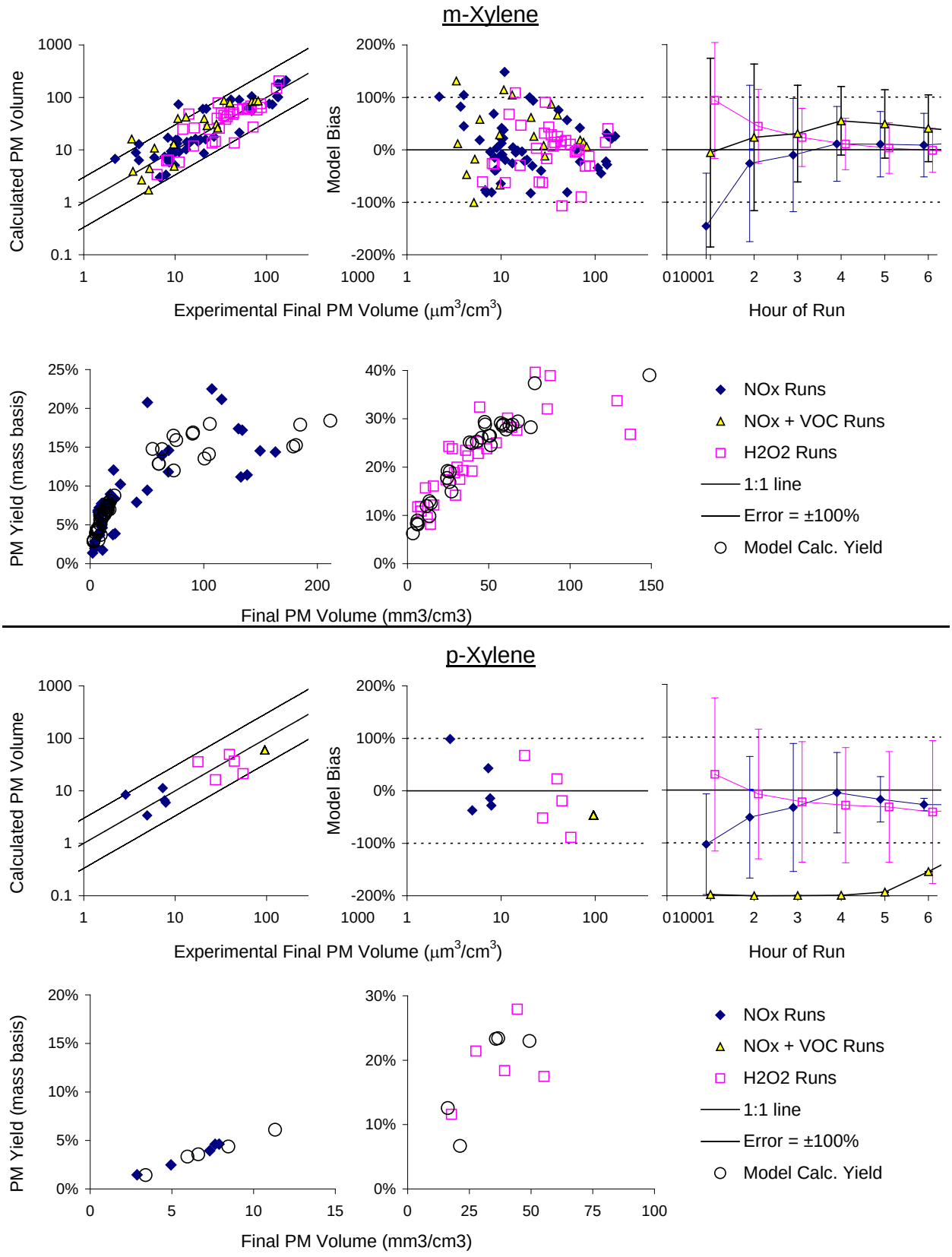

Figure A-6. Plots of SOA mechanism evaluation results for m- and p-xylenes.

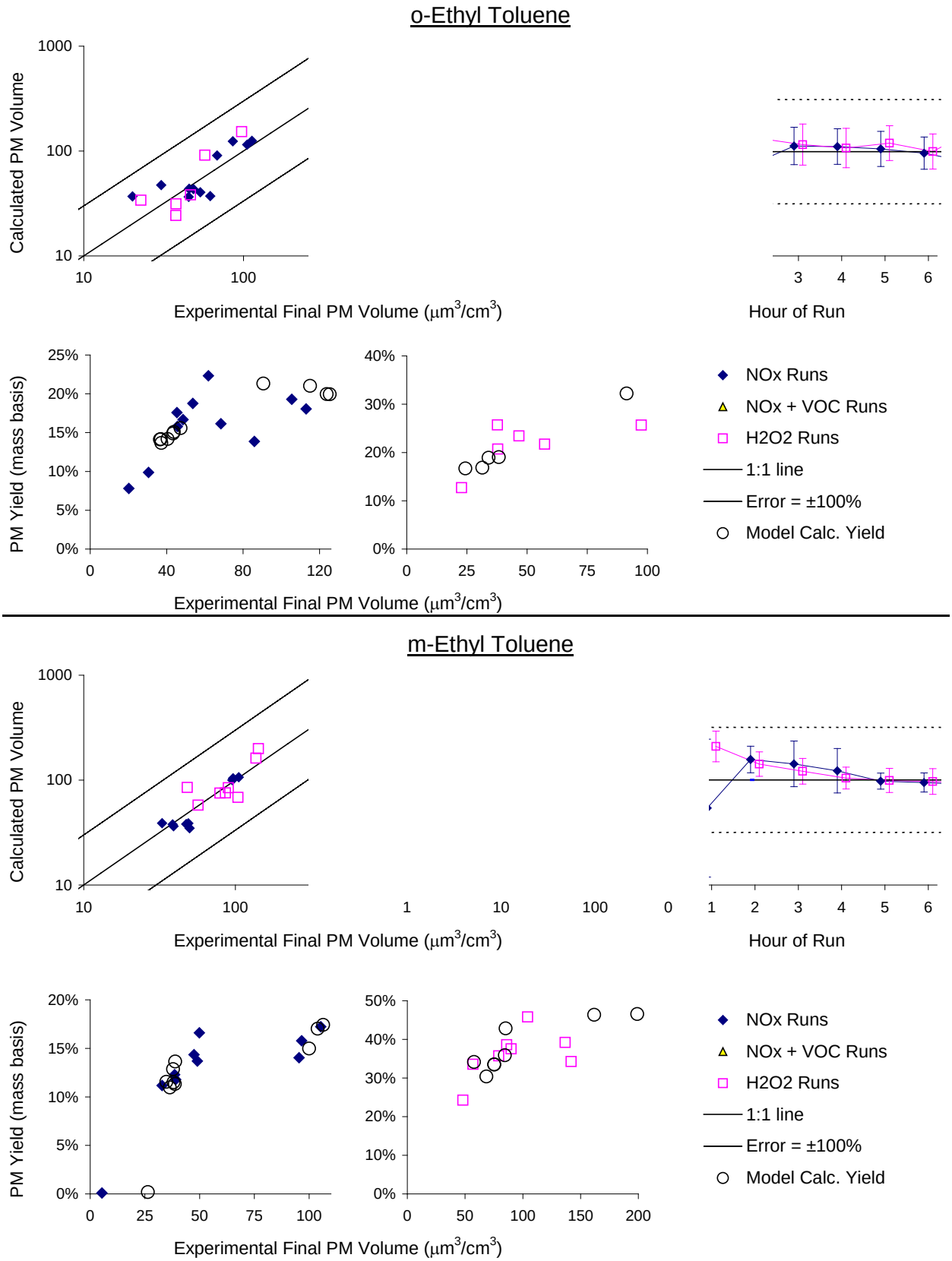

Figure A-7. Plots of SOA mechanism evaluation results for o- and m-ethyl toluene.

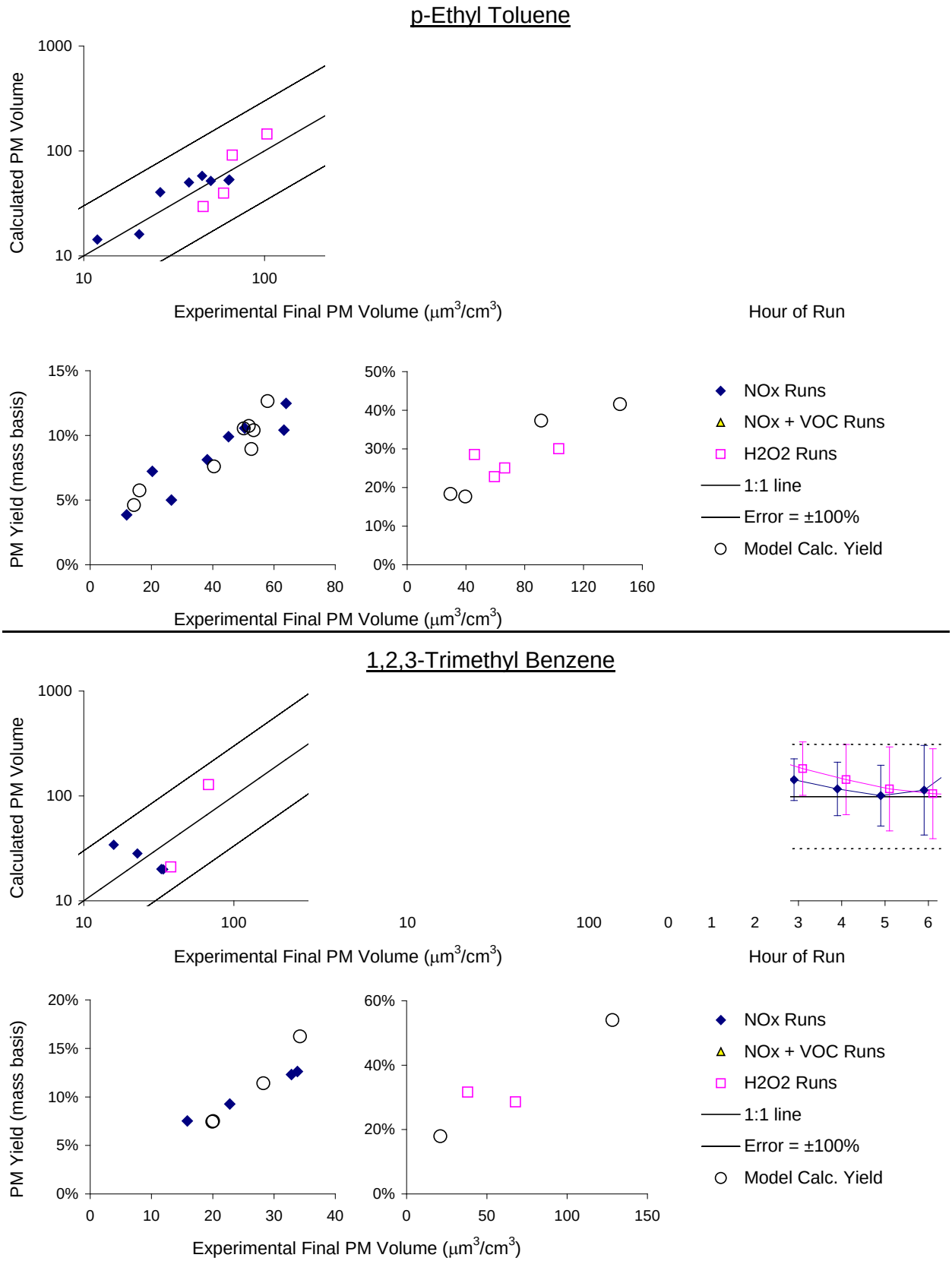

Figure A-8. Plots of SOA mechanism evaluation results for p-ethyl toluene and 1,2,3-trimethylbenzene.

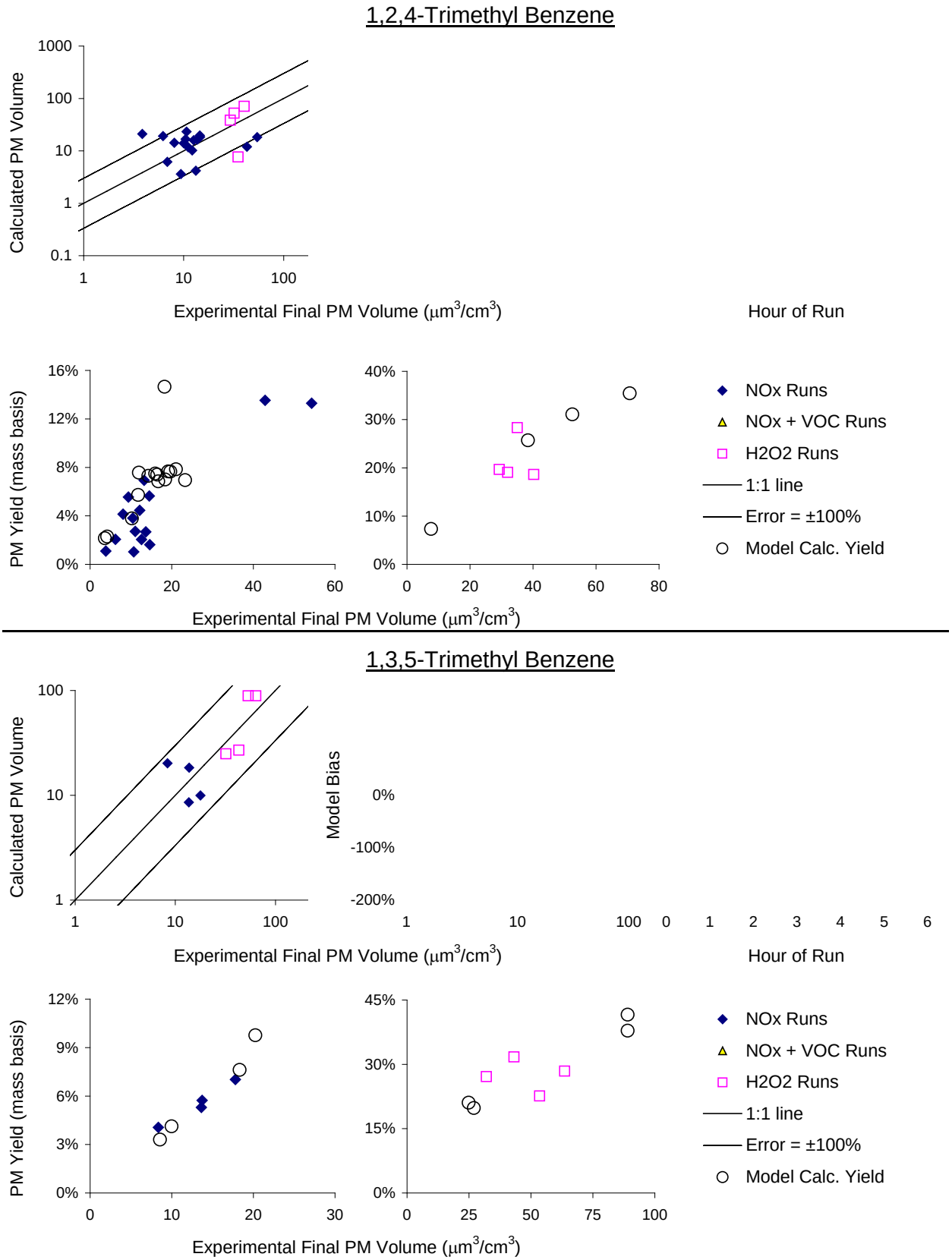

Figure A-9. Plots of SOA mechanism evaluation results for 1,2,4- and 1,3,5-trimethylbenzenes.

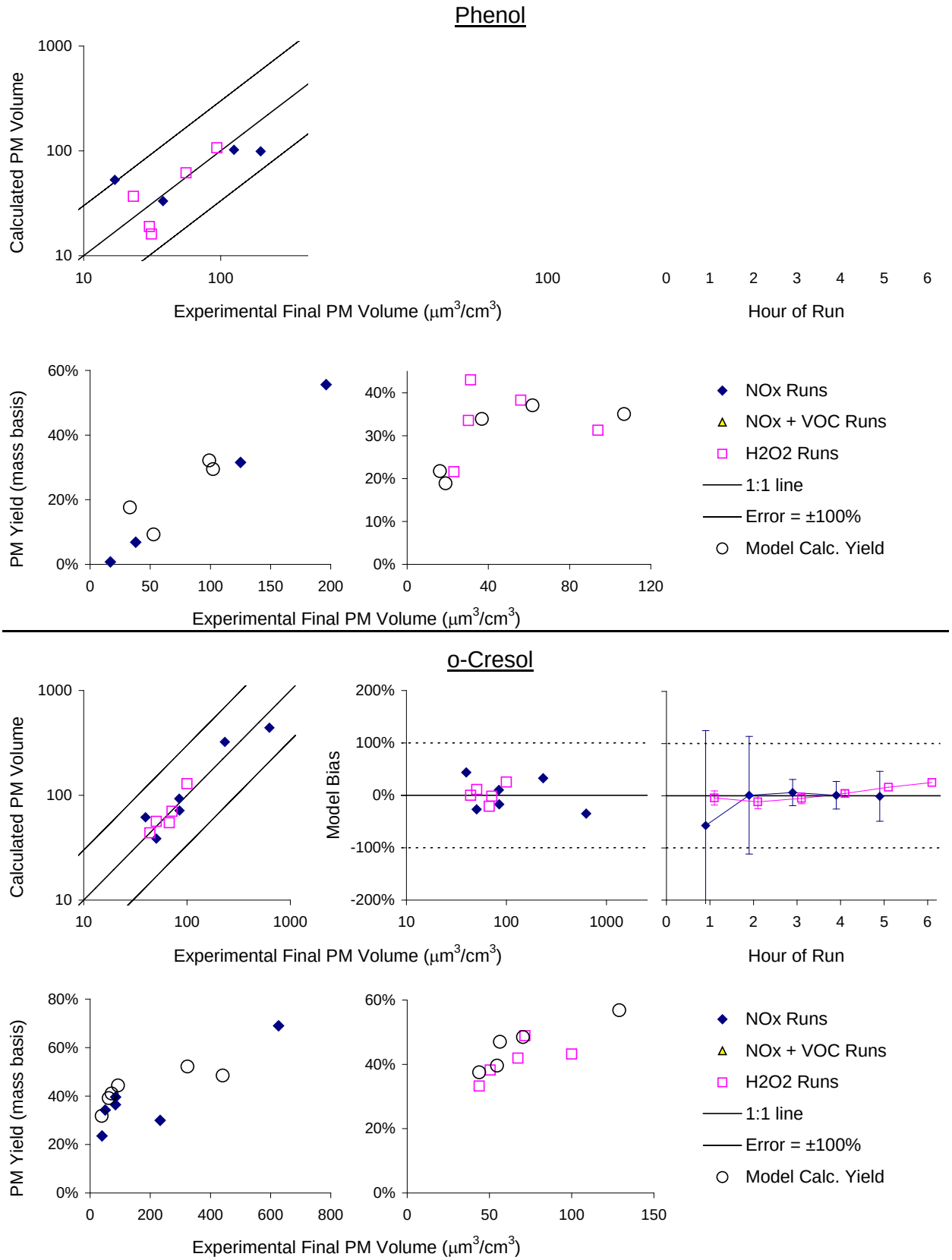

Figure A-10. Plots of SOA mechanism evaluation results for phenol and o-cresol.

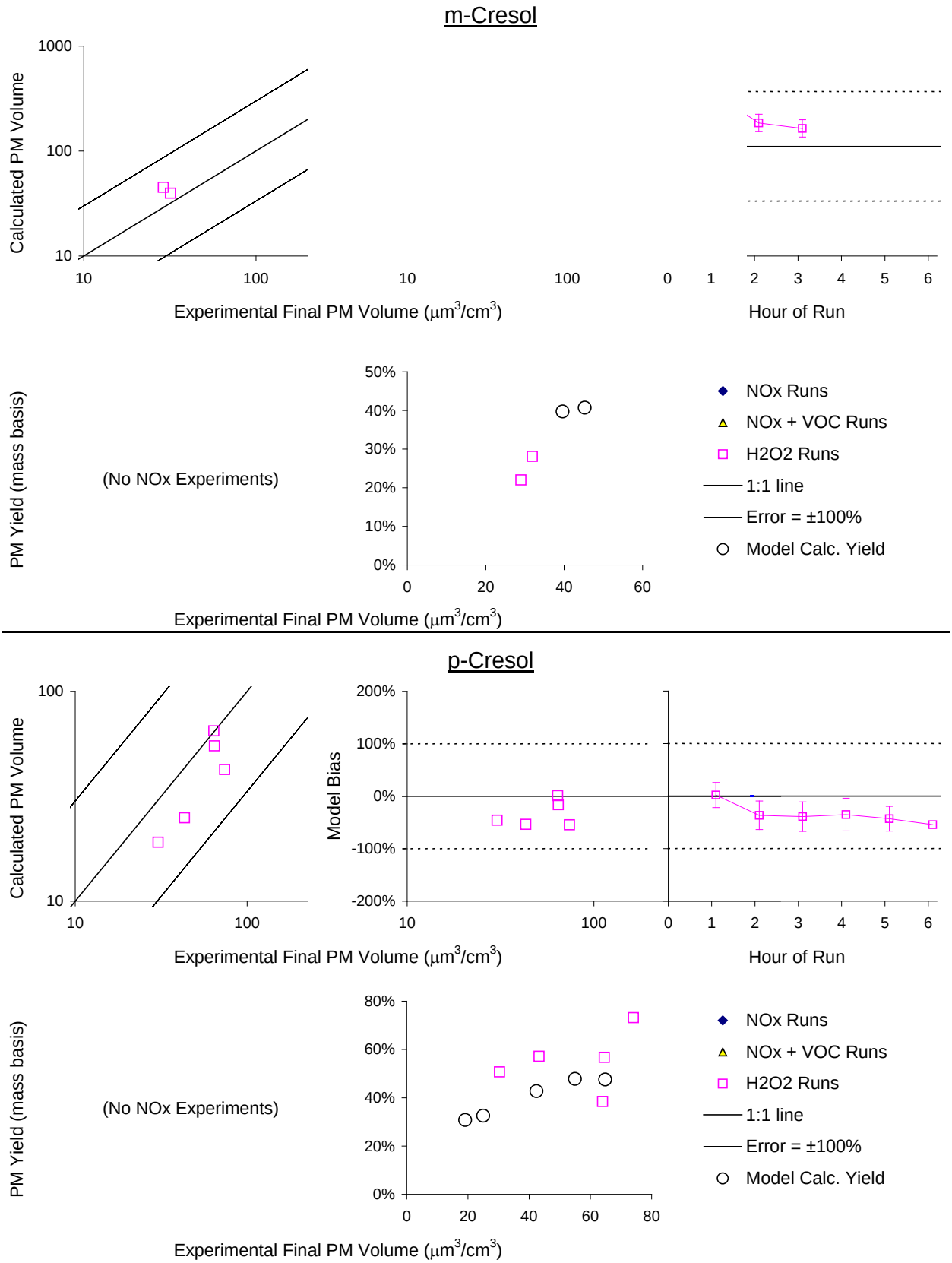

Figure A-11. Plots of SOA mechanism evaluation results for m- and p-cresols.

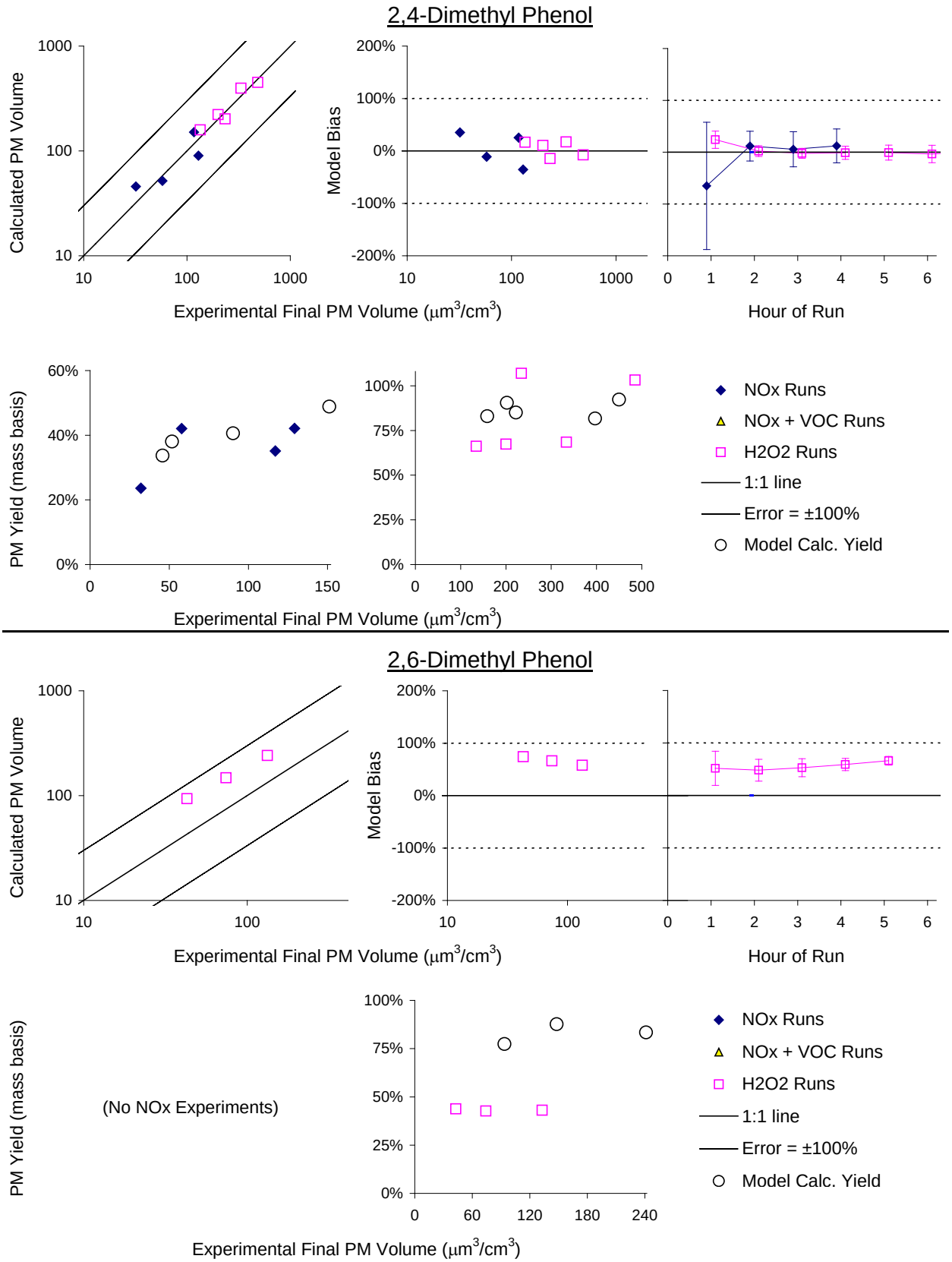

Figure A-12. Plots of SOA mechanism evaluation results for 2,4- and 2,6-dimethyl phenols.

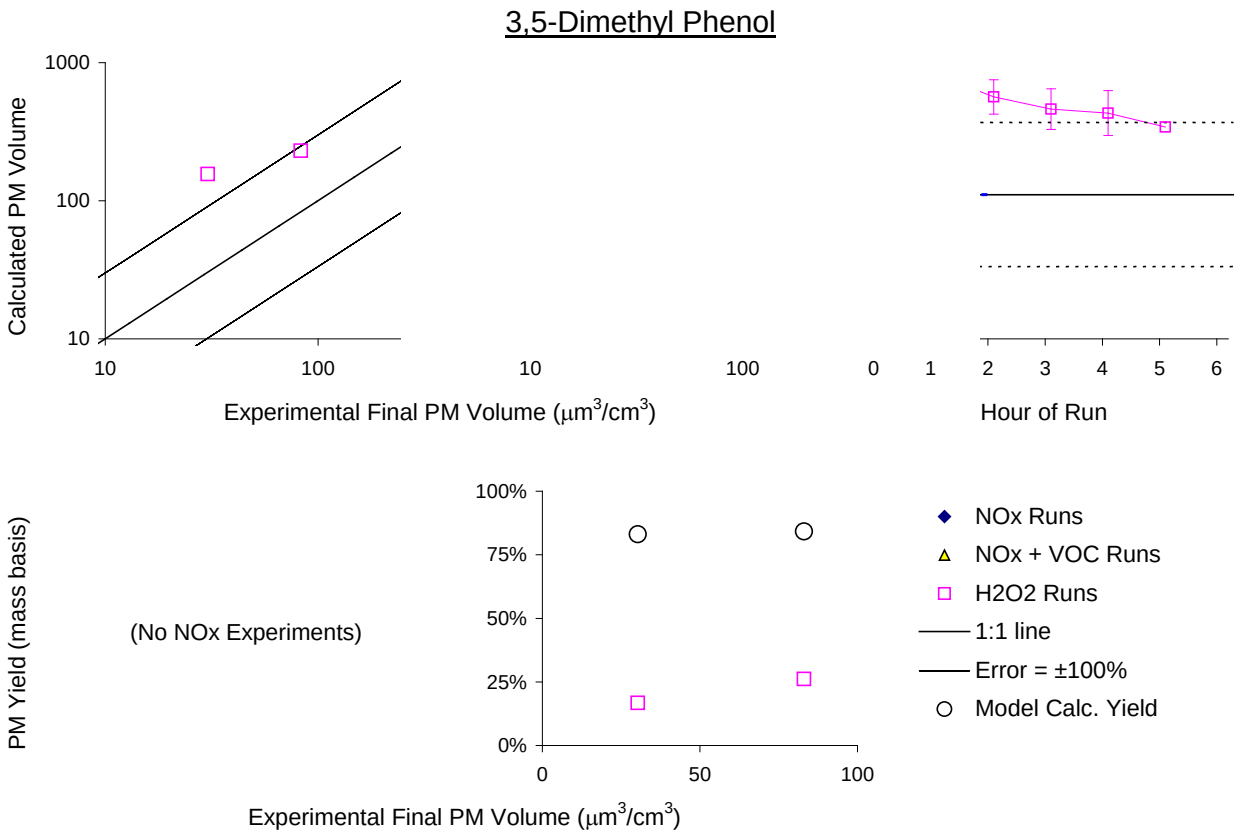

Figure A-13. Plots of SOA mechanism evaluation results for 3,5-dimethyl phenol.